

FACTORS AFFECTING THE TRANSIENT RESPONSE,  
OF DIRECT CURRENT MOTORS

By

HOWARD BRITTON HAMILTON

Bachelor of Science  
University of Oklahoma  
Norman, Oklahoma  
1949

Master of Science  
University of Minnesota  
Minneapolis, Minnesota  
1955

Submitted to the Faculty of the Graduate School  
of the Oklahoma State University  
in partial fulfillment of the requirements  
for the degree of  
DOCTOR OF PHILOSOPHY  
May, 1962

Thesis

1962D

H 2184  
J

cop. 2

NOV 8 1962

FACTORS AFFECTING THE TRANSIENT RESPONSE  
OF DIRECT CURRENT MOTORS

Thesis Approved:

*W. F. Conner*

Thesis Adviser

*Claude M. Summers*

*Harry D. Crawford*

*W. R. Ligelback*

*E. K. M<sup>s</sup> Fickler*

*Franklin*

Dean of the Graduate School

504480

## PREFACE

Direct current shunt connected motors have been used in industry for many years. Until the advent of servomechanisms, or closed loop control systems, the steady state performance of the motor was of prime interest in the majority of situations dealing with this type device.

With the development of closed loop control systems, a method of linear analysis utilizing device transfer functions, i.e., an expression relating output and input of the device, was developed, perfected, and widely accepted. Prior to this development, when the transient performance of direct current motors was considered of academic importance only, a linearized performance approximation leading to a first or second order equation evolved and was then accepted by system analysts as a true representation of motor behavior.

Cross fertilization of motor designers and closed loop control system analysts appears to have been inhibited by the tendency toward specialization of manufacturing and engineering techniques existing in industry until very recent times.

This thesis attempts to define some of the motor design parameters and their influence on transient behavior,

present experimentally determined performance compared with predicted performance using the "linearized" type analysis, and derives a procedure for obtaining a transfer function yielding valid performance calculations.

An expression of appreciation is extended to: Dr. Harry D. Crawford, Dr. William L. Hughes, and Dr. Eugene K. McLachlan, members of my advisory committee, for their encouragement and prompt consideration. I am especially indebted to Professor Charles F. Cameron, chairman of my committee, and Professor Claude M. Summers, also of my committee, for their supervision, guidance, encouragement, and help throughout my doctoral program. It was their intense interest in this area of electrical engineering study that interested and prompted me in my research leading to this thesis.

Miss Velda Davis, who typed this thesis, is also due an expression of thanks for her promptness and diligence.

## TABLE OF CONTENTS

Chapter	Page
I. INTRODUCTION . . . . .	1
II. TORQUE LOADS . . . . .	7
General Discussion . . . . .	7
Torque Load Proportional to Speed . . . . .	13
A.C. Motor as Adjustable Torque Load . . . . .	15
III. D.C. MOTOR ANALYSIS . . . . .	37
No Series Field, No $L_f$ , $L_A$ , $J$ . . . . .	43
No Shunt Field, No $L_A$ , $J$ . . . . .	44
Compound Motor, No $L_a$ , $L_f$ , $J$ , $M_{af}$ . . . . .	45
Shunt Motor Including $J$ and $L_a$ . . . . .	45
Shunt Motor Including $J$ , $L_A$ , and Torque $\propto \omega^2$ . . . . .	53
Shunt Motor Including Linear $L_f$ , Inertia Loading . . . . .	56
IV. ANALYSIS OF FACTORS OFTEN IGNORED IN LINEAR ANALYSIS . . . . .	59
Introduction . . . . .	59
A. Switching Saturated D.C. Circuits . . . . .	60
A-1. Sample Calculation - Determination of Actual Response Time . . . . .	67
A-2. Summary of $G$ , $D$ Variations . . . . .	82
B. Eddy Currents in the Iron Core . . . . .	83
C. Demagnetizing Effect of Armature MMF . . . . .	101
D. Coupling Between Field and Armature Circuits Due to Brush Shift . . . . .	117
E. Commutating Field Time Lag . . . . .	126
F. Armature Potential Drop Due to Brushes . . . . .	132
G. Induced Currents in Closed Conducting Circuits . . . . .	134

Chapter	Page
Effect of Above Factors in Linear Type Analysis . . . . .	150
V. EXPERIMENTAL TRANSIENT STUDIES . . . . .	157
Experimental Equipment . . . . .	157
Equipment Calibration . . . . .	162
Machine Characteristics . . . . .	165
Calculated and Observed Shunt Motor Transients . . . . .	182
VI. MODIFIED PERFORMANCE EQUATIONS . . . . .	217
The "Describing Function" Technique . . . . .	220
Curve Fitting Procedures Involving Polynomials . . . . .	221
Additions of "Poles" to Modify Equation (6-1) . . . . .	227
Calculation of Response Using Curve Segments . . . . .	229
VII. SUMMARY AND CONCLUSIONS . . . . .	237
Summary . . . . .	237
Conclusions . . . . .	238
A. Brushes and Rigging . . . . .	239
B. Armature Windings . . . . .	240
C. Use of Additional Windings . . . . .	241
D. Core Fastening Methods . . . . .	242
E. Core Material, Configuration and Excitation Requirements. . . . .	243
SELECTED BIBLIOGRAPHY . . . . .	245
APPENDIX A . . . . .	247
GOTRAN PROGRAM . . . . .	248
SAMPLE DATA PRINT OUT . . . . .	249

## LIST OF TABLES

Table	Page
IV-I. Current Versus Time - Typical Nonlinear Response . . . . .	70
IV-II. Armature Reaction Test Data . . . . .	116
IV-III. Brush Shift Data . . . . .	127
V-I. Machine Parameters (GE Mod. 5BC44AB65) . .	179
VI-II. Data Points, $\omega$ Versus $t$ (Figure 5.19) . . .	230



## LIST OF FIGURES

Figure		Page
2.1.	Driven System Block Diagram . . . . .	9
2.2.	D.C. Generator Equivalent Circuit . . . . .	14
2.3.	T - $\omega$ for GE Co. 5BC44AB65F (1/4 HP), Fixed Load, Separate Excitation . . . . .	16
2.4a.	Single Phase Motor With D.C. Excitation . . .	17
2.4b.	Three Phase Motor With D.C. Excitation . . .	17
2.5.	Air Gap Flux and Rotor MMF Relationship . . .	20
2.6.	Closed Path Integration in the Air Gap . . .	21
2.7.	Flux-Current Relationships - Main Winding Excitation . . . . .	25
2.8.	Flux-Current Relationship - Two Winding Excitation . . . . .	27
2.9.	Torque Direction (Two Winding Excitation). . .	31
2.10.	Torque Speed Curve for Equation (2-54) . . .	33
4.1.	Shunt Field Equivalent Circuit . . . . .	60
4.2.	Typical Open Circuit Characteristic . . . . .	68
4.3.	Typical Linear and Nonlinear Response . . . . .	71
4.4.	Effect of G/DN on $\mu_i$ for Various G . . . . .	74
4.5.	Effect of G/DN on $\mu_i$ for Various D . . . . .	75
4.6.	$i/I_{SS}$ Versus t for Various G/DN . . . . .	76
4.7.	Effect of G/N for Constant N, D . . . . .	78
4.8.	Effect of D for Constant G/N . . . . .	79
4.9.	Effect of D, G/N for Fixed Current . . . . .	80

Figure		Page
4.10.	$i$ Versus $t$ for Various $N, D$ . . . . .	81
4.11.	Electric and Magnetic Field Relationships. .	86
4.12.	Eddy Current Formation, $I_y$ . . . . .	88
4.13.	Eddy Current Formation, $I_x$ . . . . .	88
4.14.	Core Cross Section . . . . .	90
4.15.	Rectangular Wave, $f(y)$ . . . . .	91
4.16.	Eddy Current Time Constants . . . . .	98
4.17.	Elementary D.C. Machine - Developed Air Gap.	102
4.18.	Armature MMF Space Relationship . . . . .	104
4.19.	Armature Circuit Voltage Drop (Westinghouse Generalized Machine) . . . . .	111
4.20.	Open Circuit Characteristic (Westinghouse Generalized Machine) . . . . .	112
4.21.	Voltage Reduction due to Armature Reaction .	113
4.22.	Calculation of Effective Turns (Westinghouse Generalized Machine) . . .	115
4.23.	Brush Shift (Simple D.C. Machine) . . . . .	119
4.24.	Air Gap Physical Arrangement (Simple D.C. Machine) . . . . .	122
4.25.	MMF Relationship, Brushes on Neutral . . . .	122
4.26.	MMF Relationship, Brushes $\alpha$ Radians off Neutral . . . . .	122
4.27.	Induced Voltage as a Function of Brush Shift (Westinghouse Generalized Machine).	128
4.28.	Commutating Field Equivalent Circuit . . . .	131
4.29.	Lamination Fastener Arrangement (Bolted or Riveted) . . . . .	135
4.30.	Lamination Fastener Arrangement (Clamp) . .	136
4.31.	Closed Circuits Formed on Armature for Simple Winding . . . . .	136

Figure		Page
4.32.	Field Current Build up . . . . .	146
4.33.	Induced Voltage Build up (Step Voltage on Field) . . . . .	147
4.34.	Open Circuit Characteristics, GE Model 5BC44AB65F . . . . .	148
5.1.	Four Element Strain Gage Bridge . . . . .	158
5.2.	Experimental Circuitry . . . . .	163
5.3.	Filter Details . . . . .	164
5.4.	Open Circuit Saturation Characteristic GE Model No. 5BC44AB65F . . . . .	167
5.5.	System Friction and Windage Load Versus Speed . . . . .	170
5.6.	Brush System - Effective Resistance Variation . . . . .	174
5.7.	Self Inductances . . . . .	175
5.8.	Self Inductances, Continued . . . . .	178
5.9.	Mutual Inductances . . . . .	180
5.10.	Shunt Field Current Build up . . . . .	181
5.11.	Speed Versus Time (No External Load) . . . . .	184
5.12.	Shunt Field Current Versus Time (No External Load) . . . . .	186
5.13.	Torque Versus Time (No External Load) . . . . .	188
5.14.	Current Versus Time (No External Load) . . . . .	189
5.15.	Dynamic Torque Constant as a Function of Armature Current . . . . .	192
5.16.	Speed Versus Torque (No External Load) . . . . .	193
5.17.	Speed Versus Time (Various Commutating Field Arrangements) . . . . .	196
5.18.	Effect of Series Field on Shunt Field Current (No External Load) . . . . .	199

Figure		Page
5.19.	Speed Versus Time (Torque Proportional to Speed) . . . . .	201
5.20.	Torque Versus Time (Torque Proportional to Speed) . . . . .	203
5.21.	Effect of Series Field on Shunt Field Current Variations (Torque Proportional to Speed) . . . . .	204
5.22.	Armature Current Versus Time (Torque Proportional to Speed) . . . . .	205
5.23.	Dynamic Torque Constant as a Function of Armature Current (Under Load). . . . .	207
5.24.	Speed Versus Torque (Torque Proportional to Speed) . . . . .	209
5.25.	Speed Versus Time (Impact Loading) . . . . .	210
5.26.	Torque Versus Time (Impact Loading) . . . . .	211
5.27.	Current Versus Time (Impact Loading) . . . . .	212
5.28.	Speed Versus Torque (Impact Loading) . . . . .	213
5.29.	Torque Constant Variation (Impact Loading) . . . . .	214
6.1.	Second Order System Response to Step Input . . . . .	219
6.2.	Delay and Shift Using Laplace Transforms . . . . .	223
6.3.	Typical $\omega$ Versus $t$ Characteristics . . . . .	224
6.4.	Generating Non-Periodic Functions by Delay and Shift . . . . .	225
6.5.	Curve Fitted Segments (Speed Versus Time). . . . .	231
6.6.	Torque Versus Time, Observed and Calculated . . . . .	235

## CHAPTER I

### INTRODUCTION

Direct-current motors have been designed and utilized for many years in substantially the physical form presently used. During the years since the advent of this form of electrical to mechanical conversion device, there have been many improvements in the state of the art but these improvements were, for the most part, incorporation of advances in insulation, magnetic materials, brush materials, etc. Electrically, there have been few changes other than the addition of pole face windings (rather than movable brush rigging) to compensate for the effect on the main field of magneto motive force due to armature currents, commutating windings for aiding commutation, etc.

Few changes in the method of analysis, insofar as performance is concerned, have occurred. Until the advent of closed-loop control systems, transient response of d-c motors was relegated to secondary importance - the steady-state characteristics, such as the speed-torque relationship, were considered prime factors. Since d.c. motors are widely used as power stages in closed-loop systems, their transient response characteristics are becoming of extreme

importance, not only to the system analyst who is interested in the external behavior, but also to the designer who is striving to examine the factors contributing to undesirable external characteristics and to take steps to correct or mitigate these factors.

One of the earliest references dealing with transient performance was published in 1917. (1). It deals with the characteristics of shunt, series, and compound wound d.c. motors with various load combinations. The analysis is for a linear relationship between magnetizing force and resultant flux (B-H curve) for the shunt and compound wound machines and includes mutual coupling between the shunt and series field in the latter case. The shunt and series field self inductances are also considered although they are assumed to be of constant value (which later investigators, especially Koenig (2), have experimentally shown not to be the case). The analysis for the series and the shunt motor is based on no inductance in the armature and no coupling between the armature and the main field for the shunt connection. Frohlich's representation of the B-H curve is utilized in the series motor analysis.

Since the appearance of Hansen's (1) 1917 publication, numerous works have been published pertaining to the electrodynamics of d.c. machines, but these are, for the most part, with either constant or linear parameters and for the condition of constant, full excitation prior to any disturbance investigated. (2, 3, 4, 5, 6, 7). Inclusion

of conditions within the field circuit (for varying field) leads to mathematical obstacles not easily overcome in straight forward analytical work. White and Woodson (4) presents a block diagram of a realistic d.c. shunt machine which incorporates nonlinearity of the B-H curve and lends itself to analog computer study. Some works do circumvent the mathematic obstacles associated with the nonlinear B-H curve by graphical methods. (8, 9, 10). However, the effect of flux build up with time in the shunt field is ignored. The closest approach to a true analysis is given by Rao (11), although it is limited in scope since it covers a specific two machine oscillating system. In the course of study of short circuit phenomena associated with d.c. machines, effects have been noted and accounted for empirically that appear to retard the rise of current in machines under short circuit conditions. (12, 13, 14). These effects do not manifest themselves in a linear analysis where the effects of eddy currents and currents circulating in closed iron paths formed by rivets, bolts etc., used in fastening the core together, are ignored.

The most common and widely used analysis of d.c. motors is based on a so called "steady-state" analysis which, in effect, is for a device with no inductance and no electrical time delays. The most enlightening reference for this type of analysis is presented by Ahlquist (15). The practical effect of the no-inductance assumption is that there are infinite number of equilibrium conditions

relating torque and speed, which are the externally manifested parameters of a motor considered of first importance. These equilibrium points are mathematically related and can be so expressed. In operation, any departure from a condition of equilibrium is along a line, which can be mathematically expressed (called the speed-torque characteristic) by a relatively simple first or second order equation, to a new equilibrium point. This speed-torque characteristic can be experimentally obtained by slowly changing electrical and mechanical system parameters and measuring average values. Due to the realities of the situation, the actual physical phenomena will most probably depart from the static or "steady state" curve except for average values. In other words, the instantaneous values depart from the average values of speed and torque and a "steady state" analysis may lead to misleading or false results.

Some factors responsible for the departure of instantaneous values from average values are:

1. Nonlinear B-H Characteristic
  - (a) Armature magnetomotive forces.
  - (b) Constantly changing ratio of inductance to resistance.
2. Armature to Field Coupling
3. Commutation
  - (a) Brush shift.
  - (b) Use of diverter resistors in the series and commutating fields.



4. Circulating Currents in Core Fastener and Other Closed Conducting Circuits.
5. Eddy Currents in the Magnetic Core.
6. Nature of Mechanical Load, Inertia, and Damping.

The inclusion of any of the above factors in a mathematical analysis of the motor performance leads to unwieldy and often impossible-to-solve expressions. Linear analysis ignoring the above factors does admit to mathematical solution and does serve a useful purpose, i.e., an appreciation of factors influencing the transient response can be obtained. In order to intelligently evaluate electromechanical dynamics based on the linear analysis, each of the above factors must be examined and their effect on the linear analysis assessed by judicious application of appropriate engineering judgment.

In this thesis, the various influencing factors are examined analytically and experimentally and their probable effects summarized. In addition, experimentally derived data for various loadings on the shunt connected d.c. motors is presented.

The objectives of this thesis are:

1. A comparison between the predicted and actual transient response of direct current motors.
2. Mathematical derivation and evaluation of factors contributing to discrepancies between actual and theoretical performance.

3. To present a summary of steps and precautions that can be taken in the design stage of a motor to minimize the effect of the factors referred to in (2).
4. To develop a procedure for obtaining a transfer function for the motor which will result in more faithful representation of motor behavior.

If these objectives have been fulfilled, it is felt that a substantial contribution will have been made to the motor design and systems analysis area, because it will materially aid motor designers in their attempts to design relatively small direct current motors (for inclusion in closed-loop control systems) whose performance can be reliably and accurately predicted by present day, straight forward, easily managed techniques of system analysis.

The rationalized MKS system of units is used throughout this thesis.

## CHAPTER II

### TORQUE LOADS

#### General Discussion

In general, motors are devices which convert electrical energy to mechanical energy. Utilization of a motor results in a mechanical load on the shaft of the motor. This mechanical load is best considered, for analytical purposes, as a resisting torque acting on the motor shaft. Electromagnetic power is defined as the power converted from electrical to mechanical form, or vice versa. Electromagnetic torque is related to mechanical power by:

$$T_m = \frac{P_m}{\omega} \quad (2-1)$$

where:

$T_m$  = electromagnetic torque, newton-meters

$P_m$  = electromagnetic power, watts

$\omega$  = angular velocity, radians/sec.

For a motor, electromagnetic torque corresponds, at the given angular velocity, to the power converted from electrical to mechanical form and acts against friction and windage effects of the rotor of the motor (commonly referred

to as "rotating losses") as well as the external resisting effect of the load and the inertia of the load and rotor.

Considering the mechanical load as a resisting torque which includes friction and windage effects, and applying d'Alembert's principle, the equation of equilibrium for the motor and load is:

$$T_m = T_L \pm J \frac{d\omega}{dt} \quad (2-2)$$

where:

$T_L$  = resisting torque of load, friction, and windage in newton-meters.

$J$  = polar moment of inertia of combined motor and load referred to motor shaft, in kilogram-meters<sup>2</sup>.

$\frac{d\omega}{dt}$  = angular acceleration of motor and load, referred to the motor shaft in radians/second<sup>2</sup>.

Note: If  $T_m > T_L$ , the + sign is used;

If  $T_m < T_L$ , the - sign is used.

Loads which can only oppose rotation, such as friction, are designated as passive loads. Loads having the ability to drive the motor are said to be active loads.  $J \frac{d\omega}{dt}$  is commonly referred to as an inertia load. Both passive and active loads may be of a type which are (a) independent of speed, (b) some function of speed, and (c) a combination of (a) and (b) plus the inertia load.

If the load shaft revolves at a different angular

velocity than the motor shaft, a torque transformation may occur (as in the case of gearing, pulleys, etc.) and this must be considered when determining net  $T_L$  and  $J$ .

Consider a drive system, as shown in Figure 2-1, with a speed-changing gear between the motor drive shaft and the load shaft.

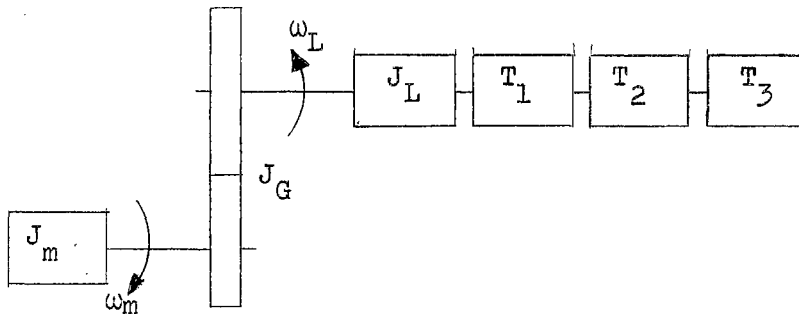


Figure 2-1. Driven System Block Diagram

Where:

$J_m$  = polar moment of inertia of motor

$J_L$  = polar moment of inertia of load

$J_G$  = polar moment of inertia of gears (referred to the motor shaft)

$a$  = speed ratio  $\omega_L/\omega_m$

$\omega_L$  = angular velocity of load shaft

$\omega_m$  = angular velocity of motor shaft

$T_1$  = a load torque independent of speed =  $C_1$

$$T_2 = \text{a load torque varying as } \omega_L = C_2 \omega_L$$

$$T_3 = \text{a load torque varying as } \omega_L^2 = C_3 \omega_L^2$$

( $T_1$ ,  $T_2$  and  $T_3$  referred to the load shaft)

$$\text{Now } T \omega_L = T' \omega_m, \text{ or } T = \frac{\omega_m}{\omega_L} T', \text{ or } T' = aT$$

where:

$T$  = torque referred to load shaft with angular velocity  $\omega_L$

$T'$  = torque referred to motor shaft with angular velocity  $\omega_m$ .

$$\text{For the inertia load, } T = J_L \frac{d\omega_L}{dt}$$

$$\frac{T'}{a} = J_L \frac{d(a\omega_m)}{dt} \text{ or } T' = a^2 J_L \frac{d\omega_m}{dt}$$

referred to the motor shaft.

$$\text{For } T_1; T = C_1; T' = aC_1$$

$$T_2; T = \omega_L C_2; T' = a^2 C_2 \omega_m$$

referred to the motor shaft.

$$T_3; T = \omega_L^2 C_3; T' = a^3 C_3 \omega_m^2$$

For the complete solution, referred to the motor shaft, the equation of equilibrium is:

$$T_m = (J_m + J_G + a^2 J_L) \frac{d\omega_m}{dt} + aC_1 + a^2 C_2 \omega_m + a^3 C_3 \omega_m^2.$$

(2-3)

Thus, any combination of motor-load-gearing arrangements can be reduced to an equivalent system for which the

equation of equilibrium is applicable. Although the overall gear ratio,  $a$ , is fixed, it is possible to minimize the total inertia by securing the speed change,  $a$ , in several, rather than one, steps of speed changing. (16).

The stability of a system may be defined as that attribute of a system which enables it to develop forces of such a nature as to restore equilibrium after any small departure therefrom. A simplified evaluation of stability considers the system to be at some equilibrium position defined by:

$$\frac{d\omega}{dt} = 0 ; T_m = T_L. \quad (2-4)$$

And, for a decrease in speed, if  $T_m > T_L$ , the system accelerates to its former position; for a speed increase beyond the equilibrium speed, if  $T_L > T_m$ , the system returns to equilibrium. For these conditions, the system is said to be stable.

A more sophisticated, and exacting, approach is as follows: Assume a small deviation from equilibrium and denote the changes by  $\Delta T_m$ ,  $\Delta T_L$  and  $\Delta\omega$ . The equation of equilibrium (2-2) becomes:

$$J \frac{d(\omega + \Delta\omega)}{dt} + (T_L + \Delta T_L) = T_m + \Delta T_m. \quad (2-5)$$

From this, subtract equation (2-2), resulting in:

$$J \frac{d(\Delta\omega)}{dt} + \Delta T_L = \Delta T_m. \quad (2-6)$$

If the departures are truly quite small, they may be expressed as linear functions of  $\Delta\omega$ , in which case Equation (2-6) becomes:

$$J \frac{d(\Delta\omega)}{dt} + \frac{dT_L}{d\omega} (\Delta\omega) = \frac{dT_m}{d\omega} (\Delta\omega) . \quad (2-7)$$

This is an ordinary differential equation in  $\Delta\omega$ , of the "variables separable" type, yielding for a solution,

$$\Delta\omega = \Delta\omega_0 \varepsilon^{-\frac{1}{J} \left[ \frac{dT_L}{d\omega} - \frac{dT_m}{d\omega} \right] t} \quad (2-8)$$

where  $\Delta\omega_0$  is the change in angular velocity at time,  $t = 0^+$ .

If  $\Delta\omega$  is to approach zero with passage of time (and equilibrium is to be restored), the exponent of  $\varepsilon$  must be negative and, from Equation (2-8), this can be so only if

$$\frac{dT_L}{d\omega} > \frac{dT_m}{d\omega} . \quad (2-9)$$

The condition of  $\Delta T_m = \frac{dT_m}{d\omega} (\Delta\omega)$  and  $\Delta T_L = \frac{dT_L}{d\omega} (\Delta\omega)$  utilizes the derivatives of  $T_m$  and  $T_L$  with respect to  $\omega$  at the point of equilibrium. The values of  $\frac{dT_m}{d\omega}$  and  $\frac{dT_L}{d\omega}$  must be evaluated in the light of the actual  $\Delta\omega$ , which may or may not be small enough to yield valid results using Equation (2-8).



## Torque Load Proportional to Speed

In order to investigate, experimentally, transient loading of motors, several possibilities for obtaining adjustable torque loads were considered. The most feasible method of obtaining an adjustable load with minimum transient effects within the load device appears to be a separately excited shunt generator with a small (less than 10% effect) series field and interpoles. For such a generator, the total armature inductance is:

$$L = L_{\text{armature}} + L_{\text{series fld}} + L_{\text{interpoles}} - 2M_{\text{AI}} - 2M_{\text{SI}} + 2M_{\text{SA}}$$

where:

$L$  = appropriate self inductances

$M_{\text{AI}}$  = armature to interpole mutual inductance

$M_{\text{SI}}$  = series field to interpole mutual inductance

$M_{\text{SA}}$  = series field to armature mutual inductance.

For many machines, the net inductance is very nearly zero. Under this circumstance, the equivalent loading circuit of the generator, neglecting rotating losses, is as shown in Figure 2-2.

With constant excitation, the induced voltage is proportional to angular velocity and the power absorbed by the total circuit resistance,  $R_T$ , is:

$$P = EI = \frac{E^2}{R_T} = \frac{K^2 \omega^2}{R_T} \quad (2-10)$$

where:

$E$  = induced voltage in the armature.

$K$  = constant of proportionality =  $\frac{E}{\omega}$ .

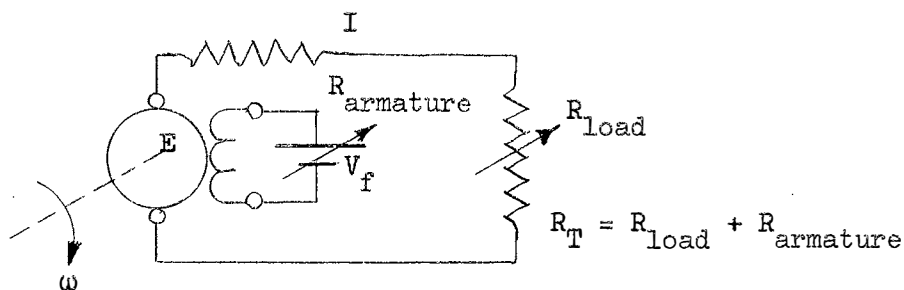


Figure 2.2. D.C. Generator Equivalent Circuit

Under the assumption of no rotating losses, the electrical power absorbed is also equal to the mechanical power input to the generator. The mechanical torque input is thus:

$$T_{\text{mech}} = \frac{EI}{\omega} = \frac{K^2\omega}{R_T} \quad (2-11)$$

It can be seen then that for constant excitation and fixed load resistance, the mechanical torque input to the generator will be directly proportional to the angular velocity of the armature of the generator. Tests made on the generator used for load in the experimental portion of

this thesis displayed the torque versus angular velocity relationship shown in Figure 2-3.

As can be seen, the torque-speed relationship is extremely linear. It does have a constant component due to the nearly constant rotating losses associated with the generator, the torque meter and the tachometer.

The net armature circuit inductance was found to be a maximum (low saturation value) of 0.008 henrys with an armature circuit resistance of 4 ohms, resulting in a time constant of 0.002 seconds. The actual measured time for the input torque to rise from zero to rated value upon closing the armature circuit was found to be less than 0.005 seconds. Thus, the self excited generator displays very desirable characteristics for obtaining this type of loading and was used experimentally in this investigation.

#### A.C. Motor as Adjustable Torque Load

In the course of the evaluation of various devices as to suitability for the experimental portion of this thesis, an analysis was made on the use of conventional alternating current motors, with direct current supplied to the stator windings, as load devices. Although this means of providing loading does not appear to be satisfactory for transient studies, due to the electrical transients within the loading device, it does offer unique properties for steady state studies. This analysis was original with this investigator and the results were experimentally

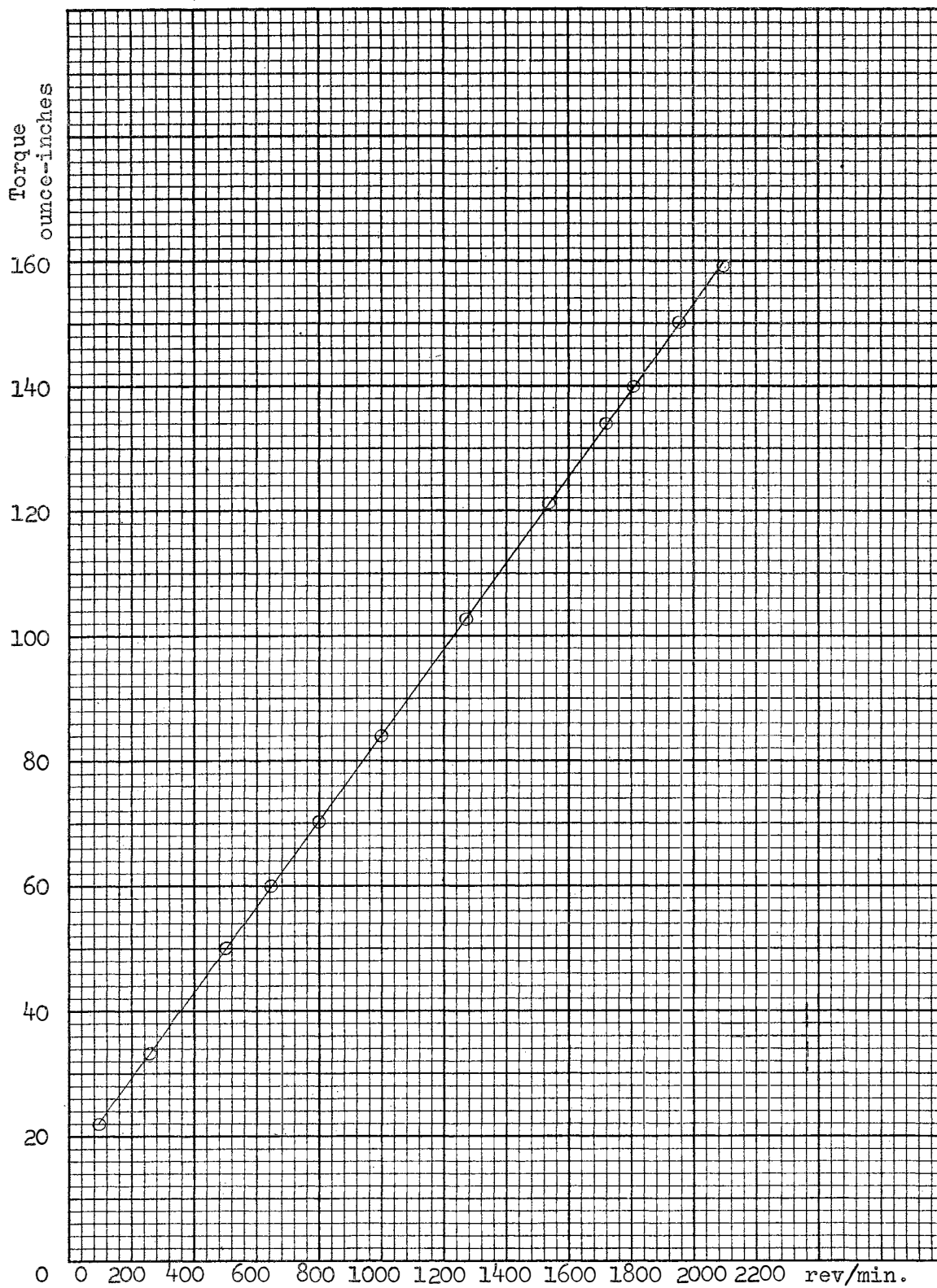


Figure 2.3. T- $\omega$  for GE Co. 5BC44AB65F ( $\frac{1}{4}$  HP), Fixed Load, Separate Excitation

substantiated by others and it is felt that its inclusion in this thesis is a positive contribution to the field of energy conversion device analysis.

This analysis is based on the use of a single-phase alternating current motor of conventional design utilizing a main and an auxiliary winding in space quadrature as shown in Figure 2.4a, but the results are equally applicable to a conventional three-phase induction motor with windings excited as shown in Figure 2.4b which in effect establishes two magnetic fields in space quadrature.

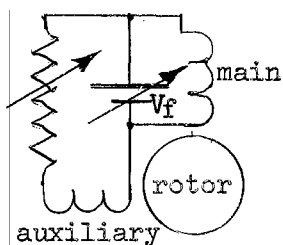


Figure 2.4A. Single Phase Motor With D.C. Excitation

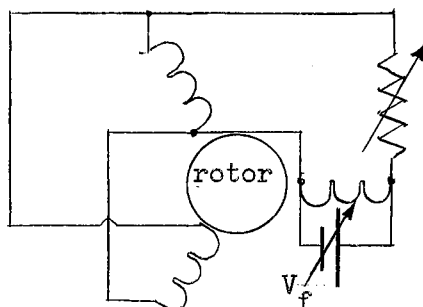


Figure 2.4B. Three Phase Motor With D.C. Excitation

For purposes of analysis, consider a single-phase motor consisting of a cylindrical rotor and stator. The stator has two distinct windings. Although the windings are distributed in space, each winding has an axis and the axis of the windings are in quadrature, i.e., separated in

space by  $\pi/2$  electrical radians. The windings are such that  $p$  poles exist and the windings will be designated  $m$ , for main and  $a$ , for auxiliary. Further, assume the following:

- (1) The effect of slot openings can be neglected, i.e., a cylindrical rotor and stator with magnetic properties independent of rotor position.
- (2) The iron used in the magnetic circuit has infinite permeability. All magnetomotive force drop is in the air gap of the machine.
- (3) There are a sufficient number of inductors on the rotor so the closed rotor winding can be considered to consist of an infinite number of fine inductors and rotor current can be considered the equivalent of a "current sheet".
- (4) The stator winding configuration is such that a stator current establishes a magnetic field with sinusoidal distribution in space.
- (5) The influence of saturation, hysteresis and eddy currents is neglected.
- (6) Air gap width,  $g$ , is small compared with the diameter and length of the rotor and stator.
- (7) Flux crosses the air gap normal to the rotor and fringing at the ends of the rotor and stator is neglected.

- (8) Harmonics in the current and flux density sinusoids are neglected.
- (9) All leakage flux is neglected.

In order to establish the relationship between torque, flux and magnetomotive force, consider excitation on one winding only with the rotor revolving  $\omega$  radians per second. If the excitation is time varying, a "transformer" and a "speed" voltage are induced in the rotor. Since the rotor winding is closed upon itself, currents flow in the rotor winding. The transformer voltage, if present, acts along the same axis as that of the winding (stator) and would appear to the stator terminals as a voltage drop in the stator. Since the stator field and the field due to the rotor transformer voltage are in space phase, no mechanical torques are involved. Under the assumptions made and with constant speed,  $\omega$ , the "speed" voltage, is sinusoidal and is in space quadrature and time phase with the magnetic field of the stator winding. With no leakage flux, and consequent leakage inductance, the resulting rotor current is in time and space phase with the rotor speed voltage. If leakage flux does exist, the voltage and current are displaced with respect to each other in time and, consequently, in space due to rotor movement.

For two poles, the developed air gap situation would be as shown in Figure 2.5, assuming  $\theta = 0$  is along the axis of the exciting winding.

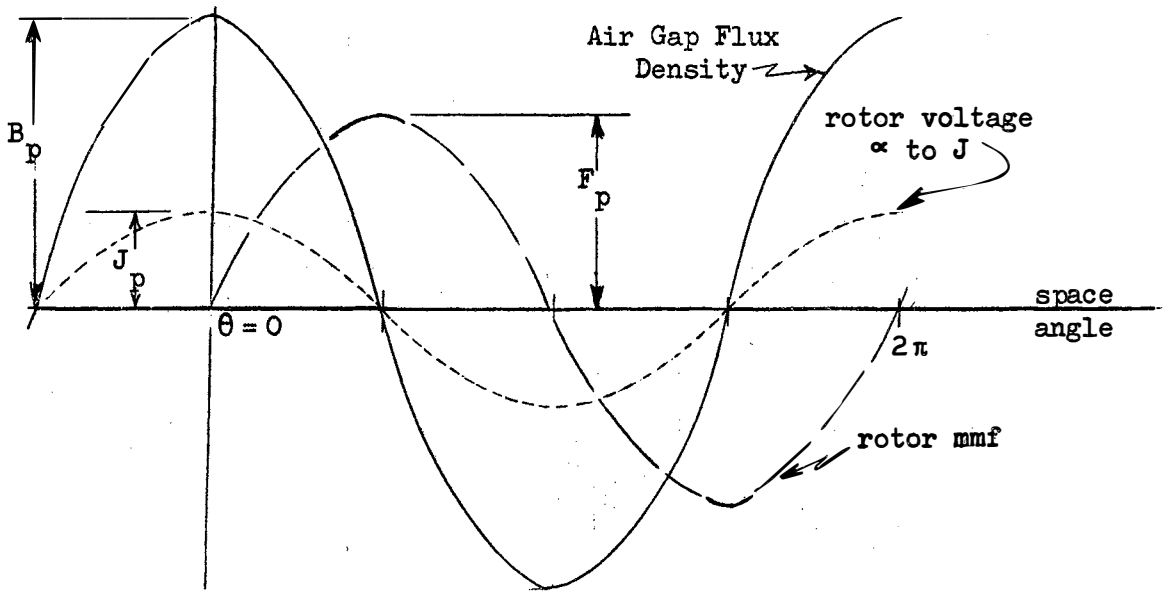


Figure 2.5. Air Gap Flux and Rotor MMF Relationship

The relationship between current density and mmf is determined from the fact that, in the mks (rationalized) system of units, the mmf acting around any closed path is equal to the current enclosed by the path, or

$$I = \oint H \cdot dl . \quad (2-12)$$

With sinusoidal current density distribution, i.e.,  $J = J_p \cos \theta$ , the mmf,  $F$ , at any point can be determined as follows: Refer to Figure 2.6. Assume integration around closed path "a". The net current enclosed is zero. Therefore,  $F$ , at points where path "a" crosses the air gap must be zero. Integrating around closed path "b" yields, for net current:



$$I_{\text{net}} = \int_0^\pi J d\theta = \int_0^\pi J_p \cos \theta d\theta = 2J_p, \quad (2-13)$$

since current density is in amperes/radian.

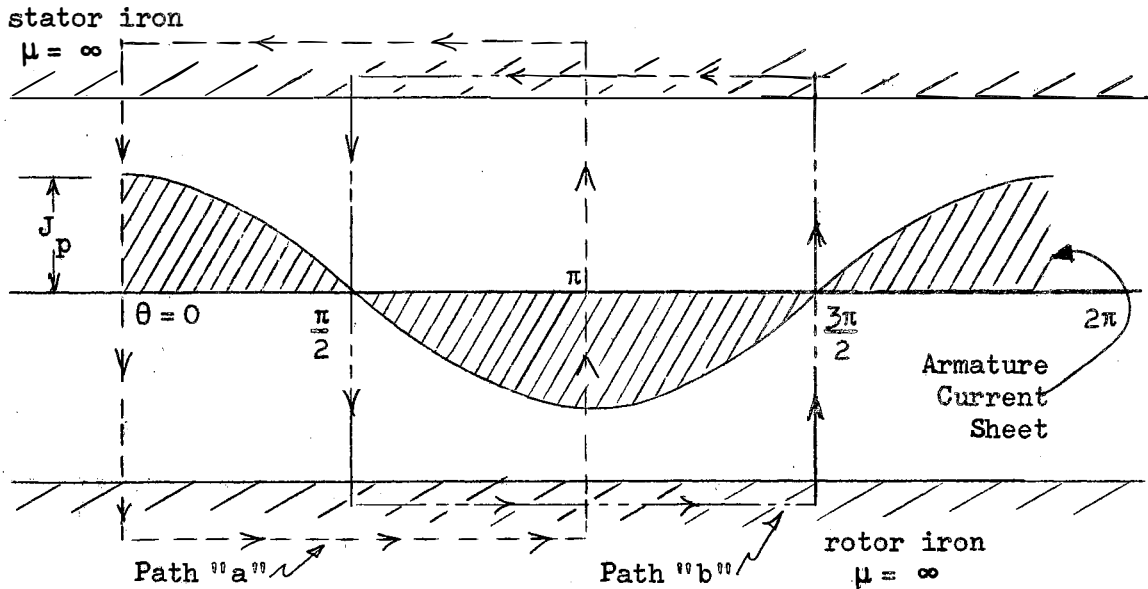


Figure 2.6 Closed Path Integration in the Air Gap

With a total mmf of  $2J_p$  and no drop in mmf in the iron, there must be a drop in mmf of  $J_p$  across the air gap at each crossing of path "b". Since path "b" corresponds to the maximum enclosed current, these points, in space, must correspond to the locations of maximum rotor mmf,  $F_p$ , which is also equal to  $J_p$ . Performing the same thought process for all other possible paths, where the air gap

crossings are  $\pi$  radians apart, leads to the conclusion that the mmf wave is sinusoidal and can be expressed as:

$$F = F_p \sin \theta = J_p \sin \theta. \quad (2-14)$$

From elementary electrical and mechanical relationships, the following results:

$$p_{\text{elec}} = ei \quad ; \quad e = \frac{d\lambda}{dt} \quad \text{and} \quad p_{\text{elec}} = i \frac{d\lambda}{dt}$$

$$p_{\text{mech}} = \frac{T\omega}{p/2} \quad ; \quad \omega = \frac{d\theta}{dt} \quad \text{and} \quad p_{\text{mech}} = \frac{2T}{p} \frac{d\theta}{dt}$$

where:

$p_{\text{elec}}$  = instantaneous electric power

$e, i$  = instantaneous voltage and current

$\lambda$  = flux linkages

$p_{\text{mech}}$  = instantaneous mechanical power

$T, \omega$  = instantaneous torque and angular velocity

$\theta$  = instantaneous space angle

$p$  = number of poles in the electrical machine.

$$\text{If } p_{\text{mech}} = p_{\text{elec}} \quad ; \quad i \frac{d\lambda}{dt} = \frac{2T}{p} \frac{d\theta}{dt}. \quad (2-15)$$

Equation (2-15) can be solved for torque, yielding

$$T = \frac{p}{2} i \frac{d\lambda}{d\theta}. \quad (2-16)$$

Now consider an elemental 1 turn coil located on the rotor. One side of the coil is of width  $d\alpha$  at angle  $\theta$ , the other side of the coil being  $d\alpha_{\theta + \pi}$ , located at  $\theta + \pi$  radians, (for a full pitch coil).

The flux linkages,  $\lambda$ , with this coil are

$$\lambda = \int_{\theta}^{\theta} + \pi B l (r d\theta) \quad (2-17)$$

where  $r$  and  $l$  are the radius and length of the stator and rotor iron and  $B$  is space distributed flux density.

$$\text{From Figure 2.5, } B = B_p \cos \theta. \quad (2-18)$$

$$\text{Then, } \lambda = \int_{\theta}^{\theta} + \pi B_p l r \cos \theta \, d\theta = 2B_p l r \sin \theta \quad (2-19)$$

and

$$\frac{d\lambda}{d\theta} = 2B_p l r \cos \theta. \quad (2-20)$$

$$\text{Since } i = J d\theta = J_p \cos \theta \, d\theta \quad (2-21)$$

the torque,  $dT$  on this elemental one turn coil is

$$dT = \frac{id\lambda}{d\theta} = (J_p \cos \theta \, d\theta)(2B_p l r \cos \theta). \quad (2-22)$$

The total torque on the current sheet is

$$T = \frac{p}{2} \int_0^{\pi} dT.$$

When Equation (2-22) is used for  $dT$ ,

$$T = \frac{p}{2} \int_0^{\pi} 2J_p B_p l r \cos^2 \theta \, d\theta = \pi B_p J_p l r \left(\frac{p}{2}\right) \quad (2-23)$$

and since  $J_p = F_p$

$$T = B_p F_p l r \pi \left(\frac{p}{2}\right). \quad (2-24)$$

If angle  $(\pi/2 - \delta)$  had existed between the current

sheet and the flux density, due to leakage reactance, the derivation would have proceeded in the same fashion except

$$J = J_p \cos\left[\theta + \left(\frac{\pi}{2} - \delta\right)\right] = J_p \sin(\theta - \delta)$$

and

$$F = F_p \cos(\theta - \delta) \quad (2-25)$$

$$di = Jd\theta = J_p \sin(\theta - \delta)$$

and Equation (2-24) becomes

$$T = B_p F_p l r \pi \left(\frac{p}{2}\right) \sin \delta . \quad (2-26)$$

Noting that flux,  $\phi$ , and flux density are related by

$$\phi = \int_0^\pi \frac{B l r}{p/2} d\theta = \frac{2}{p} l r \int_0^\pi B_p \cos\theta d\theta \quad (2-27)$$

results in:

$$\phi = \frac{4 l r B_p}{p} . \quad (2-28)$$

Substituting Equation (2-28) into Equation (2-26) yields:

$$T = \frac{\pi}{8} p^2 \phi F_p \sin \delta . \quad (2-29)$$

In Equation (2-29),  $F_p$  is a function of  $\phi$  and rotor velocity  $\omega$ . If the excitation is time varying, both  $\phi$  and  $F_p$  will be functions of time and  $T$ , as determined from Equation (2-29), will be instantaneous torque. Average torque can then be obtained from:

$$T_{\text{ave}} = \frac{1}{2\pi} \int_0^{2\pi} T \, dt \quad (2-30)$$

where  $T$  is the value of torque from Equation (2-29).

In order to easily visualize the effect of direct current on the rotor, consider first the phenomena with only the main winding excited. Refer to Figure 2.7. The inner ring indicates the direction of current flow from the induced speed voltage resulting from conductor elements cutting the net air gap flux along the main field axis; + represents current flow onto the page and  $\cdot$  is current flow out of the page.

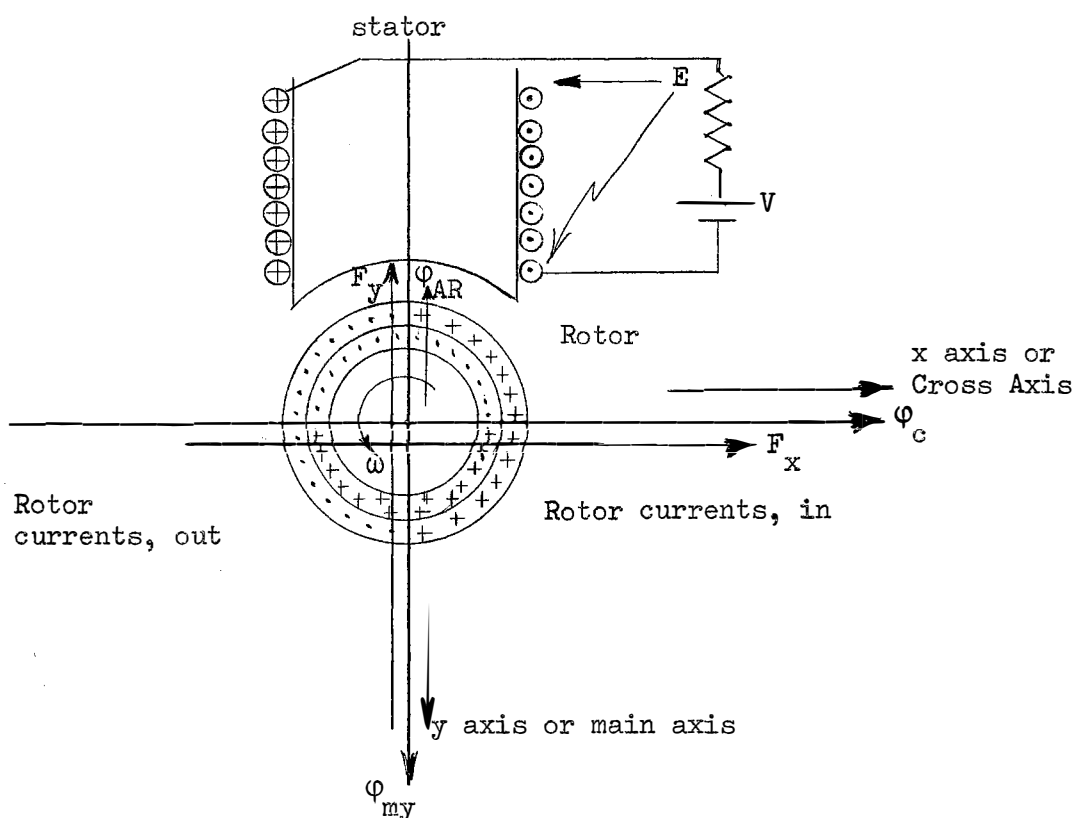


Figure 2.7. Flux-Current Relations-Main Winding Excitation

In Figure 2.7:

$\varphi_{my}$  is the flux due to winding m in the y axis.

$\varphi_c$  is flux established in the cross axis due to the current in the inner ring and is proportional to net y axis flux ( $\varphi_{my} - \varphi_{AR}$ )

$\varphi_{AR}$  is flux arising as a result of current flow from speed voltage due to  $\varphi_c$ .

The outer ring indicates the direction of current flow due to the speed voltage arising from  $\varphi_c$ . The resulting current establishes flux  $\varphi_{AR}$ .

From the speed voltage form of Faraday's Law:

$$\varphi_c = K_1 \omega (\varphi_{my} - \varphi_{AR}) \quad (2-31)$$

$$\varphi_{AR} = K_2 \omega \varphi_c \quad (2-32)$$

and

$$\varphi_{my} = K_3 E \quad (2-33)$$

where  $K_1$ ,  $K_2$ , and  $K_3$  are constants of proportionality.

Therefore:

$$\varphi_c = K_1 \omega (K_3 E - K_2 \omega \varphi_c)$$

$$\text{or } \varphi_c = \frac{K_1 K_3 \omega E}{1 - K_1 K_2 \omega^2} \quad (2-34)$$

$$\text{and } \varphi_{AR} = \frac{K_1 K_2 K_3 \omega^2 E}{1 - K_1 K_2 \omega^2} \quad (2-35)$$

The mmf's  $F_x$  and  $F_y$  are the result of the currents shown in the inner and outer ring - bearing in mind that the inner and outer ring are fictitious separations for the purpose of easy visualization, whereas in the actual rotor, these currents exist simultaneously in the single set of rotor inductors.

From Equation (2-29), torque is developed between  $F_y$  and  $\varphi_c$  and also between  $F_x$  and  $(\varphi_{my} - \varphi_{AR})$ .

The analysis will now be extended to cover the case where both windings  $m$  and  $a$  are excited by direct current as shown in Figure 2.8. Since flux density and mmf can be related via the permeability, flux density will be used rather than flux.

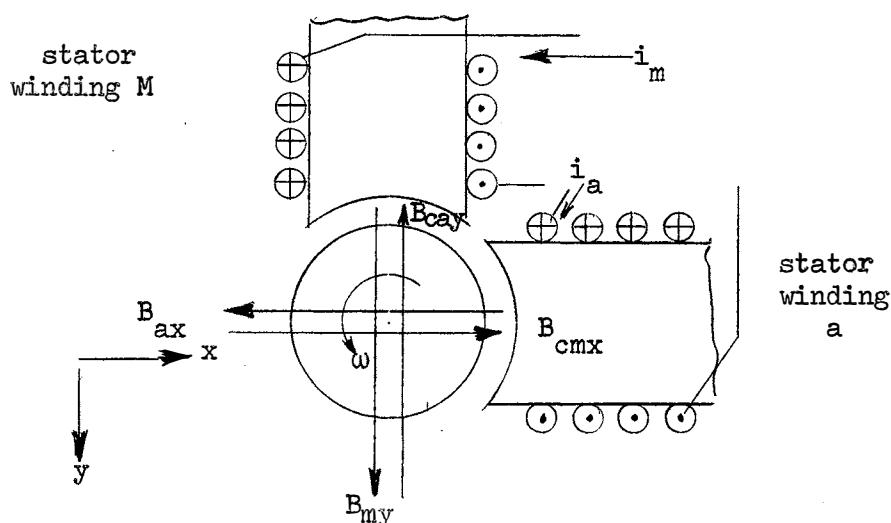


Figure 2.8. Flux Current Relationship - Two Winding Excitation

In Figure 2.8:

$B_{my}$  = magnetic field established by  $i_m$  (in y axis)

$B_{cmx}$  = cross field due to speed voltage from net main axis flux (in x axis)

$B_{ax}$  = magnetic field established by  $i_a$  (in x axis)

$B_{cay}$  = a main axis field due to speed voltage from net cross axis flux (in y axis).

$$\text{Now } H_y = \frac{i_m N_{me}}{2g} \quad \text{and} \quad H_x = \frac{i_a N_{ae}}{2g} \quad (2-36)$$

where  $N_{me}$  and  $N_{ae}$  are the effective number of turns on m and a,  $H_y$  and  $H_x$  are stator winding magnetomotive forces, and  $g$  is air gap length.

Then:

$$B_{my} = H_y \mu_o = \frac{i_m N_{me} \mu_o}{2g} ; B_{ax} = H_x \mu_o = \frac{i_a N_{ae} \mu_o}{2g} \quad (2-37)$$

where

$\mu_o$  is air gap permeability =  $4\pi \cdot 10^{-7}$  (free space).

Also,  $B_y$  and  $B_x$  can be defined as:

$$B_y = B_{my} - B_{cay} \quad B_x = B_{cmx} - B_{ax} \quad (2-38)$$

where:

$B_y$  and  $B_x$  are net flux densities in the y and x axis.



As demonstrated in the preceding section, the combination of  $B_y$  and  $\omega$  induce a rotor voltage with accompanying rotor current,  $i_x$ . An mmf,  $F_x$  arises from  $i_x$  and  $F_x$  establishes  $B_{cmx}$ . Similarly  $i_y$  results from  $B_x$  and  $\omega$ , establishing  $F_y$  and  $B_{cay}$ . In order to determine these quantities, consider a small element on the rotor winding of width  $r d\theta$ , thickness  $h$ ,  $l$  units in length and with a resistivity of  $\rho$ . A voltage,  $e_x$  (or  $e_y$ ) is induced and current flows in the element.

$$e_x = B_y l r \omega \quad (2-39)$$

$$i_x = \frac{e_x}{\rho l} h r d\theta \quad (2-40)$$

From Equation (2-14):

$$J_p = F_p \quad \text{and} \quad i_x = J_x d\theta \quad .$$

Therefore:

$$J_x = F_x = \frac{i_x}{d\theta} = \frac{e_x h r}{\rho l} \quad (2-41)$$

Using the value of  $e_x$  from Equation (2-39)

$$F_x = \frac{B_y r^2 \omega h}{\rho} \quad ; \quad \text{and} \quad F_y = \frac{B_x r^2 \omega h}{\rho} \quad (2-42)$$

If  $B_y$  and  $B_x$  are defined as maximum values, then  $F_x$  and  $F_y$  in Equation (2-42) are the peak values of sinusoidally distributed mmf's. Now that  $F_x$  and  $F_y$  are determined,  $B_{cmx}$  and  $B_{cay}$  can be evaluated, thus

$$B_{cmx} = \frac{F_x \mu_o}{2g} = \frac{B_y r^2 \omega h \mu_o}{2\rho g}$$

and

$$B_{cay} = \frac{F_y \mu_o}{2g} = \frac{B_x r^2 \omega h \mu_o}{2\rho g} \quad (2-43)$$

Since

$$B_y = B_{my} - B_{cay} \quad ; \quad B_x = B_{cmx} - B_{ax} \quad (2-44)$$

From Equation (2-43):

$$B_y = \frac{K B_{cmx}}{\omega} \quad ; \quad B_x = \frac{K B_{cay}}{\omega} \quad (2-45)$$

where:

$$K = \frac{2g\rho}{r^2 h \mu_o}$$

Substituting Equation (2-45) into Equation (2-44):

$$\frac{K}{\omega} B_{cmx} = B_{my} - B_{cay} \quad ; \quad \frac{K}{\omega} B_{cay} = B_{cmx} - B_{ax} \quad (2-46)$$

The two equations in Equation (2-46) can be solved for

$B_{cmx}$  and  $B_{cay}$ , yielding:

$$B_{cmx} = \frac{\frac{K}{\omega} B_{my} + B_{ax}}{\left(1 + \frac{K^2}{\omega^2}\right)} \quad (2-47)$$

$$B_{cay} = \frac{B_{my} - \frac{K}{\omega} B_{ax}}{\left(1 + \frac{K^2}{\omega^2}\right)} \quad (2-48)$$

The values of  $B_{cmx}$  and  $B_{cay}$  from Equation (2-47) and Equation (2-48) can be substituted in Equation (2-45) to obtain:

$$B_y = \frac{K}{\omega} \frac{\left( \frac{K}{\omega} B_{my} + B_{ax} \right)}{1 + \frac{K^2}{\omega^2}} \quad (2-49)$$

$$B_x = \frac{K}{\omega} \frac{\left( B_{my} - \frac{K}{\omega} B_{ax} \right)}{1 + \frac{K^2}{\omega^2}} \quad (2-50)$$

There are two mmf's,  $F_y$  and  $F_x$  acting with the two fields  $B_x$  and  $B_y$  to produce torque on the rotor in accordance with Equation (2-26). Refer to Figure 2.9.



Figure 2.9. Torque Directions (Two Winding Excitation)

From Equation (2-26), since the quantities are in quadrature,

$$T = \pi l r \frac{p}{2} [B_y F_x + B_x F_y] \quad (2-51)$$

The value of  $F_x$  and  $F_y$  are given by Equation (2-42) and  $B_x$  and  $B_y$  by Equation (2-49) and Equation (2-50). Using these values in Equation (2-51), gives:

$$\begin{aligned} T &= \pi l r \frac{\rho}{2} \left[ \frac{B_y^2 r^2 \omega h}{\rho} + \frac{B_x^2 r^2 \omega h}{\rho} \right] \\ &= \pi \frac{l r^3 \omega h}{2 \rho} \rho [B_y^2 + B_x^2] . \end{aligned} \quad (2-52)$$

From Equation (2-49) and Equation (2-50):

$$B_x^2 + B_y^2 = \frac{K^2}{K^2 + \omega^2} [B_{my}^2 + B_{mx}^2] . \quad (2-53)$$

Since, from Equation (2-37),

$$B_{my} = \frac{i_m N_{me} \mu_o}{2g} \quad \text{and} \quad B_{mx} = \frac{i_a N_{ae} \mu_o}{2g} ,$$

Equation (2-53) can be written:

$$B_x^2 + B_y^2 = \frac{K^2 \mu_o^2}{4g^2 (K^2 + \omega^2)} [N_{me}^2 i_m^2 + N_{ae}^2 i_a^2]$$

where

$$K = \frac{2g}{r^2 h \mu_o} .$$

Then

$$T = \frac{\pi l \rho \omega}{2 r h \left( \omega^2 + \frac{4g^2 \rho^2}{r^4 h^2 \mu_o^2} \right)} [N_{me}^2 i_m^2 + N_{ae}^2 i_a^2] . \quad (2-54)$$

An analytical derivation, proceeding along the same general lines, but for rectangular rather than sinusoidal flux distribution, corresponding to concentrated, rather than distributed coils, results in an expression for torque which is exactly the same as Equation (2-54) if the total flux per pole is the same for the concentrated and for the distributed windings. This is in harmony with direct current dynamo performance which is based on total flux per pole and is not dependent upon the flux density distribution under the pole.

Examination of Equation (2-54) indicates it has the form of the curve shown in Figure 2.10, for fixed  $i_a$  and  $i_m$ .

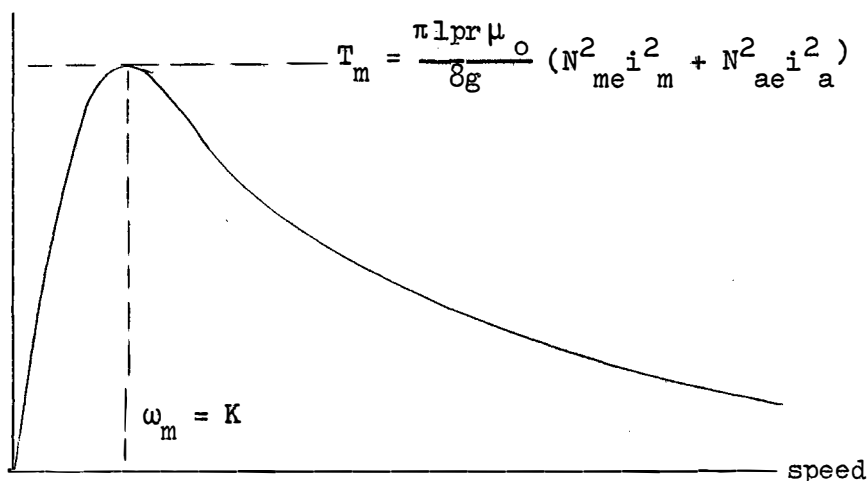


Figure 2.10. Torque-Speed Curve for Equation (2-54)

The speed at which the maximum torque occurs,  $\omega_m$ , was obtained by setting  $\frac{dT}{d\omega} = 0$ , solving for  $\omega_m$ . When  $\omega_m$  is substituted in the expression for torque, Equation (2-54), maximum torque,  $T_m$  results. In general, this is on the order of 25-50 rev/min for a normal design induction motor.

In an effort to verify this behavior, tests were run by this investigator on a 1 h.p., 1800 rpm, 220 volt, three-phase induction motor at the University of Wichita Electrical Engineering Laboratory in March, 1961. Since the complete design data on the motor was not known, the form of the equation was changed to:

$$T = \frac{K' \omega}{\omega^2 + K^2} [a^2 i_m^2 + i_a^2] \quad (2-55)$$

where

$$a = \frac{N_{me}}{N_{ae}} \quad ; \quad K' = \frac{N_{ae}^2 \pi l p \rho}{2rh} \quad ; \quad K = \frac{2g\rho}{r^2 h \mu_0} \quad (2-56)$$

The value of  $a$  is, of course, easily determined and values of  $K$  and  $K'$  were calculated, based on two separate conditions of  $i_m$ ,  $i_a$ , and  $T$ . Complete data was then taken over a range of values of the variables and the correlation between calculated and observed data was extremely good - much closer than anticipated, based on the large number of assumptions inherent in the derivation. Certainly, the data was within commonly accepted engineering limits,

i.e., within 2 or 3 per cent of calculated values. Since this device is not the main topic of this thesis, the actual experimental results are omitted.

The above work was concluded in March, 1961 and in April, 1961, an article appeared in a technical magazine detailing experimental work and a graphical analysis on this same topic conducted at the Allis Chalmers Company, Milwaukee, Wisconsin. (17). The analysis in this reference was based upon the fact that the speed-torque characteristic obtained experimentally (see Figure 2.10) is of the same shape (but inverted with respect to speed) as the speed-torque characteristic of the motor operating in its normal mode with alternating current excitation. Their experimental work was conducted on a 157 h.p., 1200 rpm, 2300 volt induction motor. This investigator selected two points from their data, calculated  $K$  and  $K'$  in Equation (2-55) and then used Equation (2-55) to calculate additional operating conditions. The correspondence between calculated and experimental values was again excellent. Also, as is pointed out by Moore (17), the calculated values from the graphical method using the regular induction motor speed-torque curve is excellent, but their method has the inherent disadvantage in that it is applicable only for the condition where  $i_a = i_m$  and the windings are symmetrical, i.e., identical. The development by this investigator overcomes these limitations and also lends itself to calculating procedures rather than graphical methods.

An analysis, limited in scope, was made to evaluate the performance of this device as a suitable load, i.e., constant torque, for transient studies of the type made in this thesis. Due to the two stator fields being coupled through the rotor circuit, self and mutual inductances have a very marked effect upon its transient behavior and it was felt that transient phenomena within this device, when used as a load, would possibly mask transient behavior to be observed within the motor under study. For this reason, it was not used in the investigation. However, this does not detract from its usefulness in applications involving, for example, dynamic braking analysis as exemplified by the use of direct current on the windings of three-phase motors.

It also will find use in situations involving an easily adjusted variable torque load for investigations where the transient characteristic is not objectionable. The analysis and suggestion for this usage is original with this investigator.



## CHAPTER III

### D.C. MOTOR ANALYSIS

For a d.c. motor, or generator, the induced voltage or counter electromotive force (cemf) is given by Fitzgerald (9).

$$E = \frac{Z\phi p\omega}{2\pi a} = K\phi\omega \quad (3-1)$$

where:

$Z$  = number of active armature inductors

$\phi$  = flux per pole, webers

$p$  = number of poles

$a$  = number of paths in parallel through the armature

$\omega$  = angular velocity, radians/second

$$K = \frac{Zp}{2\pi a} .$$

The electromechanical power,  $P_m$ , which is power converted from electrical to mechanical form (or vice versa) and differs from shaft power by the amount of so called "rotating losses" (friction, windage, etc., and also some core losses) is given by:

$$P_m = EI_a = \omega T_m$$

where:

$I_a$  = armature current

$T_m$  = electromagnetic torque corresponding to  
electromagnetic power

or

$$T_m = \frac{EI_a}{\omega} = \frac{Z\phi p \omega}{2\pi a} \frac{I_a}{\omega} = K\phi I_a \quad (3-2)$$

where:

$K$  has the same value as in Equation (3-1).

The equations of motion describing the internal situation within the motor as well as external load are:

$$V = E + I_a R_a + V_B + L_A \frac{dI_a}{dt} + \sum_{n=0}^N M_{na} \frac{dI_n}{dt} \quad (3-3)$$

$$E = K\phi\omega \quad (3-4)$$

$$\phi = f\left(\sum_{i=0}^n N_i I_i\right) \quad (3-5)$$

$$V_f = I_f R_f + L_f \frac{dI_f}{dt} + \sum_{n=0}^N M_{nf} \frac{dI_n}{dt} \quad (3-6)$$

$$K\phi I_a = T_L(\omega) \pm J \frac{d\omega}{dt} \quad (3-7)$$

where:

$R_a$  = armature circuit resistance

$V_B$  = voltage drop across the brush system

$L_A$  = armature circuit inductance (self)

$M_{na}$  = mutual inductance due to coupling between the armature circuit and any arbitrary circuit  $n$  with current  $I_n$

$\sum N_i I_i$  = effect of the total magnetizing force (mmf) on the saturation (or B-H) curve of all currents with an effective mmf.

$V_f$  = shunt field voltage

$I_f$  = shunt field current

$R_f$  = shunt field circuit resistance

$L_f$  = shunt field circuit self inductance

$T_L(\omega)$  = load torque, a function of speed

$J \frac{d\omega}{dt}$  = inertia torque resulting from angular acceleration of an inertia  $J$ , which relates the electrical and mechanical parameters of the system under study.

Although these equations are for a machine with desired excitation in one axis only, they do express the feature of any excitation, insofar as its effect in the one axis is concerned, by virtue of Equation (3-5), because the generalized manner of expressing Equation (3-5) provides for the nonlinearity between the flux and any contributing current.

Now, many of the defined quantities above are functions of other variables. Specifically:

$$V_b = f_1(\omega, I_a)$$

$$L_A = f_2(I_f, I_a)$$

$$M_{na} = f_3(I_n, I_a)$$

$$\begin{aligned}\phi &= f_4(I_n, I_a) \\ L_f &= f_5(I_n, I_a) \quad .\end{aligned}$$

The exact manner in which each of the parameters vary with respect to the appropriate variables cannot be predicted with any degree of accuracy due to flux fringing and leakage. If empirical relationships, based on experimental results, are established, mathematical relationships so formidable as to be all but impossible to solve result.

For this reason, analytical analysis of performance is made based upon neglect of some factors and linearizing of relationships of the remaining factors. The assumptions necessary for a linear analysis are:

- (1) The B-H curve of the magnetic circuit is linear.
- (2) No mmf is required for the iron, i.e., it has infinite permeability whereas the air gap has finite permeability and the drop in magnetic potential across the air gap is equal to the net mmf.
- (3) No coupling exists between the field circuit and the armature circuit except via the shunt and series fields.
- (4) There is negligible brush shift effect, i.e., the brushes are centered on the magnetic neutral.
- (5) Linear commutation, i.e., the current in the commutated coil changes linearly with respect to

time and the commutator brush area of contact is also changing linearly with respect to time.

- (6) All inductors are active and making a positive contribution to the induced cempf.
- (7) Negligible voltage drop across the brush system or inclusion of this phenomena in the total armature circuit resistance which is considered constant.
- (8) There are no closed circuits within the magnetic structure which allow circulating currents to manifest themselves, i.e., there are no closed circuits formed by fasteners and the iron structure is built up of infinitely thin laminations, etc.

Applying the above assumptions, the equations of motion, Equations (3-3), (3-4), (3-5), and (3-6) become:

$$V = E + I_a R_a + L_A \frac{dI_a}{dt} + M_{fa} \frac{dI_f}{dt} \quad (3-8)$$

$$E = K\phi\omega \quad (3-9)$$

$$\phi = K' I_f + K'' I_a \quad (3-10)$$

$$V_f = I_f R_f + L_f \frac{dI_f}{dt} + M_{af} \frac{dI_a}{dt} \quad (3-11)$$

In addition, the analysis may be made for negligible field circuit self inductance, which is tacitly assumed

when the field is considered constant, at full strength from the instant of switching.

Several authors have published works dealing with transient response of d.c. motors based on the eight previously stated assumptions and, in some cases, additional simplifying assumptions. In all instances known by this writer, the resisting torque is either inertia only or restricted to a particular type only, such as varying with the square of the angular velocity - leaving out the inertia, the damping torque and the constant component of torque completely. (1, 3, 4, 5, 7, 10). Even in a linear analysis, inclusion of the effects of flux build up in the shunt field leads to expressions which have not been solved (so far as is known by this writer). The expressions are nonlinear and involve transcendental expressions as coefficients. Doubtless, with persistence they can be evaluated, but it is doubtful if their solution contributes information of sufficient validity to warrant the difficulty of solution, since the premises upon which the solutions are based do not appear valid.

One of the most promising new attacks on linear analysis is presented by Koenig (2) which is based upon experimentally measured couplings. However, the experimentally obtained values are clearly shown to be non-constant in nature and his analysis is described as valid only for small disturbances about a given equilibrium point, similar in scope to well-known small signal analysis techniques

used in electronic tube circuit analysis. This is also the approach presented by Adkins (7).

The analysis for several different situations are presented in the following pages. There are, of course, a large number of variations which can be investigated. A limited number are presented, the criteria being either to present situations contributing to an understanding of the over-all problem or an analysis which is mathematically feasible and is believed original with this study - the originality being, for the most part, concerned with the type of torque load considered. In the cases examined, the designation of no inductance reduces the study to that for the steady state case.

#### No Series Field, No $L_f$ , No $L_A$ , No J

This is in effect a shunt motor (idealized) connected to a constant torque load and corresponds to an actual shunt motor subjected to disturbances occurring so slowly as to not disturb the operating equilibrium.

Then:

$$V = K\phi\omega + I_a R_a \quad (3-12)$$

$$I_a = \frac{T_L}{K\phi} \quad (3-13)$$

Substituting Equation (3-13) into Equation (3-12) and rearranging,

$$T_L = \frac{-K^2 \phi^2}{R_A} \omega + K \phi V . \quad (3-14)$$

If

$$\phi = K' I_f \quad \text{and} \quad I_f = \frac{V}{R_f}$$

then

$$\phi = \frac{K' V}{R_f}$$

and Equation (3-14) becomes

$$T_L = \frac{-K^2 K'^2 V^2}{R_f^2 R_A} \omega + \frac{K K' V^2}{R_f} \quad (3-15)$$

which will plot as a straight line on a  $T_L$  versus  $\omega$  rectangular plane and is the so called linear, steady state characteristic of a shunt motor.

No Shunt Field, No  $L_A$ , No J

This is in effect a series motor operating under the constraints detailed above. Following the same procedure as above, the series motor equivalent to Equation (3-15) can be shown to be:

$$T = \frac{V^2}{\omega^2 K K' + 2 R_a \omega + \frac{R_a^2}{K K'}} \quad (3-16)$$

which will plot as a hyperbola.



Compound Motor, No  $L_A$ , No  $L_f$ , No  $J$ , No  $M_{af}$

The steady state linear speed-torque characteristic can be shown to be, again using Equations (3-8), (3-9), (3-10), and (3-11):

$$V = \frac{KK'V}{R_f} + (KK'\omega + R_a) \left( \frac{-K'V}{2K''R_f} \right) \pm \sqrt{\left( \frac{K'V}{2K''R_f} \right)^2 - \frac{T}{KK''}} \quad (3-17)$$

A graphic representation of Equation (3-17) is difficult to visualize as far as exact form is concerned, but it will have the same general shape as a hyperbola except it will not be asymptotic to the speed axis. In other words, at zero torque loads a finite steady state speed exists, much lower than the situation for the phenomena described in Equation (3-16). For this reason, a shunt winding, referred to as a stabilizing winding, is often added to a series motor.

Shunt Motor, Including  $J$  and  $L_A$

Since the experimental portion of this thesis deals at some length with this configuration, a detailed derivation follows. Consider a shunt motor with constant excitation, inertia  $J$ , and a torque load consisting of a constant component as well as a component varying directly with speed. Applying the equations of motion:

$$T_m = J \frac{d\omega}{dt} + C_1 + C_2\omega$$

$$E = K\phi\omega = \bar{K}\omega$$

$$T_m = K\phi I_a = \bar{K} I_a$$

$$V = E + R_A I_a + L_A \frac{d I_a}{dt}$$

now

$$I_a = \frac{T_m}{\bar{K}} = \frac{J}{\bar{K}} \frac{d\omega}{dt} + \frac{C_1}{\bar{K}} + \frac{C_2 \omega}{\bar{K}}$$

$$\frac{d I_a}{dt} = \frac{J}{\bar{K}} \frac{d^2 \omega}{dt^2} + \frac{C_2}{\bar{K}} \frac{d\omega}{dt}$$

$$V = \bar{K}\omega + \frac{R_A J}{\bar{K}} \frac{d\omega}{dt} + \frac{R_A C_1}{\bar{K}} + \frac{R_A C_2 \omega}{\bar{K}} + \frac{L_A J}{\bar{K}} \frac{d^2 \omega}{dt^2} + \frac{L_A C_2}{\bar{K}} \frac{d\omega}{dt}$$

or, collecting terms,

$$(\bar{K}V - R_A C_1) = L_A J \frac{d^2 \omega}{dt^2} + (L_A C_2 + R_A J) \frac{d\omega}{dt} + (\bar{K}^2 + R_A C_2)\omega$$

(3-18)

The steady state portion of the expression for  $\omega$  can be found from the equations of motion, setting  $\frac{d\omega}{dt} = 0$  and  $\frac{d I_a}{dt} = 0$ .

Thus:

$$T_m = C_1 + C_2 \omega_\infty = \bar{K} I_a$$

$$E = \bar{K} \omega_\infty$$

$$V = \bar{K} \omega_\infty + I_a R_A$$

$$\frac{V - K\omega_{\infty}}{R_A} = \frac{C_1 + C_2\omega_{\infty}}{K}$$

$$\frac{KV - R_A C_1}{K^2 + R_A C_2} = \omega_{\infty}$$

where

$$\omega_{\infty} = \omega \text{ at } t = \infty . \quad (3-19)$$

The transient portion of the expression for  $\omega$  can be found from the roots of the auxiliary equation:

$$L_A J m^2 + (L_A C_2 + R_A J)m + (K^2 + R_A C_2) = 0$$

$$m_{1,2} = \frac{-(L_A C_2 + R_A J) \pm \sqrt{(L_A C_2 + R_A J)^2 - 4JL_A(K^2 + R_A C_2)}}{2JL_A} \quad (3-20)$$

The complete solution of the differential equation (3-18) is then:

$$\omega = \omega_{\infty} + A_1 \varepsilon^{m_1 t} + A_2 \varepsilon^{m_2 t} \quad (3-21)$$

where  $\omega_{\infty}$  is given by Equation (3-19),  $m_1$  and  $m_2$  are given by Equation (3-20), and  $A_1$ ,  $A_2$  are constants to be determined from the initial conditions. For initial conditions, assume that at  $t = 0$ ,  $\omega = \omega_0$  and  $\frac{d\omega}{dt} = 0$ .

Then,  $\omega_0 = \omega_{\infty} + A_1 + A_2$

$$\text{and } 0 = m_1 A_1 + m_2 A_2$$

from which,

$$A_2 = \frac{m_1[\omega_0 - \omega_\infty]}{m_1 - m_2} \quad \text{and} \quad A_1 = \frac{-m_2[\omega_0 - \omega_\infty]}{m_1 - m_2} \quad (3-22)$$

and the final solution is:

$$\omega = \omega_\infty + \frac{[\omega_0 - \omega_\infty]}{m_1 - m_2} \left[ -m_2 \epsilon^{m_1 t} + m_1 \epsilon^{m_2 t} \right] \quad (3-23)$$

where

$$m_1, m_2 = \frac{-(L_A C_2 + R_A J) \pm \sqrt{(L_A C_2 + R_A J)^2 - 4JL_A(\bar{K}^2 + R_A C_2)}}{2JL_A}$$

and

$$\omega_\infty = \frac{\bar{K}V - R_A C_1}{\bar{K}^2 + R_A C_2}.$$

The solution, given by Equation (3-23) can be either exponential or oscillatory, depending upon the sign of the term under the radical for the expression for  $m_1, m_2$ .

If:

$$4JL_A(\bar{K}^2 + R_A C_2) > (L_A C_2 + R_A J)^2 \quad (3-24)$$

the speed will oscillate with time about its steady state value,  $\omega_\infty$ . Specifically, as  $R_A$  approaches zero, the criteria for oscillation becomes:

$$2\bar{K} \sqrt{\frac{J}{L_A}} > C_2 \quad (3-25)$$

which harmonizes with the physical reality of the situation because  $C_2$  corresponds to the magnitude of a viscous damping term and increasing  $C_2$  above the fixed value of

$$2\bar{K} \sqrt{\frac{J}{L_A}}$$

should eliminate oscillations.

Another insight into the transient behavior can be gained by setting  $J = 0$  in Equation (3-18). The differential equation becomes:

$$\bar{K}V - R_A C_1 = L_A C_2 \frac{d\omega}{dt} + (\bar{K}^2 + R_A C_2)\omega . \quad (3-26)$$

This differential equation has, for a solution (considering  $\omega = \omega_0$  at  $t = 0$ )

$$\omega = \omega_\infty + (\omega_0 - \omega_\infty) e^{-\frac{(\bar{K}^2 + R_A C_2)t}{L_A C_2}} \quad (3-27)$$

where

$$\omega_\infty = \frac{\bar{K}V - R_A C_1}{\bar{K}^2 + R_A C_2} .$$

From Equation (3-27), the term

$$\frac{L_A C_2}{\bar{K}^2 + R_A C_2} \quad (3-28)$$

appears as what is commonly referred to as a "time constant" which is by definition the time required for approximately 63.2% of the total change to be made in speed to occur. Since the system considered has no mechanical inertia, by virtue of the assumption that  $J = 0$ , Equation (3-28) can be considered an "electrical" time constant.

Similarly, reducing the electrical inertia,  $L_A$ , to zero in Equation (3-18) results in

$$KV - R_A C_1 = R_A J \frac{d\omega}{dt} + (K^2 + R_A C_2)\omega \quad (3-29)$$

which has as a solution, considering  $\omega = \omega_0$  at  $t = 0$ :

$$\omega = \omega_\infty + (\omega_0 - \omega_\infty) e^{-\left(\frac{K^2 + R_A C_2}{R_A J}\right)t} \quad (3-30)$$

and following the same reasoning as immediately above, the "mechanical" time constant is:

$$\frac{R_A J}{K^2 + R_A C_2} \quad (3-31)$$

Both the electrical and mechanical time constants given in Equation (3-28) and Equation (3-31) indicate both electrical and mechanical terms in their make-up, thus decreased time constants, corresponding to rapidly decaying transients can be accomplished by parameter changes in the electrical circuit as well as reduction of moment of

inertia in the mechanical system, for a given value of  $C_2$ .

In Equation (3-28), dividing numerator and denominator by  $C_2$  indicates that any of the following will reduce the electrical time constant (in the limiting case considered, i.e.,  $J = 0$ ):

- (a) decreasing  $L_A$
- (b) increasing  $R_A$
- (c) increasing  $\bar{K}$
- (d) decreasing  $C_2$ .

In Equation (3-31), dividing numerator and denominator by  $R_A$  indicates that any of the following will reduce the mechanical time constant (in the limiting case considered, i.e.,  $L_A = 0$ ):

- (a) decreasing  $J$
- (b) decreasing  $R_A$
- (c) increasing  $\bar{K}$
- (d) increasing  $C_2$ .

Note that decreasing  $L_A$  and  $J$  and increasing  $\bar{K}$  has a positive effect in reducing both time constants, whereas changing  $R_A$  and  $C_2$  has opposite effects on the two time constants.

Referring back to Equation (3-23), there are three criteria which must be met if  $m_1$ ,  $m_2$  are to have negative

values essential for disappearance of the transient components of speed. They are:

$$\begin{aligned}
 JL_A &> 0 \\
 (L_A C_2 + R_A J) &> 0 \\
 4JL_A(K^2 + R_A C_2) &> 0 .
 \end{aligned}
 \tag{3-32}$$

If these criteria are not met, "negative damping" and instability occur.

To investigate torque as a function of time, using the equations of motion:

$$\begin{aligned}
 T &= J \frac{d\omega}{dt} + C_1 + C_2 \omega \\
 &= (C_1 + C_2 \omega_\infty) - \frac{(Jm_1 + C_2)m_2(\omega_0 - \omega_\infty)}{m_1 - m_2} \epsilon^{m_1 t} + \\
 &\quad + m_1 \frac{(Jm_2 + C_2)(\omega_0 - \omega_\infty)}{m_1 - m_2} \epsilon^{m_2 t}
 \end{aligned}
 \tag{3-33}$$

where  $m_1$  and  $m_2$  and  $\omega_\infty$  are as defined in Equation (3-23).

Since neither the expression for  $\omega$  versus  $t$  (Equation 3-23) nor  $T$  versus  $t$  (Equation 3-33) can be solved explicitly for  $t$  and substituted back to obtain an expression for  $T$  versus  $\omega$ , one must calculate and plot the values of  $\omega$  and  $T$  corresponding to various times,  $t$ , and then for specific times,  $t$ , during the transient period, pick off corresponding values of  $T$  and  $\omega$ .



Shunt Motor Including  $J$ ,  $L_A$ , and Torque  $\propto \omega^2$ 

This is the same as the preceding section except a torque component varying as the square of the speed is included in the load torque. This detailed derivation is believed to be original with this author and for that reason is presented complete. The equations of motion are:

$$T_m = J \frac{d\omega}{dt} + C_1 + C_2\omega + C_3\omega^2$$

$$E = K\omega$$

$$T_m = KI_a$$

$$V = E + I_a R_A + L_A \frac{dI_a}{dt}$$

now,

$$I_a = \frac{J}{K} \frac{d\omega}{dt} + \frac{C_1}{K} + \frac{C_2\omega}{K} + \frac{C_3\omega^2}{K}$$

$$\frac{dI_a}{dt} = \frac{J}{K} \frac{d^2\omega}{dt^2} + \frac{C_2}{K} \frac{d\omega}{dt} + \frac{2C_3\omega}{K} \frac{d\omega}{dt}$$

and

$$\begin{aligned} KV - C_1 R_A &= L_A J \frac{d^2\omega}{dt^2} + (L_A C_2 + 2\omega C_3 L_A + R_A J) \frac{d\omega}{dt} + \\ &+ (C_2 R_A \omega + K^2 \omega + C_3 K \omega^2) . \end{aligned} \quad (3-34)$$

Equation (3-34) can be solved rather easily if the net

armature inductance can be considered negligible. As discussed earlier, with a commutating winding present, this is usually considered a valid assumption. Then Equation (3-34) reduces to:

$$R_A J \frac{d\omega}{dt} = - [(C_1 R_A - KV) + (C_2 R_A + K^2)\omega + C_3 R_A \omega^2] \quad (3-35)$$

Let:

$$\begin{aligned} a &= C_3 R_A \\ b &= C_2 R_A + K^2 \\ c &= C_1 R_A - KV \end{aligned} \quad (3-36)$$

Separating the variables and integrating each side of Equation (3-35) yields:

$$\int \frac{d\omega}{a\omega^2 + b\omega + c} = - \frac{t}{R_A J} \quad (3-37)$$

The left hand side of Equation (3-37) integrates to:

$$\frac{1}{\sqrt{b^2 - 4ac}} \ln \frac{2a\omega + b - \sqrt{b^2 - 4ac}}{2a\omega + b + \sqrt{b^2 - 4ac}} \text{ for } b^2 > 4ac \quad (3-38)$$

or

$$\frac{2}{\sqrt{4ac - b^2}} \tan^{-1} \frac{2a\omega + b}{\sqrt{4ac - b^2}} \text{ for } b^2 < 4ac \quad (3-39)$$

For the condition where  $b^2 > 4ac$ , Equation (3-37) becomes (with  $b^2 - 4ac = p^2$ ):

$$\frac{\omega + \frac{b-p}{2a}}{\omega + \frac{b+p}{2a}} = M\epsilon^{-\frac{pt}{R_A J}} \quad (3-40)$$

If  $\omega = \omega_0$  at  $t = 0$ , the constant of integration,  $M$  can be evaluated as:

$$M = \frac{\omega_0 + \frac{b-p}{2a}}{\omega_0 + \frac{b+p}{2a}} \quad (3-41)$$

when  $M$  is substituted in Equation (3-40), and the resulting expression solved for  $\omega$ , one has:

$$\omega = \frac{(p-b)(2a\omega_0 + b+p) + (p+b)(2a\omega_0 + b-p)\epsilon^{-\frac{pt}{R_A J}}}{2a \left[ (2a\omega_0 + b+p) - (2a\omega_0 + b-p)\epsilon^{-\frac{pt}{R_A J}} \right]} \quad (3-42)$$

If, at  $t = 0$ ,  $\omega_0 = 0$ , Equation (3-42) reduces to

$$\omega = \frac{1 - \epsilon^{-\frac{pt}{R_A J}}}{2a \left[ \frac{1}{(p-b)} + \frac{\epsilon^{-\frac{pt}{R_A J}}}{p+b} \right]} \quad (3-43)$$

where  $p$ ,  $a$ , and  $b$  have the values assigned in Equation (3-36). If  $b^2 < 4ac$ , again with  $p^2 = 4ac - b^2$ , using Equation (3-39), Equation (3-37) evaluates as:

$$\omega = \frac{p\omega_0 - 2(c + b\omega_0) \tan \frac{pt}{2R_A J}}{p + (2a\omega_0 + 2b) \tan \frac{pt}{2R_A J}} \quad (3-44)$$

The expression of Equation (3-43) is for an angular velocity that does not have a sustained oscillation whereas the angular velocity given by Equation (3-44) will exhibit sustained steady state oscillations.

In order to obtain an expression for torque as a function of time, it would be necessary to evaluate  $\omega$ ,  $\omega^2$  and  $\frac{d\omega}{dt}$  for various values of time and substitute in:

$$T_m = J \frac{d\omega}{dt} + C_1 + C_2\omega + C_3\omega^2 \quad (3-45)$$

Shunt Motor Including  $L_f$  but With no Coupling  
Between Armature and Shunt Field  
Inertia Loading

The equations of motion become:

$$V = E + I_a R_A \quad (3-46)$$

$$E = K\Phi\omega \quad (3-47)$$

$$\Phi = K'I_f \quad (3-48)$$

$$V_f = R_f I_f + L_f \frac{dI_f}{dt} \quad (3-49)$$

$$T_m = K\Phi I_a = J \frac{d\omega}{dt} \quad (3-50)$$

Equation (3-49) has for solution,

$$I_f = \frac{V_f}{R_f} \left( 1 - e^{-\frac{R_f t}{L_f}} \right) \quad (3-51)$$

Also, from Equation (3-50):

$$I_a = \frac{J}{K\phi} \frac{d\omega}{dt} \quad (3-52)$$

$$\frac{dI_a}{dt} = \frac{J}{K} \left[ \frac{\phi \frac{d^2\omega}{dt^2} - \frac{d\phi}{dt} \frac{d\omega}{dt}}{\phi^2} \right] . \quad (3-53)$$

Substituting Equations (3-47), (3-52), and (3-53) into Equation (3-46) yields:

$$V = K\phi\omega + \left( \frac{R_a J}{K\phi} - \frac{L_A J}{K\phi^2} \frac{d\phi}{dt} \right) \frac{d\omega}{dt} + \frac{L_A J}{K\phi} \frac{d^2\omega}{dt^2} . \quad (3-54)$$

Recognizing that, from Equation (3-48) and Equation (3-51):

$$\phi = \frac{K' V_f}{R_f} \left( 1 - \epsilon^{-\frac{R_f t}{L_f}} \right) \quad (3-55)$$

and

$$\frac{d\phi}{dt} = \frac{K' V_f}{L_f} \epsilon^{-\frac{R_f t}{L_f}} . \quad (3-56)$$

These relationships, when substituted in Equation (3-54), result in:

$$V = \frac{L_A J R_f}{K K' V_f} \left[ \frac{1}{\left( 1 - \epsilon^{-\frac{R_f t}{L_f}} \right)} \right] \frac{d^2\omega}{dt^2} + \frac{J R_f}{K K' V_f} \left[ \frac{R_A \left( 1 - \epsilon^{-\frac{R_f t}{L_f}} \right) - \frac{L_A R_f}{L_f} \epsilon^{-\frac{R_f t}{L_f}}}{\left( 1 - \epsilon^{-\frac{R_f t}{L_f}} \right)^2} \right] \frac{d\omega}{dt} +$$

$$+ \frac{KK' V_f}{R_f} \left( 1 - \varepsilon - \frac{R_f t}{L_f} \right) \omega . \quad (3-57)$$

Obviously, Equation (3-57) is an extremely difficult expression to cope with analytically. Also, it is, in reality, not realistic because coupling actually will manifest itself between the field and armature circuit. If the effect of the coupling is included, prospects of a solution are even more dismal.

The various analyses and discussion presented above do not purport to include all combinations possible. However, they do present a cross-section of the over-all problem and point up the necessity for an empirical approach based on observations of instantaneous torque-speed characteristics of various d.c. machines.

## CHAPTER IV

### ANALYSIS OF FACTORS OFTEN IGNORED IN LINEAR ANALYSIS

#### Introduction

In Chapter III, methods of analysis are presented based on various simplifying assumptions. These simplifying assumptions lead to expressions which are useful insofar as the insight they provide, but they also can lead to erroneous and misleading results. In this portion of the thesis, the effects of some of the factors eliminated by the assumptions are examined. Not only will this examination be helpful in forming engineering judgment to evaluate so called linear analysis of the machines, but it will also indicate to a designer the areas of the design where transient response can be improved by exercising prudence in the design.

Topics to be discussed in this chapter include:

- A. Switching Saturated D.C. Circuits.
- B. Eddy Current Formation in the Magnetic Circuit.
- C. The Demagnetizing Effect of Armature Reaction.

- D. Coupling Between Field and Armature Circuit due to Brush Shift.
- E. Commutating Field Time Lag.
- F. Armature Circuit Potential Drop due to Carbon Brushes.
- G. Induced Currents in Closed Conducting Circuits.
- H. Effect of the Above Factors on Linear Analysis Results.

#### A. Switching Saturated D.C. Circuits

In order to evaluate the effects of magnetic saturation in the magnetic material comprising the magnetic circuit of the motor, consider the equivalent circuit of the shunt field of a d.c. motor with no armature to field circuit coupling. It can be represented as shown in Figure 4-1.

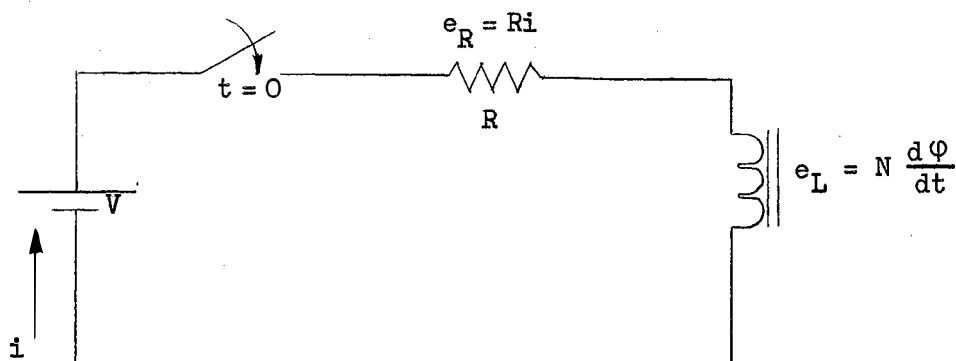


Figure 4.1. Shunt Field Equivalent Circuit



Applying Kirchoff's Law to the closed loop after the switch is closed,

$$V - iR = N \frac{d\phi}{dt} = N \frac{d\phi}{di} \frac{di}{dt} \quad (4-1)$$

where:

R = lumped circuit resistance

V = impressed step voltage

i = resulting current

N = number of turns (effective) linked by  $\phi$

$\phi$  = flux in webers.

If the B-H curve is linear (as is considered in the linear analysis),  $N \frac{d\phi}{di}$  is a constant for a given configuration and is termed the self inductance, L, in henrys.

If L is constant, the current can be expressed as a function of time in accordance with the well-known solution to the differential equation (4-1) and is:

$$i = I_s \left( 1 - e^{-\frac{Rt}{L}} \right) \quad (4-2)$$

where:

$$I_s = \frac{V}{R} = i \text{ at } t = \infty .$$

In actuality, with a finite air gap and a ferromagnetic core material driven to values of flux density near saturation, the B-H curve is not linear. Designating

$\frac{dB}{dH}$  by  $\mu$ , where  $\mu$  is the permeability, examination of the B-H curve for a ferromagnetic material indicates a trend toward decreasing  $\mu$  with increasing H. For a specific configuration, the following relationship can be derived:

$$\mu = \frac{\Delta B}{\Delta H} = \frac{\Delta \Phi l}{A \Delta i N} \left( \frac{N}{N} \right) = \frac{L l}{A N^2} \text{ or } L = \frac{N^2 \mu A}{l} \quad (4-3)$$

where:

$\Delta \Phi$  is the incremental change in flux (for an incremental change in current  $\Delta i$ ) in a magnetic circuit of effective cross sectional area, A, and length, l.

If  $\mu$  decreases because of saturation, L decreases also with current growth, resulting in an i versus t relationship with a quicker time of response than is obtained with a constant  $\mu$  and L.

In order to evaluate time of response based on actual B-H relationships rather than on a linear approximation, the actual curve can be represented by the empirical relationship known as Frohlich's Equation:

$$B = \frac{\bar{D} H}{\bar{G} + H} \quad (4-4)$$

where:

$\bar{D}$  and  $\bar{G}$  are constants of the core material.

Even in a complex (relatively) magnetic structure, such as is found in a d.c. machine where the structure is

composed of air gaps, pole structures, frame, yoke, etc., the different cross-sectional areas, lengths and permeabilities combine in some unique fashion to have a resultant  $\Phi$  versus  $Ni$  characteristic. On this basis, it is more enlightening from an analytical standpoint to express Equation (4-4) as:

$$\Phi = \frac{Di}{\frac{G}{N} + i} \quad (4-5)$$

where:

$D$  and  $G$  are different constants than  $\bar{D}$  and  $\bar{G}$  and are unique for the specific configuration of the core structure, including material.

Since  $\frac{d\Phi}{di} = \frac{GD}{N(\frac{G}{N} + i)^2}$ , Equation (4-1) becomes:

$$V - Ri = \frac{GD}{(\frac{G}{N} + i)^2} \frac{di}{dt} \quad (4-6)$$

Separating the variables and expanding  $\frac{GD}{(\frac{G}{N} + i)^2 (V - Ri)}$  by the method of partial fractions, gives:

$$dt = \left[ \frac{K_1}{V - Ri} + \frac{K_2}{(\frac{G}{N} + i)} + \frac{K_3}{(\frac{G}{N} + i)^2} \right] di \quad (4-7)$$

where  $K_1$ ,  $K_2$ , and  $K_3$  are determined by equating coefficients of  $i$  in the equation:

$$GD = K_1 \left( \frac{G}{N} + i \right)^2 + K_2 \left( \frac{G}{N} + i \right) (V - Ri) + K_3 (V - Ri). \quad (4-8)$$

Solution of Equation (4-8) results in three equations in three unknowns, and, when solved, lead to values as follows:

$$K_1 = RK_2, \quad K_2 = \frac{RGD}{(V + \frac{RG}{N})^2}, \quad K_3 = \frac{K_2}{R} (V + \frac{RG}{N}). \quad (4-9)$$

Integrating each side of Equation (4-7),

$$t = -\frac{K_1}{R} \ln(V - Ri) + K_2 \ln\left(\frac{G}{N} + i\right) - K_3 \left(\frac{1}{\frac{G}{N} + i}\right) + M \quad (4-10)$$

where:

M is the constant of integration which can be evaluated for any switching condition by consideration of the appropriate initial conditions. In this thesis, the initial condition of  $i = 0$  at  $t = 0$  will be examined.

$$0 = -\frac{K_1}{R} \ln V + K_2 \ln \frac{G}{N} - \frac{K_3}{G/N} + M. \quad (4-11)$$

Subtracting Equation (4-11) from Equation (4-10),

$$t = \frac{K_1}{R} \ln \frac{V}{V - Ri} + K_2 \ln \frac{G/N + i}{G/N} + \frac{K_3 i}{G/N(G/N + i)}. \quad (4-12)$$

Using the values of  $K_1$  and  $K_3$  from Equation (4-9), and noting  $\frac{V}{R} = I_s$ , the steady state current, results in:

$$t = \epsilon \frac{K_2 \left(\frac{I_s}{G/N} + 1\right) i}{(G/N + 1)} \left[ \frac{1 + \frac{i}{G/N}}{1 - \frac{i}{I_s}} \right]^{K_2} \quad (4-13)$$

where:

$$K_2 = \frac{RGD}{\left(V + \frac{RG}{N}\right)^2} \cdot$$

Refer to the  $\phi$  versus  $Ni$  curve for a specific material and configuration. Flux per pole and  $I_s$  are usually constrained values, i.e., they are design constants, usually operated at their maximum values. This fact, along with the design voltage,  $V$  (in this case the voltage across each pole winding), can be utilized to reduce Equation (4-13) to an equation with only  $G$  and  $N$  as variable parameters. Thus:

$$\phi_m = \frac{DI_s}{G/N + I_s}, \text{ or } D = \phi_m \frac{(G/N + I_s)}{I_s} \quad (4-14)$$

and

$$\epsilon^t = \epsilon \frac{Ni\phi_m}{V(G/N + i)} \left[ \frac{1 + i/G/N}{1 - i/I_s} \right] \frac{G\phi_m}{V(I_s + G/N)} \quad (4-15)$$

where  $\phi_m = \text{maximum}$ .

Although Equation (4-15) cannot be solved explicitly for  $i$ , the form is of a nature which lends itself to calculation of time,  $t$ , in terms of  $\frac{i}{I_s}$  for various  $N$  and  $G$  and a fixed  $\phi_m$  and  $I_s$ .

Equation (4-15) is of extreme usefulness to an analyst determining the actual time of response of a given

configuration. It has a more limited utility when used during the design stage to select a core material for minimum time of response. This limitation is due to the fact that the  $\Phi$  versus  $Ni$  relationship is unique for a given material and configuration. Since the air gap of the machine is a portion of the magnetic circuit, the relationship is determined not only by the permeability of the iron, but also by the proportion of the total excitation necessary to overcome the drop in magnetic potential across the air gap. The designer works from the B-H curve of the material. If a preponderance of the total excitation is utilized for the air gap, changing the permeability of the iron core will not appreciably alter the slope of the  $\Phi$  versus  $Ni$  curve. The only sure way to evaluate the effect of various core materials is to actually calculate the  $\Phi$  versus  $Ni$  characteristic using the different materials and then evaluate  $i$  as a function of  $t$ . However, trends in the effect upon time of response by different materials can be examined. To do this, consider that

$$\frac{d\Phi}{di} = \frac{GD}{N(\bar{G}/N + i)} \quad (\text{based on Frohlich's Equation}).$$

At  $i = 0$ ,  $\frac{d\Phi}{di}$  reduces to  $D$ .  $\frac{d\Phi}{di}$  is related to the initial permeability of the core material. Actually,  $\bar{D}$ , as defined in Equation (4-4), is the initial permeability (within the limits of accuracy imposed by the curve fitting process in determining  $\bar{D}$  and  $\bar{G}$ ). The exact

relationship between  $D$  and the initial permeability is determined by the factors enumerated above. In general, an increase in permeability results in an increase in  $D$ .

Using Equation (4-14) and Equation (4-15), the  $t$  versus  $i$  relationship can be expressed in terms of  $D$ , rather than  $G$ . Thus:

$$\epsilon^t = \epsilon \frac{Ni\phi_m^2}{V[DI_s - (I_s - i)\phi_m]} \left[ \frac{DI_s - (I_s - i)\phi_m}{(D - \phi_m)(I - i)} \right] \frac{N\phi_m(D - \phi_m)}{VD}$$

(4-16)

Numerical evaluation of this equation for changes in permeability (proportional to  $D$ ) and  $N$  will indicate the effect of variation in these parameters on time of response.

#### A-1. Sample Calculation - Determination of Actual Response Time

Assume a d.c. shunt motor with open circuit characteristic obtained by the conventional methods and shown in Figure 4.2 by the dotted line, and the following design details:

Shunt field turns per pole = 1,000

Number of inductors = 332

Wave wound, 4-pole

Rated Voltage, 250 volts

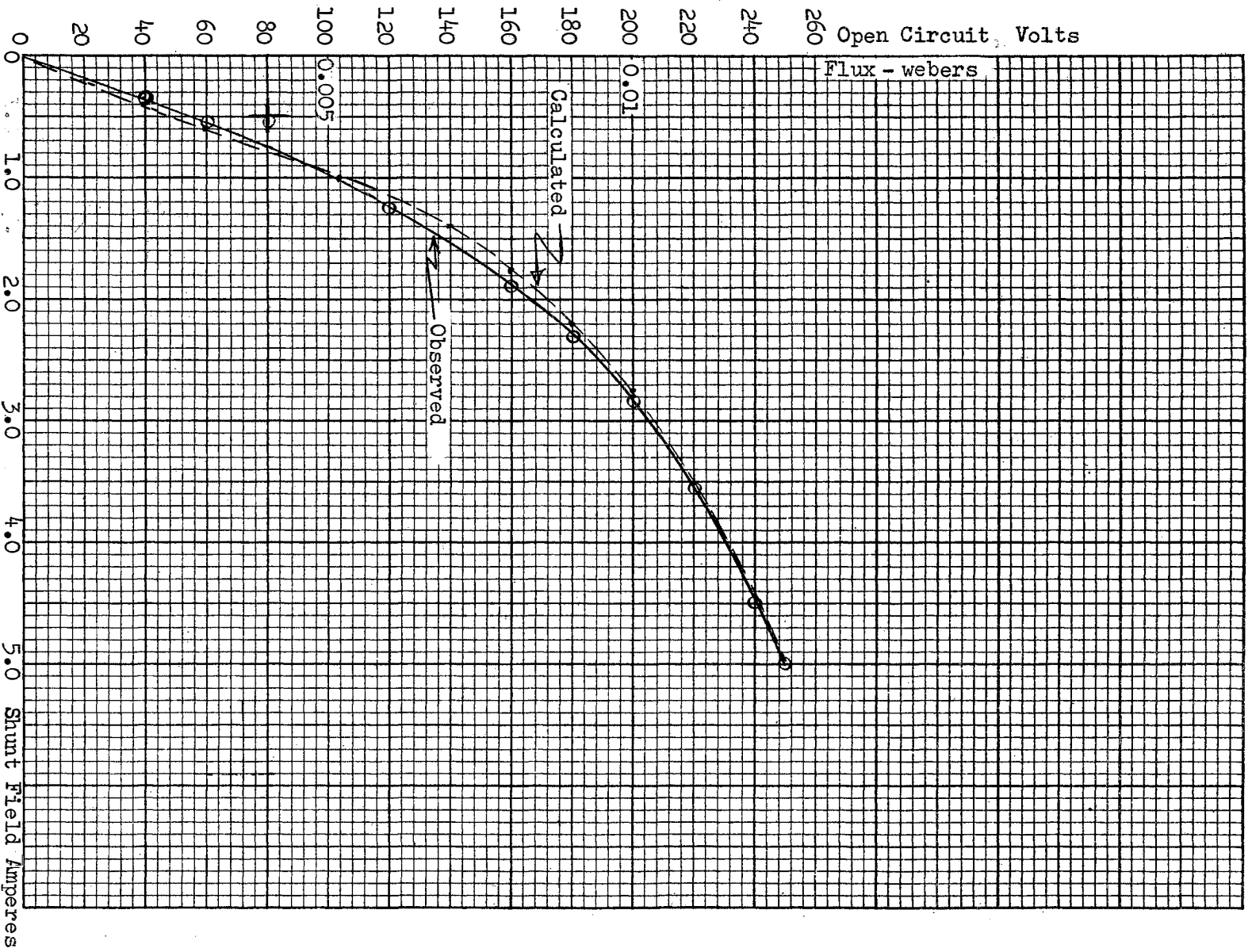


Figure 4.2. Typical Open Circuit Characteristic



Rated Speed, 1800 rpm

Resistance per field pole, 12.5 ohms (poles connected in series)

$$\text{from } E = \frac{Z\phi pn}{60a} \quad \phi_m = \frac{60 \times 2 \times 200}{332 \times 1800 \times 4} = 0.01 \text{ webers.}$$

Imposing this value of flux on the ordinate at 200 volts enables the  $\phi$  versus  $Ni$  characteristic (actual) to be represented by Frohlich's Equation:

$$\phi_m = 0.0125 \text{ webers} \quad I_s = \frac{250}{4 \times 12.5} = 5 \text{ amps.}$$

Also, at  $\phi = 0.005$  webers  $i = 0.95$  amperes.

Using these two values and  $N = 1000$ , the constants of Frohlich's Equation are determined as:

$$D = 0.019$$

$$G = 2700.$$

Thus, the  $\phi$  versus  $Ni$  characteristic is given by:

$$\phi = \frac{0.019 i}{2.7 + i} \text{ and is also plotted on Figure 4.2.}$$

In utilizing Frohlich's Equation, care must be taken to insure correspondence between actual and empirical curve at the  $\phi_m$  point and at a lower value of  $\phi$  to insure correct permeability over the linear region of the characteristic.

Values of  $i$ , such that  $0 < i < 0.95I_s$ , were chosen and times,  $t$ , calculated. From the linear portion of the characteristic, a value of inductance determined as:

$$L = \frac{N\Delta\Phi}{i} = \frac{1000 \times 0.0052}{1} = 5.2 \text{ henrys,}$$

was combined with  $R = 12.5$  ohms and used in Equation (4-2). Values for both the "linear" and actual situation are tabulated in Table IV-I and plotted in Figure 4.3. The difference between apparent time of response (based on a linearized version) and actual time is obvious from inspection of Figure 4.3. The magnitude of the discrepancies is also tabulated in Table IV-I.

TABLE IV-I  
CURRENT VERSUS TIME - TYPICAL NONLINEAR RESPONSE

Current	Actual Time	"Linear" Time	Difference	% Error
1.0	0.089	0.0925	0.0035	3.9%
2.0	0.157	0.213	0.056	35.5%
3.0	0.223	0.380	0.157	70.3%
4.0	0.297	0.668	0.371	125.0%
4.5	0.354	0.958	0.604	171.0%
4.75	0.408	1.242	0.834	204.0%

Since the departure, or noncorrespondence, becomes more pronounced with the passage of time, it appears reasonable to define an apparent field inductance based, not on one time constant,  $T = L/R$ , but rather based on a period of time equal to  $2L/R$  or  $2.5 L/R$  where  $L$  is the

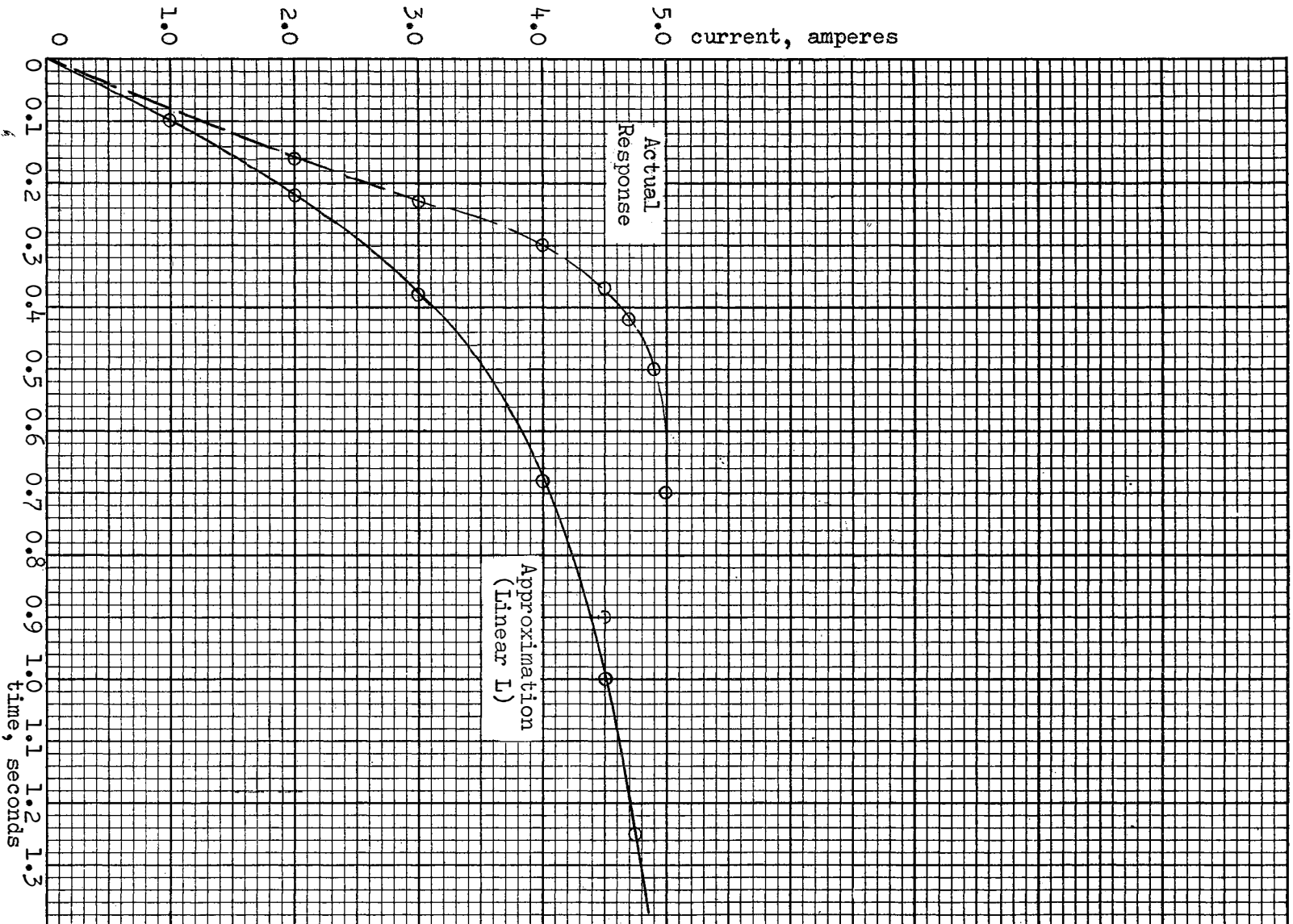


Figure 4.3. Typical Linear and Nonlinear Response

inductance calculated from the initial permeability. In a linear inductance circuit of 5.2 henrys, 5 amperes steady-state current, the actual current would be approximately 4.32 amperes after a period of time of 2 time constants. The circuit used in this example reaches this current level in 0.34 seconds and would, thus, have an "apparent" inductance of:

$$L = \frac{0.34 \times 12.5}{2} = 2.12 \text{ henrys.}$$

An effort was made to determine the effect of D, G, and N on time of response. Initially, it was hoped that it would be possible to correlate variations of G, D, and N (due to different core materials and configurations) in such a fashion as to enable one to foresee the effect upon time of response for the variations without actually carrying out the calculation of  $i$  versus  $t$  for each of several possible combinations of material and configuration. The aid of an IBM 1620 computer and its associated Gotran program processor was utilized in this investigation and was a tremendous time saver in the data evaluation. A number of variations of parameter combinations were examined, but most were found lacking in results suitable for clear conclusions. Useful variations examined and observations made are detailed below with graphic visualization presented in Figures 4.4 through 4.10. Although the specific numbers used in calculating these curves are not

important, per se, they have been retained on the graphical presentation because of their usefulness in a relative fashion.

Data Plotted:

Figure 4.4. Flux versus exciting current for fixed  $N$ , various  $G/D$  for several values of  $G$ .

Figure 4.5. Flux versus exciting current for fixed  $N$ , various  $G/D$  for several values of  $D$ .

Figure 4.6.  $i/I_s$  versus time for various  $G/D$ , fixed  $N$  and two different values of  $G$ .

Several observations were made concerning initial permeability, excitation requirements, and time of response:

(a) Initial Permeability,  $\mu_i$ , increases with decreasing values of  $G/D$  for fixed values of  $G$  or  $D$ :

$\mu_i$  increases with increasing values of  $D$  for fixed values of  $G$ .

$\mu_i$  increases with fixed values of  $G/D$  and increasing values of  $G$  or  $D$ .

$\mu_i$  increases with decreasing  $G/D$  and fixed values of  $D$ .

(b) Exciting Current:

The larger the value of  $G/D$ , for a fixed  $G$  or  $D$ , the larger the excitation current for a given flux.

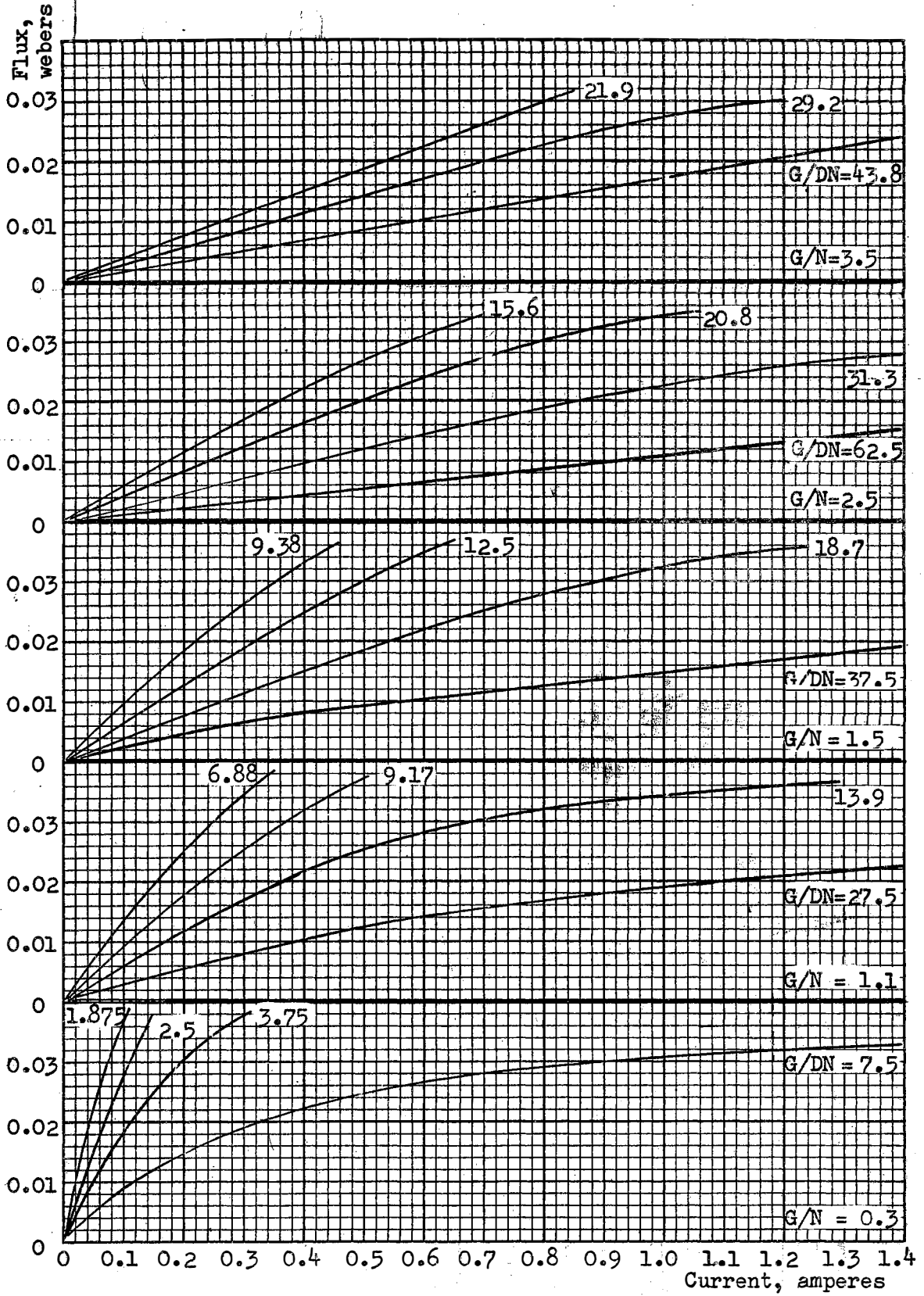


Figure 4.4. Effect of G/DN on  $\mu_i$  for Various G

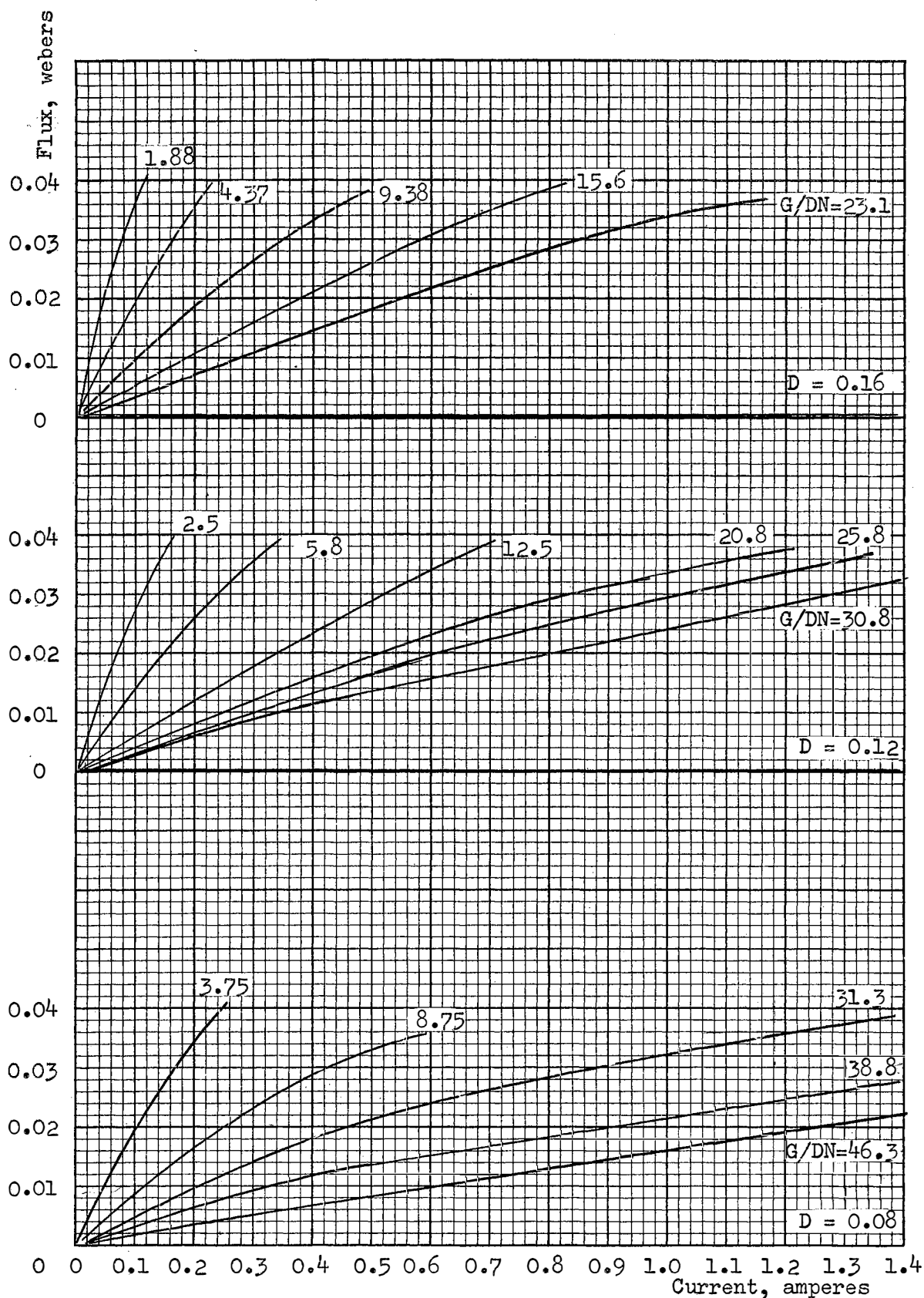


Figure 4.5. Effect of  $G/DN$  on  $\mu_i$  for Various  $D$

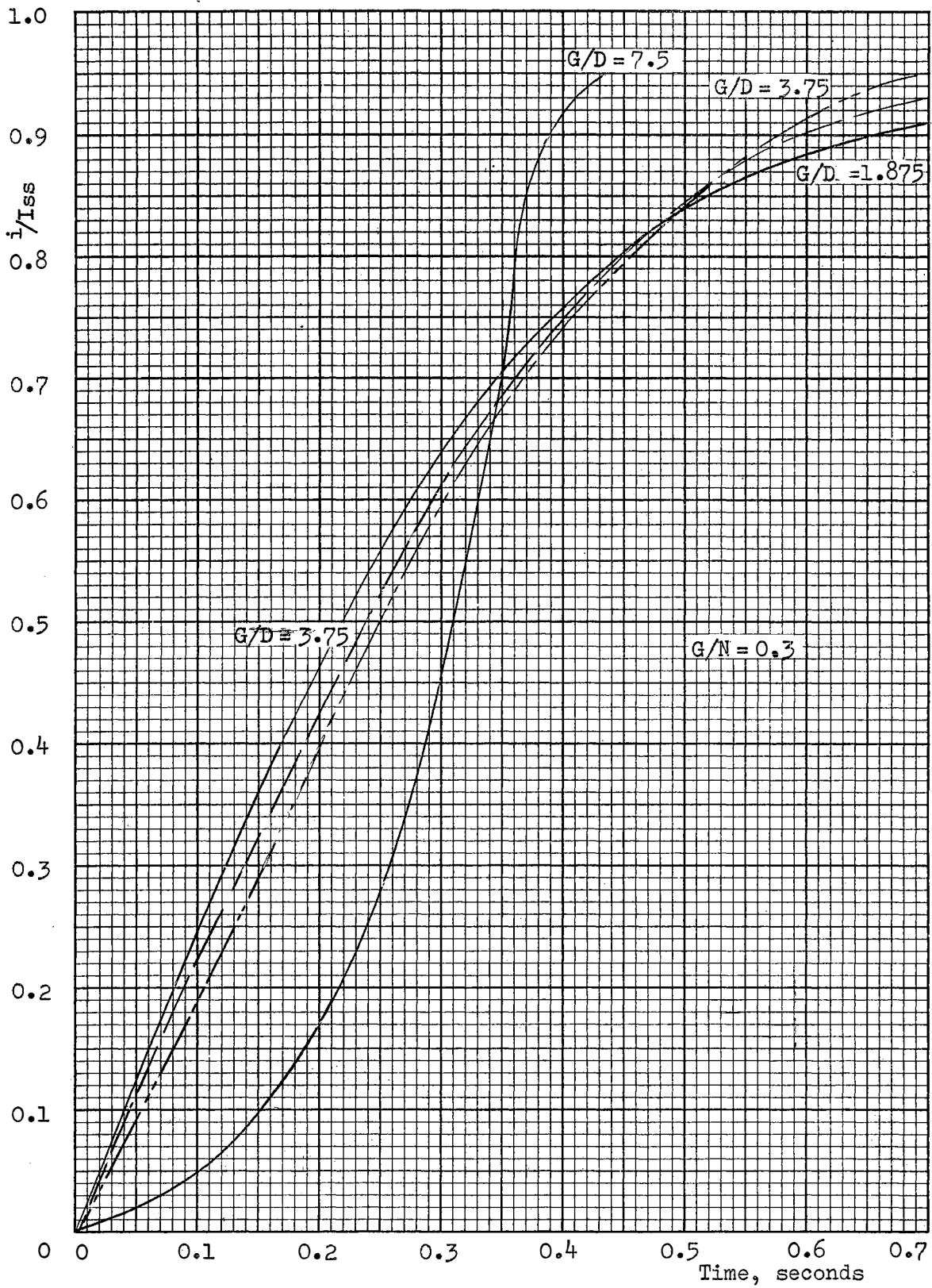


Figure 4.6.  $i/I_{ss}$  Versus  $t$  for Various  $G/DN$



## (c) Time of Response:

For a fixed  $G$ , time of response to a given value of flux decreases with increasing  $G/D$ .

For a fixed  $G/D$ , time of response to a given value of flux decreases with decreasing  $G$ .

Data Plotted:

Figure 4.7. Flux versus exciting current for fixed  $\Phi_m$ ,  $I_s$ , various fixed values of  $D$  and variable  $G/N$ .

Figure 4.8. Flux versus exciting current for fixed  $\Phi_m$ ,  $I_s$ , various fixed values of  $G/N$  and variable  $D$ .

Figure 4.9. Flux versus exciting current for fixed  $\Phi_m$ ,  $I_s$ , variable  $D$ , and variable  $G/N$ .

Figure 4.10.  $i$  versus time for various  $N$  and  $D$ .

In Figures 4.7, 4.8, 4.9, and 4.10, the same circuit conditions as in the numerical example prevailed, i.e.,  $\Phi_m = 0.0125$  webers,  $I_s = 5$  amperes. Observations made, in some cases, parallel the observations made in connection with Figures 4.4, 4.5, and 4.6.

## (a) Initial Permeability:

$\mu_i$  increases with increasing  $D$  and fixed  $G/N$ .

$\mu_i$  increases with decreasing  $G/N$  for fixed  $D$ .

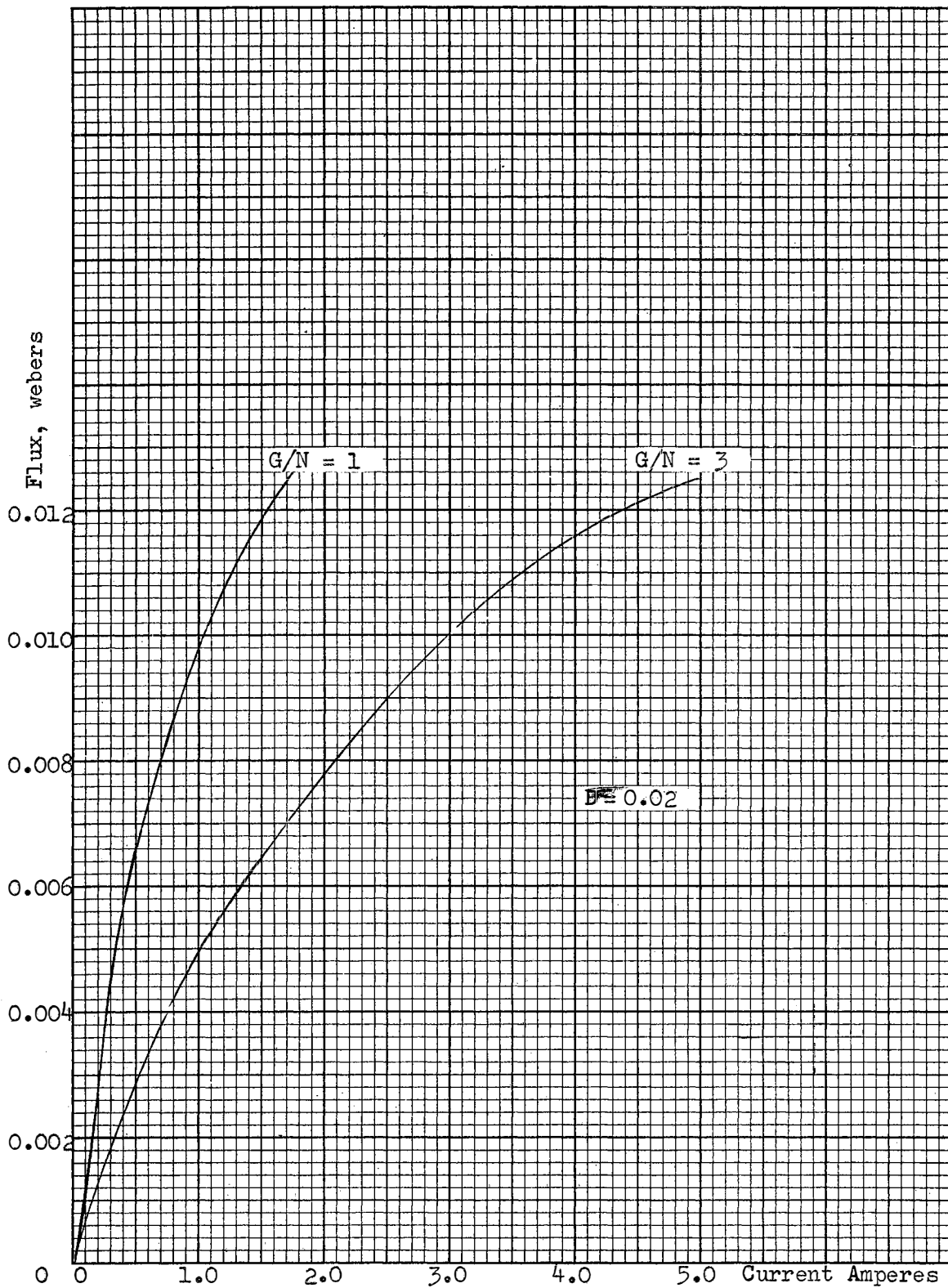


Figure 4.7 Effect of  $G/N$  for Constant  $N, D$

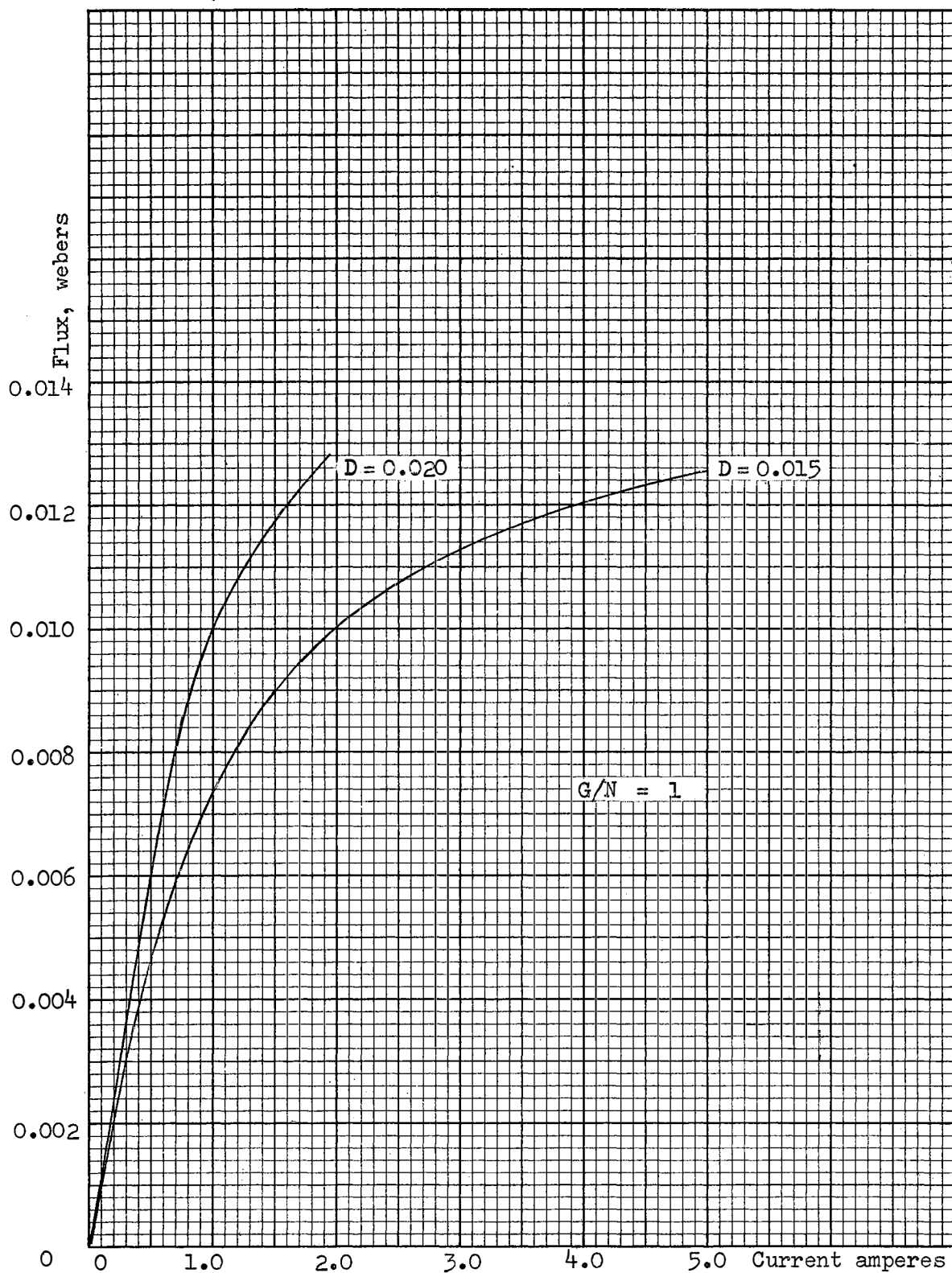


Figure 4.8. Effect of  $D$  for Constant  $G/N$

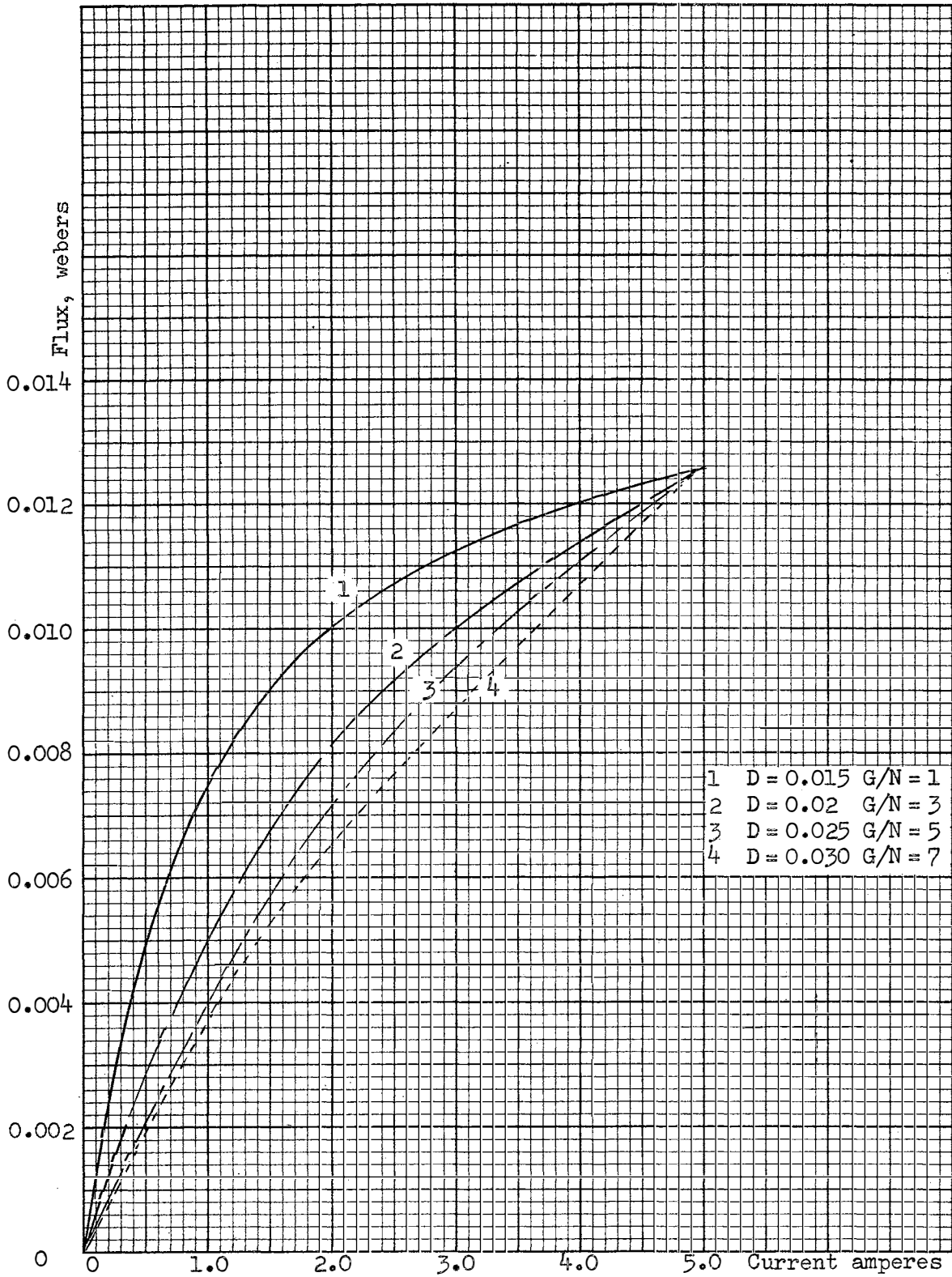


Figure 4.9. Effect of D, G/N for Fixed Current

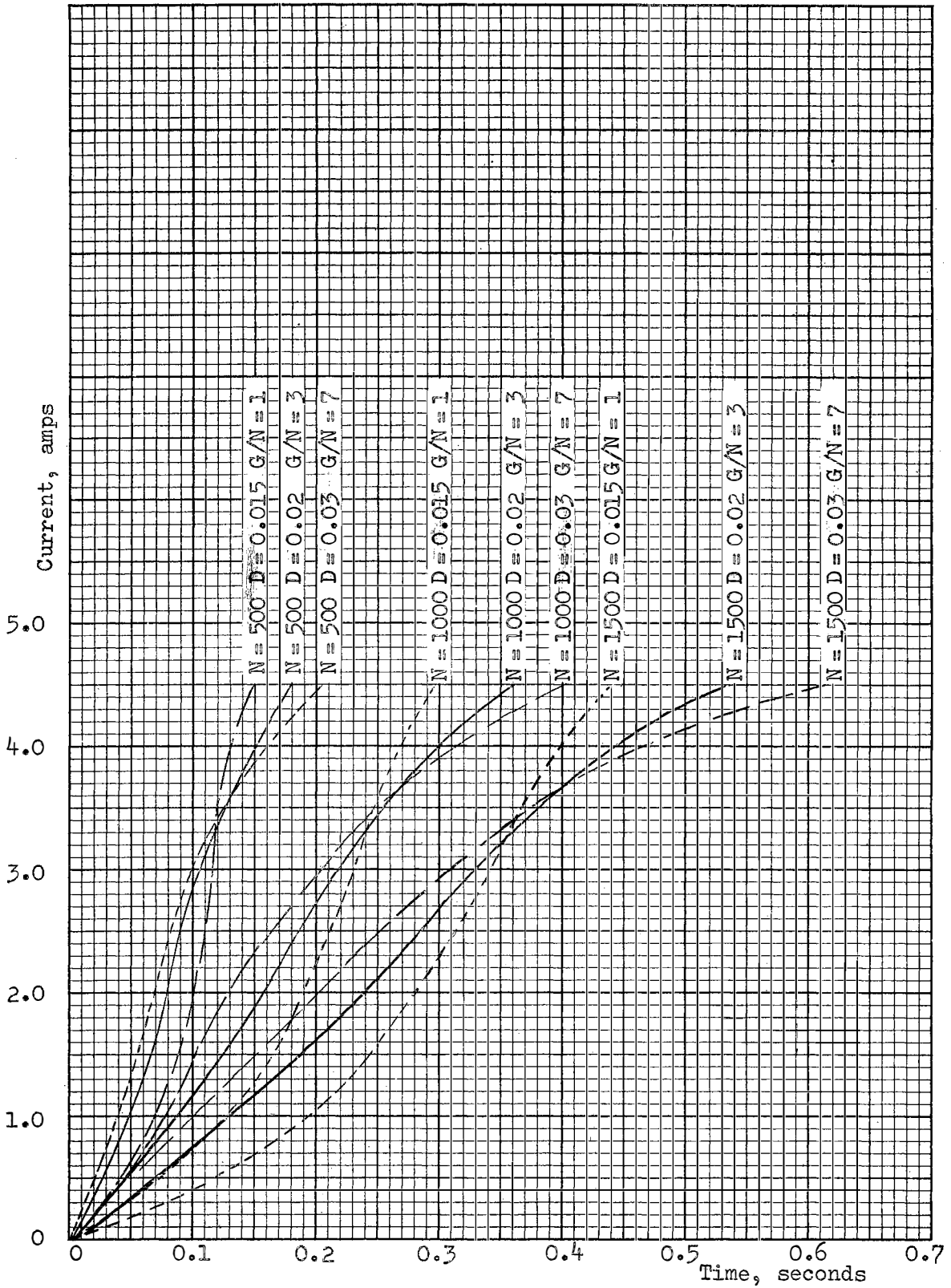


Figure 4.10.  $i$  Versus  $t$  for Various  $N$ ,  $D$

When both D and G/N are varying, the change in  $\mu_i$  depends on the relative magnitudes of G/N and D. For the values used in Figure 4.9,  $\mu_i$  increases with decreasing G/N and D decreasing as well.

(b) Time of Response:

The time of response is much more affected by the number of turns than by changes in D or G/N. However, for a given number of turns, the shortest time to reach steady state current (or very nearly) is obtained using material with the highest initial permeability.

A-2. Summary of G, D Variations

Data presented in Figures 4.7, 4.8, 4.9 and 4.10 appears to be the most realistic method of examination of core material and configuration possibilities because the designer is usually confronted with the necessity of securing some fixed value of flux and has a restraint on the maximum excitation current at his disposal. From the data, the minimum time to reach nearly steady state current is obtained by using a material with the highest initial permeability obtainable. Also, in general, quickest response will be obtained by utilizing the largest possible exciting

current (affording usage of a minimum number of turns). Changing the number of turns affects time of response in a nonlinear circuit exactly as it does in a circuit with a linear B-H characteristic (and constant inductance with respect to current). From Equation (4-3), the linear inductance varies as the square of the number of turns. Thus, doubling the number of turns would require the time for current build up to approximately 63% of its ultimate value to increase by a factor of 4. For the nonlinear circuit examined here, the time for build up to  $0.63 \times 5 = 3.16$  amperes with 500 turns is 0.115 seconds. Using the same value of D and G, but going to 1000 turns, reducing  $I_s$  to 2.5 amperes, requires 0.46 seconds for the current build up to  $0.63 \times 2.5 = 1.58$  amperes.

The Gotran Program for data evaluation of  $i$  versus  $t$  utilizing the IBM 1620 computer is enclosed in Appendix A.

## B. Eddy Currents in the Iron Core

When the flux attempts to change with time in a conducting media, a voltage is induced and currents tend to flow. In iron structures subjected to alternating magnetic fields, these currents may be responsible for an electrical loss, termed eddy current loss, due to the conversion of electrical energy to heat energy - commonly called  $i^2R$  type loss. For this reason, an iron structure which will contain a time varying field is usually built up of thin laminations insulated from each other. Physically,

this reduces eddy current loss because the currents are confined to small eddies and, as the length of the eddy path is reduced to zero, the resistance approaches zero and, consequently, the eddy current loss is decreased. This state of the art is well developed and well documented.

Many d.c. machines have solid iron structures for frame, yoke, and pole pieces although most armatures are built up of laminations in order to decrease the eddy current loss arising as a result of local variations of flux in the air gap due to teeth and slots. During switching, or other transient phenomena, if the flux attempts to change, eddy currents result and these in turn establish a short duration magnetic field superimposed upon the field due to other causes. For years, there has been speculation as to the effect these short duration fields actually exert. In this thesis, an effort has been made to evaluate this phenomena.

The most straight forward derivation of the describing equation is by use of Maxwell's Equations, enumerated below:

$$\nabla \times \mathbf{E} = - \frac{\partial \mathbf{B}}{\partial t} \quad (4-17)$$

$$\nabla \times \mathbf{H} = \mathbf{J} + \frac{\partial \mathbf{D}}{\partial t} = \frac{\mathbf{E}}{\rho} + \epsilon \frac{\partial \mathbf{E}}{\partial t} \quad (4-18)$$

$$\nabla \cdot \mathbf{D} = \sigma \quad (4-19)$$

$$\nabla \cdot \mathbf{B} = 0 \quad (4-20)$$



where:

$\epsilon$  = Electrical Permittivity

$E$  = Electric field intensity in volts/meter

$\nabla$  = Mathematical operator del

$\times$  = Vector or cross product

$H$  = Magnetizing force in ampere turns/meter

$J$  = Current density, amperes/meter<sup>2</sup>

$\frac{\partial D}{\partial t}$  = Displacement current

$D$  = Electric flux density, coulombs/meter<sup>2</sup>

$\sigma$  = Charge density, coulombs/meter<sup>3</sup>

$B$  = Magnetic flux density, webers/meter<sup>2</sup>

$\rho$  = Resistivity, ohm-meters.

For a material classified as a conductor,

$$\frac{\partial D}{\partial t} \ll J. \quad \text{Also, } J = \frac{E}{\rho} \text{ and } B = \mu H \quad (4-21)$$

where

$\mu$  = Magnetic permeability.

Therefore, from Equation (4-18) and (4-21):

$$\frac{1}{\mu} (\nabla \times B) = \frac{E}{\rho}. \quad (4-22)$$

Using Equation (4-22) in Equation (4-17):

$$\frac{\rho}{\mu} (\nabla \times \nabla \times B) = - \frac{\partial B}{\partial t}. \quad (4-23)$$

$$\text{Now, } \nabla \times \nabla \times B = \nabla(\nabla \cdot B) - (\nabla \cdot \nabla)B \quad (4-24)$$

which is a fundamental identity in vector analysis. From

Equation (4-20),  $\nabla \cdot \mathbf{B} = 0$ . Combining Equation (4-24) and Equation (4-23), results in:

$$\nabla^2 \mathbf{B} = \frac{\mu}{\rho} \frac{\partial \mathbf{B}}{\partial t} . \quad (4-25)$$

A derivation leading to the same general result, but which gives a better physical picture of events, follows from events shown in Figure 4.11.

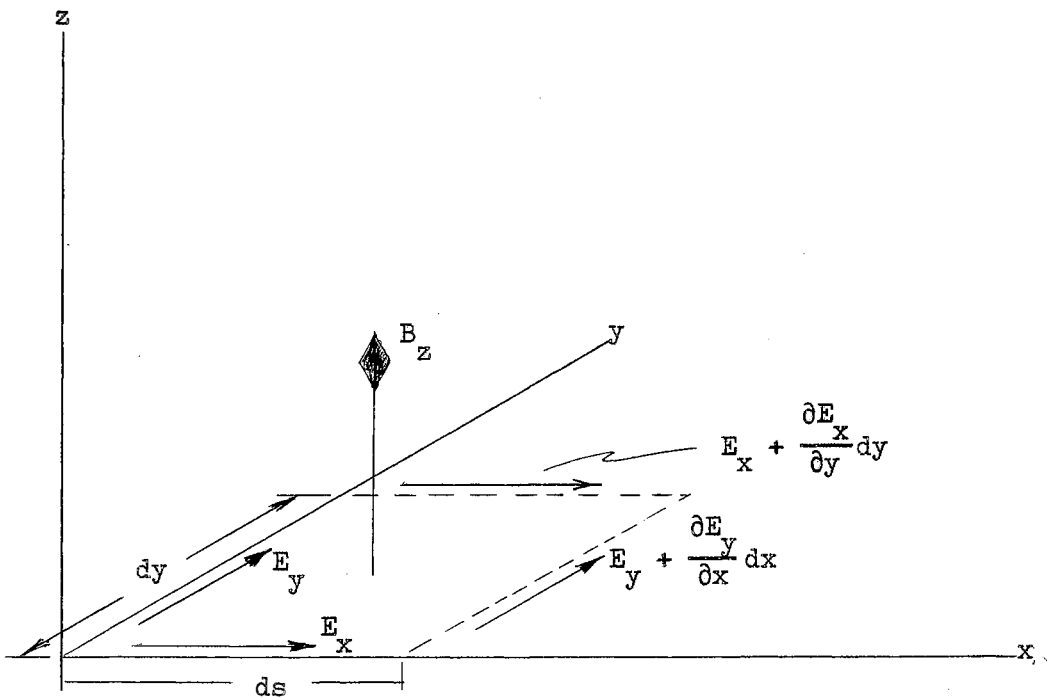


Figure 4.11. Electric and Magnetic Field Relationships

Consider a magnetic field,  $B_z$ , passing normal to a plane in the solid iron structure. Designate an element

of area through which  $B_z$  passes as  $dx dy$ . Then:

$$\Phi = B_z dx dy \quad (4-26)$$

where:

$\Phi$  is magnetic flux through area  $dx dy$ .

If  $\Phi$  varies with respect to time, electric voltages are induced along the  $x$  and  $y$  axis. By Faraday's Law and the definition of electric field intensity:

$$\oint \mathbf{E} \cdot d\mathbf{s} = - \frac{d\Phi}{dt} \quad (4-27)$$

$$\begin{aligned} \oint \mathbf{E} \cdot d\mathbf{s} &= E_x dx + (E_y + \frac{\partial E_y}{\partial x} dx) dy - (E_x + \frac{\partial E_x}{\partial y} dy) dx - E_y dy \\ &= \left( \frac{\partial E_y}{\partial x} - \frac{\partial E_x}{\partial y} \right) dy dx = - \frac{d\Phi}{dt} \quad (4-28) \end{aligned}$$

From Equations (4-26) and (4-28), then:

$$\left( \frac{\partial E_y}{\partial x} - \frac{\partial E_x}{\partial y} \right) = - \frac{\partial B_z}{\partial t} \quad (4-29)$$

This is electromagnetic induction in differential form giving the relationship between flux density and electric field strength.

For a circuit comprised of iron and air, such as the magnetic circuit of a motor:

$$H_z = \frac{B_z}{\mu} \quad \text{where } \mu_0 < \mu < \mu_{\text{iron}} \quad (4-30)$$

From Equation (4-29), currents will flow as a result of induced voltages (from  $\frac{\partial B_z}{\partial t}$ ) in the x and y directions. Designate the currents as  $I_x$  and  $I_y$ .

Consider the integral form of the vector expression of Equation (4-18) and refer to Figures 4.12 and 4.13.

$$\oint \mathbf{H} \cdot d\mathbf{s} = I \quad (4-31)$$

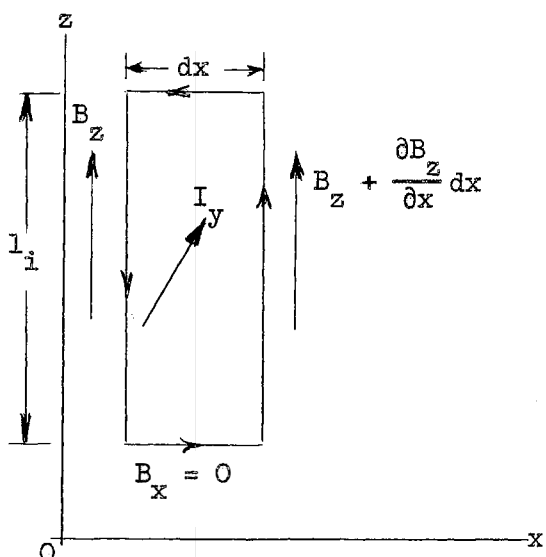


Figure 4.12. Eddy Current Formation,  $I_y$

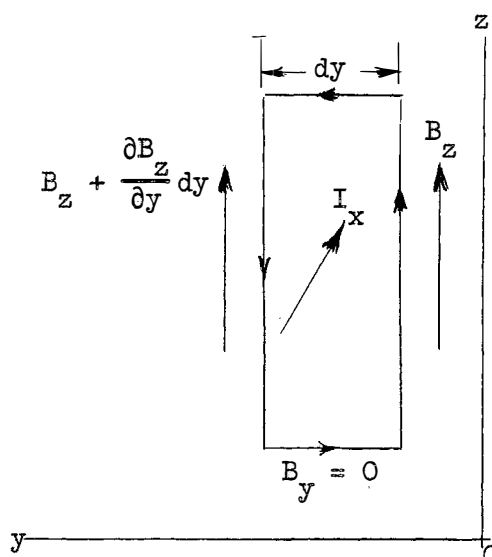


Figure 4.13. Eddy Current Formation,  $I_x$

The eddy current circulates in an elemental element and forms a 1 turn coil as shown for  $I_x$  and  $I_y$  in Figures 4.12 and 4.13. The current densities,  $J_x$  and  $J_y$  are:

$$J_x = \frac{I_y}{l_i dx} ; \quad J_y = \frac{I_x}{l_i dy}$$

$$\text{or} \quad I_x = J_x l_i dy ; \quad I_y = J_y l_i dx. \quad (4-32)$$

For  $I_y$ , using Equations (4-31) and (4-32):

$$\oint H_z \cdot ds = \oint \frac{B_z}{\mu} \cdot ds = \frac{1}{\mu} [B_z l_i - B_z l_i - \frac{\partial B_z}{\partial x} dx l_i] = J_y l_i dx$$

and

$$-\frac{1}{\mu} \frac{\partial B_z}{\partial x} = J_y \quad (4-33)$$

Similarly, for  $I_x$ :

$$\oint H \cdot ds = \oint \frac{B_z}{\mu} \cdot ds = \frac{1}{\mu} [B_z l_i + l_i \frac{\partial B_z}{\partial y} dy - B_z l_i] = J_x l_i dy$$

and

$$\frac{1}{\mu} \frac{\partial B_z}{\partial y} = J_x \quad (4-34)$$

From Ohms Law with Equations (4-33) and (4-34):

$$\rho J_x = E_x \quad ; \quad \rho J_y = E_y \quad (4-35)$$

and

$$E_x = \rho \frac{\partial B_z}{\partial y} \quad ; \quad E_y = -\rho \frac{\partial B_z}{\partial x} \quad (4-36)$$

$$\therefore \frac{\partial E_x}{\partial y} = \rho \frac{\partial^2 B_z}{\partial y^2} \quad ; \quad \frac{\partial E_y}{\partial x} = -\rho \frac{\partial^2 B_z}{\partial x^2} \quad (4-37)$$

Using the values from Equation (4-37) in Equation (4-29), gives:

$$-\frac{\rho}{\mu} \left( \frac{\partial^2 B_z}{\partial x^2} + \frac{\partial^2 B_z}{\partial y^2} \right) = -\frac{\partial B_z}{\partial t} \quad (4-38)$$

which is mathematically equivalent to:

$$\nabla^2 B_z = \frac{\mu}{\rho} \frac{\partial B_z}{\partial t} \quad (4-39)$$

which is the same as Equation (4-25).

The solution to the partial differential equation [Equation (4-39)] must, of course, be compatible with the initial condition imposed by the physical situation. The solution in this thesis is for the condition of zero flux at time  $t = 0$ , in the cross-section of core shown in Figure 4.14 and with over-all dimensions as shown.

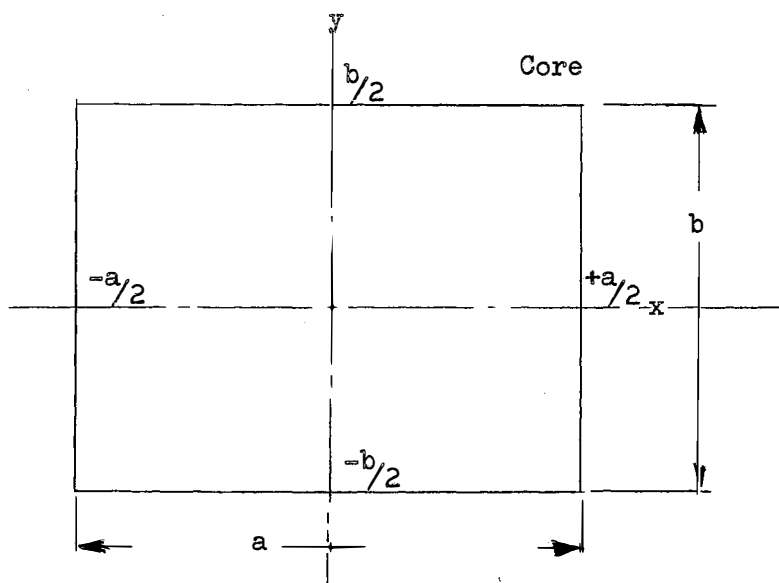


Figure 4.14. Core Cross Section

The Fourier Series for the rectangular wave shown in Figure 4.15 is: (20)

$$B = \frac{B_0}{2} - \frac{2B_0}{\pi} \sum_{m=1,3,\dots}^{\infty} \frac{(-1)^{\frac{m-1}{2}}}{m} \cos \frac{m\pi y}{b} \quad (4-40)$$

where:

$b$  is length

$B_0$  is steady state flux density.

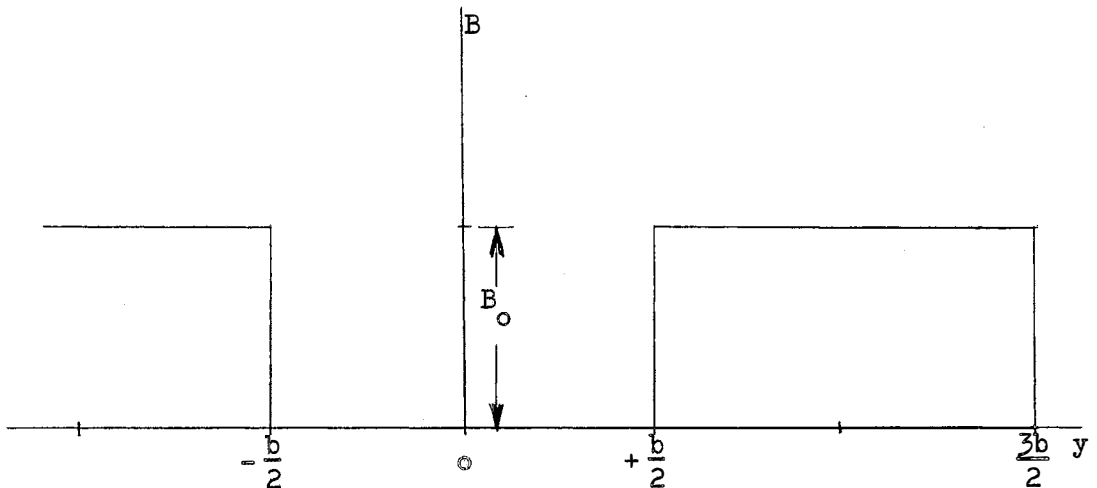


Figure 4.15. Rectangular Wave,  $f(y)$

Equation (4-40) is valid for any  $y$  and is everywhere zero for  $-\frac{b}{2} < y < \frac{b}{2}$ . If  $b$  is considered as the core dimension and a similar expression is written for the other core dimension,  $a$ , an expression is produced in terms of  $x$  which is valid for any  $x$  and is zero for  $-\frac{a}{2} < x < \frac{a}{2}$ .

Thus:

$$B = \frac{B_0}{2} - \frac{2B_0}{\pi} \sum_{n=1,3,\dots}^{\infty} \frac{(-1)^{\frac{n-1}{2}}}{n} \cos \frac{n\pi x}{a} \quad (4-41)$$

A proposed solution for  $\nabla^2 B_z = \frac{\mu}{\rho} \frac{\partial B_z}{\partial t}$  is:

$$B_z = B_0 - \frac{2B_0}{\pi} \left[ \sum_{n,m=1,3,\dots}^{\infty} \epsilon^{-\alpha_{nx}t} \frac{(-1)^{\frac{n-1}{2}}}{n} \cos \frac{n\pi x}{a} + \epsilon^{-\alpha_{my}t} \frac{(-1)^{\frac{m-1}{2}}}{m} \cos \frac{m\pi y}{b} \right] \quad (4-42)$$

where  $\alpha_{nx}$ ,  $\alpha_{my}$  are constants to be determined. As verification,

$$\nabla^2 B_z = - \frac{2B_0}{\pi} \left[ \sum_{n,m=1,3,\dots}^{\infty} -\epsilon^{-\alpha_{nx}t} \frac{n^2 \pi^2}{a^2} \frac{(-1)^{\frac{n-1}{2}}}{n} \cos \frac{n\pi x}{a} + \epsilon^{-\alpha_{my}t} \frac{m^2 \pi^2}{b^2} \frac{(-1)^{\frac{m-1}{2}}}{m} \cos \frac{m\pi y}{b} \right] \quad (4-43)$$

$$\frac{\partial B_z}{\partial t} = - \frac{2B_0}{\pi} \left[ \sum_{n,m=1,3,\dots}^{\infty} -\alpha_{nx} \epsilon^{-\alpha_{nx}t} \frac{(-1)^{\frac{n-1}{2}}}{n} \cos \frac{n\pi x}{a} + \alpha_{my} \epsilon^{-\alpha_{my}t} \frac{(-1)^{\frac{m-1}{2}}}{m} \cos \frac{m\pi y}{b} \right] \quad (4-44)$$

$$\text{Now, if } \frac{n^2 \pi^2}{a^2} = \frac{\mu \alpha_{nx}}{\rho} \quad (4-45)$$

$$\text{and } \frac{m^2 \pi^2}{b^2} = \frac{\mu \alpha_{my}}{\rho} \quad (4-46)$$

then Equation (4-42) satisfies Equation (4-39) and Equation (4-42) is a solution satisfying the mathematical and



physical situation, i.e., flux everywhere within the core is zero at  $t = 0$ . Physically, the field actions in  $x$  and  $y$  are independent. There are a large number of fluxes,  $\Phi_{m,n}$  associated with the changing field (where  $m,n$  is any combination of odd integers). The distribution of the field within the core after switching is the sum of a series of fluxes, each of which is cosinely distributed with respect to  $x$  and  $y$ . The amplitudes of the individual flux waves decrease inversely with increasing  $m,n$ . The flux waves decay proportional to the square of  $n,m$ , as can be seen from Equation (4-46).

The effect of the individual flux waves will be investigated by determining flux magnitudes, their rate of change with time and their resulting effect as viewed from a winding attempting to establish a magnetic field in the iron core.

If the magnetic field of Equation (4-42) links on  $N$  turn winding, a voltage will be induced in that winding. It is determined from:

$$e = \iint_{x,y} N \frac{\partial B}{\partial t} dx dy . \quad (4-47)$$

Since  $B$ , which is a function of  $x, y, t$  is continuous and has a continuous derivative  $\frac{\partial B}{\partial t}$ , this can be expressed as:

$$e = \frac{N \partial \Phi}{\partial t} \quad (4-48)$$

where  $\Phi$  is flux, given by:

$$\Phi = \iint_{x,y} B \, dx \, dy \quad (4-49)$$

The flux corresponding to a given  $n, m$  is determined from

$$\begin{aligned} \Phi_{m,n} = \int_{-\frac{b}{2}}^{\frac{b}{2}} \int_{-\frac{a}{2}}^{\frac{a}{2}} B_0 &= \frac{2B_0}{\pi} \left[ \epsilon^{-\alpha_{nx}t} \frac{(-1)^{\frac{n-1}{2}}}{n} \cos \frac{n\pi x}{a} + \right. \\ &+ \left. \epsilon^{-\alpha_{my}t} \frac{(-1)^{\frac{m-1}{2}}}{m} \cos \frac{m\pi y}{b} \right] dx \, dy \quad (4-50) \end{aligned}$$

when this double integral is evaluated, it yields

$$\begin{aligned} \Phi_{m,n} = B_0 ab &- \frac{2B_0}{\pi} \left[ \epsilon^{-\alpha_{nx}t} \frac{(-1)^{\frac{n-1}{2}}}{n^2} \frac{2ab}{\pi} \sin \frac{n\pi}{2} + \right. \\ &+ \left. \epsilon^{-\alpha_{my}t} \frac{(-1)^{\frac{m-1}{2}}}{m^2 \pi} 2ab \sin \frac{m\pi}{2} \right] \quad (4-51) \end{aligned}$$

$$\text{Now } (-1)^{\frac{n-1}{2}} \sin \frac{n\pi}{2} = (-1)^{\frac{m-1}{2}} \sin \frac{m\pi}{2} = +1 \text{ for } n, m = 1, 3, \text{etc.}, \quad (4-52)$$

$$\text{and defining } B_0 ab = \Phi_s, \quad (4-53)$$

where  $\Phi_s$  is steady state flux, Equation (4-51) becomes:

$$\Phi_{m,n} = \Phi_s \left[ 1 - \frac{4}{\pi^2} \left( \frac{\epsilon^{-\alpha_{nx}t}}{n^2} + \frac{\epsilon^{-\alpha_{my}t}}{m^2} \right) \right] \quad (4-54)$$

and the corresponding voltage,  $e_{m,n}$  induced in the  $N$  turn coil linked by this changing flux is:

$$e_{m,n} = \frac{N d\phi_{m,n}}{dt} = \frac{4\phi_s N}{\pi^2} \left[ \frac{\alpha_{nx} \epsilon^{-\alpha_{nx} t}}{n^2} + \frac{\alpha_{my} \epsilon^{-\alpha_{my} t}}{m^2} \right]. \quad (4-55)$$

Now, consider that the coil of  $N$  turns has an inductance  $L$ , resistance  $R$ , and provides the excitation winding for a core material with dimension  $ab$ . The magnetic circuit permeability is  $\mu$ , the iron has a resistivity  $\rho$  and the coil is to be energized from a step voltage source,  $V$ .

$$L = \frac{N\phi_s}{I} = \frac{N\phi_s R}{V} \quad (4-56)$$

for constant permeability material. Applying Kirchoff's Potential Law to the coil,

$$V = Ri + \frac{Ldi}{dt} + \sum_{m,n=1,3,\dots}^{\infty} e_{m,n}. \quad (4-57)$$

The voltages  $e_{m,n}$  are voltages appearing in the  $N$  turn coil as a result of eddy currents in the iron core. Using Equations (4-55), (4-56), and the values for  $\alpha_{nx}$ ,  $\alpha_{my}$  in Equation (4-57) yield:

$$V = Ri + \frac{Ldi}{dt} + \frac{4LV\rho}{R\mu} \sum_{m,n=1,3,\dots}^{\infty} \frac{\epsilon^{-\frac{n^2 \pi^2 \rho t}{a^2 \mu}}}{a^2} + \frac{\epsilon^{-\frac{m^2 \pi^2 \rho t}{b^2 \mu}}}{b^2}. \quad (4-58)$$

Applying Laplace Transformation techniques (initial conditions zero) to Equation (4-58) results in:

$$\frac{V}{s} = (R + sL)I(s) + \frac{4LV\rho}{R\mu} \sum_{n,m=1,3,\dots}^{\infty} \frac{1}{a^2 (s + \alpha_{nx})} + \frac{1}{b^2 (s + \alpha_{my})} \quad (4-59)$$

Solving for I(S) yields:

$$I(s) = \frac{V}{R} \left[ \frac{1}{\left(1 + \frac{Ls}{R}\right)} - \frac{4\rho}{\mu} \sum_{n,m=1,3,\dots}^{\infty} \frac{1}{Ra^2 \alpha_{nx} \left(1 + \frac{s}{\alpha_{nx}}\right) \left(1 + \frac{Ls}{R}\right)} + \frac{1}{Rb^2 \alpha_{my} \left(1 + \frac{s}{\alpha_{my}}\right) \left(1 + \frac{Ls}{R}\right)} \right] \quad (4-60)$$

Transforming back to the time domain and rearranging results in:

$$i(t) = \frac{V}{R} \left[ 1 - \epsilon^{-\frac{Rt}{L}} - \frac{4\rho}{\mu} \sum_{n,m=1,3,\dots}^{\infty} \frac{\epsilon^{-\alpha_{nx}t} - \epsilon^{-\frac{Rt}{L}}}{a^2 \left(\frac{R}{L} - \alpha_{nx}\right)} + \frac{\epsilon^{-\alpha_{my}t} - \epsilon^{-\frac{Rt}{L}}}{b^2 \left(\frac{R}{L} - \alpha_{my}\right)} \right] \quad (4-61)$$

where:

$$\alpha_{nx} = \frac{n^2 \pi^2 \rho}{a^2 \mu} \quad (4-62)$$

$$\alpha_{my} = \frac{m^2 \pi^2 \rho}{b^2 \mu} \quad (4-63)$$

This may be compared with the equation for current in

an R and L circuit with the same driving voltage and no eddy current phenomena present, i.e.:

$$i(t) = \frac{V}{R} \left( 1 - e^{-\frac{Rt}{L}} \right). \quad (4-64)$$

It is difficult to generalize on the influence of  $\rho$ ,  $\mu$  and core dimension in Equation (4-61) because of the presence of  $n$  and  $m$ , which take on all odd integer values from 1 to  $\infty$ . However, noting that  $\frac{1}{\alpha_{nx}}$  and  $\frac{1}{\alpha_{my}}$  are time constants corresponding to an iron core whereas  $\frac{L}{R}$  is the time constant of a wound winding, it is a perfectly valid assumption that:

$$\frac{1}{\alpha_{nx}} \ll \frac{L}{R} ; \quad \frac{1}{\alpha_{my}} \ll \frac{L}{R} \quad \text{and} \quad \alpha_{nx} \gg \frac{R}{L} ; \quad \alpha_{my} \gg \frac{R}{L} \quad (4-65)$$

which enables simplification of Equation (4-61). Thus, using values of  $\alpha_{nx}$ ,  $\alpha_{my}$ :

$$i(t) = \frac{V}{R} \left[ 1 - e^{-\frac{Rt}{L}} - \frac{4}{\pi^2} \sum_{n,m=1,3,\dots}^{\infty} \frac{e^{-\frac{Rt}{L}} - \frac{n^2 \pi^2 \rho t}{a^2 \mu}}{n^2} + \right. \\ \left. + \frac{e^{-\frac{Rt}{L}} - \frac{m^2 \pi^2 \rho t}{b^2 \mu}}{m^2} \right]. \quad (4-66)$$

At time  $t = 0$ , the terms inside the summation sign add to zero. As time passes, the terms involving  $\epsilon$  to a power determined by  $\rho$ ,  $n$ ,  $m$ ,  $\mu$ ,  $a$ ,  $b$  decay faster than the terms involving  $\epsilon^{-\frac{Rt}{L}}$ , because the core has a shorter time

constant than does the field. This causes the terms inside the summation sign to always be positive which is a characteristic of the physical system, i.e., the eddy currents retard field current build up. Since  $\epsilon^{-\alpha t}$  and  $\epsilon^{-\frac{Rt}{L}}$  are opposite in sign, the faster the decay of  $\epsilon^{-\alpha t}$ , the larger the magnitude of eddy current effect. This is illustrated in Figure 4.16.

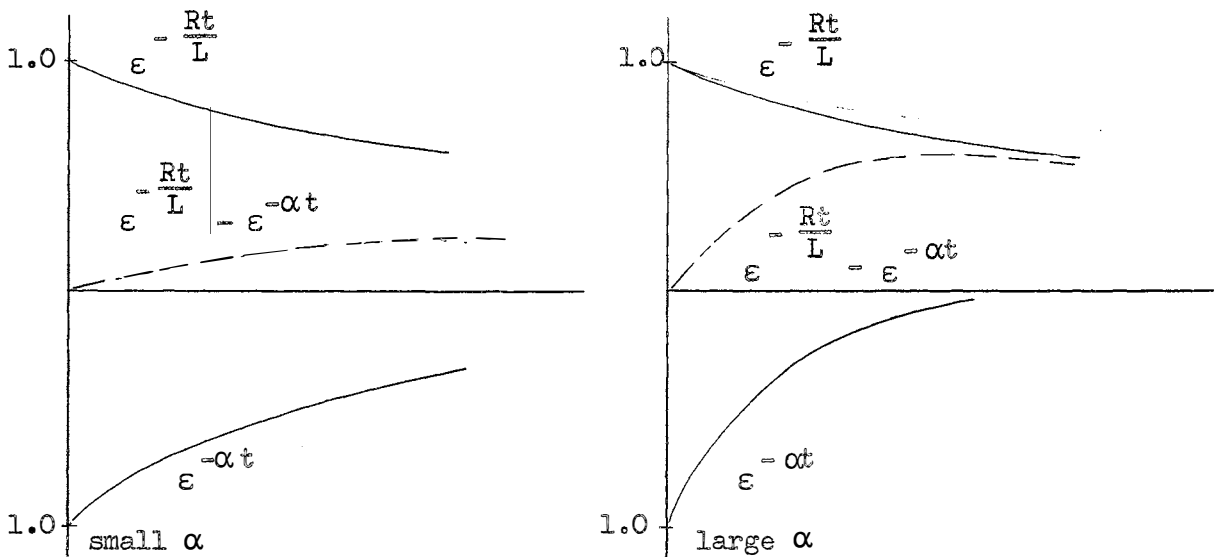


Figure 4.16. Eddy Current Time Constants

Increasing  $\alpha$  causes  $\epsilon^{-\alpha t}$  decay quicker, resulting in greater retardation of current build up in the excitation coil. Since:

$$\alpha_{nx} = \frac{\rho n^2 \pi^2}{\mu a^2} \quad (4-67)$$

$$\alpha_{my} = \frac{\rho m^2 \pi^2}{\mu b^2} \quad (4-68)$$

$\alpha_{nx}$  and  $\alpha_{my}$  become smaller as  $\rho$  is decreased and  $\mu$  is increased for a fixed core dimension. This variation of parameter effect is opposite to the variation one would expect without complete analysis.

At this point, the effect of laminating the iron can be investigated. As can be seen from the above equations, the length of the magnetic path is not a factor in the relationship between current and time, whereas, in an eddy current loss calculation, it is found that the power loss due to eddy currents is proportional to magnetic circuit length insofar as the length contributes to the total volume of iron in which the loss occurs. Laminating the iron does affect the eddy current losses in a magnetic core. The loss decreases as lamination thickness is reduced.

Consider a core made up of  $M$  laminations, each  $b$  units in width and  $a$  units in thickness. Neglecting the stacking factor, the over-all dimensions of the core would be  $abM$  square units of length. If  $\Phi_s$  is the steady state flux linking the core, the flux of harmonic  $m, n$  linking each lamination will be given by Equation (4-54) if the dimensions of the lamination are used rather than the over-all core dimensions. However, the steady state flux, Equation (4-53) is now:

$$\Phi_s = B_o abM \quad (4-69)$$

and Equation (4-54) becomes:

$$\varphi_{m,n} = \frac{\varphi_s}{M} \left[ 1 - \frac{4}{\pi^2} \left( \frac{\varepsilon \frac{-\alpha_{nx} t}{n^2}}{n^2} + \frac{\varepsilon \frac{-\alpha_{my} t}{m^2}}{m^2} \right) \right]. \quad (4-70)$$

Neglecting leakage, all of  $\varphi_{m,n}$  links the main coil of  $N$  turns and since  $\varphi_{m,n}$  varies with respect to time, it induces a voltage in the coil. It is:

$$e_{m,n} = N \frac{d\varphi_{m,n}}{dt} = \frac{4\varphi_s N}{M\pi^2} \left( \alpha_{nx} \frac{\varepsilon \frac{-\alpha_{nx} t}{n^2}}{n^2} + \alpha_{my} \frac{\varepsilon \frac{-\alpha_{my} t}{m^2}}{m^2} \right). \quad (4-71)$$

Since there are  $M$  identical laminations contributing to this effect in the main winding, the total induced voltage in the main winding due to all laminations will be  $M$  times the value given in Equation (4-70) which is identical to Equation (4-55). Thus, laminating the core has no influence on eddy current retardation of excitation coil current. The only change in the use of Equation (4-62) for laminated structure is that  $a$  and  $b$  refer to lamination dimension rather than over-all core dimensions.

Experimental verification of this specific phenomena in a machine is not feasible because of the problem of isolating the affect of core eddy currents from the effect of circulating currents as a result of induced voltages in other closed conducting circuits such as are formed by physical methods used as fastener circuits, armature turns closed upon themselves via brush and commutator paths, etc. In Section G of this chapter, experimental evidence of the existence of this phenomena will be presented in



conjunction with the discussion on the effects of the circulating currents referred to above.

The magnetic structure of a direct current machine is so complex that a precise analysis of the eddy current phenomena would be all but impossible. The utility of a derived expression, such as Equation (4-61), lies in the presentation of the part played by the various parameters in this phenomena, and steps that can be taken to minimize the manifestation of eddy currents.

The only reference to this phenomena found in the literature is a brief mention by Rudenberg (8) concerning the decay of flux of an electromagnet after the main coil is de-energized, and is for a much more easily evaluated boundary condition. It is felt that the original derivation presented here evaluates one of the most significant factors in the transient performance of direct current machines and should be of value to analysts and designers in improving the performance of direct current machines during transient conditions.

#### C. Demagnetizing Effect of Armature MMF ("Armature Reaction")

To outline the problem, consider a developed simple d.c. machine as shown in Figure 4.17, recalling that induced voltage and flux are independent of flux density distributions, being affected only by magnitude of total flux. (9).

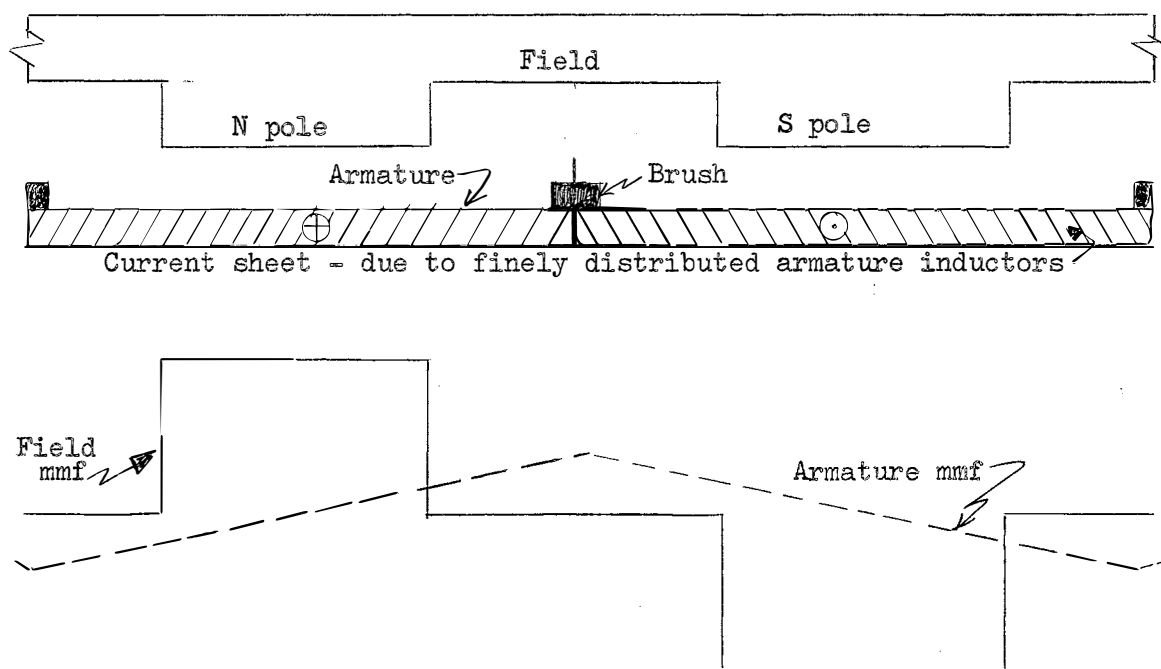


Figure 4.17. Elementary D.C. Machine - Developed Air Gap

The armature mmf, as will be demonstrated below, is triangular insofar as space distribution is concerned. Under one-half of the pole face, the mmf is in the same direction as the field mmf and under the other half of the pole face it opposes the mmf. The B-H characteristic is not linear for ferromagnetic materials, i.e., B does not increase at the same rate as does H for increasing values of H. Therefore, the increase in flux density under one pole tip is not as great as the decrease under the other. When the flux density is then integrated over the entire pole face, the net flux is less when the armature mmf is present than when no armature mmf exists. Thus, events in

the armature do affect phenomena in the field circuit and there exists armature to field coupling which cannot be expressed by some simple number as can mutual inductance.

Up to the present time, no analytical method of predicting the effect of armature reaction has been available to the machine designer. The only method of establishing the magnitude of the demagnetizing effect present in any machine has been to build a machine and experimentally determine the field ampere turns necessary to compensate for the armature reaction. (9). This investigator has devised an analytical approach based on only the assumption that the permeability of the magnetic material is so large compared to that of the air gap that it may be considered infinite. Since the relative permeability of the iron used extensively today is on the order of 100-10,000, this assumption appears warranted and will not lead to invalid results unless the machine is designed to operate in the completely saturated portion of the magnetic characteristic of the material. Also, it will be necessary to represent the B-H characteristic of the iron by Frohlich's Equation [as presented in Equation (4-4)]. If care is taken to achieve complete correspondence between the values used in Frohlich's Equation and the actual B-H curve, the analytical results will be accurate over the complete range of armature currents and field excitation. Since complete correspondence is very nearly impossible to achieve, because only two constants are available for

curve fitting in Frohlich's Equation, correspondence must be achieved in the desired operating range.

Refer to Figure 4.18; assume the pole has the structure shown, and the brushes are on magnetic neutral.

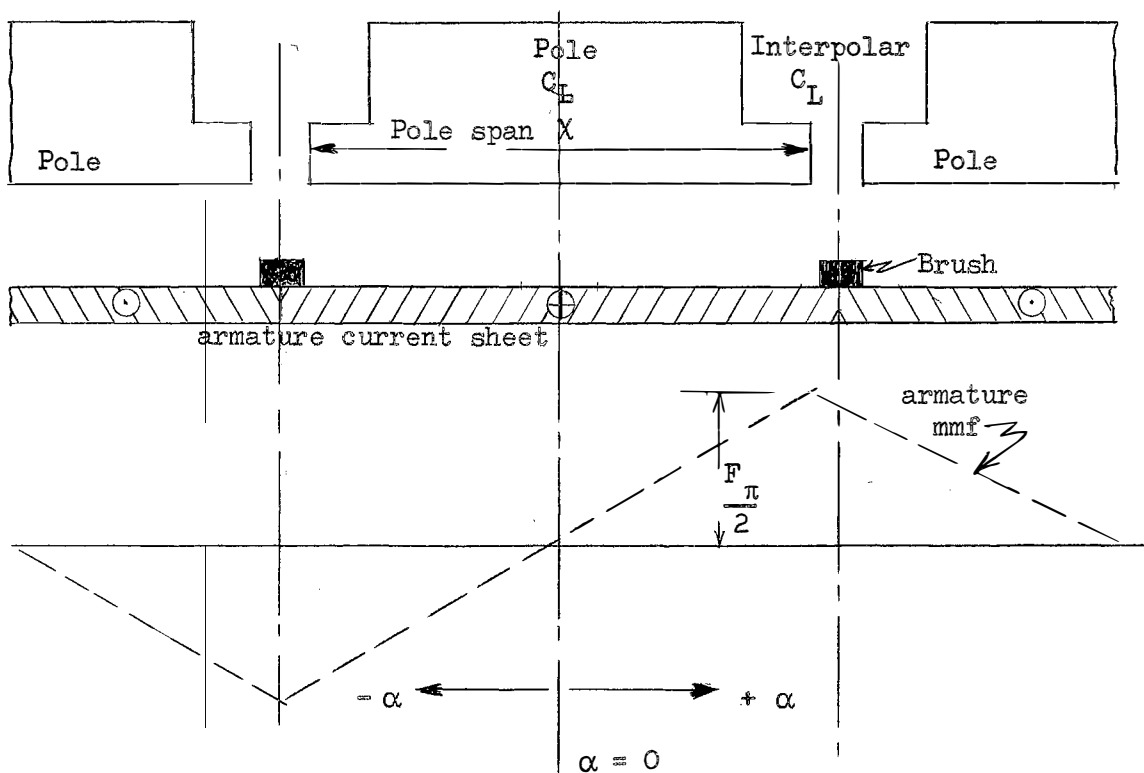


Figure 4.18. Armature MMF Space Relationship

There are  $\frac{Z}{p}$  inductors under each pole. Each inductor carries  $\frac{I}{a}$  amperes,

where:

$Z$  is total number of inductors

$p$  is the number of poles

$I$  is the "armature" current

$a$  is the number of parallel paths through the armature.

Now, 
$$F = \oint H \cdot dl \quad (4-72)$$

(a form of Amperes Law which states that the mmf,  $F$ , acting around a closed path is equal to the current enclosed by the path). If one takes a path through the iron and crossing the air gap at the interpole center line, the current enclosed is  $\frac{ZI}{pa}$ . Thus, the peak to peak value of armature mmf at the interpole locations is  $\frac{ZI}{pa}$ . If a path through the iron and crossing the air gap at the center line of the main field poles is taken, the net current enclosed is zero. By following the same procedure for other air gap crossings, it is seen that the armature mmf distribution in space is triangular.

The armature mmf at  $\alpha = \frac{\pi}{2}$  (see Figure 4.18 for the location of  $\alpha$ ) is the maximum value and is given by  $\frac{F}{2} = \frac{ZI}{2pa}$ . The mmf at any angle  $\alpha$  is:

$$F_{\alpha} = \frac{ZI\alpha}{pa\pi} \quad (4-73)$$

Now, total mmf at any point,  $F_T$ , is the sum of the total field mmf and the armature mmf at that point.

$$F_T = N_s I_s + N_f I_f + \frac{ZI\alpha}{pa\pi} \quad (4-74)$$

where:

$N_s$  = series field turns

$N_f$  = shunt field turns

$I_s$  = series field current

$I_f$  = shunt field current.

Use of the + sign is correct since  $\alpha = 0$  falls at the center line of the field pole. Dividing Equation (4-74) by  $N_f$  yields:

$$\frac{F_T}{N_f} = I_f + I_s \frac{N_s}{N_f} + \frac{ZI\alpha}{pa\pi N_f} \quad (4-75)$$

This is the mmf in equivalent shunt field amperes,  $F$ , which can be written:

$$F = I_f + K_1 I_s + K_2 I\alpha \quad (4-76)$$

where:

$$K_1 = N_s / N_f$$

$$K_2 = \frac{Z}{pa\pi N_f} \quad .$$

Consider a linear B-H curve ( $B = KF$ ). For a two pole machine, the flux per pole,  $\Phi$ , is:

$$\Phi = \int_{-\chi/2}^{+\chi/2} B dA = \int_{-\chi/2}^{+\chi/2} Br l d\alpha \quad (4-77A)$$

$$\phi = \int_{-\chi/2}^{+\chi/2} K(I_f + K_1 I_s + K_2 I \alpha) r l d\alpha = K r l [I_f + K_1 I_s] \quad (4-77)$$

where  $r$  and  $l$  are the radius and length of the armature,

$K$  is a constant of proportionality,  $K = \frac{B}{F}$ .

$\chi$  is pole span.

If there were no armature mmf,  $I_f + K_1 I_s$  would be the total mmf. Therefore, the flux has the same value with armature mmf and a linear B-H characteristic as it would have if no armature mmf were present.

Actually, of course,  $B$  and  $F$  are not linearly related and  $F = f(\alpha)$ . Using Frohlich's Equation:

$$B = \frac{DF}{F + G} \text{ where } D \text{ and } G \text{ are constants} \quad (4-78)$$

and substituting in Equation (4-77A) yields:

$$\phi = \int_{-\chi/2}^{+\chi/2} B dA = \int_{-\chi/2}^{+\chi/2} \frac{DF}{G + F} r l d\alpha \quad (4-79)$$

Since  $F = I_f + K_1 I_s + K_2 I \alpha$  and  $\frac{F}{G + F} = 1 - \frac{G}{G + F}$

$$\phi_{AR} = D r l \int_{-\chi/2}^{+\chi/2} 1 - \frac{G}{G + I_f + K_1 I_s + K_2 I \alpha} d\alpha \quad (4-80)$$

$$= D r l \left[ \alpha - \frac{G}{K_2 I} \ln (G + I_f + K_1 I_s + K_2 I \alpha) \right]_{-\chi/2}^{+\chi/2} \quad (4-81)$$

$$= DrlX \left[ 1 - \frac{G}{K_2 XI} \ln \frac{1 + \frac{K_2 XI}{2(G + I_f + K_1 I_s)}}{1 - \frac{K_2 XI}{2(G + I_f + K_1 I_s)}} \right] \quad (4-82)$$

where  $\Phi_{AR}$  designates the flux per pole with armature reaction effects in a nonlinear magnetic circuit. Now, consider the flux per pole,  $\Phi$ , with no armature reaction effect, i.e., a linear magnetic circuit for which

$$B = KF .$$

If the unsaturated permeability of the two circuits is identical, the slope of the B-F characteristics will be identically equal.

Linear Case

$$\frac{dB}{dF} = K$$

Nonlinear Case

$$\frac{dB}{dF} = \frac{d}{dF} \left( \frac{DF}{G+F} \right) . \quad (4-83)$$

Now, at low saturation  $G \gg F$  and for the nonlinear case,

$$B \approx \frac{DF}{G} \text{ at low } F \text{ and } \frac{dB}{dF} = \frac{D}{G}, \text{ or } K = \frac{D}{G} . \quad (4-84)$$

Using Equations (4-77), (4-82), and (4-84), it is now possible to determine the ratio  $\frac{\Phi_{AR}}{\Phi}$  as follows:

$$\frac{\Phi_{AR}}{\Phi} = \frac{DrlX \left\{ 1 - \frac{G}{K_2 XI} \ln \left( \frac{1 + \frac{K_2 XI}{2(G + I_f + K_1 I_s)}}{1 - \frac{K_2 XI}{2(G + I_f + K_1 I_s)}} \right) \right\}}{\frac{D}{G} rIX (I_f + K_1 I_s)} \quad (4-85A)$$



which reduces to

$$\frac{\phi_{AR}}{\phi} = \frac{G}{(I_f + K_1 I_s)} \left\{ 1 - \frac{G}{K_2 \chi I} \ln \left( \frac{1 + \frac{K_2 \chi I}{2(G + I_f + K_1 I_s)}}{1 - \frac{K_2 \chi I}{2(G + I_f + K_1 I_s)}} \right) \right\} \quad (4-85)$$

with  $K_1 = \frac{N_s}{N_f}$

$$K_2 = \frac{Z}{p a \pi N_f}$$

$\chi$  = pole span in radian

$I$  = armature current

$I_s$  = series field current

$I_f$  = shunt field current

$G$  = constant from Frohlich's Equation.

The expression given in Equation (4-85) contains only terms easily ascertained from design data and leads to results which were experimentally verified in the course of this investigation. It is felt by this investigator that the original work done in connection with this facet of machine analysis represents a signal contribution in this area which has always presented something of a mystery insofar as it lending itself to a quantitative analysis. The experimental work to verify the validity of Equation (4-85) was conducted in the Oklahoma State University Electrical Engineering Department laboratories, using a Westinghouse Electric Corporation Generalized Machine laboratory set.

The experimental procedure consisted of obtaining an open circuit saturation curve (in order to determine the constants in Frohlich's Equation), an external characteristic (armature current versus terminal voltage) of the machine under the same speed condition as the open circuit characteristic, but with fixed shunt field excitation, and armature circuit voltage drop information.

Armature circuit voltage drop due to various armature currents is displayed graphically in Figure 4.19, and the open circuit characteristic obtained is presented in Figure 4.20 (stator windings in series). The above data permitted calculation of the induced emf under various armature loadings. The ratio of induced emf,  $E$ , for various armature currents as a fraction of induced emf at zero armature current is plotted on Figure 4.21.

By trial and error curve fitting, Frohlich's Equation form representing the open circuit characteristic was found to be:

$$E = \frac{500 I_f}{6.38 + I_f} .$$

This relationship is also plotted on Figure 4.20. From the design constants using

$$\phi = \frac{60 a E}{Z_{np}} \quad \text{and} \quad B = \frac{\phi}{A}$$

with symbols previously defined, the actual form of Frohlich's Equation used was:

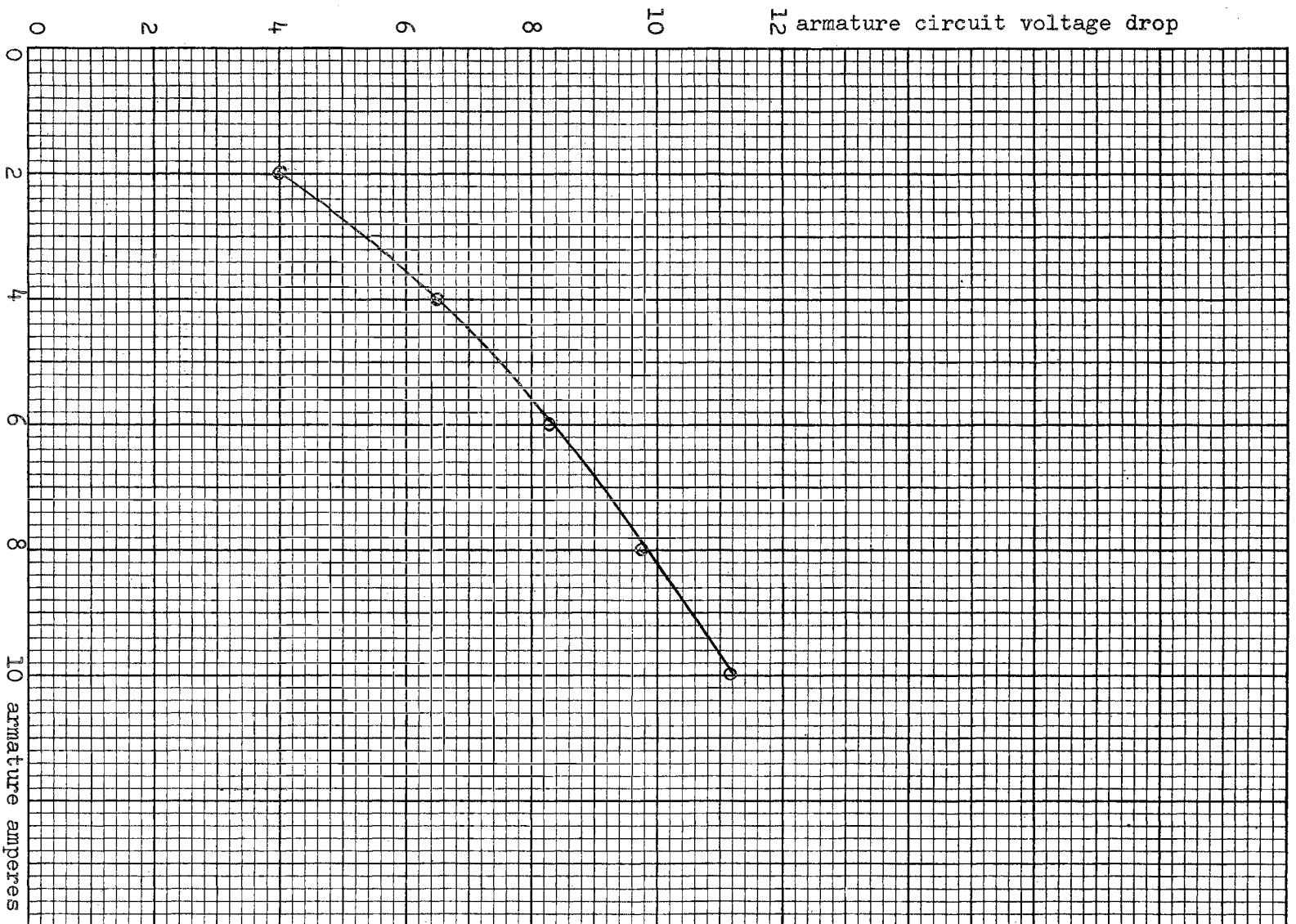


Figure 4.19. Armature Circuit Voltage Drop (Westinghouse Generalized Machine)

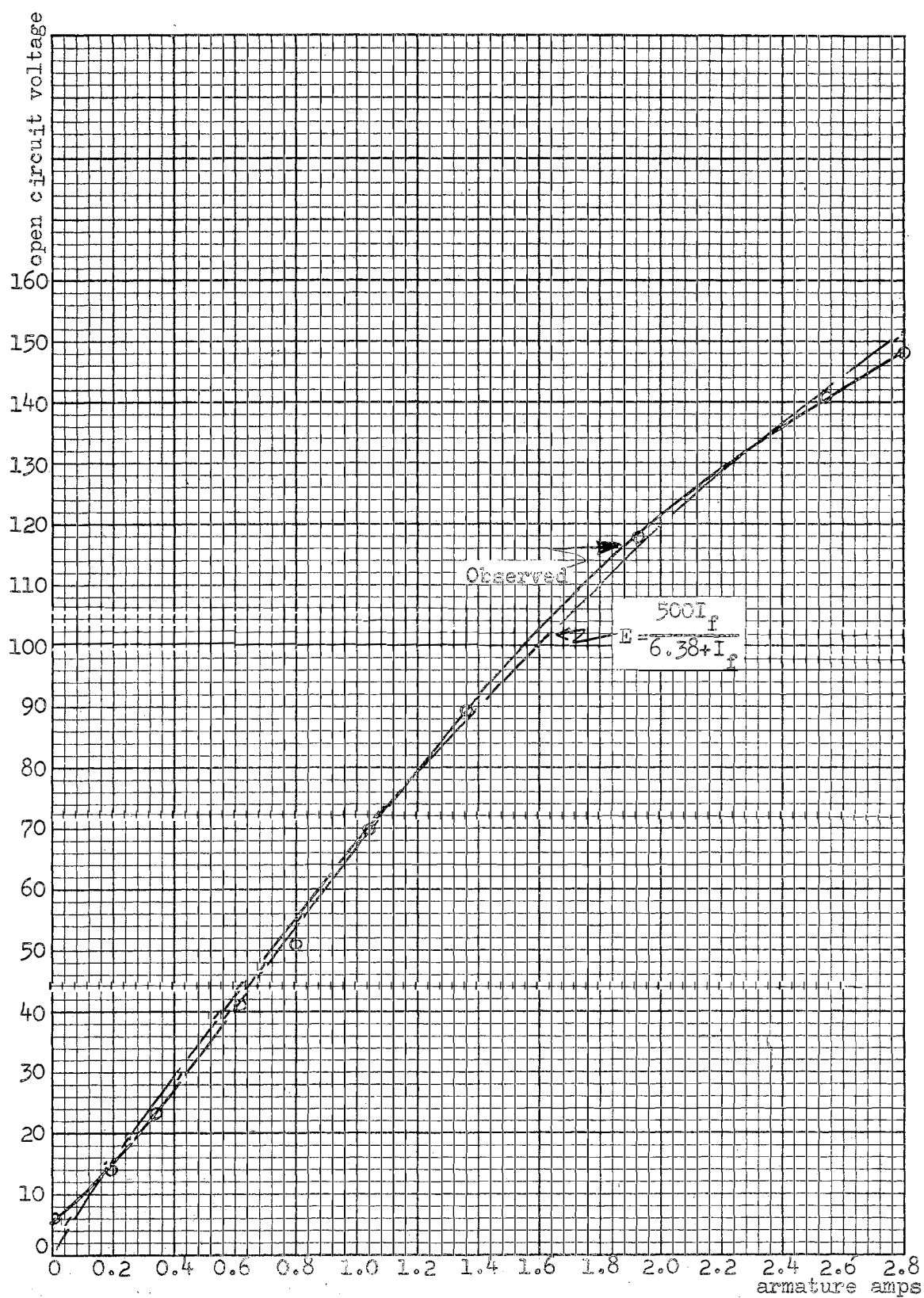


Figure 4.20: Open Circuit Characteristic (Westinghouse Generalized Machine)

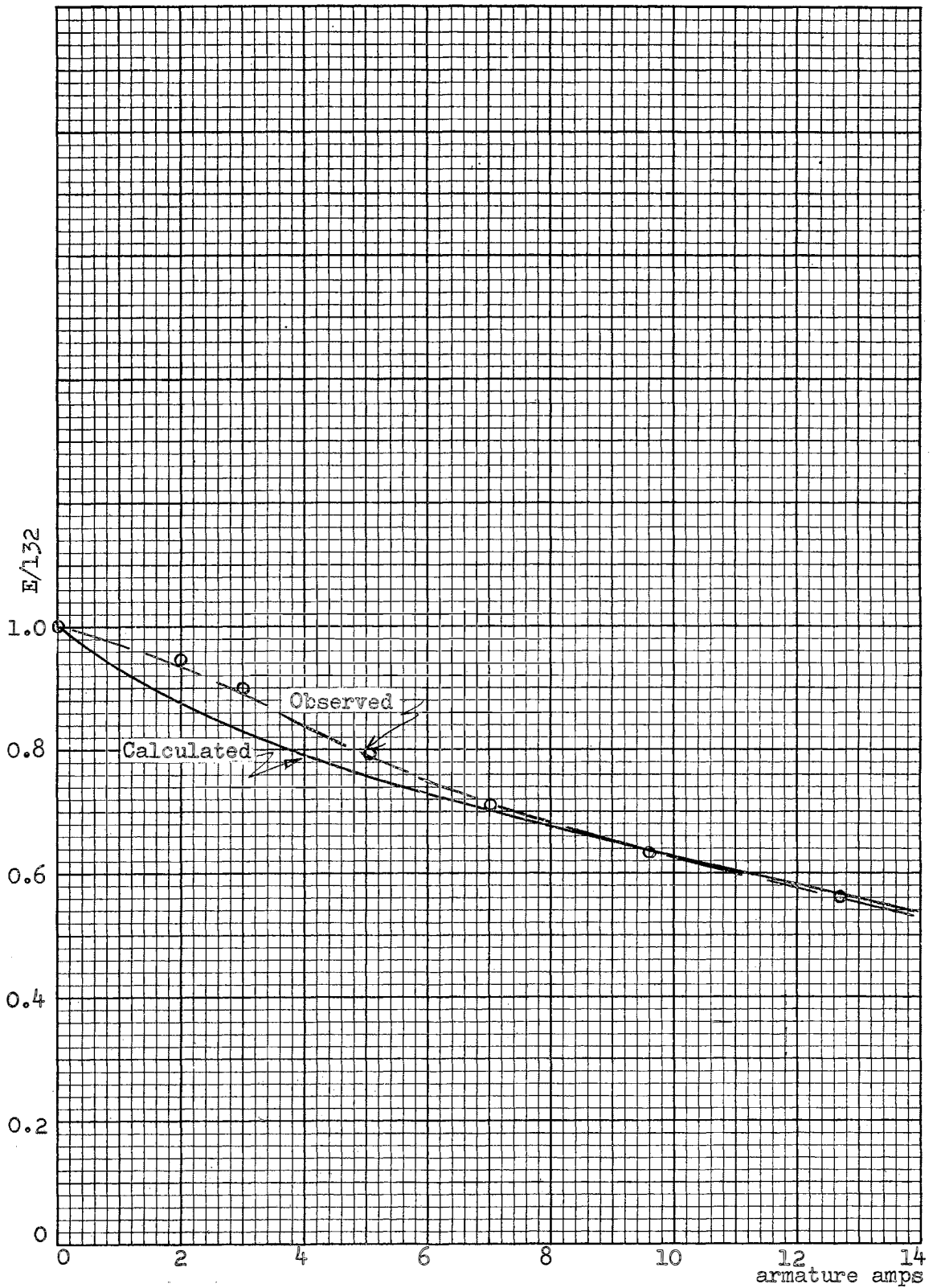


Figure 4.21. Voltage Reduction Due to Armature Reaction

$$B = \frac{1.662 I_f}{6.36 + I_f}$$

and  $D = 1.662$  ;  $G = 6.36$ .

Since the winding used for excitation in this particular machine is distributed as contrasted with the concentrated winding used for excitation in a d.c. machine of conventional design [and for which Equation (4-85) was derived], it was necessary to correct the total number of turns to obtain an effective value for use as  $N_f$ . This correction was made by considering Figure 4.22 with 36 coils, 1 coil per slot and 4 groups of 9 coils; each of the 4 poles originates by virtue of 1 group distributed over 21 slots. Thus, there is an overlapping of pole windings with each pole spanning  $\frac{21}{24} \pi$  electrical radians. By superposition, the mmf acting to establish a pole is built up as in Figure 4.22. If each coil carried unit current, the total mmf along the axis of the pole would be:

$$1 \times 21 + 1 \times 19 + 1 \times 17 + 1 \times 15 + 1 \times 13 + 1 \times 11 + 1 \times 9 + 1 \times 7 + 1 \times 5 = 117 \text{ units.}$$

If all 9 contributing coils were concentrated over 21 slots and carried unit current, the total mmf would be  $9 \times 21 = 189$  units. Thus, the total distributed winding of  $N_f$  turns behaves as if it were a concentrated winding of  $\frac{117}{189} \times N_f$  turns. For the machine used,  $N_f = 324$ ,  $\chi = \frac{21}{24} \pi$ ,  $K_1 = 0$ ,  $K_2 = 0.613$ ,  $I_f = 2.2$ ,  $G = 6.36$ . Values of  $\phi_{AR}/\phi$

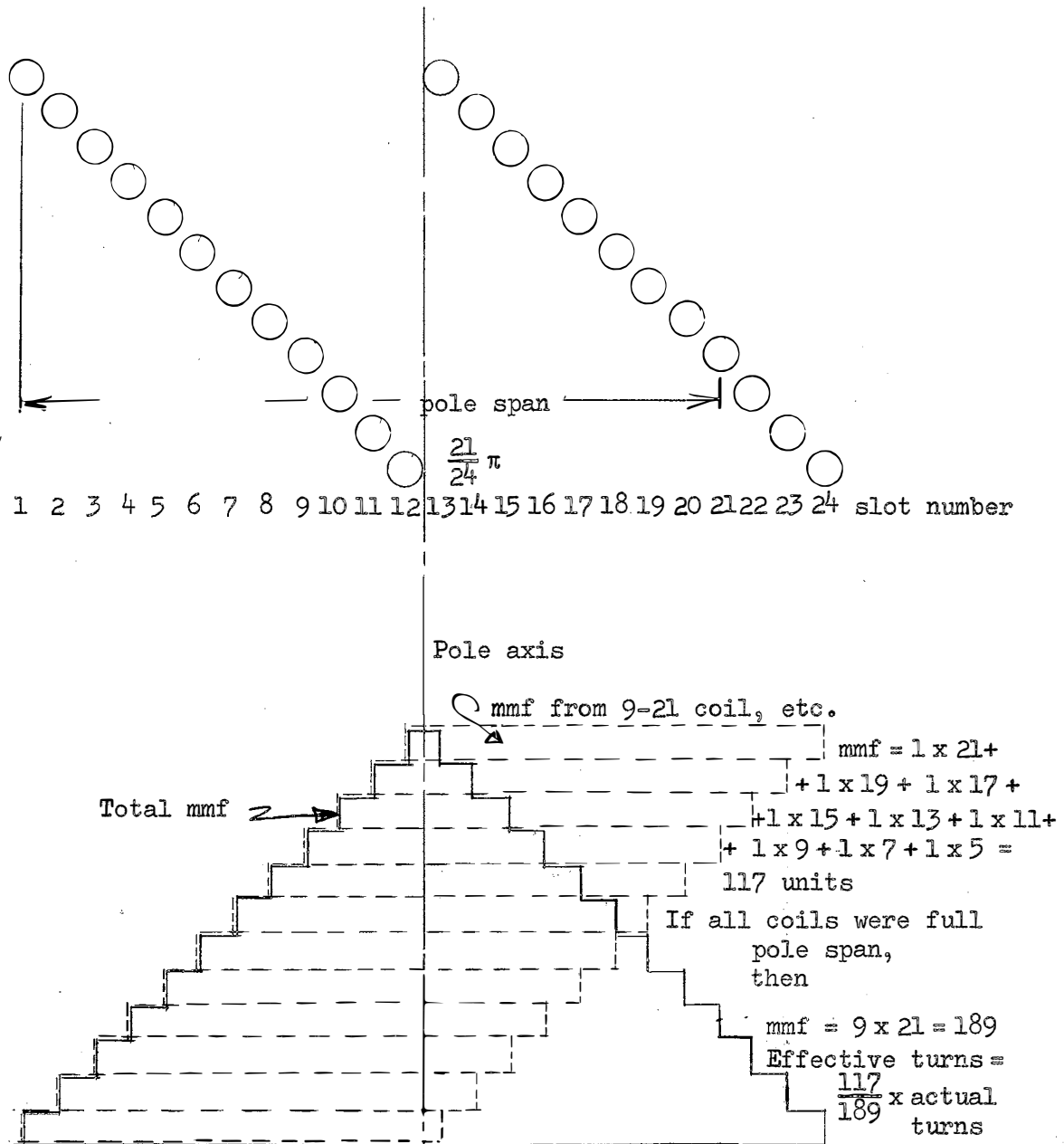


Figure 4.22. Calculation of Effective Turns  
 (Westinghouse Generalized Machine)

were calculated by using Equation (4-85) and are tabulated in Table IV-II. With constant speed,  $E$  is directly proportional to  $\Phi$ , and the normalized value of  $\Phi_{AR}$  is also the normalized value of  $E_{AR}$  or  $E_{AR}/E$  where  $E$  is the induced voltage with no armature reaction and  $E_{AR}$  is the induced voltage under the condition of armature reaction present. The machine under test was driven at 2300 rev/min with 2.2 amperes excitation and the induced voltage plus armature circuit drop was observed. The corrected value of induced voltage as a ratio with the induced voltage under the condition of no armature reaction is also tabulated in Table IV-II. The values of observed and calculated  $E_{AR}/E$  are plotted on Figure 4.21.

TABLE IV-II  
ARMATURE REACTION TEST DATA

Calculated		Observed	
I	AR/ = $\frac{E_{AR}}{E}$	I	$\frac{E_{AR}}{E}$
0	1.00	0	1.0
4.0	0.795	2.1	0.947
5.0	0.775	2.55	0.924
5.5	0.723	3.05	0.905
6.0	0.70	3.75	0.873
7.0	0.695	5.1	0.80
8.0	0.68	6.0	0.76
10	0.645	7.0	0.712
12	0.59	9.7	0.64
14	0.541	12.7	0.56



It is felt that the correspondence obtained between calculated and observed values is, within engineering accuracy, good and that Equation (4-85) can be considered as a tool in evaluation, at the design stage especially, of armature reaction effects to be encountered.

D. Coupling Between Field and Armature Circuit due to Brush Shift

If a series field is utilized, coupling exists between the armature and field circuits via the mutual inductance of the two windings. Otherwise, under the assumption of the brushes being on electrical neutral and linearity between cause and effect in the magnetic circuit, no coupling does exist between armature and field. In point of fact, however, events in the armature do have an effect upon the field configuration, not only distortion of the magnetic field, but they also have a magnetizing or demagnetizing effect upon the main field. Although events within the two portions of the device are related, the relationship is not as straightforward and as easy to predict as is phenomena associated with mutual inductance coupling. The coupling may exist because of:

- (1) brushes not located on electrical neutral,
- (2) the commutating field time lag (see Chapter IV, Sub-section E),
- (3) armature magnetomotive force or armature reaction (see Chapter IV, Sub-section C).

This section will deal with analytical evaluation of the effect of improper brush location. Although there are many references in the literature to this phenomena, they are of a qualitative nature. The derivation of the quantitative results in this section were original with this investigator.

Many machines have fixed brush locations properly located on electrical neutral. Others have moveable brush riggings which may result in the brushes being shifted from their proper position - either to accomplish sparkless commutation or inadvertently due to improper location or slippage of the rigging.

The expression for induced voltage in a d.c. machine,  $E = \frac{Z\Phi np}{60a}$ , presupposes all inductors making a positive contribution to the voltage existing between pairs of brushes at all times. Also, the torque converted from electrical to mechanical form or vice versa in a d.c. machine, with the brushes on neutral is given by Fitzgerald and Kingsley (9, p. 183):

$$T = - \frac{p^2 F_A \Phi}{\pi} \quad (4-86)$$

where:

T = torque in Newton meters

$F_A$  = armature mmf, amperes

p = number of poles

$\Phi$  = flux per pole, webers.

In order to visualize events associated with brush

shift, consider a simple two pole machine with armature inductors so finely divided they may be considered to constitute current sheets and that the field magnetomotive force is consumed in drop in magnetic potential across the two air gaps of length,  $g$ . The brushes are shifted  $\alpha$  radians from the neutral axis. Refer to Figure 4.23.

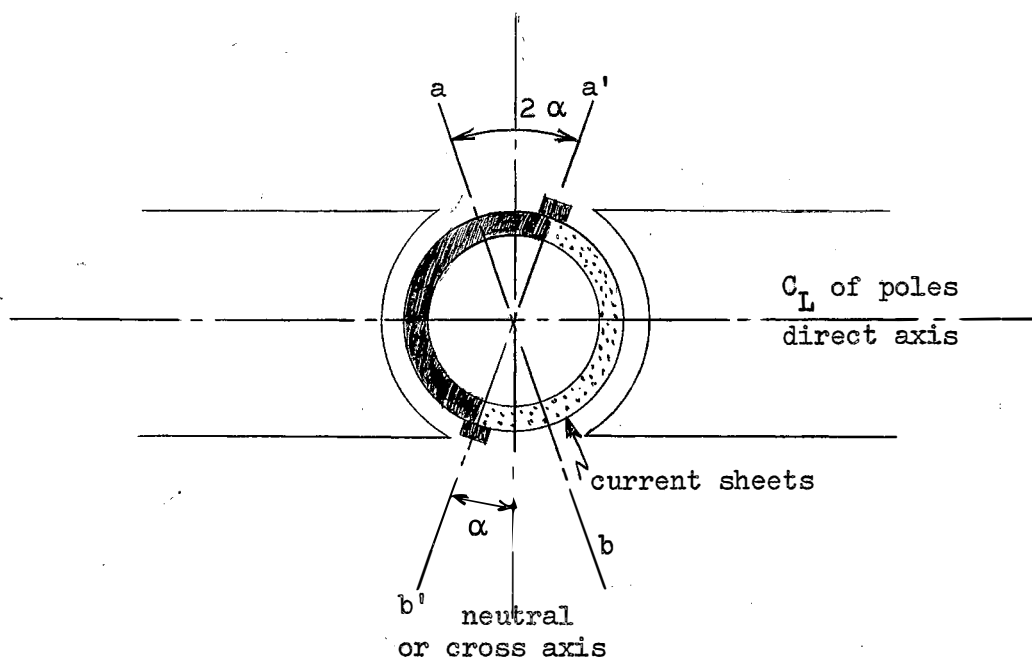


Figure 4.23. Brush Shift (Simple DC Machine)

The armature inductors between  $a - a^1$  and  $b - b^1$  establish an mmf acting along the direct axis either aiding or opposing the mmf due to the main field winding. The inductors between  $b^1 - a$  and  $a^1 - b$  establish an mmf acting along the neutral axis, or cross axis.

It is the interaction between the resulting flux from the direct axis mmf and from the cross axis mmf that is responsible for the torque produced as expressed in Equation (4-86). Equation (4-73) presents the relationship between armature mmf,  $F_A$ , armature current, and the design parameters of the machine, i.e.,

$$F_A = \frac{ZI_a}{2pa} \quad (4-87)$$

with other symbols as defined previously. Combining Equations (4-87) and (4-86) yields the well known expression for torque in a d.c. machine:

$$T = \frac{pZ\phi I_a}{2\pi a} \quad (4-88)$$

With the brushes shifted an angle  $\alpha$  from electrical neutral, the no-load voltage appearing between the brushes is reduced, because there are now only  $\left(\frac{\pi - \alpha}{\pi}\right)$  as many inductors with the same polarity voltage between brushes as there would be under the condition of no brush shift. In addition, there are  $\frac{\alpha}{\pi}$  inductors between the brushes with opposite polarity induced voltage. Thus, the induced voltage with brush shift  $E_{BS}$  is, in terms of voltage induced with no brush shift (accounting only for the loss in active inductors):

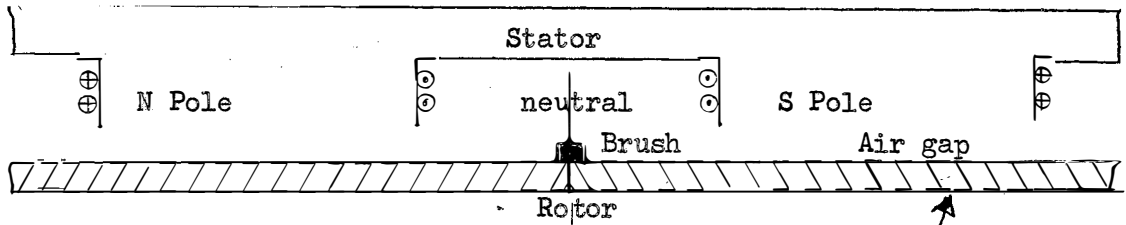
$$E_{BS} = \left(\frac{\pi - \alpha}{\pi}\right) E + \frac{\alpha}{\pi} (-E) = E \left(\frac{\pi - 2\alpha}{\pi}\right) \quad (4-89)$$

Equation (4-89) does not account for the direct axis mmf due to current flow.

With current flow, the direct axis mmf resulting can best be visualized by referring to developed views of the simple machine. Refer to Figure 4.24 for the no-brush shift situation.

The mmf, due to the main field poles, is rectangular and that due to the armature is triangular with maximum value  $\frac{ZI}{2pa}$  occurring at the brush locations [refer to Equation (4-73) for derivation of space distribution of this mmf]. With zero brush shift, this armature mmf is symmetrically located with respect to the poles and its net effect (neglecting saturation of the iron) is zero. If the brushes are shifted an angle  $\alpha$ , there is a net effect due to this mmf and it either aids or opposes the main field mmf (depending on the direction of brush shift). This can be visualized by referring to Figure 4.25, in which the armature mmf is in the same direction as the field mmf under half of the pole face and in the opposite direction under the half with a net effect of zero. Figure 4.26 portrays the relationship when the brushes are shifted an angle  $\alpha$ . As can be visualized, there is a net mmf (in this case, demagnetizing). The effect can be determined by finding the average value of armature mmf,  $F_{ave}$ , and adding or subtracting it to the main field mmf. The armature mmf can be expressed analytically as:

$$F = \frac{2F_A}{\pi} \theta + b \quad (4-90)$$



Armature winding composed of large number of inductors and considered a current sheet

Figure 4.24. Air Gap Physical Arrangement (Simple D.C. Machine)

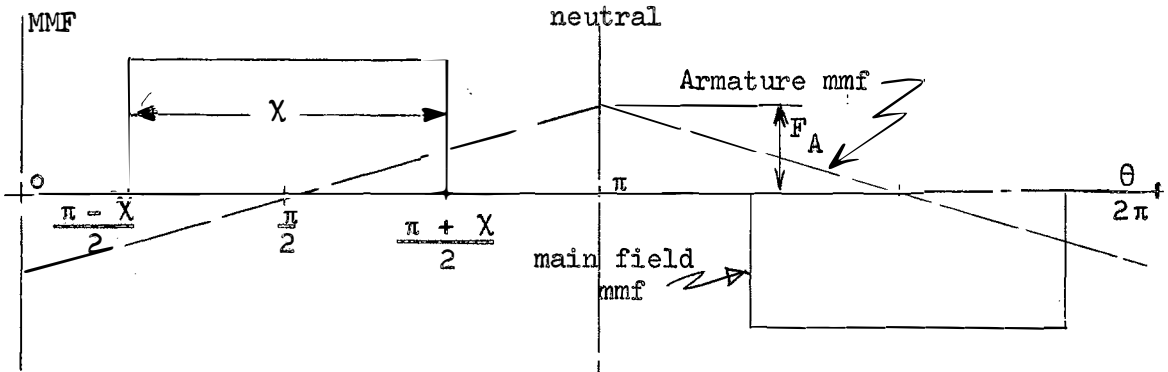


Figure 4.25. MMF Relationship, Brushes on Neutral

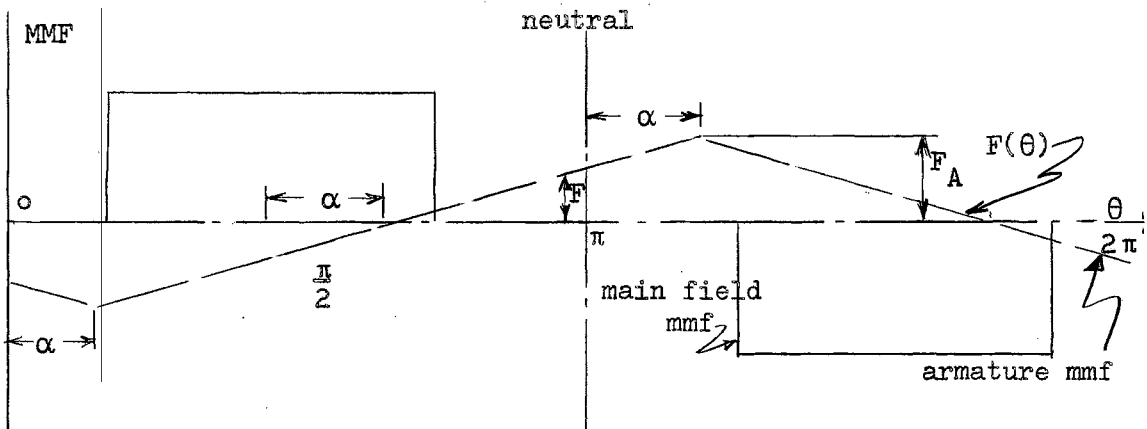


Figure 4.26. MMF Relationship, Brushes  $\alpha$  Radians Off Neutral

where  $F$  is mmf at space angle  $\theta$ :

$b$  is a constant.

$b$  can be determined when it is recognized that at  $\theta = \alpha$ ,

$$F = -F_a$$

therefore:

$$F = \frac{2F_A}{\pi} \theta - F_A \left(1 + \frac{2\alpha}{\pi}\right) \quad (4-91)$$

Now, the average value of armature mmf,  $F_{ave}$ , acting with or against the main field mmf is:

$$\begin{aligned} F_{ave} &= \frac{1}{\chi} \int_{\frac{\pi-\chi}{2}}^{\frac{\pi+\chi}{2}} F d\theta = \frac{1}{\chi} \int_{\frac{\pi-\chi}{2}}^{\frac{\pi+\chi}{2}} \frac{2F_A \theta}{\pi} - F_A \left(1 + \frac{2\alpha}{\pi}\right) d\theta \\ &= F_A \frac{2\alpha}{\pi} \text{ ampere turns.} \end{aligned} \quad (4-92)$$

Using Equation (4-87) for  $F_A$ ,

$$F_{ave} = \left(\frac{ZI}{2pa}\right) \left(\frac{2\alpha}{\pi}\right) = \frac{ZI\alpha}{pa\pi} . \quad (4-93)$$

Now, if the main field mmf is given by  $N_f I_f$ , the net mmf with brush shift is given by:

$$N_f I_f \pm \frac{ZI\alpha}{pa\pi} \quad (4-94)$$

the  $\pm$  is a sign determined by the direction of brush shift with respect to armature rotation. Also, the per unit reduction in induced voltage  $E$  would be:

$$\frac{N_f I_f \pm \frac{Z I_a}{p a \pi}}{N_f I_f} \quad (4-95)$$

Combining the two effects, reduced excitation and reduced number of active inductors, gives:

$$E_{BS} = E \frac{(N_f I_f \pm \frac{Z I_a}{p a \pi})(\pi - 2\alpha)}{N_f I_f \pi} \quad (4-96)$$

The same reasoning will lead to an expression for the effect of brush shift upon torque produced per ampere of armature current under fixed field excitation. Since there are a reduced number of inductors for producing torque and the excitation is affected by the direct axis mmf, the torque under brush shifted conditions,  $T_{BS}$ , is related to the torque under no-brush shift conditions in the same fashion as Equation (4-96), i.e.:

$$T_{BS} = T \frac{(N_f I_f \pm \frac{Z I_a}{p a \pi})(\pi - 2\alpha)}{N_f I_f \pi} \quad (4-97)$$

In order to gain perspective as to the order of magnitude involved, consider the following typical (of a large range of sizes) machine:

$$Z = 400, \quad I_a / I_f = 30 \quad ; \quad N = 1000 \quad ; \quad p = 4 \quad ; \quad a = 2$$

and assume the brushes are shifted  $\alpha = 10^\circ = \frac{\pi}{18}$  radians.

If the assumed values are inserted into Equation (4-97), the ratio of torque, as calculated, to normal torque (with



no brush shift) is

$$\frac{T_{BS}}{T} = 0.815 \text{ or } 0.962$$

depending upon the direction of brush shift relative to the direction of rotation of the armature.

The situation, with respect to this analysis, is much the same as that concerning armature reaction. The phenomena accompanying improper brush location has been long recognized, but the literature makes no mention of efforts to arrive at quantitative expressions such as Equations (4-96) and (4-97).

In order to demonstrate the validity of this derivation, the Westinghouse Electric Corporation Generalized Machine set, with brush shifting provision, was used. The rotor has the following design constants:

$$\begin{aligned} & 2 \text{ pole lap winding, } a = 2 \quad p = 2 \\ & Z = 560 \text{ inductors} \\ & N_f = 324 \text{ (effective).} \end{aligned}$$

In order to minimize saturation effects, the machine was operated at a low value of main field excitation and driven at a constant speed of 2800 rpm. After determining residual voltage and no-load induced voltage, constant current load was maintained while shifting the brushes through angles up to 40° both with and against direction of rotation of armature. The terminal voltage was observed and

recorded. Adding the armature  $iR$  drop and subtracting the residual voltage (to obtain induced voltage due to shunt field mmf) gave the induced voltage due to the net mmf in the direct axis. This is the voltage reduced by the effect of brush shift which, of course, is also manifested at the machine terminals.

Table IV-III details the calculated and observed values of  $E_{ss}/E$  for a range of brush shift of  $\pm 40^\circ$ . The results are plotted in Figure 4.27.

It is felt that the discrepancies are due to inevitable heating due to brush sparking and due to the fact that, although the flux density was kept low within the machine, nonlinearity is present, to a small degree everywhere on the saturation characteristic, and this would result in differences from calculated values because Equation (4-95) is derived for a linear relationship. Thus it is felt that the analytical work is verified by the experimental work. In particular the demagnetizing effect can be contrasted with the magnetizing effect present when direction of brush shift is reversed.

#### E. Commutating Field Time Lag

Induced voltage and torque in a d.c. machine are dependent upon total flux per pole and are not affected (in magnitude) by the actual flux density distribution, unless the distribution is such as to interfere with the commutation process. (9). When this happens, sparking accompanied

TABLE IV-III  
BRUSH SHIFT DATA

$\alpha$	$E_{BS}$ calc	$E_{BS}/E$ calc	$E_{BS}$ obs	$E_{BS}/E$ obs
0	38.5	1.00	38.5	1.00
10	35.4	0.92	37.5	0.97
20	33.0	0.86	35.0	0.91
30	29.0	0.75	31.3	0.81
40	26.0	0.68	26.9	0.70
-10	37.7	0.98	38.2	0.99
-20	36.2	0.94	36.3	0.94
-30	34.0	0.88	33.3	0.87
-40	31.0	0.80	30.0	0.78

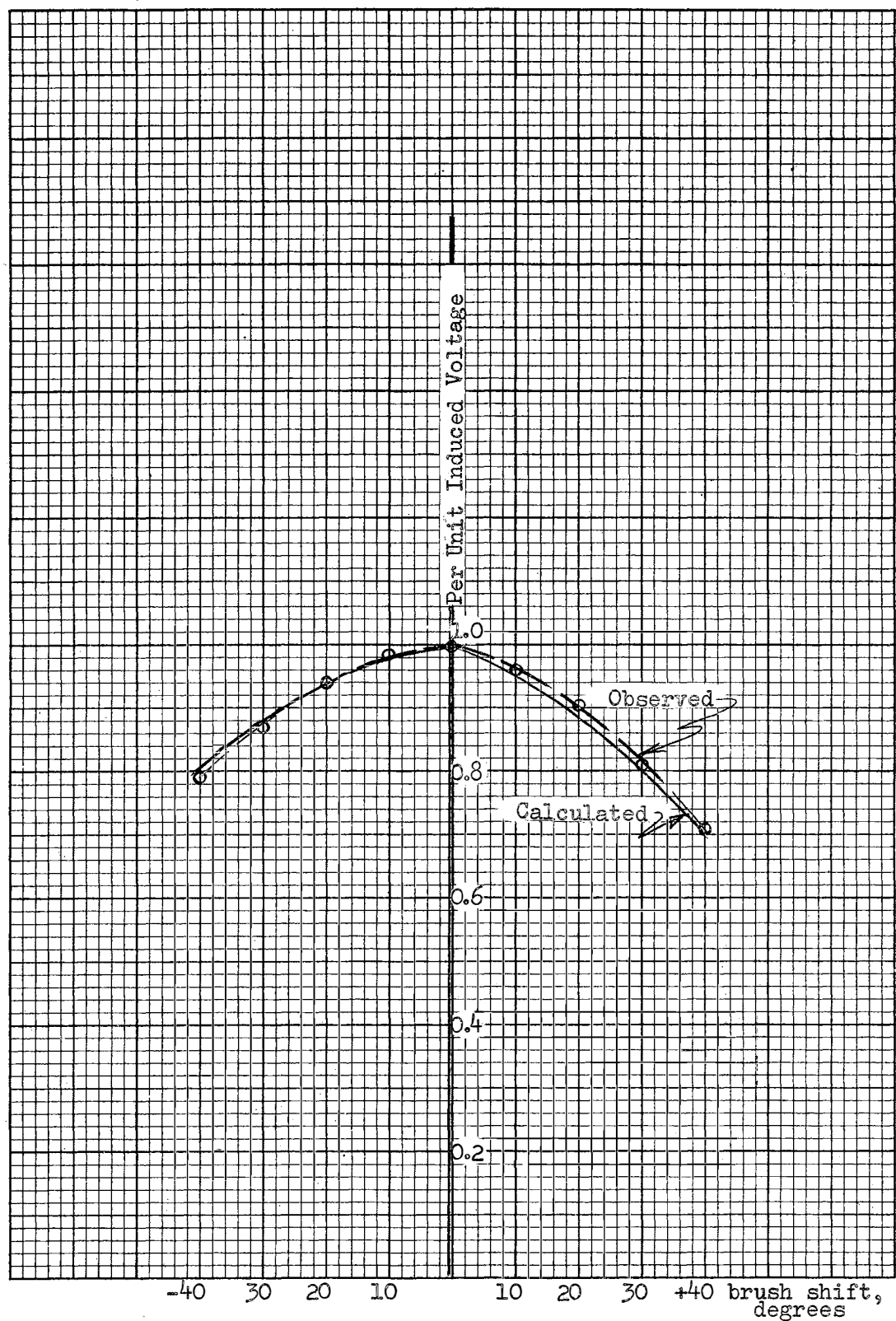


Figure 4.27. Induced Voltage as a Function of Brush Shift (Westinghouse Generalized Machine)

by local losses occur, and, besides being detrimental to the mechanical aspects of the motor, it alters the electromechanical equations written to describe the behavior of the machine. Commutation analysis is a function of so many variables, including brush material, atmospheric conditions, commutator surface condition, etc., that it is a task of extreme difficulty to describe it quantitatively. Even then, with an infinite number of possible combinations, the results may be meaningless in specific cases. Accordingly, this thesis will treat the avoidance of difficulty rather than mathematically describing the difficulty.

The commutating, or interpole winding lies in, and acts along, the cross axis. It does not participate in events along the main axis if it is connected with the proper polarity, has a strength proportional to armature current and the proper number of ampere turns. (It is, of course, possible to connect the winding in backwards.) With insufficient interpole effect, the commutation process is delayed (electrically) due to the self and mutual inductance of the coil undergoing commutation. In a motor, "under" commutation results in direct axis magnetizing effect. (9). Thus, "under" commutation (the current in the commutating coil changes less rapidly than linearly with respect to time) results in a magnetizing force opposing any demagnetizing effect due to armature mmf, treated in Chapter IV, Sub-section C. Since commutation

occurs regularly, it is a periodic transient phenomena which occurs even in steady state operation.

Over commutation (current in the commutated coil changing more rapidly than linearly with respect to time) results in a demagnetizing effect in the main axis of the motor. The brushes can be shifted to aid commutation, but must be shifted in such a manner as to establish a demagnetizing effect in the main axis (against the direction of rotation in a motor). Also, as shown in Chapter IV, Subsection D, this reduces the cross axis mmf and the combination has a very adverse effect on both torque and voltage relationships.

If interpoles, or a commutating winding, of more turns than necessary are installed for the purpose of aiding commutation, the proper number of ampere turns can be secured by diverting a portion of the armature current through a resistor connected in parallel with the commutating winding or by altering the magnetic circuit in the cross axis so as to cause the ampere turn requirement to coincide with the ampere turns existing with full armature current through the winding. From a dynamic (transient) operating standpoint, the former option will be useful if the sparking during transient periods can be tolerated, as will be demonstrated below.

Consider a commutating winding with total inductance,  $L$ , resistance,  $R$ , and shunted by a resistance,  $R_1$ , as shown in Figure 4.28 ( $R_1$  is to reduce the too many turns

winding to a winding of proper ampere-turn strength).

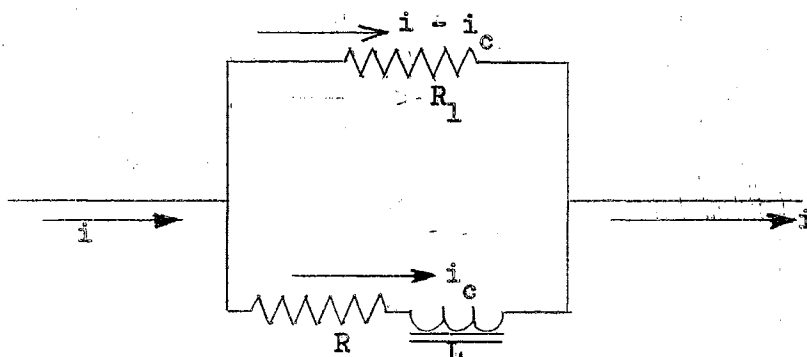


Figure 4.28. Commutating Field Equivalent Circuit

where the branch with  $R$  and  $L$  represents the commutating field circuit and  $R_1$  represents the shunting resistor.

From Kirchoff's Law:

$$R_1 i - R_1 i_c = L \frac{di_c}{dt} + R i_c \quad (4-98)$$

Assume  $i$  has a value (steady) of  $I_0$  and that some disturbance causes a step increase to  $I_D$  amperes. Transforming, by Laplace transforms, gives:

$$R_1 I(S) = [(R + R_1) + sL] I_c(S) - \frac{LR_1}{R + R_1} I_0 \quad (4-99)$$

Since  $I(S) = \frac{I_D}{s}$ , Equation (4-96) can be arranged and transformed to the time domain as:

$$i_c = \frac{R_1 I_D}{R_1 + R} \left( 1 - e^{-\frac{R_1 + R}{L} t} \right) + \frac{R_1 I_0}{R_1 + R} e^{-\frac{R + R_1}{L} t} \quad (4-100)$$

Thus, there is a transient period during which the commutating field is understrength due to the delay in current  $i_c$ . The result is under commutation with a direct magnetizing effect which can, in part, compensate for demagnetizing effects of armature mmf.

If nonmagnetic shims are placed in the interpole magnetic circuit, the mmf established by the interpole has the proper strength for desirable commutation, under transient or steady state conditions, because the mmf and flux established by the changing armature current are always of the proper magnitude. However, placing a resistance in shunt with the winding (as developed above) is a more desirable situation during any transient period such as load changes. Since the commutating field, during the transient period, is understrength, sparking will result. Thus, the aiding effect of the under commutation, insofar as direct axis magnetizing effect is concerned, is available at the expense of "proper" (sparkless) commutation during the transient period.

#### F. Armature Potential Drop due to Carbon Brushes

Various standards on testing of d.c. machines allow a constant two-volt drop in potential through the armature circuit to account for the effects of the carbon brushes and the carbon brush-copper commutator contact film. (19). As a standard procedure to follow in testing and specification, this is doubtless the most expedient method of



dealing with this variable quantity which is so difficult to assess with a high degree of accuracy. However, the literature, particularly by Saunders (18), discusses the non-constant drop in potential which has been observed in various tests. The discussion section by Saunders (18) deals with observations made in connection with a shunt connected 90 hp, 250 volt, 1750 rpm motor. Within a range of 30% of rated current, the effective armature resistance was essentially constant. At 67% above and below rated current, the effective armature resistance had changed (increased) by a factor of 67% at higher speeds and by a factor of 30% for relatively lower speeds and the trend of the data indicates a 100% change (increase) in effective armature resistance at both zero current and at 200% rated current. At zero speed, or very slow speeds, effective armature resistance is the main factor in determining current magnitude (and, thus, torque output of the machine). At near rated speeds, the current is limited by both effective armature resistance and induced rotational voltage. A large error in effective armature resistance introduces a much larger error in speed-torque calculations at low speeds than at near rated speeds.

Due to the complexity introduced in mathematical analysis by the varying voltage drop in the armature, the main utility of the above information is in qualitative explanation of departures from theoretical performance derived from mathematical analysis.

## G. Induced Currents in Closed Conducting Circuits

When a winding is switched, changes of flux linkages occur, and every change in flux linkages induces a voltage in any circuit contributing to the total flux linkages. The core structure itself forms a closed conducting circuit and eddy currents circulate throughout the core. This phenomena was discussed and analyzed in Sub-section C of this chapter. Other closed conducting circuits are formed by fastener circuits used to secure laminated cores and by armature inductors shorted from commutator bar-to-bar by the brushes and, thus, establishing a conducting circuit closed upon itself. The direction of the induced eddy currents and the currents flowing in the other closed circuits is in such a direction as to oppose any change in flux linking that particular circuit. In effect, a changing flux induces a voltage and currents flow which cause a field to be established which manifests itself in the original winding as a voltage drop, similar in nature to the voltage of self induction, which tends to retard the exciting current. In addition to delaying build up of field excitation current, the circulating current tends to demagnetize the magnetic structure by virtue of its circulating current. This same phenomena exists in every closed circuit linked by the changing flux. This portion of the thesis is concerned with the effect upon time of response of the switched winding and the core flux by the circulating

currents within the closed circuits mentioned above.

The derivation presented here is original with this investigator. However, there are so many variables which can vary from unit to unit, such as lamination tightness, brush seat condition, etc., that it is almost impossible to apply the results to a specific machine, or to characterize the phenomena by the degree of influence it wields in altering predicted performance. Its usefulness lies in pointing out the manner in which the variables influence the performance, suggesting possible means of minimizing the effects in the design stage.

A circuit can be formed by the lamination fastening circuit as shown in Figure 4.29 or Figure 4.30.

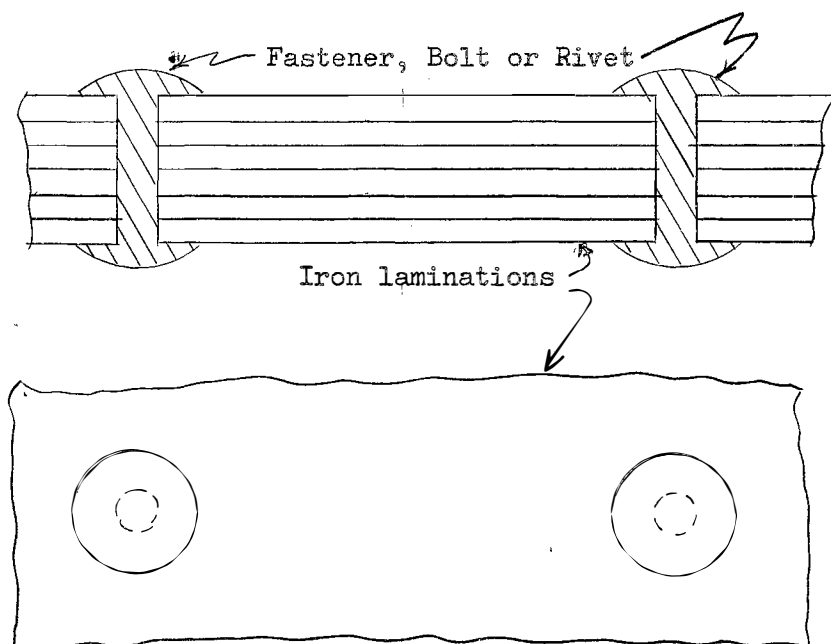


Figure 4.29. Lamination Fastener Arrangement (Bolted or Riveted)

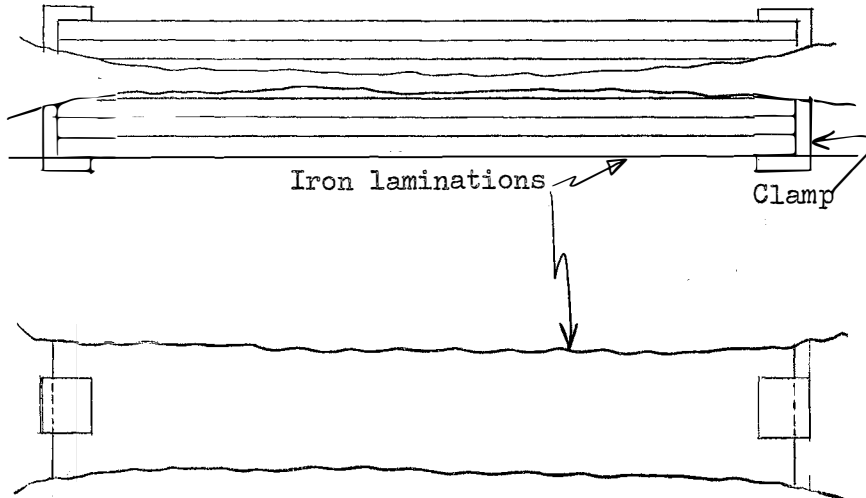


Figure 4.30. Lamination Fastener Arrangement  
(Clamp)

A multiturn closed circuit can be formed by the armature circuit as shown in Figure 4.31.

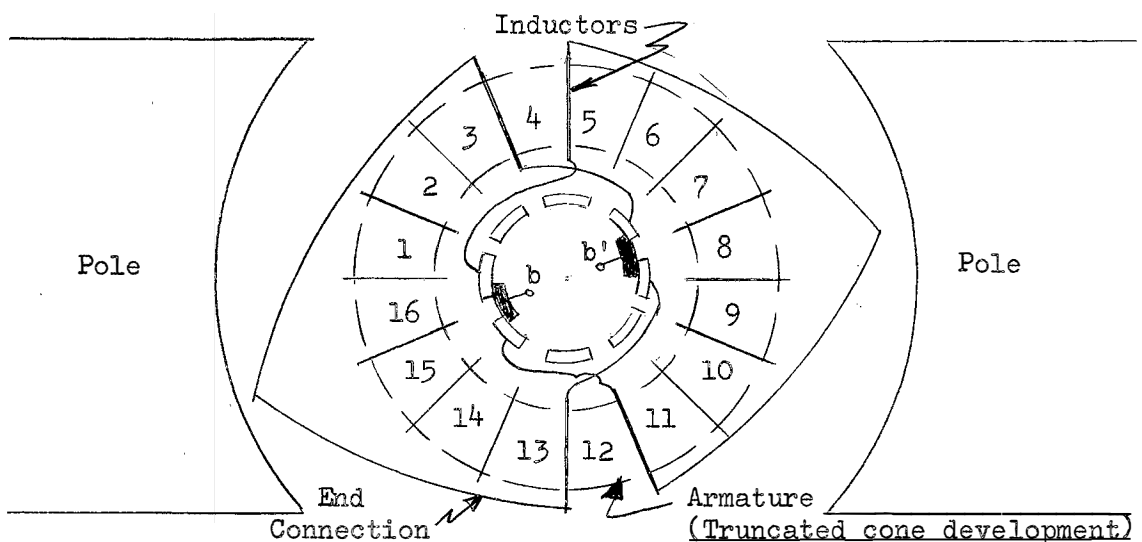



Figure 4.31. Closed Circuits Formed on Armature for  
Simple Winding

Figure 4.31 is a conical projection of a two-pole machine with 16 slots (single layer winding). Only the inductors forming closed circuits are shown connected in the interest of clarity. The commutator bars are shown as  and the brushes are shown in black, b - b'. As can be seen, inductors 12 and 5 form a closed circuit, as do inductors 4 and 13. The closed circuits shown span very nearly a complete pole and can be considered to link all of the main field flux.

For purposes of analysis, consider a laminated magnetic structure with  $q$  rows of fasteners with two fasteners per row (designated an "a" turn), each fastener circuit of resistance  $R_a$  and spanning the fraction  $\gamma$  of the total width of the magnetic circuit. Under the assumption of negligible leakage flux, the fraction  $\gamma$  of the total core flux links this closed circuit;  $r$  closed circuits of  $N_b$  turns each (such as would be formed on the armature by the short circuiting of adjacent bars of the commutator by the brushes)(designated a "b" winding), which have a resistance  $R_b$  and span the total width of the magnetic circuit; and a winding of  $N$  turns (designated the "n" winding) providing excitation for the magnetic structure.

The self inductance of each circuit can be calculated from the relationship:

$$L = \frac{N\phi}{i} = \frac{N^2\phi}{Ni} \quad (4-101)$$

and, since the reluctance  $\bar{R}$  is  $\frac{Ni}{\phi}$  by definition, Equation (4-101) can be expressed as:

$$L = \frac{N^2}{\bar{R}} . \quad (4-102)$$

Then, if the self inductance of the excitation winding is  $L_n$ ,  $\bar{R} = \frac{N^2}{L_n}$  from Equation (4-102). The self inductance  $L_b$  of each of the  $r$  full width,  $N_b$  turns windings is, under the no leakage assumption, and since it sees the same reluctance as the excitation winding:

$$L_b = \frac{N_b^2}{\bar{R}} = \frac{N_b^2}{N^2} L_n = \frac{L_n}{N^2} N_b^2 . \quad (4-103)$$

For the  $q$  fractional width windings, the reluctance as seen by these windings is larger than above and is:

$$\bar{R}_a = \frac{\bar{R}}{\gamma} \quad (4-104)$$

since reluctance is inversely proportional to area and this area is only  $\gamma$  times as great as for full width windings. ( $0 < \gamma \leq 1.0$ )

and:

$$L_a = \frac{l^2}{\bar{R}_a} = \frac{\gamma}{\bar{R}} = \frac{\gamma L_n}{N^2} . \quad (4-105)$$

To calculate the mutual inductances, consider that each "a" turn links all other "a" turns, all "b" windings and the main, or  $n$ , winding. In addition, each "b" winding links all other "b" windings, all "a" turns, and the

main winding, and the main winding links all "b" windings and "a" turns. Thus, the mutual inductances will be:

$$M_{a-a} \quad , \quad M_{a-b} \quad , \quad M_{a-n}$$

$$M_{b-b} \quad , \quad M_{b-a} \quad , \quad M_{b-n}$$

$$M_{n-a} \quad , \quad M_{n-b} \quad .$$

From considerations of symmetry:

$$M_{a-n} = M_{n-a}$$

$$M_{b-n} = M_{n-b} \quad (4-106)$$

$$M_{a-b} = M_{b-a} \quad .$$

With no leakage flux, the mutual inductance,  $M_{1-2}$ , between two windings with self inductances  $L_1$  and  $L_2$  is

$$M_{1-2} = \sqrt{L_1 L_2} \quad . \quad (4-107)$$

Equation (4-107) can be used to calculate the values expressed in Equation (4-108). Thus:

$$M_{a-a} = \frac{\gamma L_n}{N^2} \quad , \quad M_{b-b} = \frac{L_n}{N^2} N_b^2 \quad (4-108)$$

$$M_{a-n} = M_{n-a} = \sqrt{\frac{L_n \gamma L_n}{N^2}} = \frac{L_n}{N} \sqrt{\gamma} \quad (4-109)$$

$$M_{b-n} = M_{n-b} = \sqrt{\frac{L_n L_n}{N^2}} N_b = \frac{L_n N_b}{N} \quad (4-110)$$

$$M_{a-b} = M_{b-a} = \sqrt{\frac{L_n N_b^2}{N^2} \frac{\gamma L_n}{N^2}} = \frac{L_n}{N^2} \sqrt{\gamma} N_b \quad . \quad (4-111)$$

It is now possible to write Kirchoff's voltage equation for each of the closed windings present, but since all "a" turns have the same current and all "b" windings the same current, it will be necessary to write only three equations (one for the main winding, one for an "a" turn, and one for a "b" winding) to solve for the three different currents.

Assume a step voltage of magnitude  $V$  is impressed upon the main winding and that all circuits are at rest for time  $t \leq 0$ .

$$Ri_n + \frac{L_n di_n}{dt} + qM_{a-n} \frac{di_a}{dt} + rM_{b-n} \frac{di_b}{dt} = V. \quad (4-112)$$

$$M_{n-a} \frac{di_n}{dt} + L_a \frac{di_a}{dt} + (q-1)M_{a-a} \frac{di_a}{dt} + R_a i_a + rM_{a-b} \frac{di_b}{dt} = 0. \quad (4-113)$$

$$M_{n-b} \frac{di_n}{dt} + qM_{a-b} \frac{di_a}{dt} + L_b \frac{di_b}{dt} + (r-1)M_{b-b} \frac{di_b}{dt} + R_b i_b = 0. \quad (4-114)$$

Using values of self and mutual inductance from above, transforming by the use of Laplace Transforms results in:

$$(R + L_n s)I_n(s) + q \frac{L_n}{N} \sqrt{Y} sI_a(s) + \frac{rL_n}{N} N_b sI_b(s) = \frac{V}{s}. \quad (4-115)$$



$$\frac{L_n}{N} \sqrt{Y} s I_n(S) + (R_a + q s \frac{Y}{N^2} L_n) I_a(S) + r \frac{s}{N^2} L_n N_b \sqrt{Y} I_b(S) = 0 .$$

(4-116)

$$\frac{L_n}{N} N_b s I_n(S) + q \frac{L_n}{N^2} N_b \sqrt{Y} s I_a(S) + (R_b + r s \frac{L_n}{N^2} N_b^2) I_b(S) = 0 .$$

(4-117)

Equations (4-115), (4-116), (4-117) can be solved by applying Cramers Rule:

$$\Delta I_n(S) = \begin{vmatrix} \frac{V}{s} & q \frac{L_n}{N} \sqrt{Y} s & \frac{r L_n}{N} N_b s \\ 0 & R_a + \frac{s Y}{N^2} L_n q & \frac{r s L_n}{N^2} N_b \sqrt{Y} \\ 0 & q \frac{L_n N_b}{N^2} \sqrt{Y} s & R_b + r \frac{s L_n}{N^2} N_b^2 \end{vmatrix}$$

$$= \frac{R_a R_b}{s} V \left[ 1 + s \frac{q Y L_n}{N^2 R_a} + \frac{r L_n}{N^2 R_b} \right] \quad (4-118)$$

noting that  $\frac{Y L_n}{N^2} = L_a$  ,  $\frac{L_n}{N^2} N_b^2 = L_b$  , and defining  $\frac{L_b}{R_b}$  and  $\frac{L_a}{R_a}$  as the time constants,  $T_b$  and  $T_a$ , in the usual sense, of each winding a and b, Equation (4-118) can be written as:

$$\Delta I_n(S) = \frac{R_a R_b}{s} V [1 + s(q T_a + r T_b)] . \quad (4-119)$$

Also:

$$\Delta I_a(S) = \begin{vmatrix} (R + L_n s) & \frac{V}{s} & \frac{r L_n}{N} N_b s \\ \frac{L_n \sqrt{\gamma}}{N} s & 0 & r \frac{s L_n}{N^2} N_b \sqrt{\gamma} \\ \frac{L_n N_b}{N} s & 0 & (R_b + r \frac{s L_n}{N^2} N_b^2) \end{vmatrix}$$

$$\Delta I_a(S) = - \frac{V L_n \sqrt{\gamma} R_b}{N} \quad (4-120)$$

and

$$\Delta I_b(S) = \begin{vmatrix} R + L_n s & q \frac{L_n \sqrt{\gamma}}{N} s & \frac{V}{s} \\ \frac{L_n \sqrt{\gamma}}{N} s & R_a + q \frac{s \gamma}{N^2} L_n & 0 \\ \frac{L_n N_b}{N} s & q \frac{L_n N_b}{N^2} \sqrt{\gamma} s & 0 \end{vmatrix}$$

$$\Delta I_b(S) = - \frac{V L_n R_a}{N} N_b \quad (4-121)$$

 $\Delta$  is evaluated by:

$$\Delta = \begin{vmatrix} R + L_n s & q \frac{L_n \sqrt{\gamma}}{N} s & r \frac{L_n}{N} N_b s \\ \frac{L_n \sqrt{\gamma}}{N} s & R_a + q \frac{s \gamma}{N^2} L_n & r \frac{s L_n}{N^2} \sqrt{\gamma} N_b \\ \frac{L_n N_b}{N} s & q \frac{L_n \sqrt{\gamma}}{N^2} N_b s & R_b + \frac{r s}{N^2} L_n N_b^2 \end{vmatrix}$$

$$= R R_a R_b [1 + s(q T_a + r T_b + T_n)] \quad (4-122)$$

where  $T_a$  and  $T_b$  are as defined above and:

$$T_n = \frac{L_n}{R} . \quad (4-123)$$

Using Equations (4-119), (4-120), (4-121), and (4-122) results in:

$$I_n(S) = \frac{V}{R} \frac{[1 + s(q T_a + r T_b)]}{s[1 + s(q T_a + r T_b + T_n)]} . \quad (4-124)$$

$$I_a(S) = - \frac{VY}{NR_a} T_n \frac{1}{[1 + s(q T_a + r T_b + T_n)]} . \quad (4-125)$$

$$I_b(S) = - \frac{VT_n N_b}{NR_b} \frac{1}{[1 + s(q T_a + r T_b + T_n)]} . \quad (4-126)$$

As functions of time, Equations (4-124), (4-125), and (4-126) are determined by performing the inverse Laplace Transformation, resulting in:

$$i_n(t) = \frac{V}{R} \left[ 1 - \frac{T_n}{q T_a + r T_b + T_n} \epsilon^{-\frac{t}{q T_a + r T_b + T_n}} \right] \quad (4-127)$$

$$i_a(t) = - \frac{VY T_n}{NR_a} \left[ \frac{1}{q T_a + r T_b + T_n} \epsilon^{-\frac{t}{q T_a + r T_b + T_n}} \right] \quad (4-128)$$

$$i_b(t) = - \frac{VT_n N_b}{NR_b} \left[ \frac{1}{q T_a + r T_b + T_n} \epsilon^{-\frac{t}{q T_a + r T_b + T_n}} \right] \quad (4-129)$$

Since:

$$L_a = \frac{\gamma L_n}{N^2} \quad ; \quad L_b = \frac{L_n N_b^2}{N^2} \quad ; \quad L_n = \frac{L_n}{R}$$

and denoting  $T_n + q T_a + r T_b = T$ .

Equations (4-127), (4-128), and (4-129) can be expressed as:

$$i_n(t) = \frac{V}{R} \left( 1 - \frac{T_n}{T} \epsilon^{-t/T} \right) \quad (4-130)$$

$$i_a(t) = - \frac{V}{R} \left( \frac{NT_a}{T} \epsilon^{-t/T} \right) \quad (4-131)$$

$$i_b(t) = - \frac{V}{R} \left( \frac{N}{N_b} \frac{T_b}{T} \epsilon^{-t/T} \right). \quad (4-132)$$

The specific effect on the excitation circuit by the closed circuits and eddy current formation is to increase the apparent time constant of the circuit - or in other words, the time required for main field excitation current to reach a certain value is increased. The over-all effect of importance to transient analysis is that the net excitation tending to establish a magnetic field is reduced because the transient currents in the closed conducting circuits have a magnetizing effect opposite to that of the main winding. If one considers the  $q$  circuits associated with  $L_a$ ,  $R_a$  as fastener circuits and the  $r$  circuits associated with  $L_b$ ,  $R_b$  as being shorted armature inductor circuits, it is theoretically possible to determine the net

magnetizing force in the magnetic circuit. It should be noted that  $R_b$  can vary between wide limits, being a function of the "tightness" with which the core is secured, core dimensions, fastener resistivity and dimensions, and lamination insulation. Since the fastener is made up with relatively large cross sectional area,  $R_b$  can be quite low, making  $T_b$  possibly on the order of magnitude of  $T_n$ . In order to experimentally verify the analytically predicted effects of the closed circuits discussed in this section, it would be necessary to account for other phenomena discussed earlier, i.e.:

- (i) the nonlinear relationships in the core
- (ii) eddy currents induced in the core structure
- (iii) the effect of armature reaction
- (iv) the effect of changing brush contact resistance
- (v) alterations in the commutating process during the transient period.

Attempts to cope, analytically, with all of these factors is not feasible due mainly to the complex geometry of the machine. Superposition of the individual factors is not possible because of the nonlinearities involved.

The influence of all these factors can be visualized by reference to Figures 4.32, 4.33, and 4.34.

Figure 4.32 is a plot of shunt field current as a function of time as actually measured when a step voltage of rated value was impressed on the shunt field of a motor, (General Electric Model 5BC44AB65F,  $\frac{1}{4}$  hp, 115 volts, d.c.)

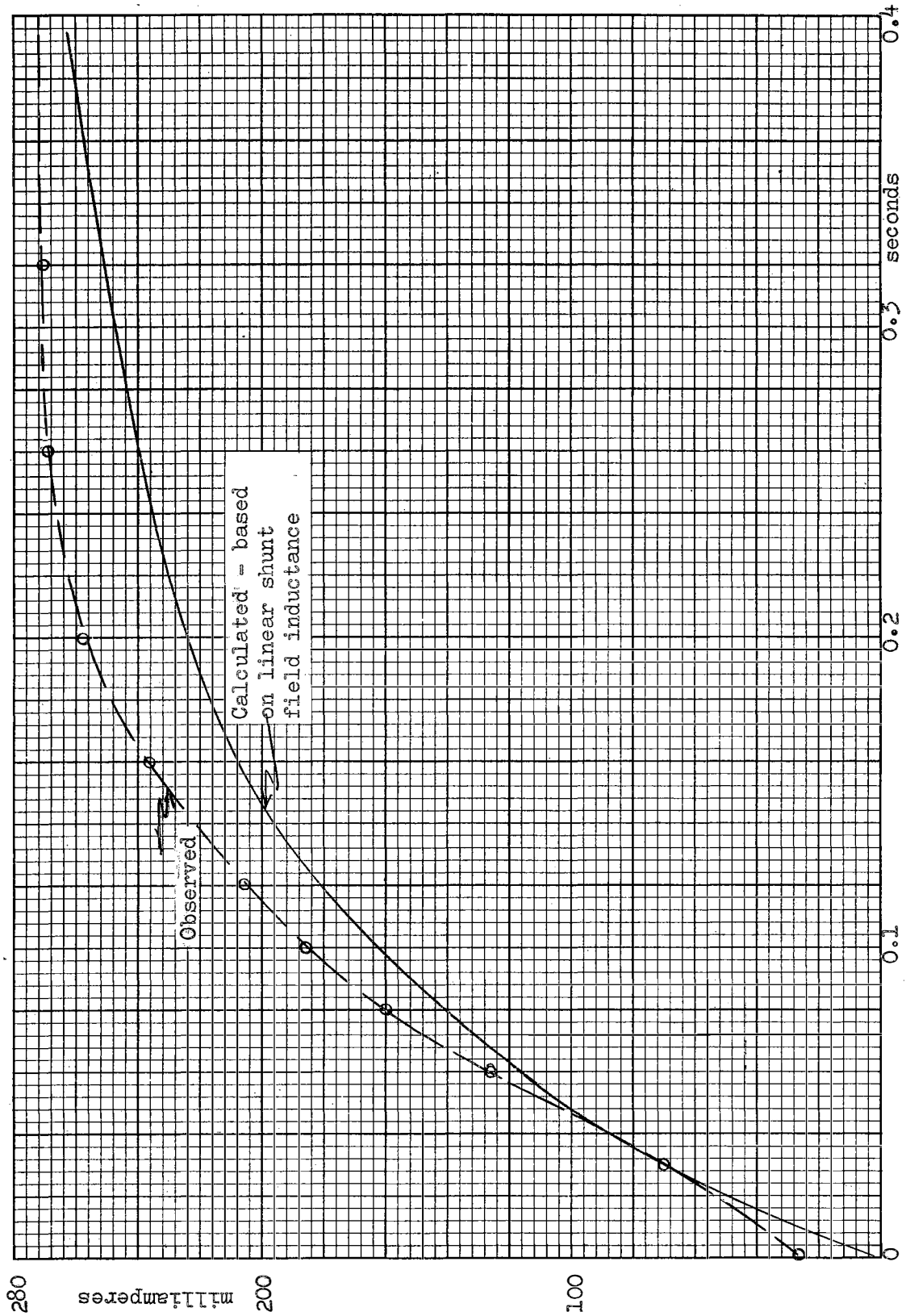


Figure 4.32. Field Current Buildup

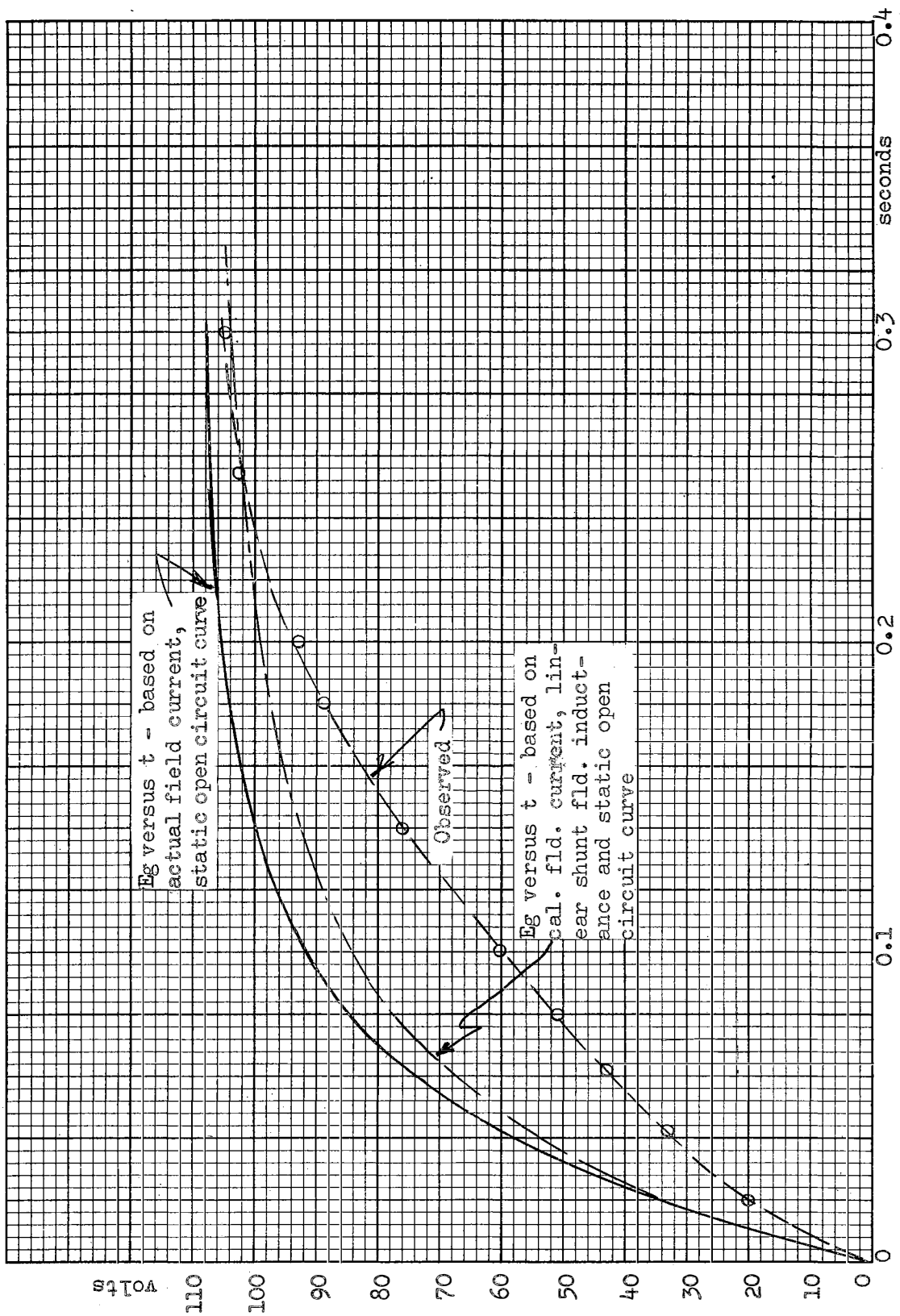


Figure 4.33. Induced Voltage Buildup (Step Voltage on Field)

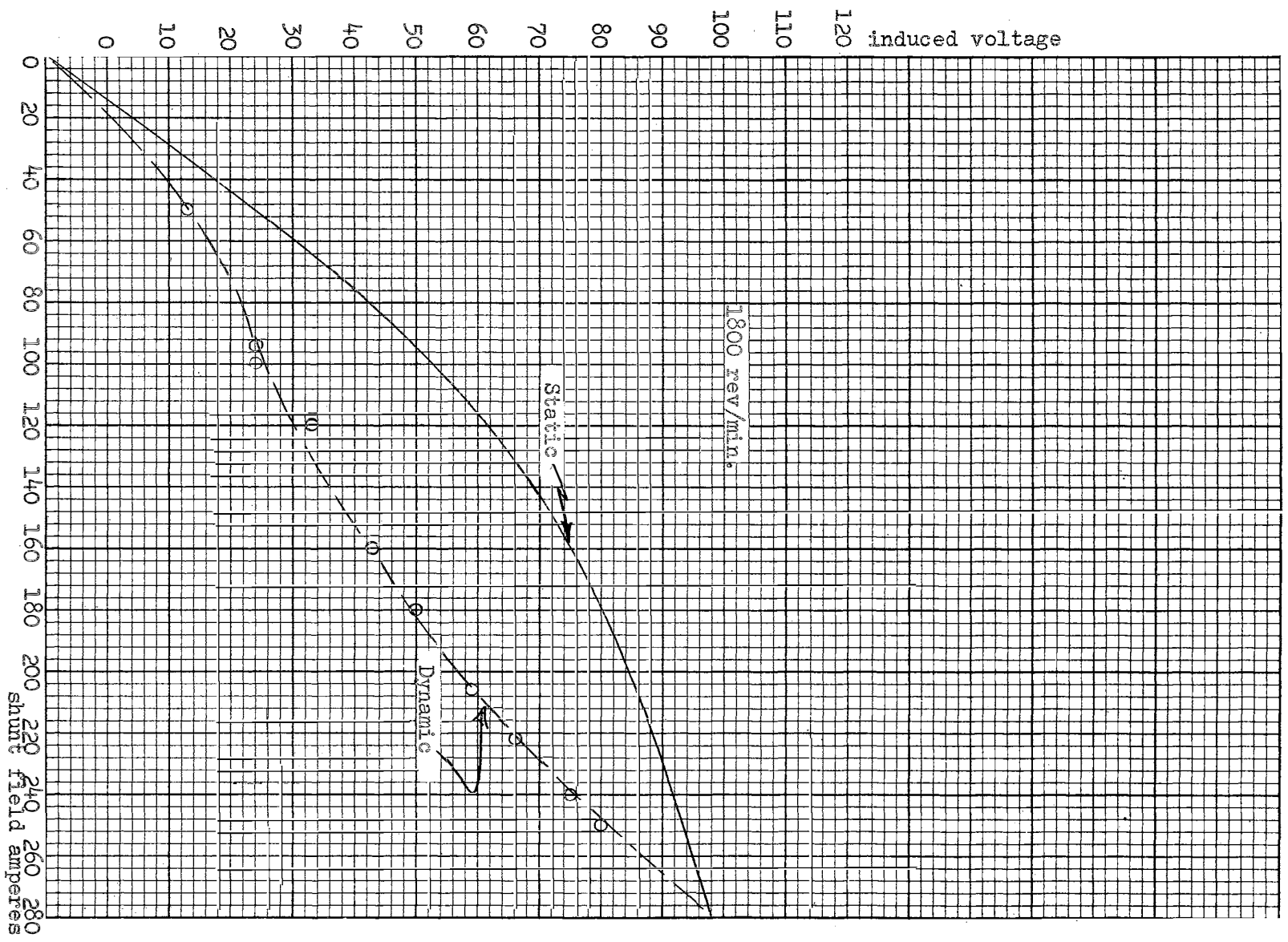


Figure 4.34. Open Circuit Characteristics, GE Model 5BC44AB65F



when being driven at rated speed, and as calculated, based on constant shunt field inductance for this motor. Two features of the actual current versus time curve are of note: (1) The actual current is larger than the calculated current at a specific time. This is in agreement with the analysis of a nonlinear circuit presented in Chapter IV, Sub-section A; (2) At time  $t = 0$ , the current has a finite value which is in agreement with results predicted in Equation (4-130) in this section. The shunt field current must assume this posture in order for the total flux linkages in the magnetic circuit to be zero at  $t = 0$ , since both circuits a and b have finite currents (and flux linkages) in opposition to the main excitation winding at time  $t = 0$ , as shown in Equations (4-131), and (4-132).

Figure 4.33 displays open-circuit voltage at 1800 rpm plotted as a function of time for the same motor as detailed above. Three relationships are shown. They are the actual observed voltage, the voltage obtained from the open-circuit saturation curve of the motor and the calculated field current based on constant inductance and the voltage from the open-circuit saturation curve and the actual field current. As can be seen, there are discrepancies between these three curves of as much as 30% at some periods of time, with the actual voltage being the lesser value throughout the transient period. In effect, the voltage (and, of course, flux) are retarded in time

which is a result of factors discussed in this chapter.

Figure 4.34 is a plot of open-circuit voltage under static conditions, i.e., the open-circuit saturation curve - as a function of shunt field current and the same variables under dynamic conditions. The latter was obtained graphically by selecting specific times during the transient period, obtaining actual shunt field current and voltage for those times and plotting the voltage as a function of actual existing shunt field current.

The effect of the discrepancy between actual voltage and voltage calculated in an analysis ignoring factors presented in this chapter is that at any instant of time during the transient period, the counter emf, the flux, and the armature current will not have the values one anticipates. Also, the torque and voltage "constants" are not really constant and are not easily predicted. Thus, results calculated with assumptions previously discussed will be in error.

#### Effect of Above Factors on Linear Type Analysis

As is apparent from Chapter III, even a linear analysis based on many simplifying assumptions can lead to mathematical expressions which are difficult, tedious and sometimes impossible, with known techniques, to solve. If the effects of the simplifying assumptions were included in the analysis, the mathematical obstacles would be even more formidable. Rather, it seems appropriate to examine

the effect of neglecting the various factors, when the factors are considered one at a time and then draw overall conclusions concerning the results of the linear analysis.

The all important primary result of the phenomena discussed in this chapter is that the magnetic field-armature current relationship has values other than linear analysis predicted values at specific times. Armature reaction and brush potential drop as well as brush shift effects alter the steady state as well as transient operating conditions. However, these alterations are such that compensation for steady state operation can be accomplished with inherent features of a d.c. motor, such as variation of shunt field and armature resistance, compensating windings, etc. Thus, over-design and subsequent adjustment can be accomplished to achieve a desired steady state characteristic. In contrast to this mode of usage of a d.c. machine is the inclusion of a d.c. motor in a closed-loop control system. By the very nature of the concept of a closed-loop system, the necessary adjustments and corrections for steady state performance are accomplished by the closed-loop system. However, from one steady state situation to another condition of steady state operation (but with different speed-torque relationship) will involve a transient period and it is this transient period that requires skill on the part of the analyst or designer and which will be a criteria of the performance of the system

as a whole. The items of paramount performance during the transient period are time of response, overshoot, rise time, settle time, and rate of change of such variables as speed and torque. These are the items which will determine stability and suitability of a given system.

Mathematically, nonlinear analysis of closed-loop systems is in its infancy. At the present time, if a device of known extreme nonlinearity is to be incorporated into a closed-loop system, the usual procedure followed is to represent the linear portions of the system on an analog type computer and to connect the actual physical nonlinear device into the computer circuitry. This is permissible for low power devices used for error sensing, correction, amplification, etc., type of components, but is not a suitable procedure, nor is it feasible, for the actual power output or controlling portion of the circuitry, where the d.c. motor is utilized.

It appears desirable to minimize as much as possible the factors (presented in this chapter) contributing to nonlinearity of performance of d.c. motors to be used in areas where transient performance is of prime importance. This, of course, requires a knowledge of these factors and the variables pertinent to the individual factors.

The linear analysis which can be analytically handled is made for a condition of full field at all times, or in the event computer simulation is made for a known relationship between field current and time and an assumed constant

relationship between field current and flux, which directly affects both torque produced and voltages generated. As shown in Chapter IV, Sub-section A, use of core materials with nonlinear relationship between cause and effect results in a current build up versus time characteristic which is certainly different than would be predicted by methods involving assumptions of constant permeability and inductance. It is possible, by proper choice of Frohlich constants, to achieve a more linear rate of rise of current and a more rapid rate of rise (theoretically) than would be achieved using constant permeability material. The fact that this is demonstrated for the condition of no eddy currents or currents circulating in closed conducting circuits does not nullify the usefulness of the derivation since the factors contributing to the phenomena are presented, i.e., proper choice of Frohlich constants, minimum turns, maximum excitation current, etc. Chapter IV, Sub-sections C and G, present the effects of the eddy currents and circulating currents as well as their variation with respect to their pertinent parameters, such as the desirability of low resistivity, high or medium permeability iron for core structure to decrease eddy currents and also show that the presence of laminations is not effective in controlling this phenomena directly. The manner in which the laminations are secured and the armature coil design (resistance and number of turns per coil) play a prominent part in determining the effect of the circulating current

phenomena on the flux-time relationship, as does the type of winding placed on the armature, such as simplex, duplex, triplex re-entrant order, etc., since the winding type will determine how many commutator bars (and armature turns) are closed upon themselves by the brushes.

The analysis of brush shift effect indicates that it can result in either magnetizing or demagnetizing effect, depending upon the direction of brush shift relative to direction of rotation, whereas the effect of armature reaction is always demagnetizing. If a motor is for use in a control system, the desirability of compensating windings to eliminate armature reaction effects should certainly be considered, although it is not the practice of industry to use compensating windings in small d.c. motors. (The exact minimum size motor to be manufactured with this type winding as standard equipment has not been clearly defined as an industry standard; varying from manufacturer to manufacturer.) Another possibility for nullifying the effect of armature reaction is presented by the deliberate installation of over strength commutating windings or interpoles and then diverting a sufficient amount of armature current to cause good commutation under steady state conditions with a resulting "under commutation" during transient periods. This under commutation phenomena results in direct magnetizing effect which can overcome the demagnetizing effect of armature reaction accompanying the increased current present during transient periods. At high

currents, as at low currents, the potential drop across the brush system is something different than the usual assumed two volts. Speed also has an effect upon this voltage drop. Since the changing voltage drop across the brush system is a manifestation of a changing contact resistance between the carbon brush and the copper commutator, adding resistance to the armature circuit will "swamp" out the small changes. In addition, as discussed previously, adding armature resistance will decrease armature influence on the shunt field circuit.

Flux variations due to the above may have a side effect of much more influence on performance than merely altering the speed-torque values and the voltage and torque constants. Specifically, it in effect can form a feedback loop within the device itself, causing unwanted oscillations which, when combined with the remainder of the system, can result in unanticipated system instability. This can come about if the load is a relatively high inertia load with low damping component and the driving motor has a slow time of response in its shunt field. If the motor has a pronounced armature reaction, or other defect causing demagnetization of the field (and the demagnetizing effect changes in magnitude when armature current changes) oscillations may develop through the following sequence: With the field demagnetized, the motor tends to turn up to a higher speed (denoted as an apparent equilibrium speed). As the motor approaches this apparent equilibrium speed,

armature current (and demagnetizing effect) will change and may even reverse, strengthening the field, establishing a new, lower, equilibrium speed; the current changes again, (increasing if the actual speed becomes less than the latest apparent equilibrium speed) and the field is again weakened, the motor starts to accelerate and the cycle is repeated.

As will be demonstrated in the next chapter, a typical motor, of so called good design, will exhibit such performance features as:

- (1) varying torque and voltage "constant"
- (2) speed and torque oscillations and over shoots
- (3) dynamic characteristics vastly different from predicted steady state or static performance
- (4) coupling between shunt and armature circuits where none theoretically exists
- (5) varying speed-time relationships whose variation is opposite to variations expected of a linear second order system
- (6) significant behavior patterns involving the usage of interpoles whose function supposedly is to aid commutation only.

At the conclusion of this thesis, recommended practice possible in the design stage as well as in operational environment will be presented.



## CHAPTER V

### EXPERIMENTAL TRANSIENT STUDIES

#### Experimental Equipment

Transient studies involving instantaneous torque were not possible until comparatively recently because of the lack of suitable transducers for detecting time variations of torque. The common method of measuring torque was by means of a prony brake or an electrical input dynamometer, both of which are satisfactory for measuring average torque under steady state conditions. The torque read-out was by means of a mechanical arm of known length exerting force against a calibrated weighing scale. Within the past three years, a torque sensing device, known as a Torque-Meter, has been developed which utilizes bridge connected, bonded strain gages to yield an electrical signal proportional to torque being transferred through a rotating shaft. This is an indirect result of Hooke's Law which states that "a body acted on by external forces will deform in proportion to the stress developed, so long as the stress remains below a certain value, known as the proportional limit". The torque causes the stress, the shaft deforms and the bonded strain gages deform in the same

fashion as the shaft, the deformation manifesting itself as a change in length of the strain gages. Since the strain gages are electrical resistance elements and resistance is proportional to length of a conducting material, the change of resistance of the strain gage can be mathematically related to the shaft stress. In order to render the strain gage circuit insensitive to temperature changes and to give maximum electrical response per unit strain, the gages are usually connected in a four element bridge, as shown in Figure 5.1.

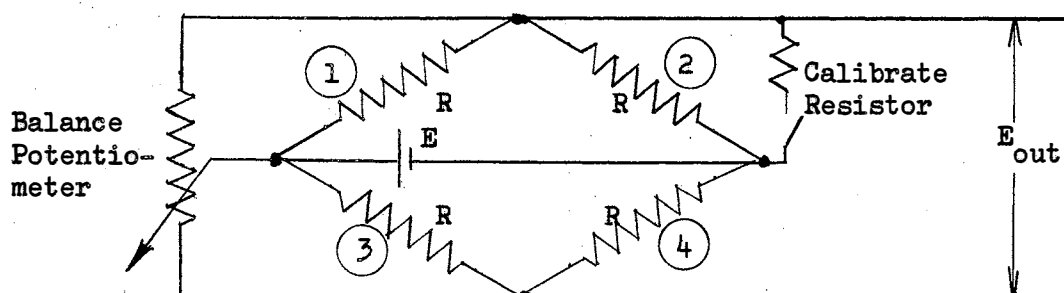


Figure 5.1. Four Element Strain Gage Bridge

The four strain gages are shown as having a nominal resistance of  $R$  ohms. The Balance Potentiometer is available to compensate for small variations of individual gage resistance and insure  $E_{out} = 0$  when the gages are in a "no strain" condition. The gages are physically located

on the member, whose stress is to be measured, in such a manner that a given stress lengthens two gages, such as 2 and 3, and shortens the other two, 1 and 4, or vice versa. This stress then would result in resistance increase in two arms, resistance decrease in the other two. The relationship between the voltage output and the resistance changes,  $\Delta R$ , can be shown to be:

For a four arm bridge,

$$E_{out} = E \frac{\Delta R}{R} . \quad (5-1)$$

The gage factor of the strain gages,  $G$ , is defined as:

$$G = \frac{\Delta R}{\Delta l/l} \quad (5-2)$$

and since, by Hookes Law:

$$\frac{\Delta l}{l} = HS = H'T \quad (5-3)$$

where  $S$  is stress proportional to torque,  $T$ , and  $H$  and  $H'$  are versions of Hookes constant. Combining Equations (5-3), (5-2), and (5-1) yields, assuming torque,  $T(t)$ , is a function of time:

$$E_{out} (t) = \frac{E}{R} GH'T (t) . \quad (5-4)$$

The voltage  $E_{out} (t)$  is then amplified and presented on a cathode ray oscilloscope or suitable recorder for obtaining torque as a function of time. The switched Calibrate Resistor is a precision resistor used to obtain

a bridge unbalance corresponding to a specific torque in order to calibrate  $E_{out}$  in terms of torque units.

Shaft speed, in the form of a voltage, as a function of time can be obtained by means of a small direct current generator, with permanent magnet excitation, caused to rotate at the same speed as the shaft transmitting torque into the Torque-Meter. Here again, the voltage corresponding to speed can be presented on a cathode ray oscilloscope or suitable recorder. If the read-out device has sufficiently high input resistance, it does not impose a load on the permanent magnet generator and the induced voltage of the generator is recorded and is very nearly exactly proportional to shaft speed. If the instantaneous torque and shaft speed are recorded on the same time base, i.e., a dual channel recorder, speed versus torque can be easily obtained. This is the scheme used in this investigation.

For demonstrating the transient behavior of direct current motors,  $\frac{1}{4}$  horsepower motors, were chosen for the following reasons:

- (1) Power requirements are sufficiently small so that the supply circuit resistance drops are negligible and voltage at the motor terminals would not be subject to fluctuations under various motor loading conditions.
- (2) Torque-Meters, capable of measuring the maximum developed torque of this size motor are commercially available.

- (3) Motors in this size range are widely used as components in closed-loop systems or servo-mechanisms.

The only departure in performance of this size motor from the performance of larger motors is that the rotating losses of the smaller motors is a much larger percentage of the rated power output of the motor than for the larger motors. Since this is usually a neglected factor in linear analysis, with consequent error in analysis results, it was felt that results obtained using small motors would serve to illuminate the misleading results arising from too careless methods of analysis.

The equipment actually used in this study was:

- 2 - direct-current machines, General Electric Model 5BC44AB65F,  $\frac{1}{4}$  HP, 1725 rpm, 115 volts, 2.4 amps  $\frac{S}{N}$  UVS with interpoles and small series field. (One used as a motor, the other as a generator for loading the motor.)
- 2 - direct-writing dual channel recorders, Sanborn Model 320, maximum chart speed 100 mm/sec, voltage sensitivity from 25 millivolts to 100 volts full chart scale (adjustable), minimum input resistance of 0.5 meg ohms, response from d.c. to 125 cps within 3db at 10 mm peak to peak.

1 - Torque-Meter, Lebow Associates No. 265-6, 1000 ounce-inches, 20,000 rpm, 0.5% accuracy to 20,000 cps variation and Ellis Associates BAM-1 Amplifier and Power Supply with precision wire wound calibrating resistors.

1 - Tachometer, Elinco Midget PM - 1 - M with permanent magnet excitation, S/N 60543, 21.8 volts/1000 rpm.

Misc. - Voltmeters, ammeters, ohmmeters, cathode ray, oscilloscopes, amplifiers, audio oscillators, strobotac tachometers, rheostats, etc.

All of the experimental work was performed in the Electrical Engineering Laboratories at Oklahoma State University.

The physical connection of the major items of equipment was as is shown in Figure 5.2.

#### Equipment Calibration

Electrical noise was observed in both the tachometer and torque meter outputs. The source of the noise in the tachometer was attributed to commutator ripple, whereas the torque meter interference was traced to two sources, i.e., the brush-slip ring arrangement within the torque meter proper and a high frequency component (about 200 cps) due to mechanical oscillation in the sponge rubber couplings connecting the torque meter to the two direct-current machines.

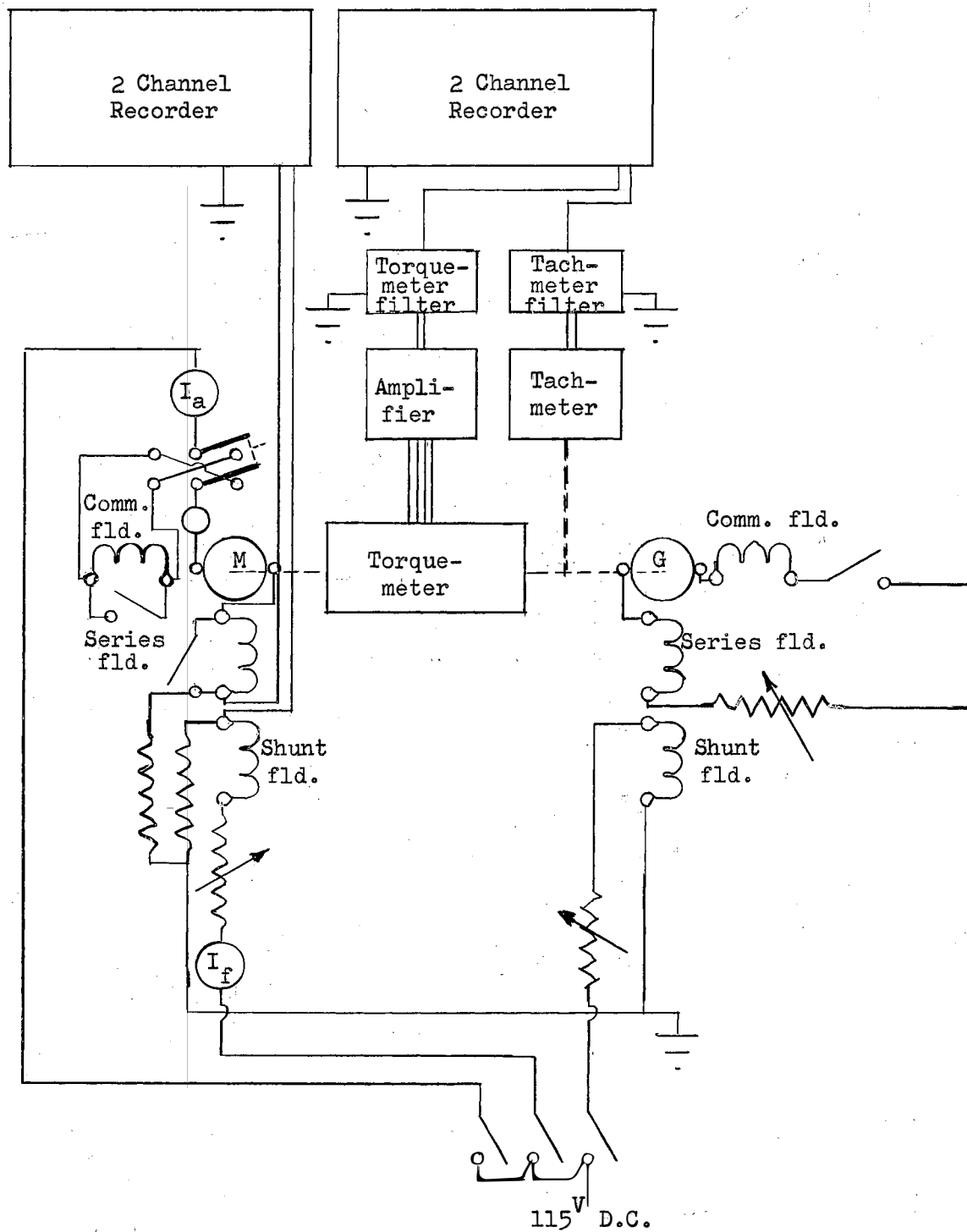


Figure 5.2. Experimental Circuitry

Satisfactory RC filters were designed with the circuit arrangement and values shown in Figure 5.3 which attenuated the noise to a level which would not interfere with accurate scaling of the recorder tracings and at the same time had no detrimental influence on recorder response to actual motor transients.

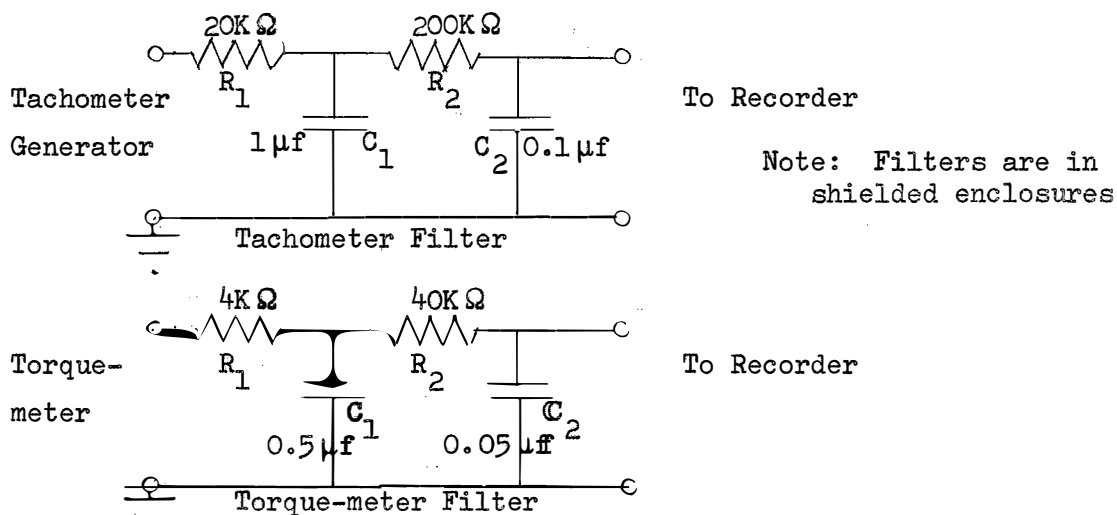


Figure 5.3. Filter Details

The torque meter and Ellis Amplifier were calibrated using the precision wire wound resistors within the amplifier in accordance with the following formula:

$$T = \frac{149.7 \times 10^5}{R_{\text{calibration}}} \text{ ounce-inches.} \quad (5-6)$$



The secondary standard use for speed calibration was a General Radio Company Strobotac flashing from "Line", which corresponds to 1800 rpm within the accuracy of the sixty cycle per second power supply which in turn is accurate with  $\pm \frac{1}{10}$  of a cycle (0.16%). This accuracy is attained by virtue of the interconnection of the local power generating system into the major midwest power grid which has precise frequency control on their generating equipment.

The voltmeters and ammeters used were from the Electrical Engineering School's precision instrument stock and were of the  $\frac{1}{4}\%$  accuracy class. Each instrument was standardized against two other instruments selected at random from the same stock and the three instruments were observed reading within their reputed accuracy.

The above precautions insured that the measuring equipment would measure faithfully within the line width as recorded on the recorders. Recorder response and chart speed were checked against the sixty cycle per second power source and their linearity was insured by comparison with the  $\frac{1}{4}\%$  accuracy voltmeters. No departures or errors were detected.

#### Machine Characteristics

Winding information on the identical machines supplied by the manufacturer is as follows:

2 poles, 2800 turns/pole shunt field, 420 ohms

33 turns/pole series field, 0.635 ohms.

1 commutating field, 215 turns of commutation field, 0.59 ohms.

Armature: 18 slots,  $21\frac{1}{2}$  turns per coil, 2 coils per slot. Coil span 8 teeth, 3.7 ohms.

Air Gap Flux: 0.00234 webers (with 115 volts across the two series connected 2800 turn windings).

Armature Inertia: 0.0014 Kg-meter-sec<sup>2</sup>.

The torque and voltage "constant" can be calculated from Equation (5-1) as:

$$K = \frac{Zp}{2\pi a} = \frac{(21.5 \times 2 \times 2 \times 18) \times 2}{2\pi \times 2} = 246 \frac{\text{volt} - \text{seconds}}{\text{radian} - \text{weber}}$$

$$= 246 \frac{\text{volts}}{\text{rad/sec} - \text{weber}} = 246 \frac{\text{newton} - \text{meters}}{\text{weber} - \text{ampere}}$$

(5-7)

The open circuit saturation characteristic, as supplied by the manufacturer and presented in Figure 5.4 was verified in the laboratory by driving the motor at 1725 rpm, varying the shunt field excitation and measuring the open circuit voltage (induced voltage).

The friction and windage (rotating losses) of the system were determined by varying the speed of the machine designated as a "motor" and observing the average torque absorbed by the idle generator, tachometer and torque

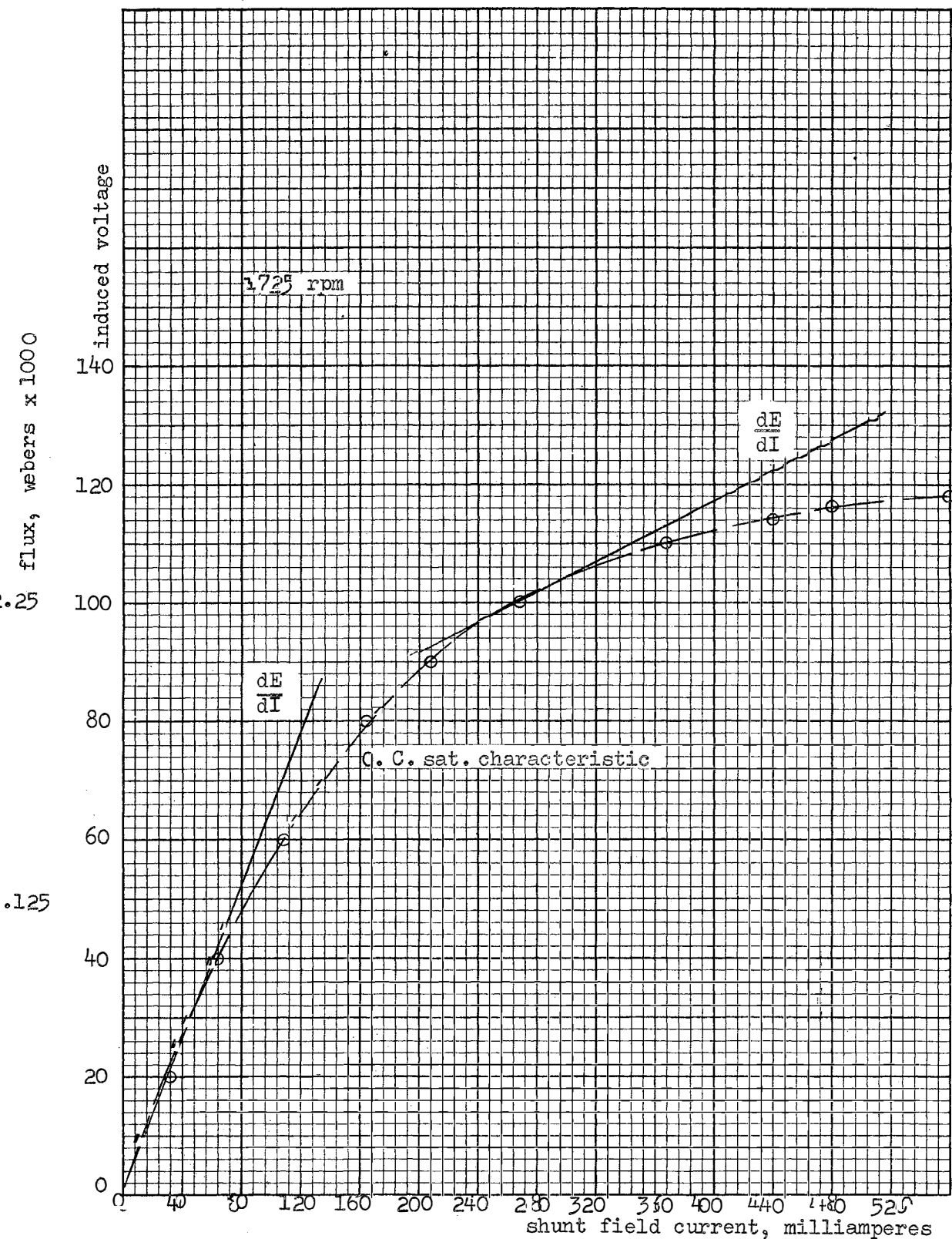


Figure 5.4. Open Circuit Saturation Characteristic  
GE Model 5BC44AB65F

meter as the speed was varied from zero to 2000 rpm and then, with the "generator" being operated as a motor, driving the idle machine over the zero to 2000 rpm range and observing the average torque required by this machine designated "motor". The torque versus speed characteristics obtained are plotted in Figure 5.5. The two characteristics were graphically combined to obtain total rotating losses as a function of speed,  $\omega$ .

The total rotating loss torque,  $T_{f+w}$ , can be represented by a linear relationship and expressed as:

$$T_{f+w} = \frac{2.94\omega}{10^4} + 0.1427 \text{ newton-meters.} \quad (5-8)$$

Equation (5-8) was determined by calculating the slope of the speed-torque relationship,  $m$ , and utilizing the ordinate intercept,  $b$ , in the straight line relationship:

$$T = m\omega + b . \quad (5-9)$$

The system moment of inertia,  $J$ , was determined by the conventional retardation method which consists of motoring the system up to above 2000 rpm and disconnecting the electrical power supply. A recording of speed as a function of time was made as the system decelerated under the influence of the torque of friction and windage. The slope of the speed-time recording was ascertained graphically, combined with the  $T_{f+w}$  corresponding to the speed

at which  $\frac{\Delta\omega}{\Delta t}$  was determined and J calculated from:

$$T_{f+w} = -J \frac{d\omega}{dt} \quad \text{or} \quad J = \frac{-T_{f+w}}{\Delta\omega/\Delta t} . \quad (5-10)$$

The measured value for the system was determined to be 0.0032 Kg-meter-sec<sup>2</sup> (compared with a value of 0.0014 Kg-meter-sec<sup>2</sup> from the manufacturer for one machine - the difference between 0.0028 and 0.0032 being due to the torque meter and tachometer).

In order to determine the effective resistance of the brush system and the manner in which the voltage drop across the brushes varied, the potential drop across the armature was observed and recorded for various values of armature current with the armature stationary after thermal equilibrium was reached. This is not strictly accurate since armature speed does influence this as discussed in Chapter IV, but the effect of residual magnetism when rotating and consequent induced voltage prohibits a more accurate determination. The calculated values of brush potential drop and contact resistance as a function of armature current are displayed in Figure 5.6.

Selection of a single value of self inductance of each field and mutual inductance between fields is a task requiring engineering judgment and an appreciation of the manner in which the inductance will change as the excitation level is varied. By definition, self inductance, L, is:

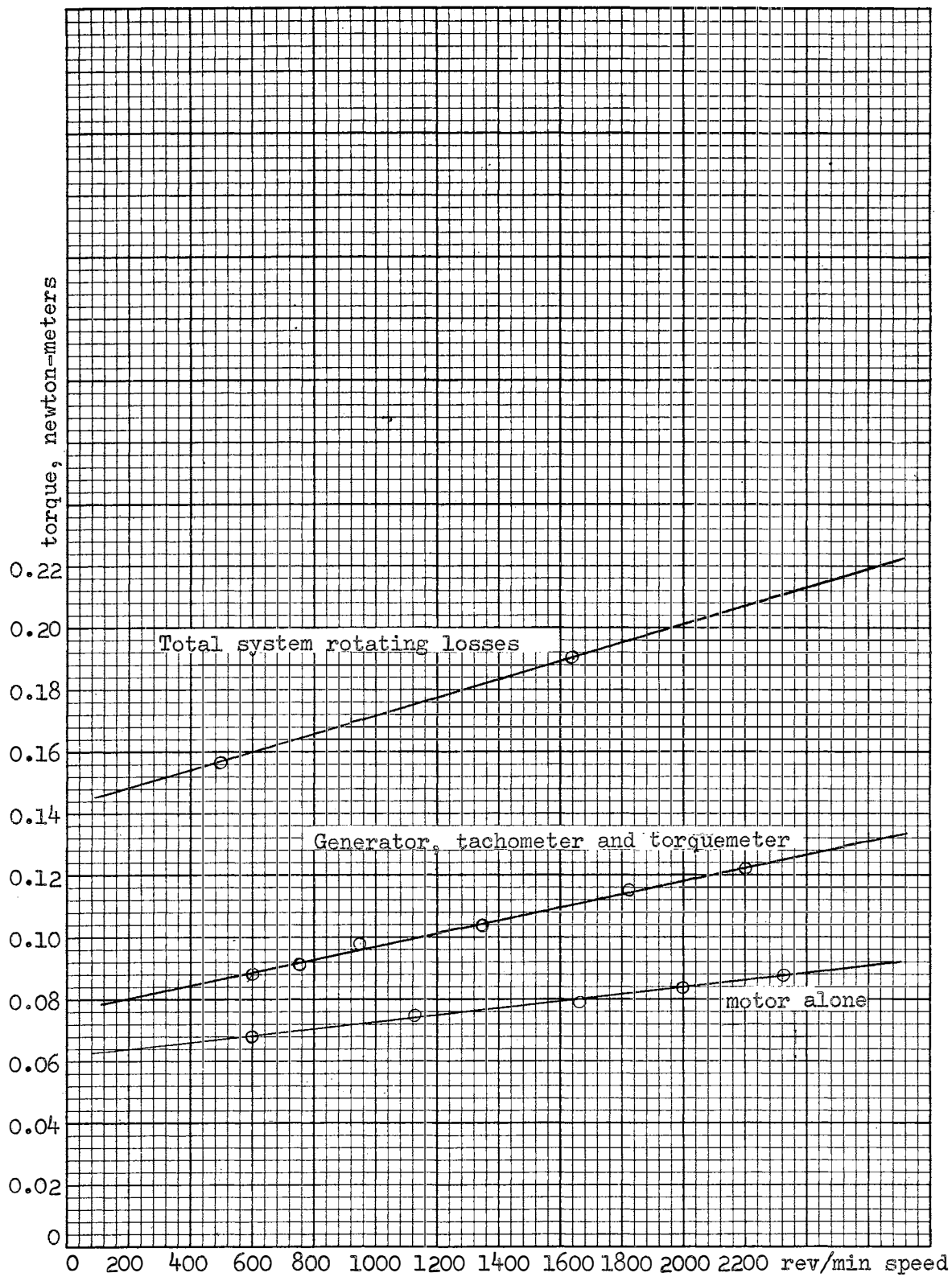


Figure 5.5. System Friction and Windage Load Versus Speed

$$L = \frac{\lambda}{I} = \frac{N_{\text{eff}} \phi}{I} \quad (5-11)$$

where

$\lambda$  = total flux linkages

$I$  = excitation current

$\phi$  = total flux

$$N_{\text{eff}} = \frac{\lambda}{\phi}$$

recalling that  $\phi = \frac{E}{K\omega}$

$$L = \frac{K_{\text{eff}} E}{K\omega I} = K' \frac{E}{I} \quad (5-12)$$

As can be seen from Equation (5-12), the self inductance is proportional to the ratio of induced voltage to excitation current. Since this ratio is constantly changing, it appears necessary to define an incremental inductance,  $L_i$ , where:

$$L_i = K' \frac{dE}{dI} \quad (5-13)$$

$\frac{dE}{dI}$ , which is the slope of the open circuit saturation characteristic, and  $L_i$ , therefore, is a function of the degree of saturation present in the magnetic circuit. Reference to Figure 5.4, the open circuit saturation characteristic of the machine under test, indicates that the angle of the tangent changes from approximately 65 degrees along the unsaturated portion of the curve to approximately

30 degrees at the saturated portion corresponding to rated operating conditions. Now,

$$\text{Tangent } 65^\circ = 2.14$$

$$\text{Tangent } 30^\circ = 0.58 .$$

This is a change of 3.7 to 1. When the inductance of the various windings was measured under saturated and unsaturated conditions, it was found to change by a factor of approximately 3 to 1 in the case of the commutating field plus armature and approximately 2.2 to 1 for the commutating field, armature, and series field combined. The difference in ratio between actual and theoretical ratios is due to the change in percentage of leakage flux, i.e., flux which links something less than all circuits because of some of the flux choosing a path through air rather than through the iron completely. The ratio without series field is much closer to the theoretical ratio than when the series field is included because different portions of the magnetic path are effected when the series field is not included and the leakage is not as severe.

The self inductances were determined in accordance with American Institute of Electrical Engineers Standard 501, "Test Code for Direct Current Machines" (effective date: July 31, 1957), Section 23-7.6. This code prescribes that armature and armature circuit windings, (such as commutating windings and series field windings) shall be tested by applying a single phase, 60 cycle per second



voltage to the winding to be tested, measuring current through the winding,  $I$ , voltage across the winding,  $V$ , and calculating the self inductance by:

$$L = \sqrt{\frac{\left(\frac{V}{I}\right)^2 - R^2}{2\pi f}} \quad (5-14)$$

where

$R$  is the winding resistance

$f$  is frequency, 60 cps.

The value calculated is the unsaturated or saturated value depending upon the absence or presence of shunt field excitation of rated ampere-turns. Since the degree of saturation does not increase appreciably after the "knee" of the saturation characteristic is passed, it is not necessary to exceed rated current in these tests.

Figures 5.7 and 5.8 portray the self inductance variation of various windings and combinations of windings under saturated and unsaturated conditions.

In Figure 5.7, it will be noted that the sum of the armature and commutating field combination is less than that of the armature alone. This arises as a result of having the mmf's associated with the two windings in opposition, such that the total inductance of the combination in series is the sum of the self inductances decreased by twice the mutual inductance. Since the mmf's of the series winding and the armature are aiding each other, the

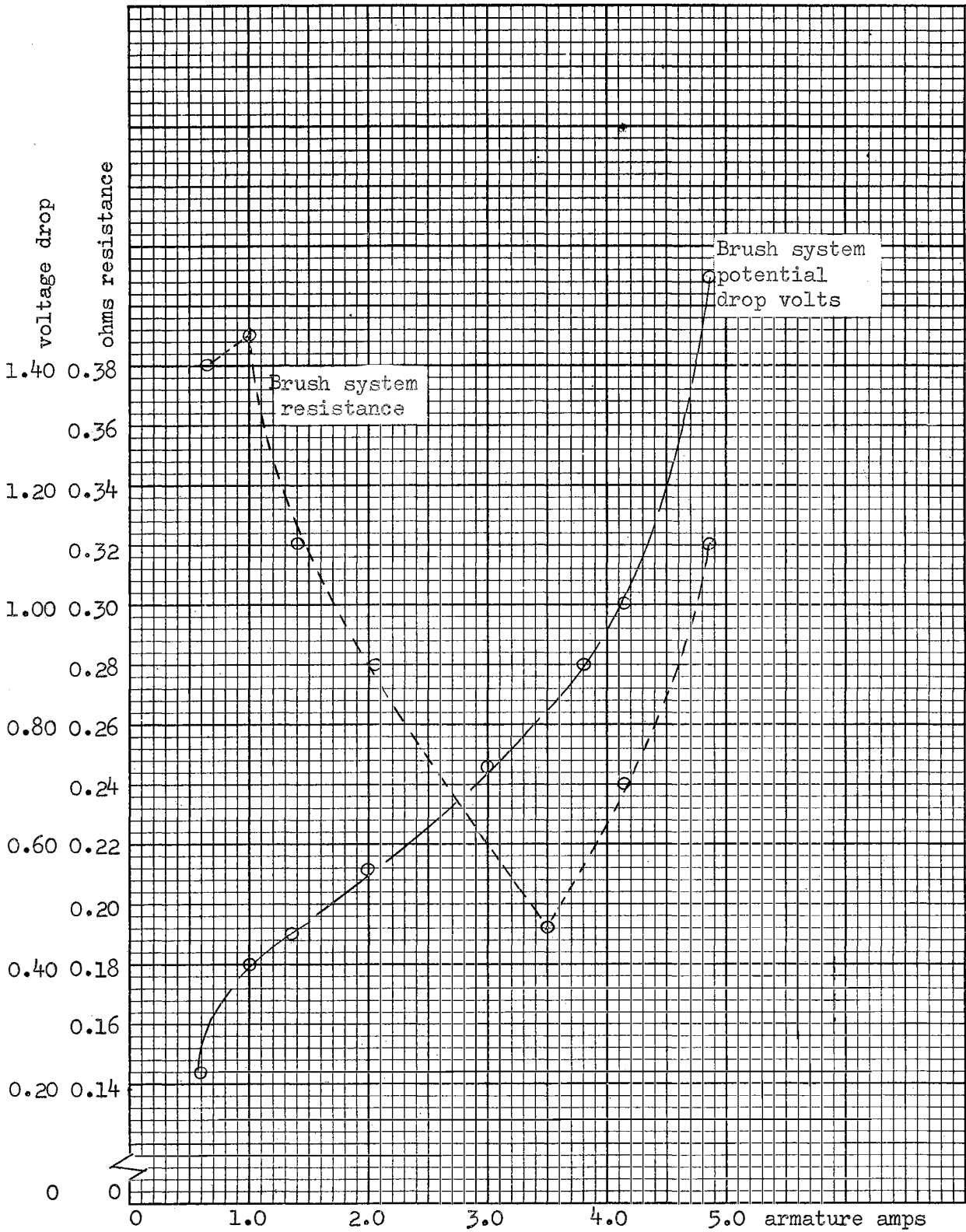


Figure 5.6. Brush System-Effective Resistance Variation

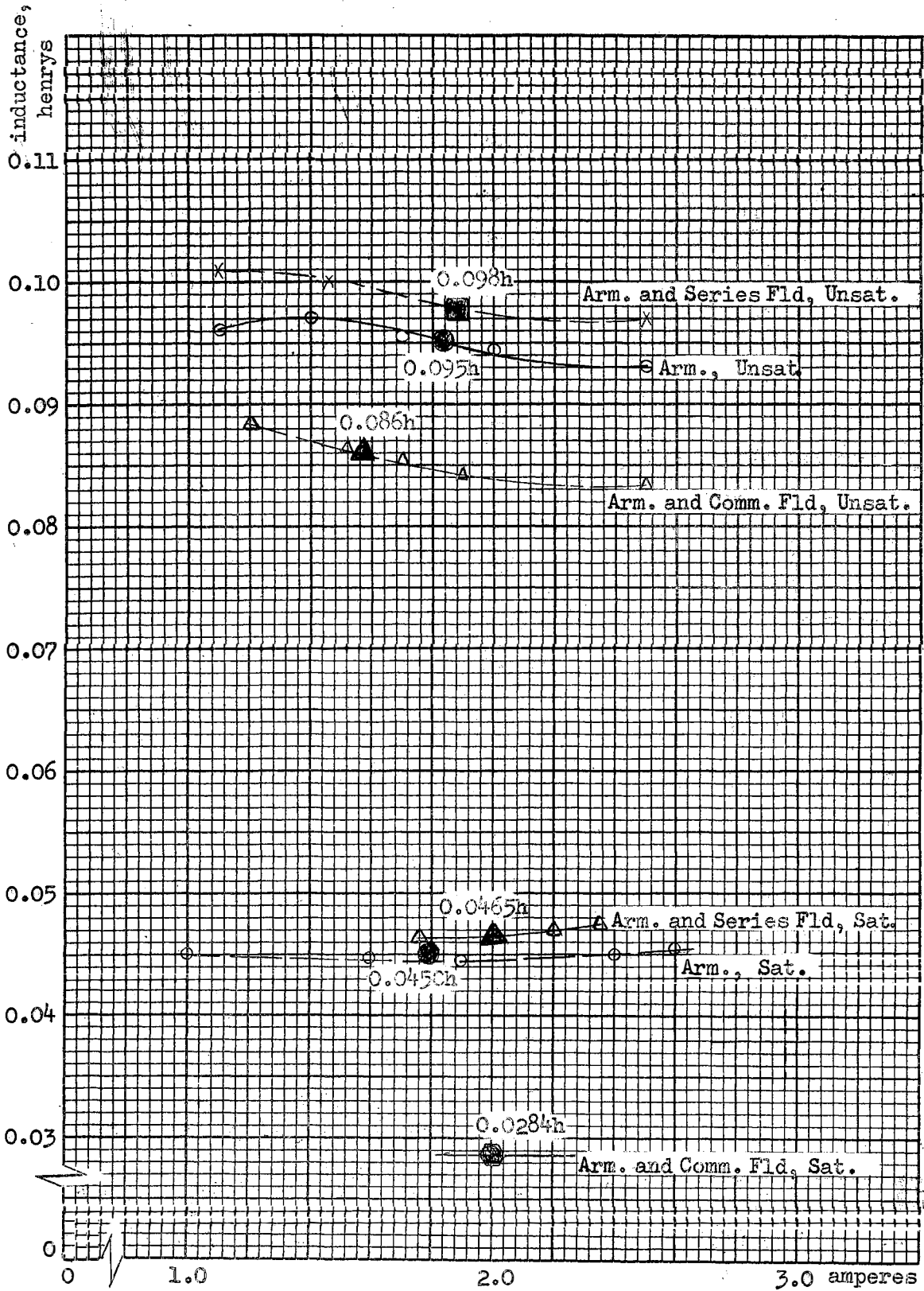


Figure 5.7. Self Inductances

total inductance of the combination is the sum of the individual self inductances plus twice the mutual inductance of the combination.

From Figures 5.7 and 5.8, the values of self inductance of the various combinations selected for this study are:

	<u>Unsaturated</u>	<u>Saturated</u>
Armature Only	0.861 h.	0.045 h.
Series Field Only	0.0048 h.	0.0014 h.
Commutating Field Only	0.026 h.	0.0223 h.
Armature and Series Field	0.0989 h.	0.0465 h.
Armature and Commutating Field	0.0861 h.	0.0284 h.
Armature, Commutating and Series Field	0.0895 h.	0.0375 h.

The test code alluded to above does not contain provision for a standardized measurement of mutual inductance between the shunt field and the various armature circuit windings. For this study, a procedure was devised which gives values that appears (based on turns, ratios and anticipated couplings) to give satisfactory results. It consisted of impressing a sinusoidal 60 cycle per second voltage on the armature circuit, measuring the resulting current flow,  $I_a$ , and measuring the open circuit voltage,  $V_f$ , induced in the shunt field. If  $\omega$  is the angular frequency of the currents and voltages, the mutual inductance,  $M$ , can be found from:

$$M = \frac{V_f}{\omega I_a} . \quad (5-15)$$

The results of the tests to determine shunt to armature circuit mutual inductance are plotted in Figure 5.9. Since the armature and commutating fields are in quadrature with the shunt field, their theoretical coupling is zero, although a small degree does manifest itself.

From Figure 5.9, the values of mutual inductance assumed proper for this investigation are:

	<u>Saturated</u>
Shunt Field to Armature and Commutating Field	0.002 h.
Shunt Field to Series Field	0.0132 h.
Shunt Field to Armature, Commutating and Series Field	0.014 h.

The nature of this test precludes obtaining an unsaturated value.

In order to determine the self inductance of the shunt field, the test code referred to above requires a time recording of shunt field current,  $I_f$ , build up after a step voltage,  $V_{f0}$ , is impressed upon the field, when the machine is being driven at rated speed, no load. ( $V_{f0}$  is of the proper value to result in rated shunt field current at time,  $t = \infty$ .) The slope of the  $I_f$  versus  $t$  curve,  $\frac{dI_f}{dt}$ , is obtained for  $t = 0$  and  $L_f$ , the shunt field self inductance is:

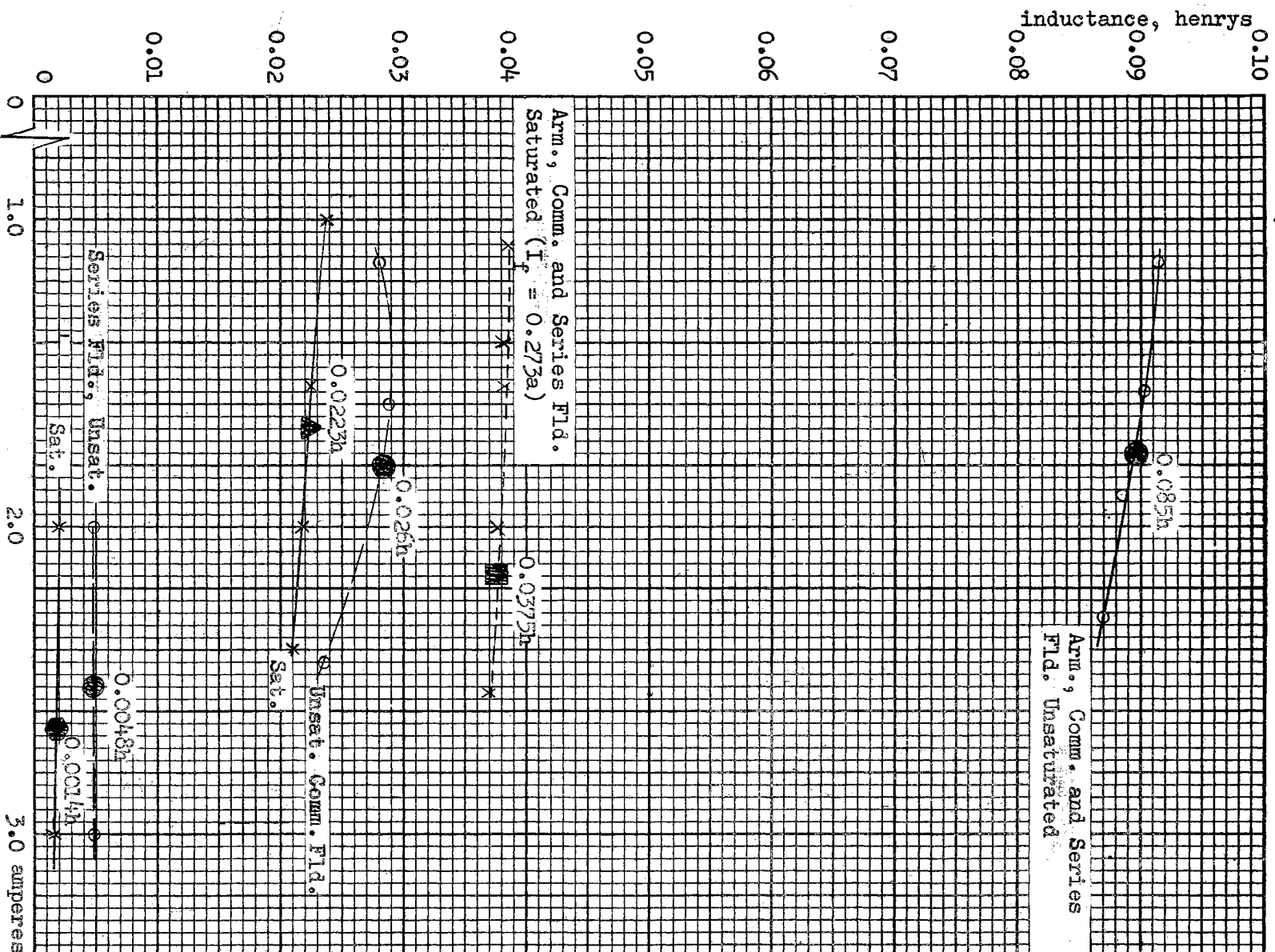


Figure 5.8. Self Inductances, Continued

$$L_f = \frac{V_{fo}}{\left(\frac{dI_f}{dt}\right)_{t=0}} \quad (5-16)$$

Figure 5.10 is a plot of shunt field current as a function of time. The self inductance of the shunt field is calculated as 46h.

The motor and system parameters supplied by the manufacturer and/or measured and computed in connection with this investigation can be summarized in Table V-I.

TABLE V-I

MACHINE PARAMETER (G. E. Mod. 5BC44AB65F)

---

Torque (friction and windage): =  $\frac{2.94\omega}{10^4} + 0.1427$  newton-

meters

System moment of inertia: = 0.0032 Kg - meter - sec<sup>2</sup>

Voltage-Torque constant: = 246  $\frac{\text{volt - seconds}}{\text{radian - weber}}$  or

$\frac{\text{newton - meters}}{\text{ampere - weber}}$

Resistance:

Armature	3.7	ohms	
Commutating Field	0.59	ohms	215 turns
Series Field	0.635	ohms	66 turns
Shunt Field	420	ohms	5600 turns

---

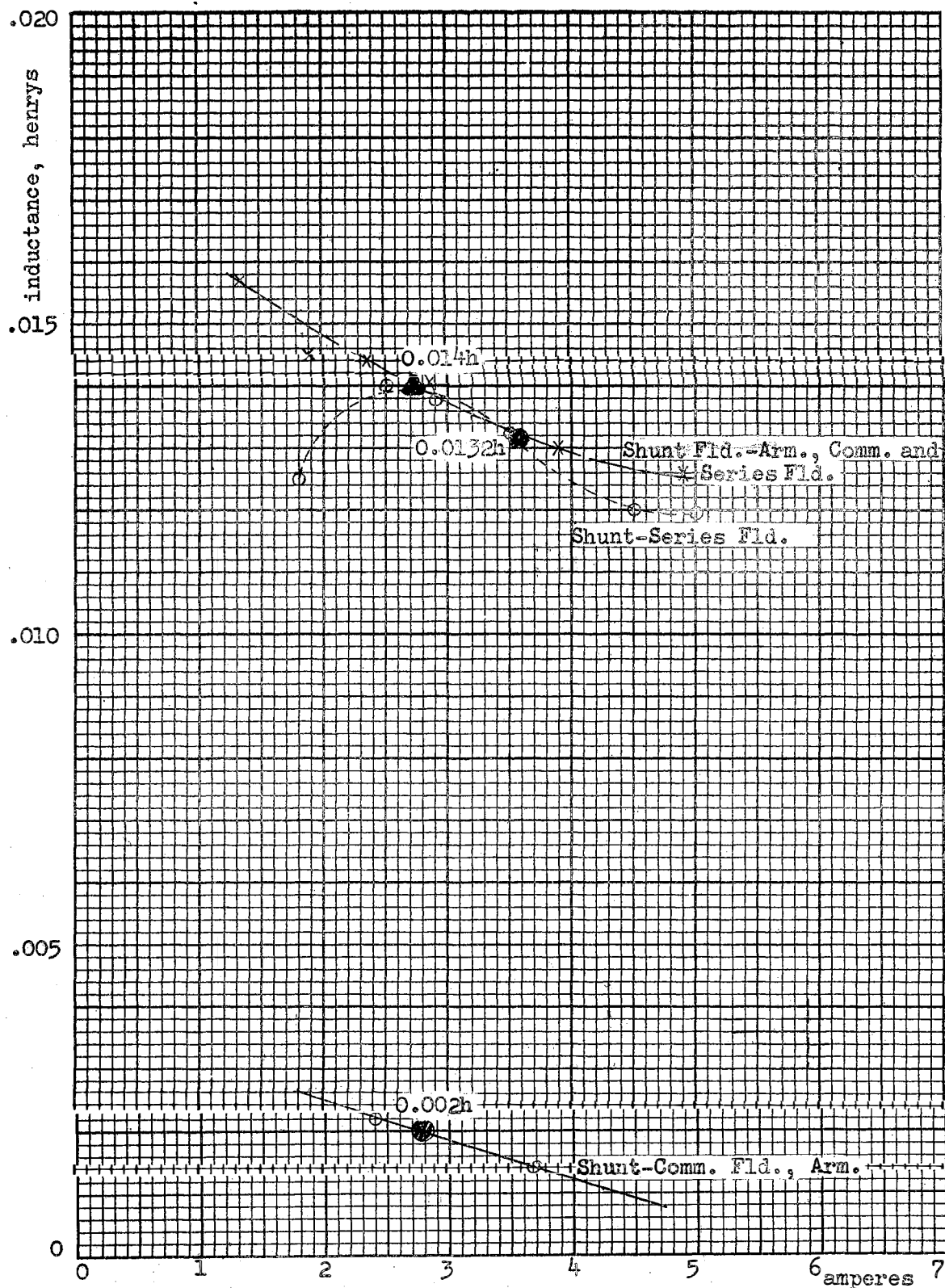


Figure 5.9. Mutual Inductances



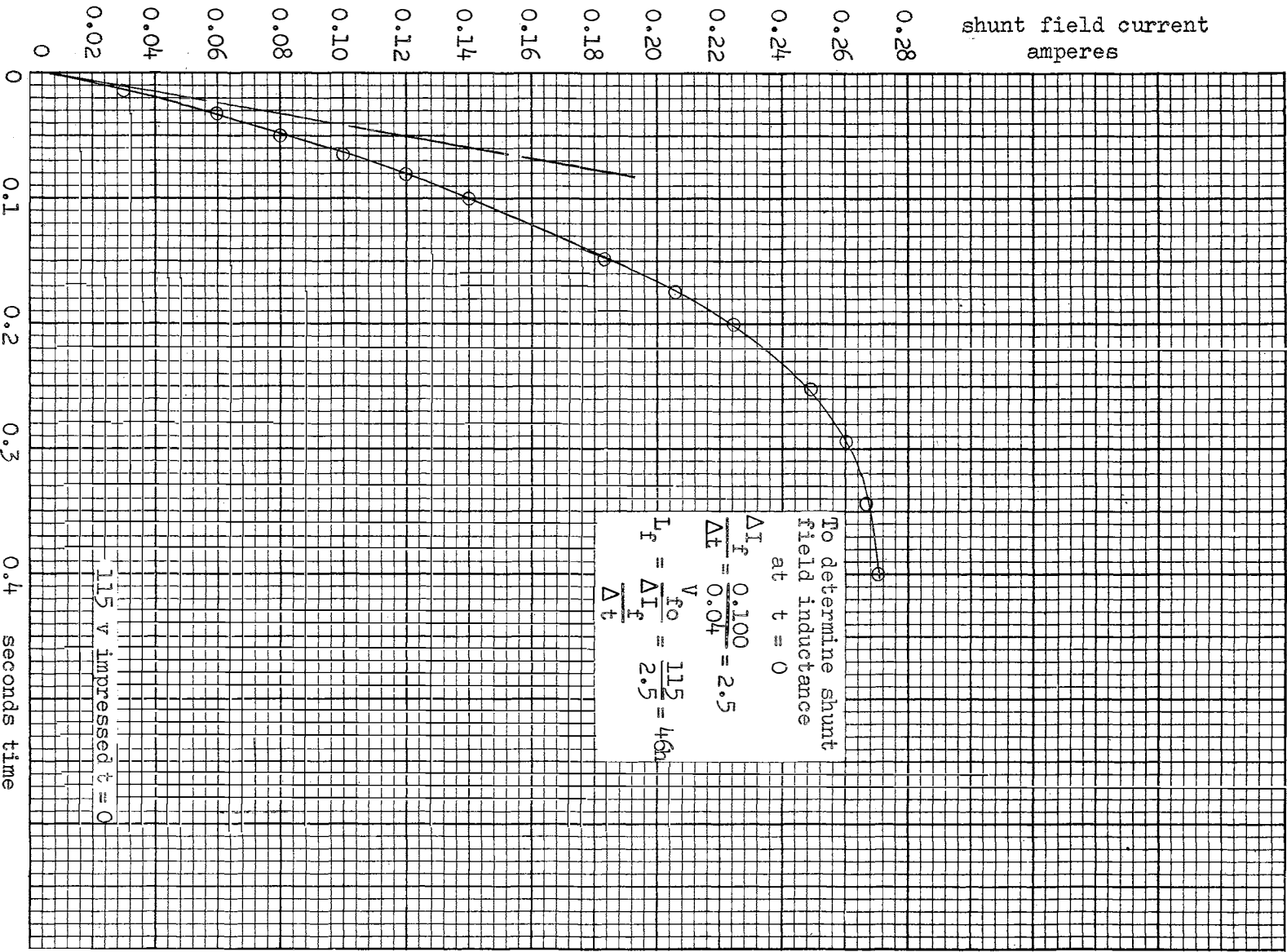


Figure 5.10. Shunt Field Current Buildup

Air Gap Flux: Figure 5.4

0.00234 webers at rated excitation

Open Circuit Characteristic: Figure 5.4

Brush Potential Drop: 0.6 Volts at 2.4 amps, 1 volt at  
4.2 amps

Self Inductance	Unsaturated	Saturated
Armature Only	0.0861 h	0.045 h
Series Field Only	0.0048 h	0.0014 h
Commutating Field Only	0.026 h	0.0223 h
Armature and Series Field	0.0989 h	0.0465 h
Armature and Commutator Field	0.0861 h	0.0284 h
Armature, Commutating and Series Field	0.0895 h	0.0375 h
Shunt Field	46 h	

Mutual Inductance	Saturated
Shunt to Armature and Commutating Field	0.002 h
Shunt to Series Field	0.0132 h
Shunt to Armature, Commutating and Series Field	0.014 h

#### Calculated and Observed Shunt Motor Transients

As pointed out in Chapter III, the usual analysis for a shunt machine, a so called linear analysis, neglects all internal loading due to friction and windage within the system and also assumes that the shunt field excitation is

at rated value and remains at this value during the transient period.

In Chapter III, Equation (3-23) was developed for a shunt motor with rated excitation when the armature was switched and with no external loading. When the values from Table V.I are inserted in that equation, angular velocity as a function of time can be calculated for the motor under investigation. In order to visualize the effect of saturation and rotating losses,  $\omega$  is calculated for various conditions. The resulting equations, determined from Equation (3-23) for this motor, are:

$L_A$  unsaturated, friction and windage neglected

$$\omega = 200[1 + 1.44e^{-24.8t} \sin(24.2t - 2.375)] \text{rad/sec.} \quad (5-17)$$

$L_A$  saturated, friction and windage neglected

$$\omega = 200[1 + 0.662e^{-108t} - 1.662e^{-43t}] \text{rad/sec.} \quad (5-18)$$

$L_A$  saturated, friction and windage included

$$\omega = 197[1 + 0.335e^{-120.8t} - 1.335e^{-30.2t}]. \quad (5-19)$$

Figure 5.11 is a plot of Equations (5-17), (5-18) and (5-19). In addition, the actual  $\omega$  versus  $t$  determined experimentally for this motor (under the two conditions of shunt field at steady state at time  $t = 0$  and of shunt field switched with the armature) are plotted on the same sheet.

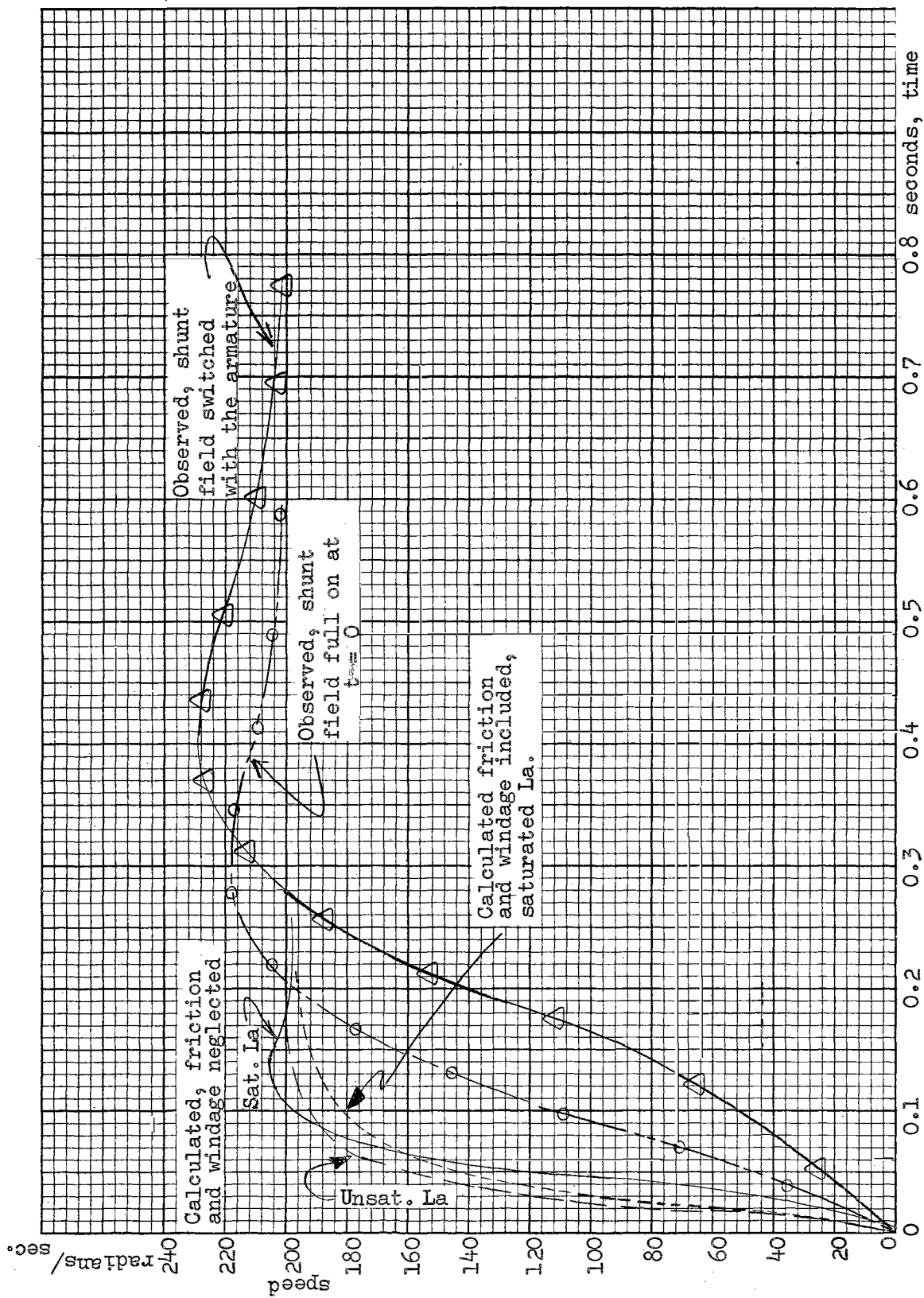


Figure 5.11. Speed Versus Time (No External Load)

The motor magnetic circuit is in a saturated condition during most of the transient period (having an approximate shunt field time constant of  $< \frac{46}{420} < .11$  seconds.) Also, the torque required to overcome friction and windage is a physical reality, so the performance depicted by Equation (5-19) should be taken as the best available by so called linear analysis methods. Obviously, it leaves a great deal to be desired insofar as its accuracy is concerned. In order to qualitatively analyze the phenomena in Figure 5.11, the actual field current variation was recorded and is displayed in Figure 5.12; the armature current is plotted in Figure 5.13, and shaft torque in Figure 5.14. The two notable differences between analytical and actual  $\omega$  versus  $t$  relationships are the lesser slope in the actual curve during the rising portion of the curve and the overshoot during the approach to steady state speed. The situation involving the test with the field at steady state prior to armature switching indicates a faster rise of speed and less overshoot than when the field is switched; Refer to Figure 5.12. The shunt field current rises momentarily to greater than twice rated value shortly after switching. Since the torque is proportional to the flux, there is more torque for acceleration of the motor during this period, so the angular velocity increases faster than when the field is zero at  $t = 0$ . After about 0.1 seconds, the shunt field current drops to about 70% of rated value so the torque decreases. The minimum value of

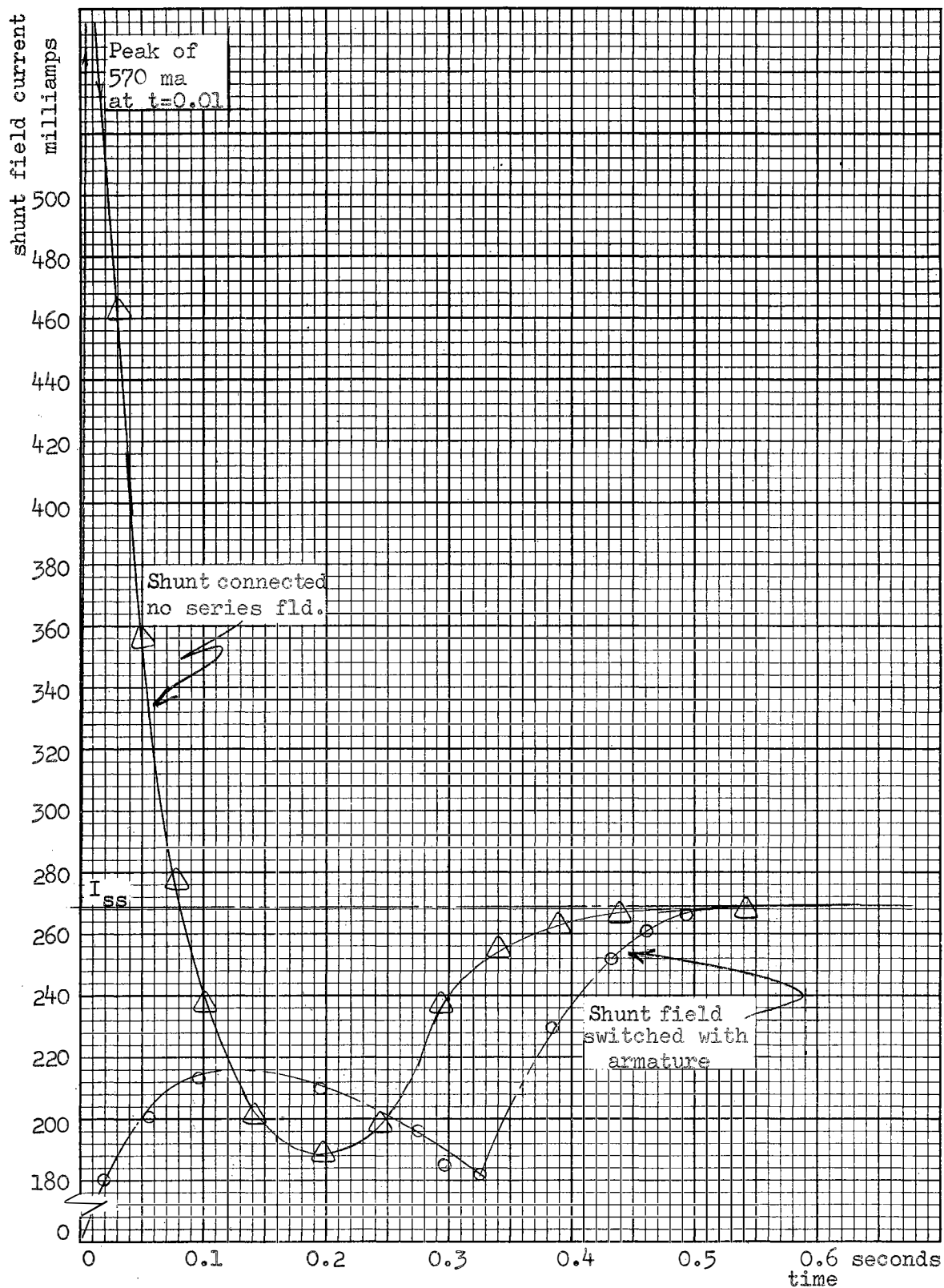


Figure 5.12. Shunt Field Current Versus Time (No External Load)

excitation occurs at 0.2 seconds. From Figure 5.11, the motor speed is at its ultimate steady state value and increasing at this time. (Since the excitation is low, its apparent steady state equilibrium speed is much higher.) The speed increases to 10% above true steady state speed, the maximum occurring about 0.35 seconds after the armature was switched. Meanwhile, the field strength is increasing with a consequence lowering of apparent steady state speed so the motor begins to slow down, reaching true equilibrium after approximately 0.8 seconds. The speed characteristic of the motor with switched shunt field is similar except the angular acceleration is less, the speed overshoot greater and the time to reach true steady state speed is longer, all because the shunt field excitation is always less than rated value prior to reaching steady state (Figure 5.12). This figure clearly indicates that some degree of coupling must exist between the shunt field and the armature circuit, even though it is theoretically zero. The coupling exists by virtue of the factors discussed in Chapter IV.

Figures 5.13 and 5.14 are plots of calculated and observed values of torque and armature current as a function of time. The experimentally obtained values and the calculated value which includes friction and windage (and saturated  $L_A$ ) are plotted.

The expressions used for calculating torque and current result from Equations (5-19) and (3-18):

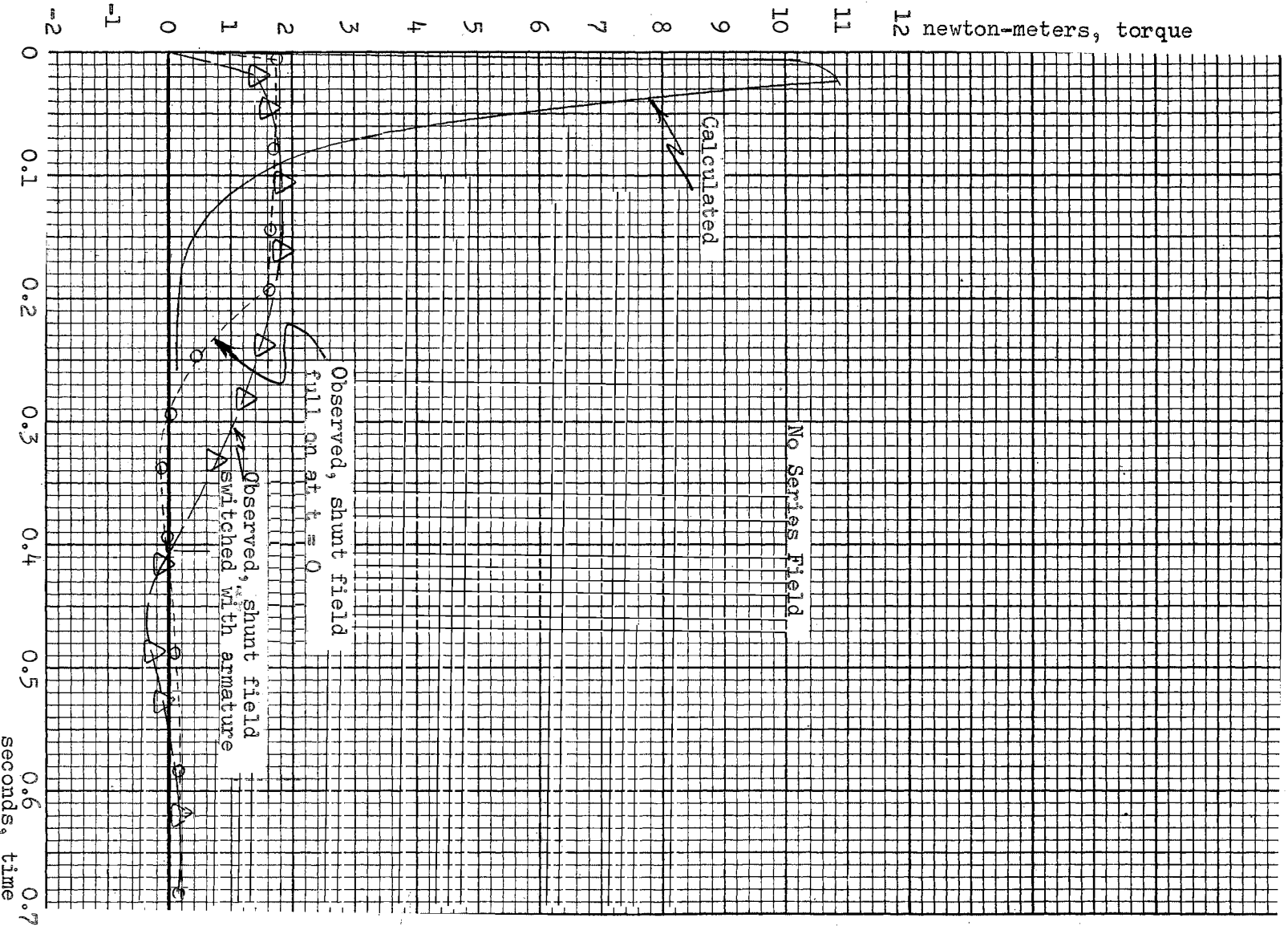


Figure 5.13. Torque Versus Time (No External Load)



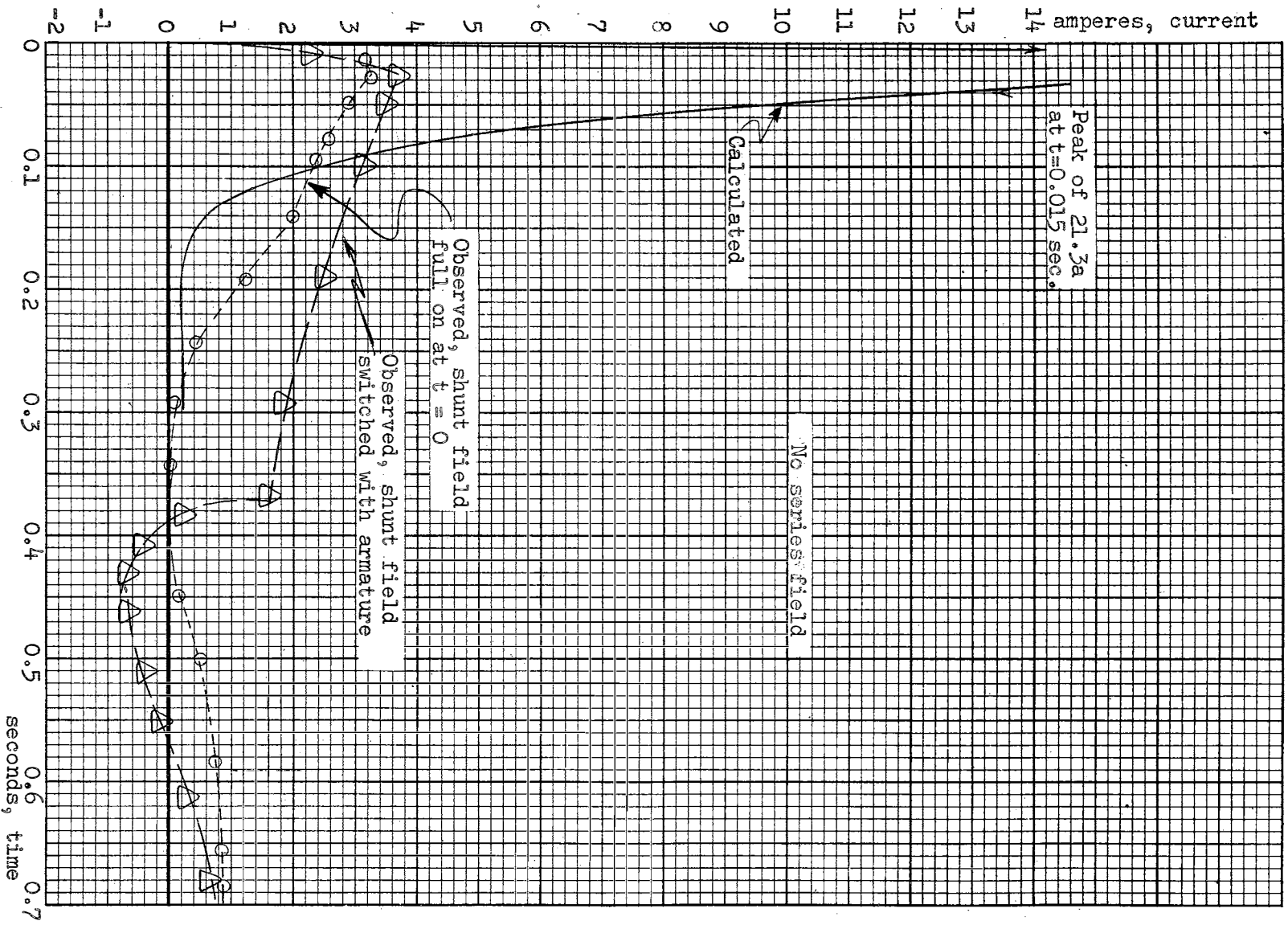


Figure 5.14. Current Versus Time (No External Load)

$$\text{Since } T = J \frac{d\omega}{dt} + C_1 + C_2\omega \quad \text{and} \quad I = \frac{T}{K}$$

$$T = 25.4(\epsilon^{-30.2t} - \epsilon^{-120.8t}) + \frac{2.94}{10^4} + 0.1427 \quad (5-20)$$

$$I = 44.2(\epsilon^{-30.2t} - \epsilon^{-120.8t}) + \frac{5.11}{10^4} + 0.248 \quad (5-21)$$

The calculated values of current rise to values very nearly that of line voltage divided by armature resistance but actual maximum current is less than this value. This phenomena has been noted in connection with rate of rise of short circuit current in generators (12, 13, and 14) and has led to an empirical quantity, "apparent resistance", defined by Linville and Darling (13). Actually, it is not some form of resistance appearing during transient periods, but rather is the armature circuit manifestation of factors discussed in Chapter IV. It is more appropriately an apparent "inductance" of transient nature because it appears to be an electromagnetic field phenomena. Since the actual current is less than the theoretical value, the actual torque also is something less than theoretically predicted. Since the motor does not accelerate as quickly, the armature counter emf does not build up as fast as one would expect from theoretical considerations and, thus, the increased current (and torque) persist for a longer period of time than it does in the calculated version.

Figure 5.15 is a plot of  $\bar{K}$ , the torque "constant", as obtained from dividing observed values of torque (Figure 5.13) by the observed value of armature current (Figure 5.14) existing at the same time. The theoretical value of  $\bar{K}$  for this motor is 0.575 newton-meters/ampere. The values plotted are "dynamic" values and vary widely from the theoretical value and are far from constant due to factors discussed in Chapter IV.

If motor operation was always steady state, i.e., any departures from one operating condition toward another operating condition were to take place extremely slowly; so slowly that electrical and mechanical transients were nonexistent, the equations describing the performance could be written as:

$$V - IR = \bar{K}\omega \quad (5-22)$$

$$T = \bar{K}I \quad (5-23)$$

or, combining Equations (5-22) and (5-23),

$$T = \left( \frac{-K^2}{R} \right) \omega + \frac{KV}{R} . \quad (5-24)$$

Equation (5-24) is plotted in Figure 5.16. The dynamic relationship between torque and speed as obtained for this motor accelerating from zero to steady state speed is also shown on this graph. Here again, a tremendous difference exists. Unfortunately, the steady state theoretical relationship shown is too often used in

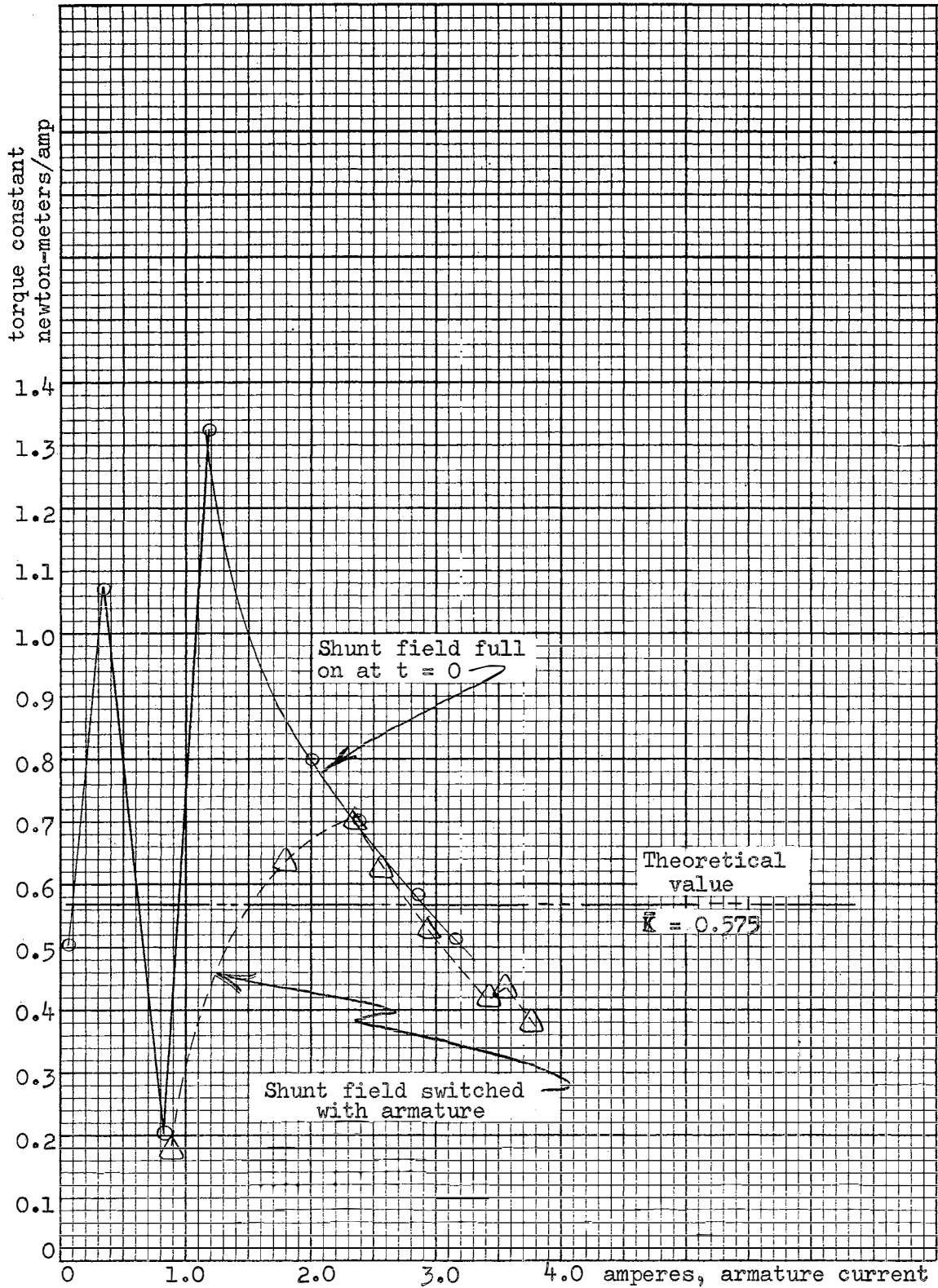


Figure 5.15. Dynamic Torque Constant as a Function of Armature Current

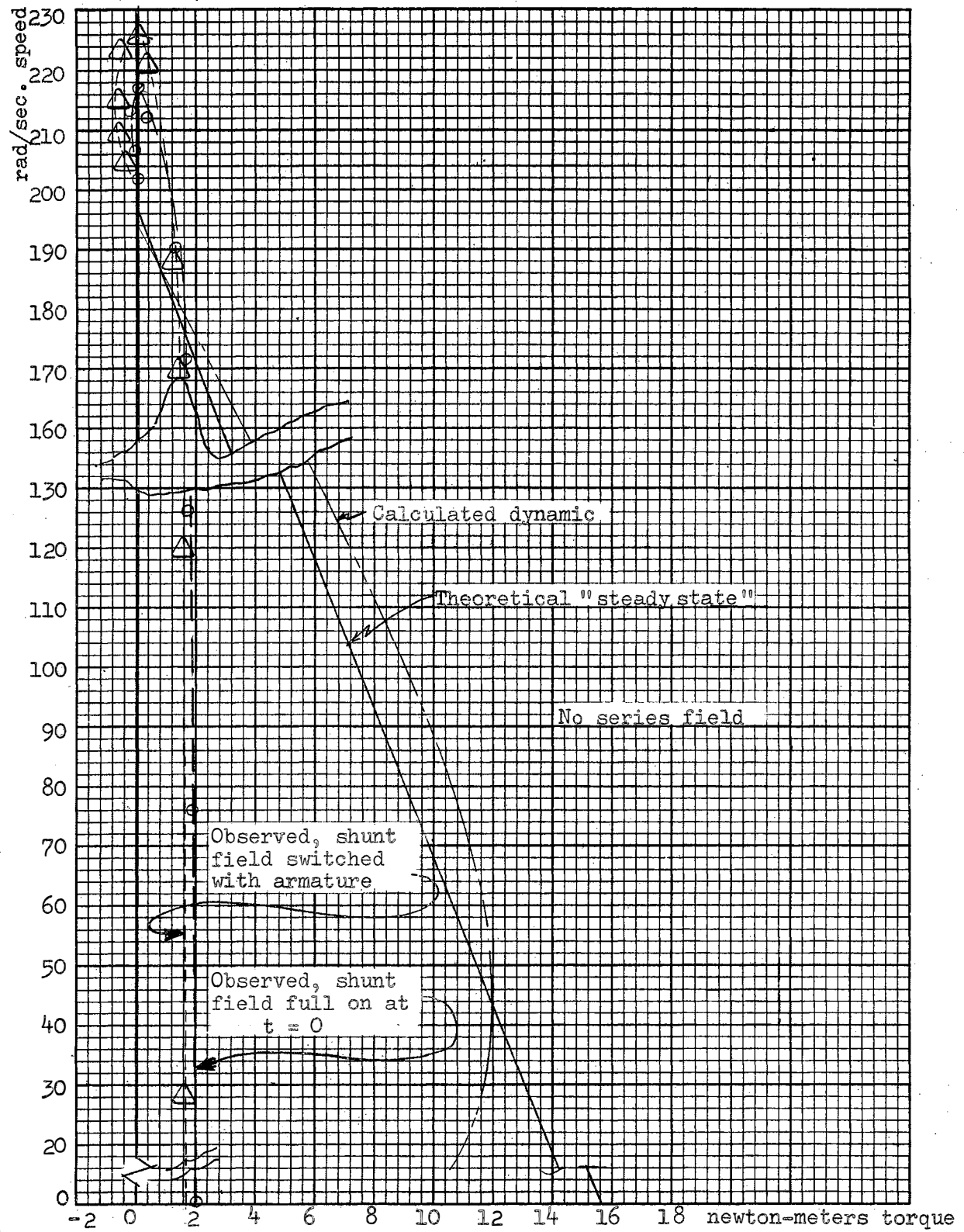


Figure 5.16. Speed Versus Torque (No External Load)

system analysis and is widely accepted as a representative relationship. The fact that the speed-torque relationship is double valued in areas near steady state speed results from the speed overshoot.

In order to investigate the effect of the commutating field on the transient performance, one must recall that the commutating field acts in the quadrature axis and that the only effect in the direct axis is by virtue of the net armature circuit inductance being influenced by the presence of the self inductance of the commutating field and the mutual coupling between the armature and the commutating field. When the commutating field and the armature are interconnected with the proper polarity, the magnetic fields of the two oppose each other. If:

$L_A$  = armature self inductance

$L_{CF}$  = commutating field self inductance

$M_{CFA}$  = mutual inductance between the two windings.

Then, for proper interconnection:

$$L_T = L_A + L_{CF} - 2M_{CFA} \quad (5-25)$$

The response depicted in Figure 5.11 is for proper connection of the armature and commutating field and is for a net armature circuit inductance of 0.0284 henrys. If no commutating field were present, the armature circuit inductance is measured as 0.045 henrys and if the

commutating field was improperly connected, the net inductance can be calculated as:

$$\begin{aligned} 2M_{CAF} &= L_A + L_{CF} - L_{TP} = 0.045 + 0.0223 - 0.0284 \\ &= 0.0389 \end{aligned}$$

$$\text{and } L_{T1} = L_A + L_{CF} + 2M_{CAF} = 0.045 + 0.0223 + 0.0389$$

$$L_{T1} = 0.106h$$

where  $L_{TP}$  is proper polarity between commutating field and armature and  $L_{T1}$  is for improper connection.

Using these values of armature circuit inductance, the equations for angular velocity as a function of time become:

for properly connected commutating field

$$\omega = 197[1 + 0.335e^{-120.8t} - 1.335e^{-30.2t}] \quad (5-19)$$

for no commutating field

$$\omega = 199.5[1 + 2.03e^{-42.3t} \sin(24.5t + 3.66)] \quad (5-26)$$

for improperly connected commutating field

$$\omega = 197[1 + 1.22e^{-18t} \sin(25.6t + 4.1)]. \quad (5-27)$$

The response based on these expressions is plotted in Figure 5.17. The actual response, obtained experimentally, is plotted on the same sheet. Since the calculation was for full shunt excitation at instant of switching, the

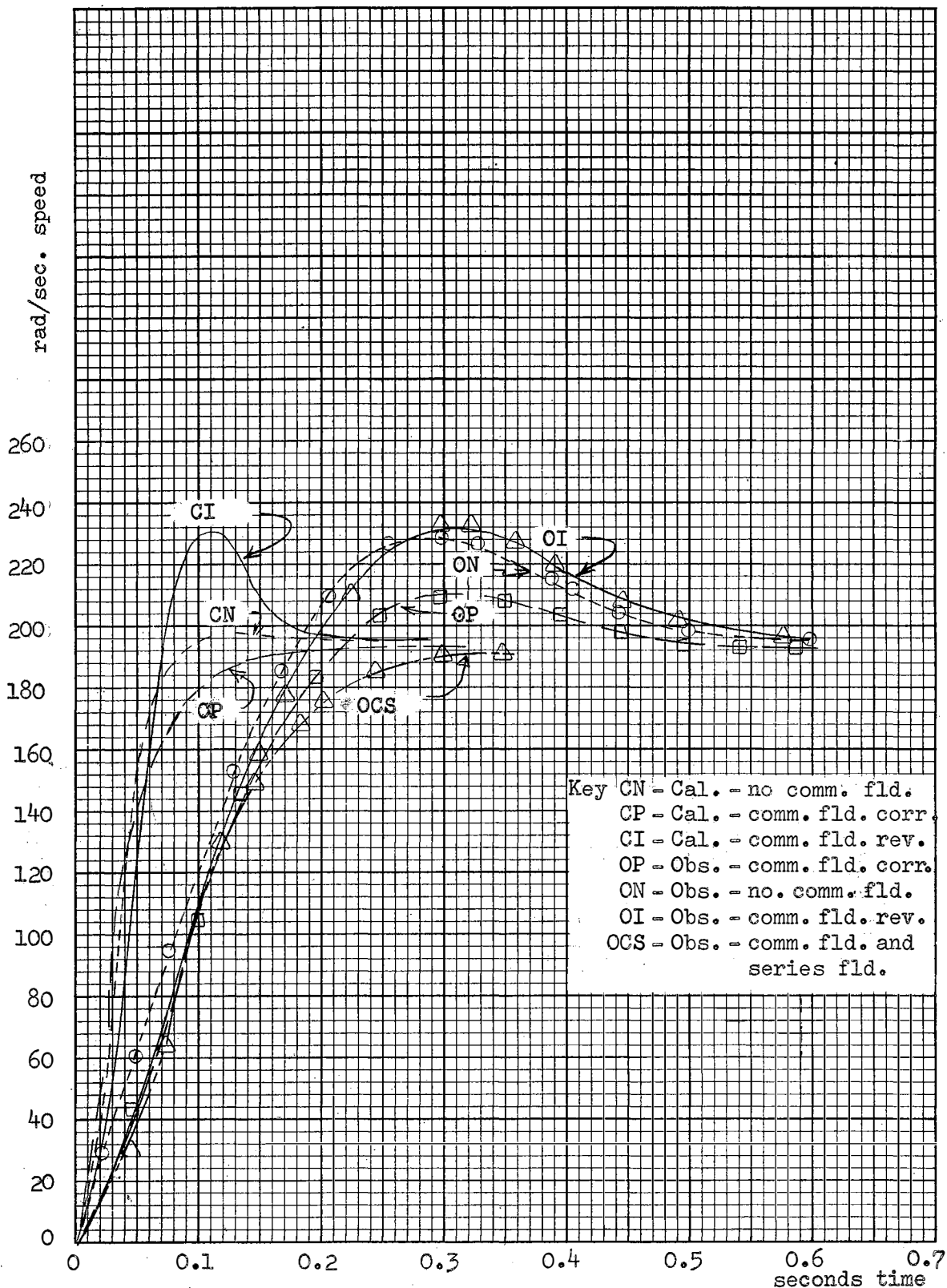


Figure 5.17. Speed Versus Time (Various Commutating Field Arrangements)



experimental data shown is for the same condition. Records were also obtained for the situation in which the shunt field was switched with the armature. Since no calculated data was obtainable for this condition, the results are not portrayed graphically. However, for each of the three configurations of commutating field for which the shunt field was switched with the armature, the overshoot was approximately 10% higher and the time at which maximum speed was attained was about 15% greater than the corresponding configuration observed with the shunt field at steady state at the instant of switching.

Obviously, the fact that the actual angular acceleration is only about one-third of the predicted value and the fact that speed overshoot occurs is directly related to the variations in shunt field current (discussed above) during the transient period. No doubt, magnetic circuit nonlinearities (in addition to armature reaction) affect this, but it is believed that the majority of the discrepancies are a result of armature to shunt field coupling. As can be seen from Figure 5.17, the presence of the commutating field does not materially affect the accelerating characteristics of the motor, but it does have a stabilizing influence (in that it very nearly eliminates speed overshoot) if properly connected. This is due to the reduction in net armature inductance from what it would be if armature inductance were the net inductance. The reduced inductance results in less energy storage capability

with consequent reduced oscillation (and overshoot).

For the machine used in this study, rated shunt excitation is  $0.270 \times 5600 = 1510$  ampere turns. With an armature current of 2.4 amperes (rated current) and the series field connected, the series field contributes an additional  $2.40 \times 66 = 158$  ampere-turns. This additional 10% excitation results in only 2% additional flux (due to the magnetic circuit nonlinearity). Accordingly, one would not expect the acceleration with series field to be greatly different from that without series field and this was experimentally verified. The response with series field for acceleration with no external load is plotted on Figure 5.17. However, use of the series field does introduce an armature-shunt coupling and this coupling tends to "smooth out" the variations of excitation experienced during transient periods with shunt excitation only. This can be readily seen from Figures 5.17 and 5.18. No overshoot was noted and steady state speed was attained in about 50% of the elapsed time taken by the shunt motor with no series field. The tendency of manufacturers to refer to this winding as a "compound" winding appears to be a misnomer, i.e., its added torque is nil under conditions where the shunt field is full or when the armature is switched. This is the usual situation in automatic control systems. It should more properly be designed a "damping" or "stabilizing" winding. Figure 5.18 shows the shunt field current variation with respect to time (when the shunt

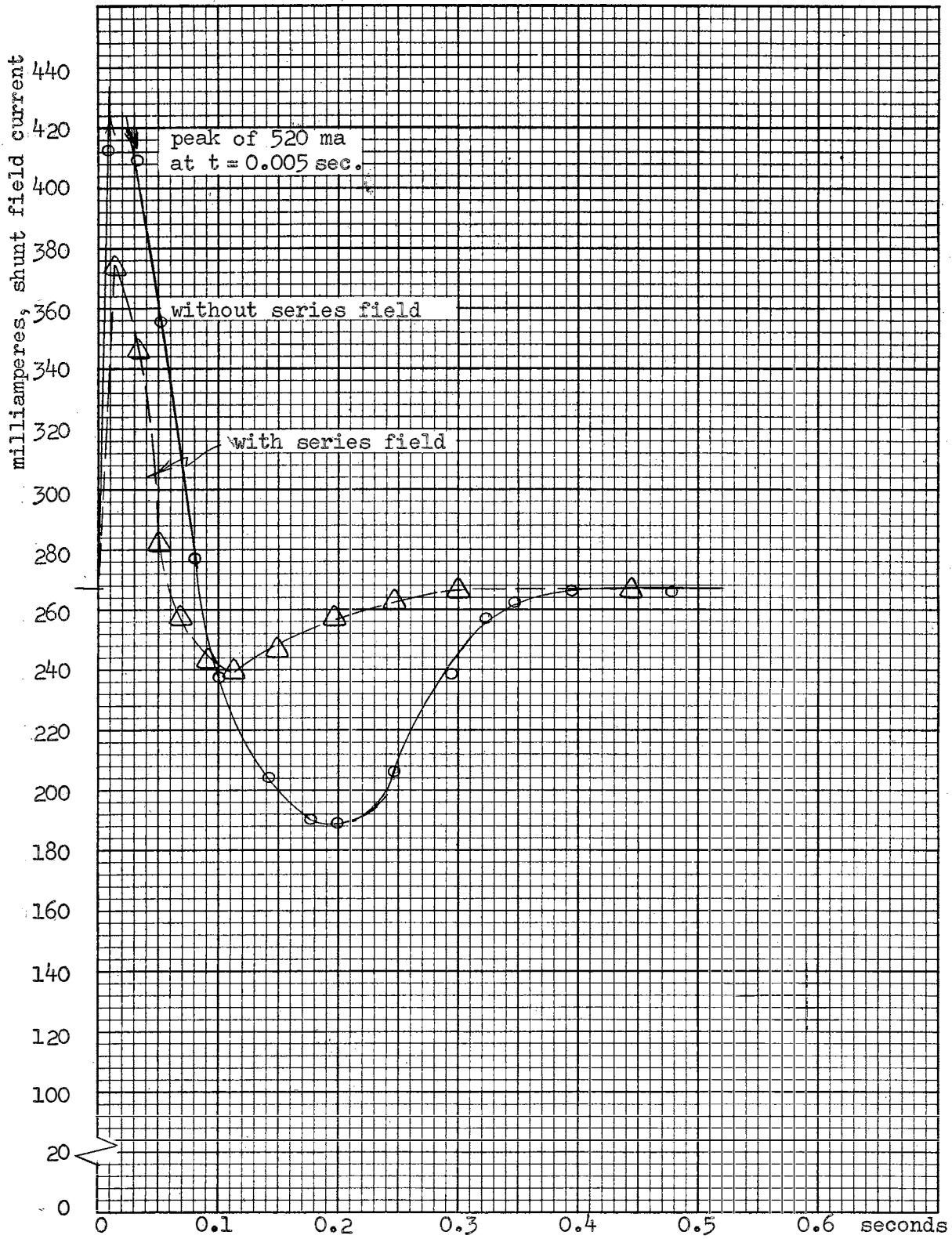


Figure 5.18. Effect of Series Field on Shunt Field Current (No External Load)

field is at rated excitation prior to switching) for the condition of series field and no series field. As can be seen, the variations are of much smaller magnitude when the series field is present and the maximum and minimum "apparent" equilibrium speeds are much less when the series field is present.

The addition of an external load to the shaft of the motor does not appreciably alter the speed response of the system, as can be seen from an inspection of results plotted in Figure 5.19. Here, the external load consisted of a fixed resistance in the armature circuit of the generator in the system. The generator had full shunt field excitation during the transient period. The shunt field current was monitored and was observed to remain substantially constant due to the nature of build up of the generator voltage. The generator resulted in a load (torque) proportional to angular velocity being imposed upon the motor under observation. Using the appropriate parameters for the motor and load, the following expressions were obtained for predicting the system performance (under the assumption of full shunt field at the instant of switching):

$$\omega = 183.5[1 + 0.345e^{-121.5t} - 1.345e^{-31.1t}] \text{ rad/sec.}$$

(5-28)

$$T = 1.255 + 23.1e^{-31.1t} - 24.35e^{-121.5t} \text{ newton-meters}$$

(5-29)

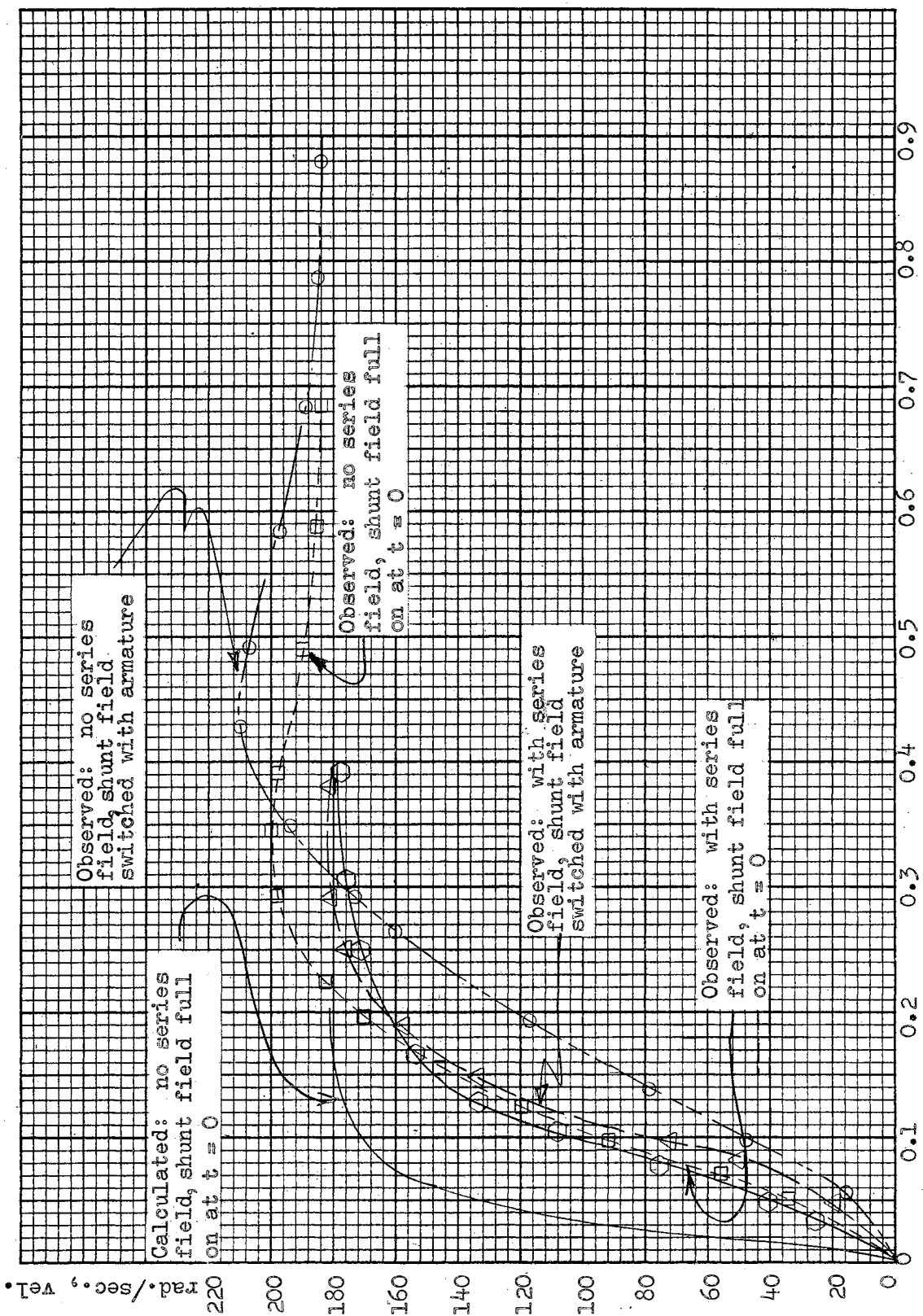


Figure 5.19. Speed Versus Time (Torque Proportional to Speed)

$$I = 2.18 + 40.5e^{-31.1t} - 42.3e^{-121.5t} \text{ amperes.} \quad (5-30)$$

In comparison with Equations (5-19), (5-20) and (5-21), which have a time constant (maximum) of 0.0332 seconds, the system now has a time constant (maximum) of .0321 seconds which is a slightly smaller value. The observed data (Figure 5.19) bears out that the addition of load had negligible affect upon the rate of increase of speed (acceleration).

Also, the amount of speed overshoot and the maximum value of speed overshoot are approximately the same for the loaded and unloaded conditions. The observed torque and current variations as a function of time are plotted in Figures 5.20 and 5.22. The observed torque, with load, as shown in Figure 5.20 is different than in the no-load case because an appreciable torque is required in the steady state condition. The transient portions observed exhibit the same behavior in each case, just as do the calculated expressions, but it persists for a longer period of time in the loaded case. If the current versus time relationship for the two situations is examined (Figure 5.14 and Figure 5.22) a tremendous difference in current magnitude during the transient period is quite obvious, i.e., 3.8 amperes versus 19.5 amperes peak. This large difference is a result of a delay in build up of counter electromotive force in the loaded motor immediately after switching the armature (due to lag in system speed) as can

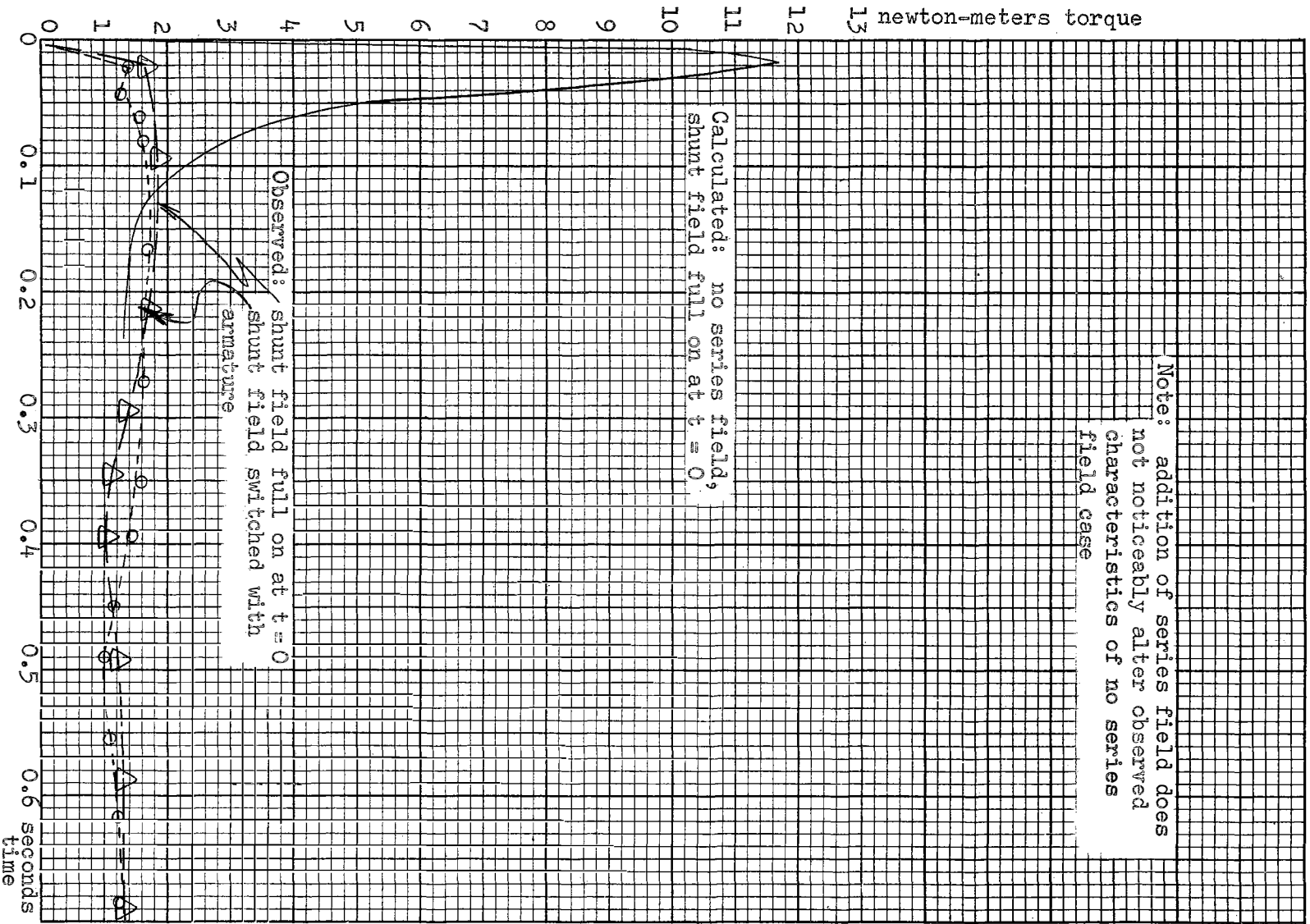


Figure 5.20. Torque Versus Time (Torque Proportional to Speed)

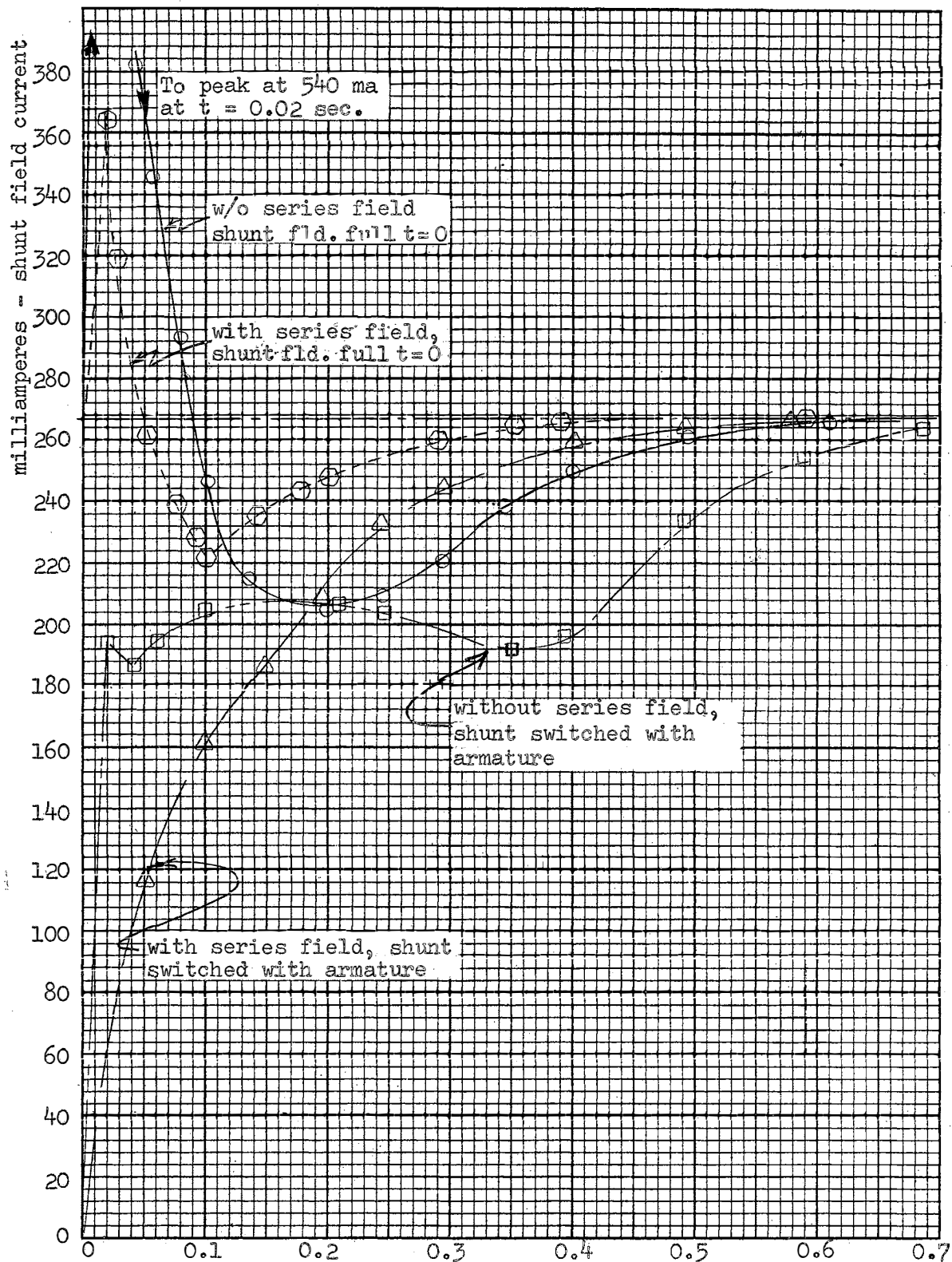


Figure 5.21. Effect of Series Field on Shunt Field.  
Current Variations (Torque Proportional to Speed)



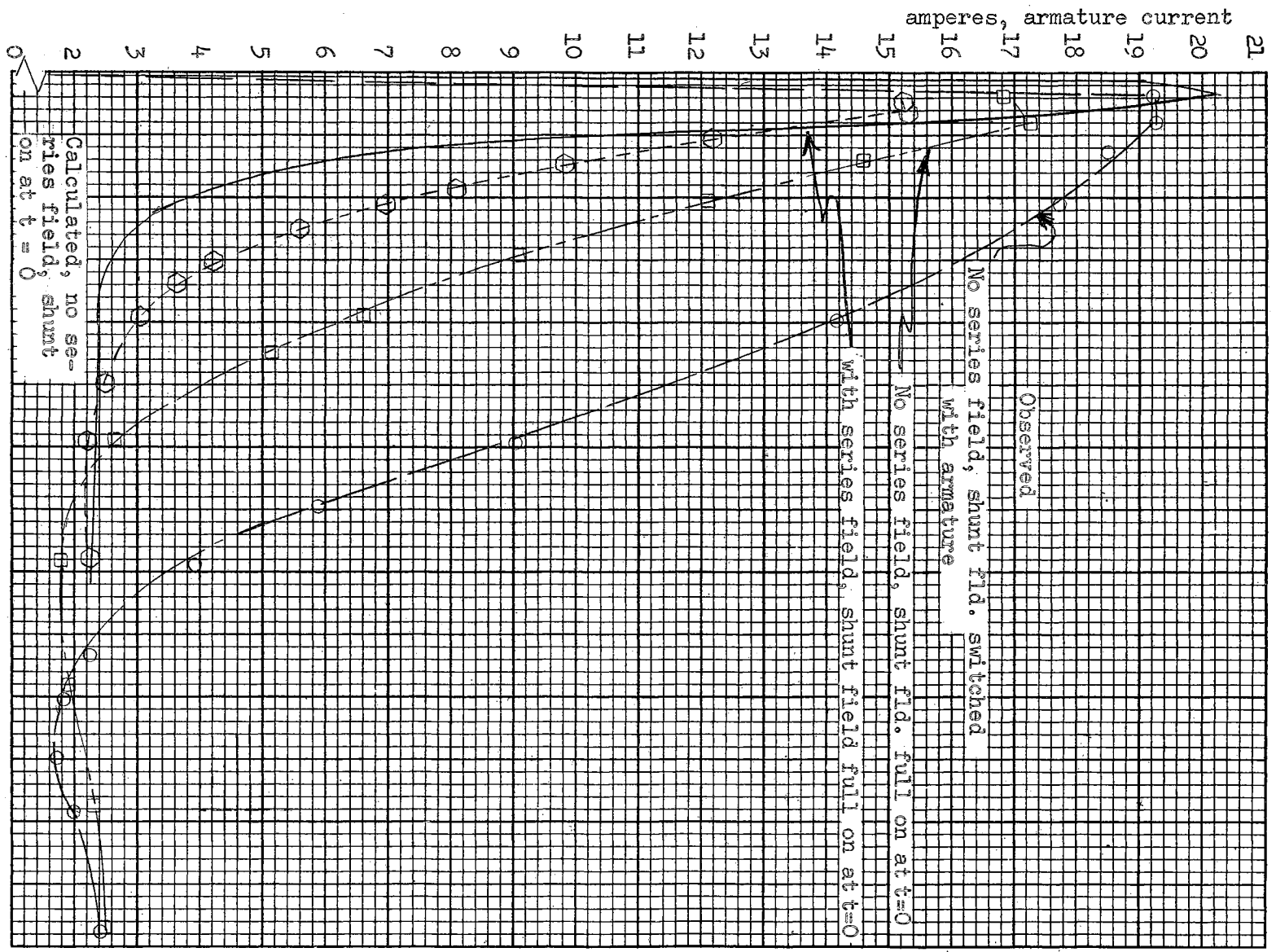


Figure 5.22. Armature Current Versus Time (Torque Proportional to Speed)

be visualized from an inspection of Figures 5.11 and 5.19). For example, with the shunt field full on at  $t = 0$ , the unloaded motor attains an angular velocity of 20 radians/second in 0.02 seconds, whereas, the loaded motor required 0.03 seconds. Since the theoretical value of the armature circuit time constant is  $0.0284/4.29 = 0.006$ , the extra 0.01 seconds delay is sufficient to allow the armature current to build up nearly to a value limited only by armature circuit resistance ( $115/4.29 = 26.8$  amperes). Excessive torque (corresponding to the 19.5 ampere peak) is not developed due to the demagnetizing effect of armature current and eddy and circulating currents discussed in Chapter IV. The dynamic torque constant, calculated from observed values of torque and current is plotted in Figure 5.23 for various conditions of shunt field switching and for the presence or absence of the series field. No discernable variation in the dynamic value of torque constant was detectable, lending additional credence to this author's previous statement that a small series field does not provide true "compounding" effect, but rather provides stabilization or damping. Additional verification can be obtained from an inspection of Figures 5.21 and 5.19 which point out that presence of the series field reduces shunt field current variations and eliminates speed overshoot under a loaded condition in the same manner that it does for the unloaded case.

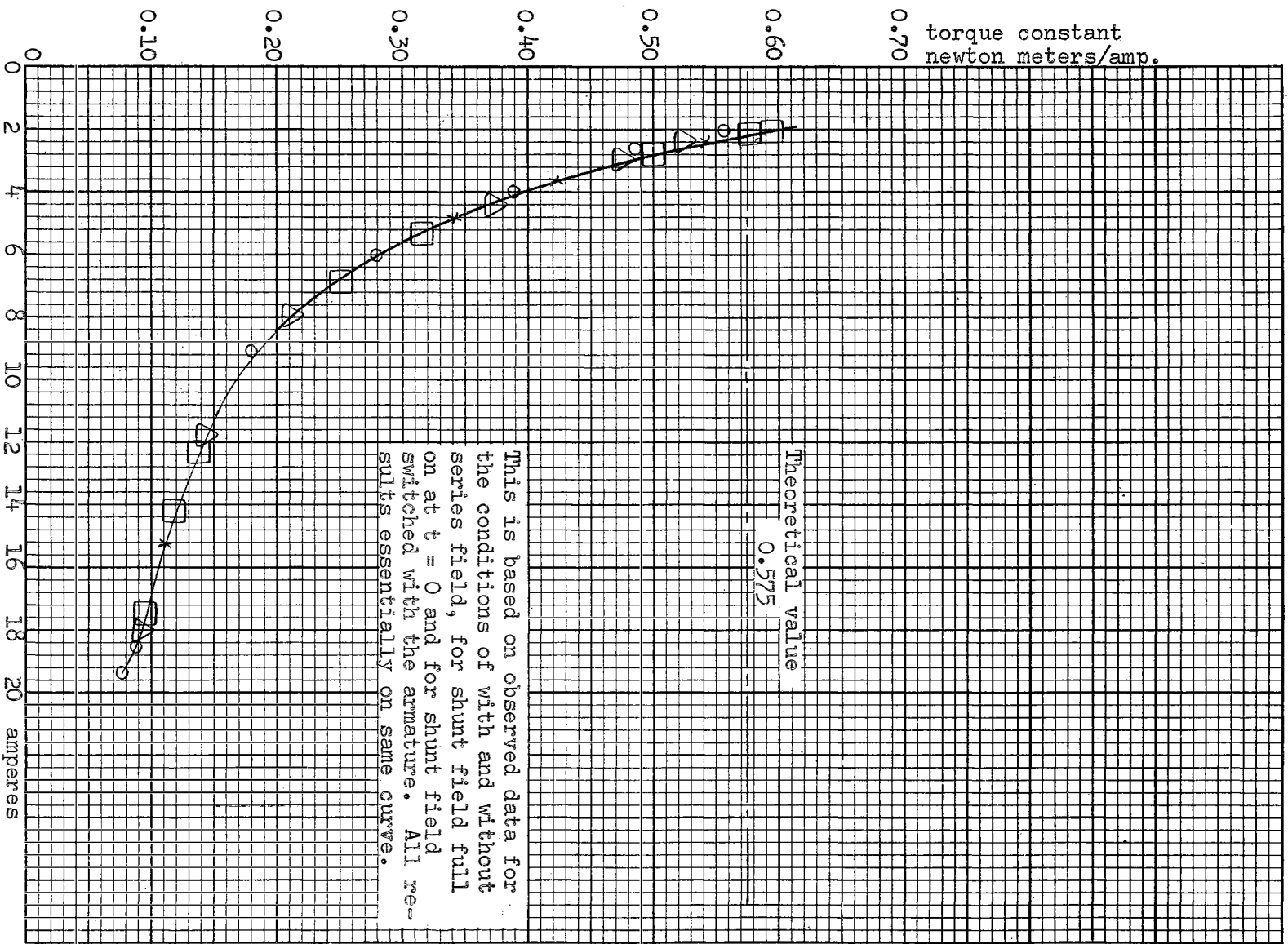


Figure 5.23. Dynamic Torque Constant as a Function of Armature Current (Underload)

When speed versus torque for the loaded system (Figure 5.24) is compared with the same variables for the unloaded system (Figure 5.16), it is obvious that the behavior is again very nearly identical for each situation.

Figures 5.25 through 5.29 depict the dynamic performance of the system when subjected to impact loads. Here again, the same type of system load was utilized, i.e., a separately excited generator. With the system at no-load equilibrium, a fixed value of resistance load was switched into the generator armature circuit and after new equilibrium was achieved, the load was removed. The equations of performance, based on Equation (3-18), and the appropriate variables are:

Load switched on

$$\omega = 189 + 22.85e^{-31.1t} - 5.85e^{-121.5t} \text{ rad/sec. (5-31)}$$

$$T = 1.27 + 2.25e^{-121.t} - 2.12e^{-31.1t} \text{ newton-meters. (5-32)}$$

$$I = 2.21 + 3.91e^{-121.t} - 3.68e^{-31.1t} \text{ amperes. (5-33)}$$

Load switched off

$$\omega = 206 + 5.67e^{-120.8t} - 22.67e^{-30.2t} \text{ rad/sec. (5-34)}$$

$$T = 0.203 + 2.190e^{-120.8t} - 2.195e^{-30.2t} \text{ newton-meters. (5-35)}$$

$$I = 0.353 + 3.81e^{-120.8t} - 3.82e^{-30.2t} \text{ amperes. (5-36)}$$

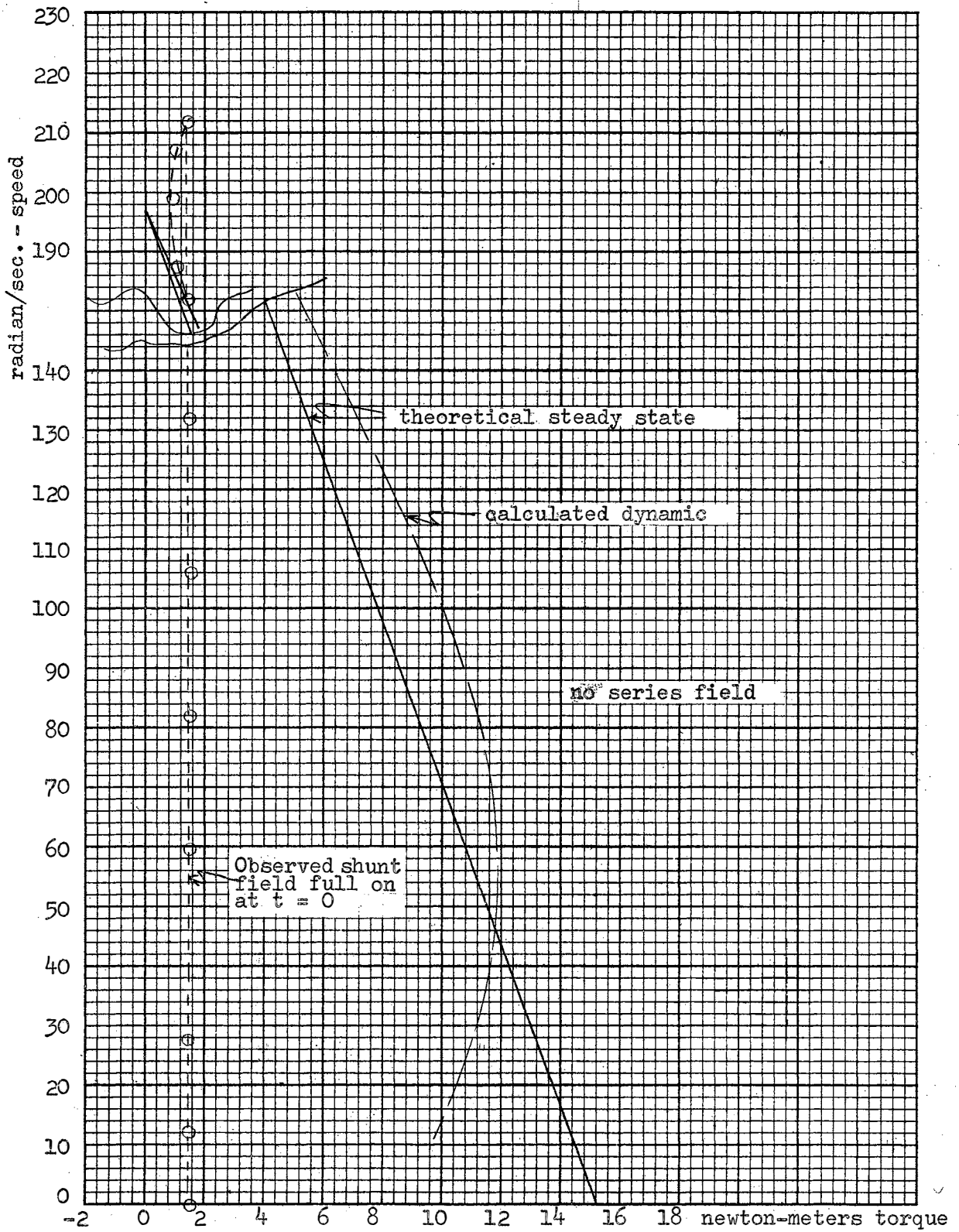


Figure 5.24. Speed Versus Torque (Torque Proportional to Speed)

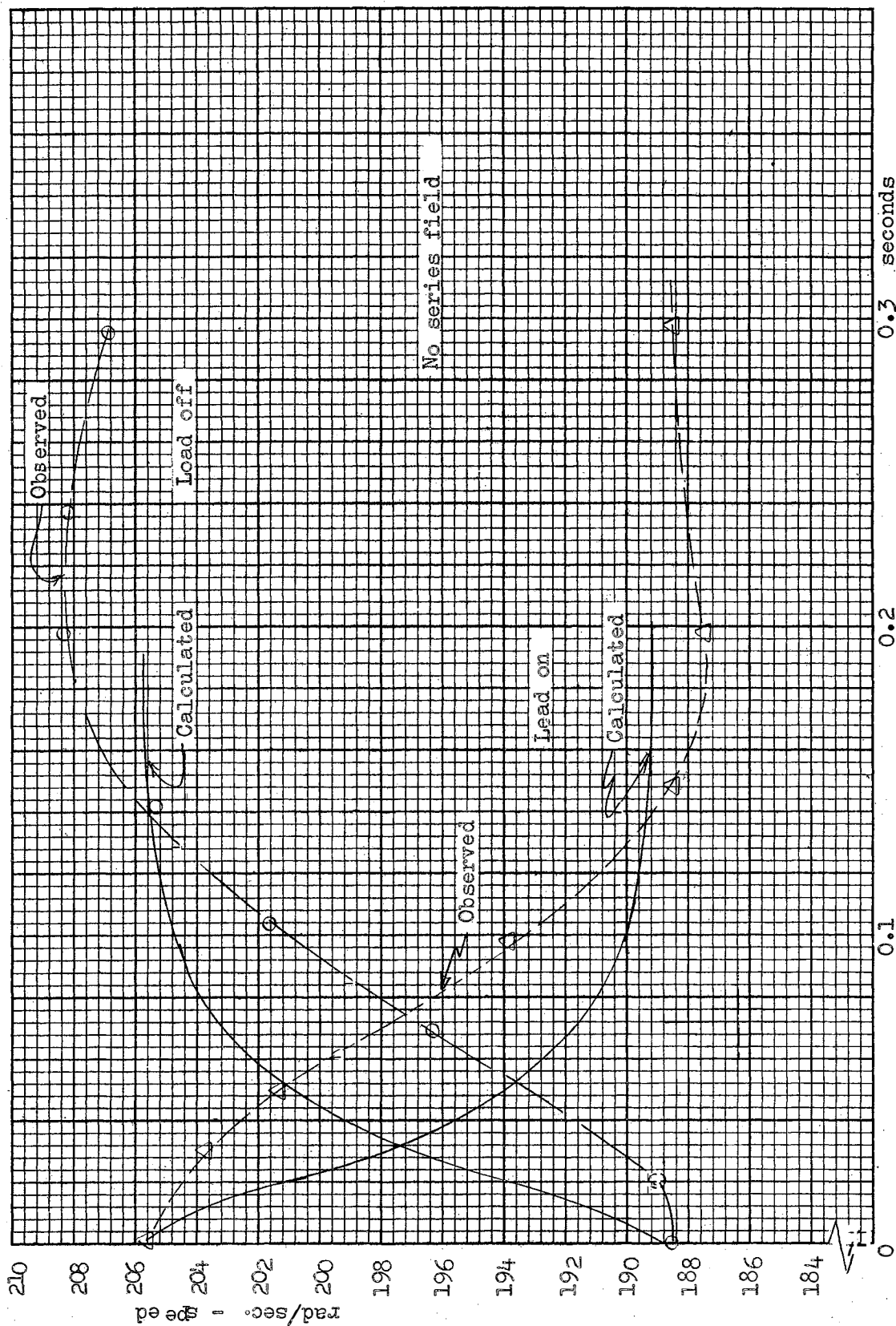


Figure 5.25. Speed Versus Time (Impact Loading)

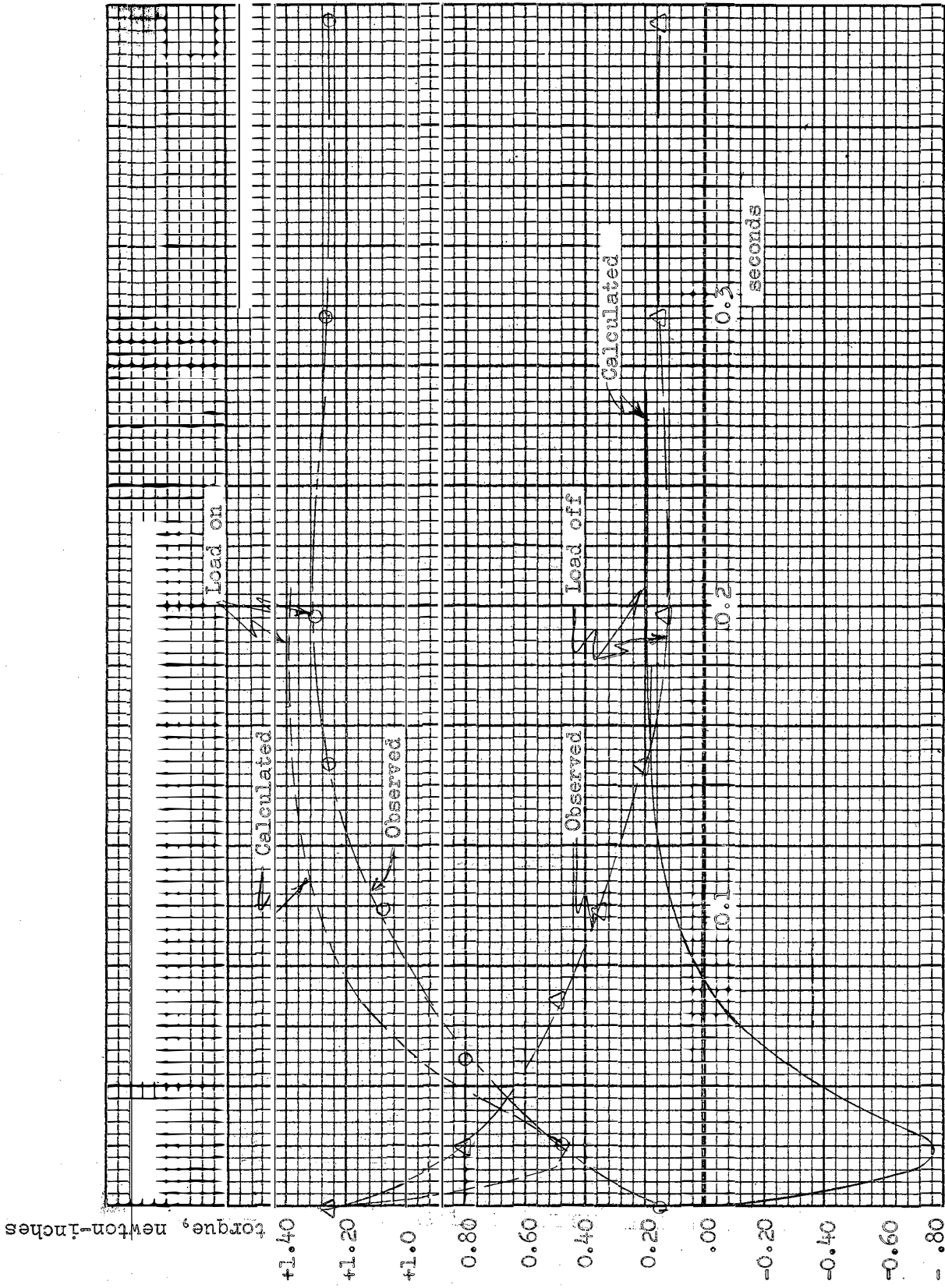


Figure 5.26. Torque Versus Time (Impact Load)

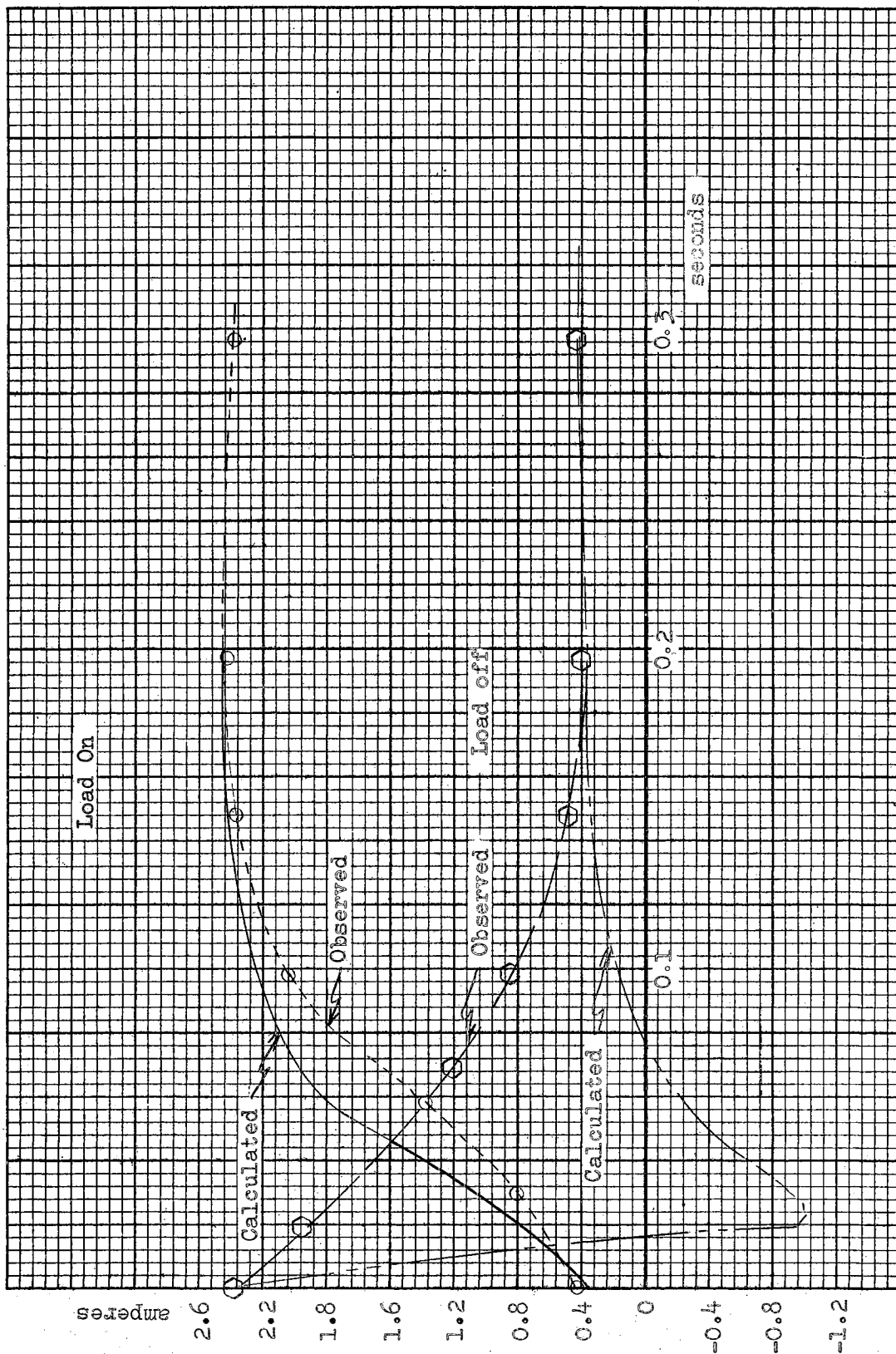


Figure 5.27. Current Versus Time (Impact Loading)



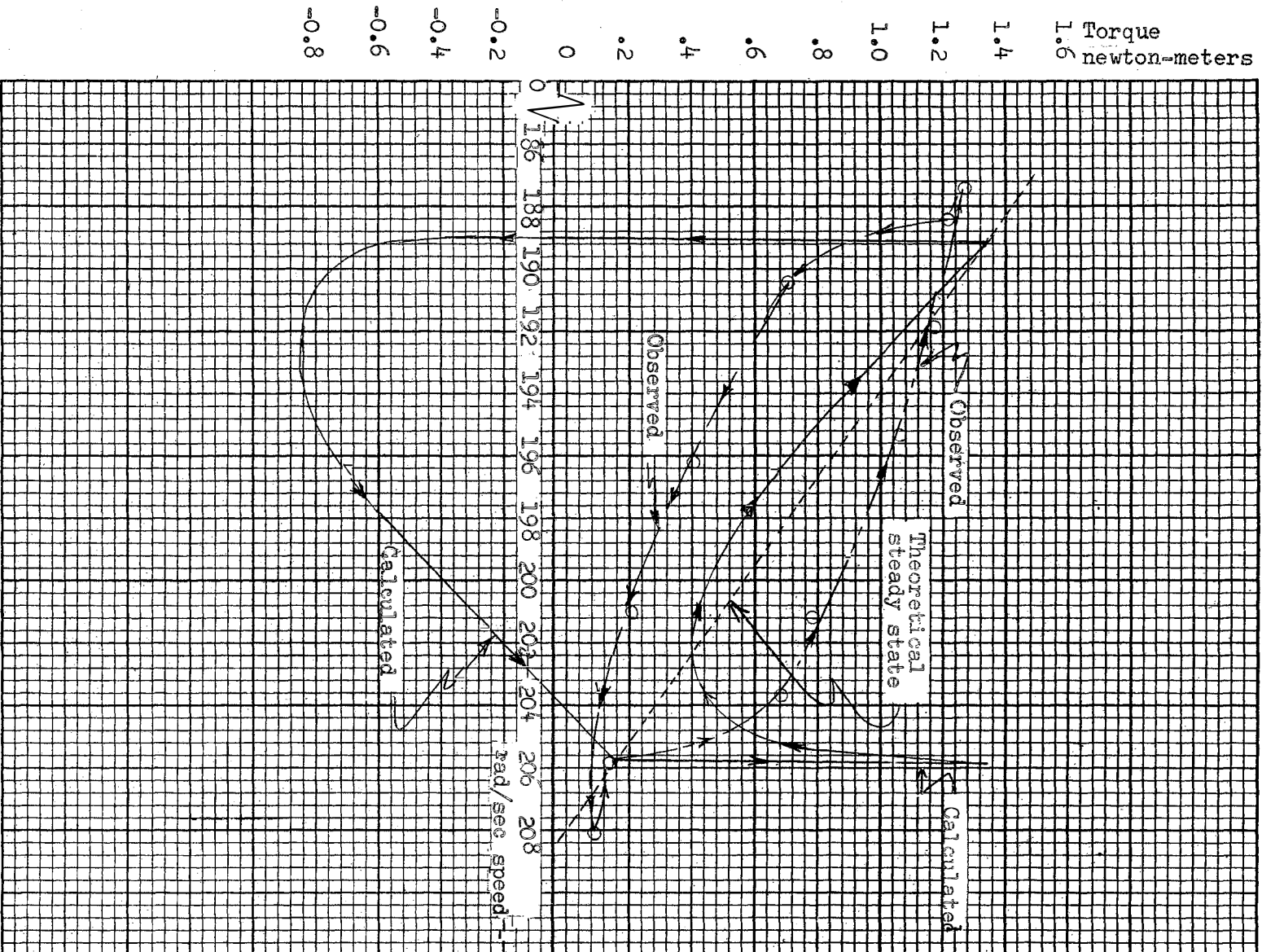


Figure 5.28. Speed Versus Torque (Impact Loading)

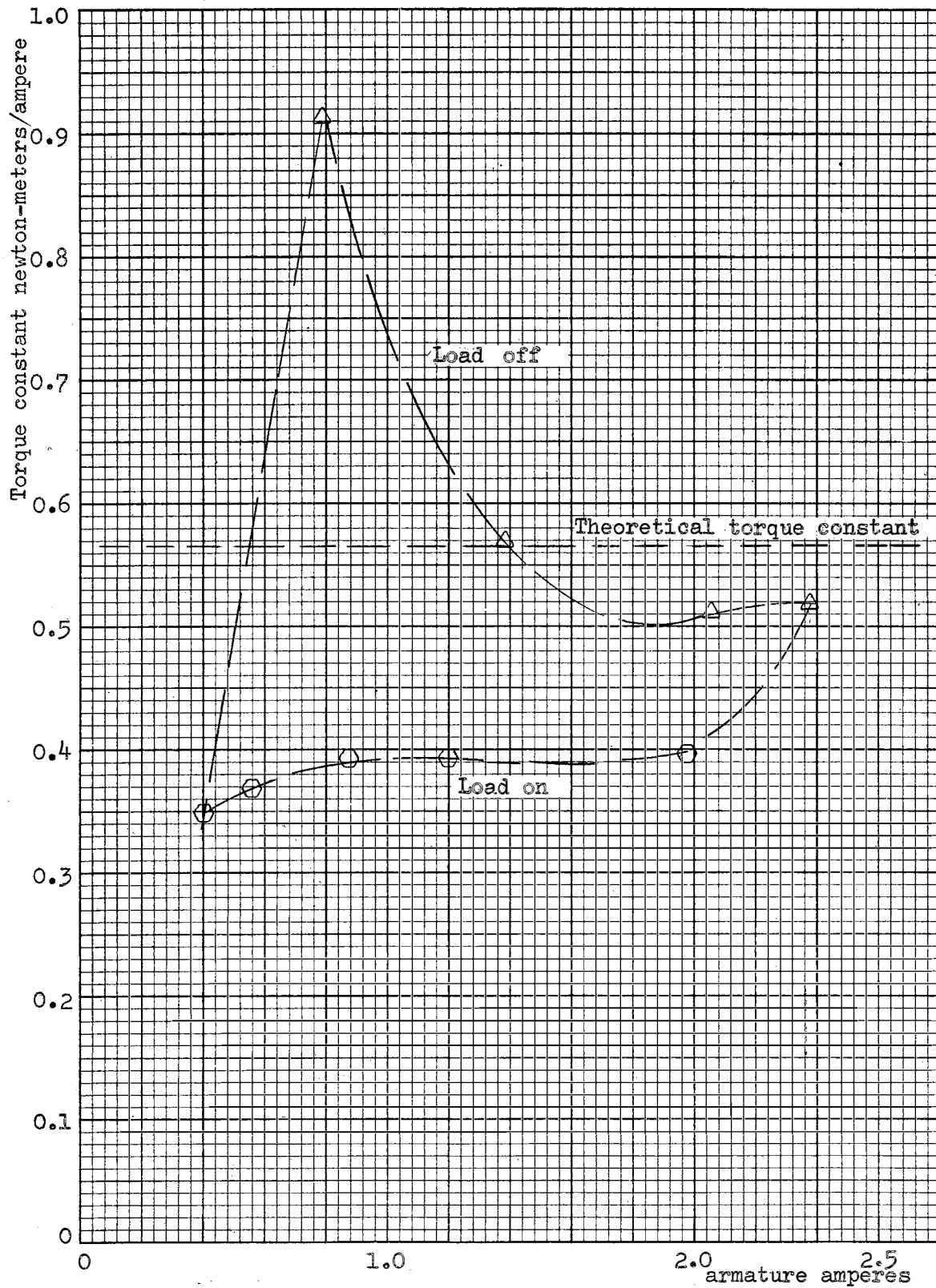


Figure 5.29. Torque Constant Variation (Impact Loading)

When the load is suddenly removed, the energy level stored in the air-gap must change, since a new equilibrium current will be established. Theoretically, a quantity of energy is transferred back to the supply system and the instantaneous current and torque should reverse, briefly. Figures 5.26, 5.27, and 5.28 illustrate this phenomena in the calculated performance curves. However, the observed characteristics do not display this predicted reversal. It is felt by this author that the reversal is present, but of such short duration as to not be present on the relatively "slow" recordings taken in this study. The shunt field current was monitored during the impact loading tests and was found to vary over a range of from rated (value at time  $t = 0$ ) down to 94.5% of rated during the transient period, with the minimum value occurring at  $t = 0.07$  seconds. Tests made when the series field was added indicate an elimination of shunt field current variation during the transient period, but the other performance characteristics were so close in value to those obtained without the series field that it was felt that no useful purpose would be served in presenting them.

In general, the actual performance departs quite widely from the theoretical performance in each instance, pointing up the need for a modification to the presently used methods of representation and analysis, especially for control system use. Two alternatives present themselves:

- (i) To take precautions, in the design stage, to insure that phenomena discussed in Chapter IV are minimized and attempt to design a motor that behaves, as closely as possible, as present analysis methods predict.
- (ii) To derive a modified expression for performance, based either on test results of a specific motor or an observed performance of a large number of motors of different size and design. Chapter VI of this thesis will concern itself with this procedure.

## CHAPTER VI

### MODIFIED PERFORMANCE EQUATIONS

In order to gain insight into the complexity of analytically describing shunt motor performance, consider Equation (3-18) which is used to describe the "linearized" shunt motor speed versus time behavior. It is a linear second order differential equation, and the motor, as described, can be said to be a "second order system".

The differential equation of a second order system, when transformed from the time domain to the "s-plane" by Laplace Transform techniques, has the following general form (with step type input):

$$\omega(S) = \omega_{\infty} \left[ \frac{1}{s \left( 1 + \frac{2\xi s}{\omega} + \frac{s^2}{\omega^2} \right)} \right] \quad (6-1)$$

where:

$\omega_{\infty}$  = steady state speed

$\xi$  = system damping factor

$\omega$  = system natural frequency

$\omega(S)$  = Laplace transform of instantaneous speed as a function of time. (21, 22).

Speed, as a function of time, can be obtained from the inverse transformation of Equation (6-1):

$$\omega(t) = \omega_{\infty} \left[ 1 + \frac{1}{\sqrt{1 - \xi^2}} e^{-\xi\omega t} \sin(\omega\sqrt{1 - \xi^2} t - \chi) \right] \quad (6-2)$$

where:

$$\chi = \tan^{-1} \frac{\sqrt{1 - \xi^2}}{-\xi} . \quad (21).$$

Equation (6-2) is a solution of Equation (3-18) whose form is preferred over Equation (3-21) when the roots of the auxiliary equation (Equation 3-20) are imaginary. As pointed out in Equation (3-24), the criteria for oscillation, or overshoot, about the ultimate value of the dependent variable is that the roots of the auxiliary equation be imaginary. In Equation (6-1), the denominator has imaginary roots if:

$$\xi < 1.0 . \quad (6-3)$$

In control system technology, the value of damping which corresponds to  $\xi = 1.0$  is referred to as "critical damping" and values less than this result in "under damping" and the response displays an oscillation or overshoot of its ultimate steady state position. Actually, for an overshoot of 10% of its ultimate equilibrium position, the necessary value of  $\xi$  is:

$$\xi \approx 0.6 . \quad (6-4)$$

Now, when Equation (6-2) is plotted on a rectangular coordinate system, it displays the general form shown in Figure 6-1.

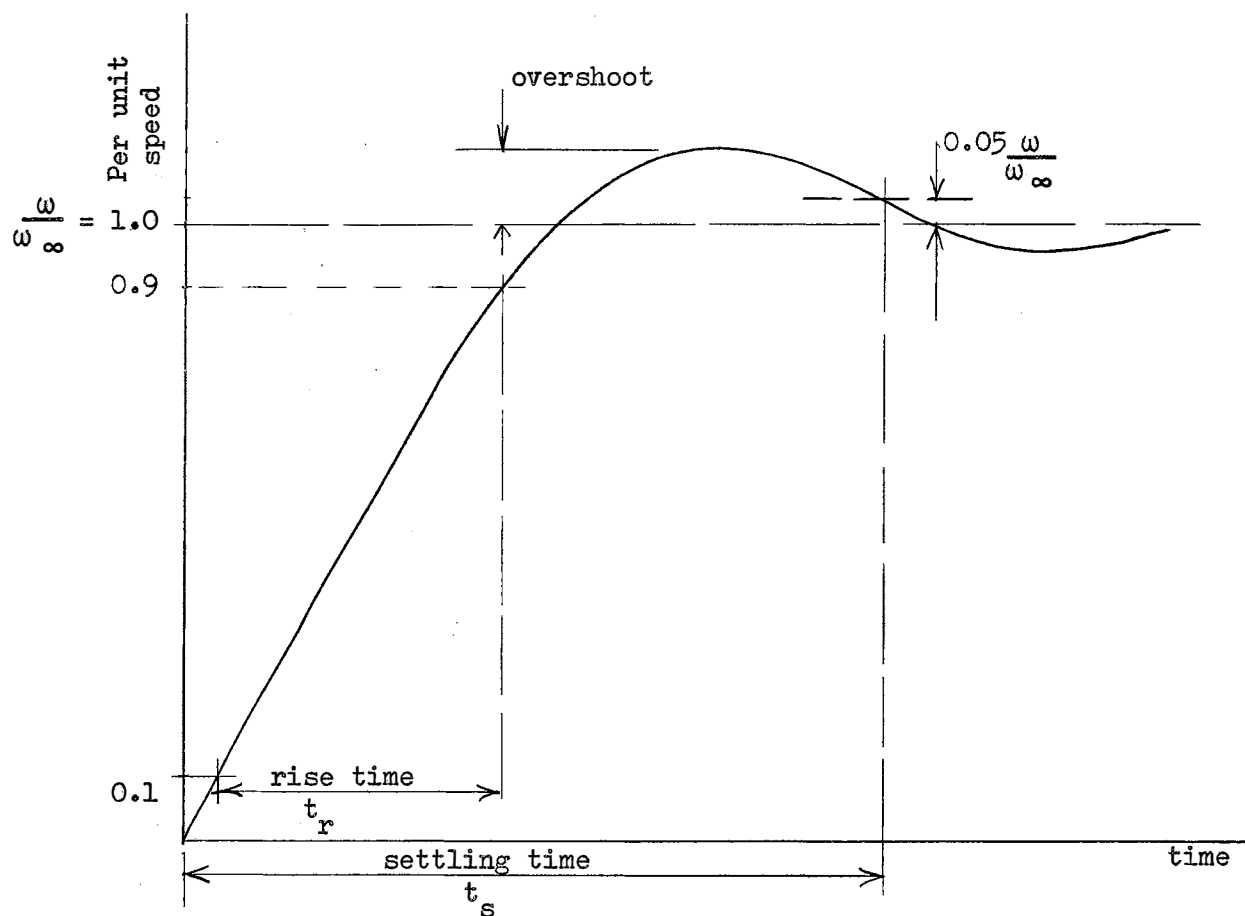


Figure 6.1. Second Order System Response to Step Input

Two specifications for second order linear systems that are related to  $\xi$  and  $\omega$  are rise time,  $t_r$ , and settling time,  $t_s$ . These are arbitrarily defined parameters and are shown in Figure 6.1. It can be shown that:

$$t_s = \frac{3}{\xi\omega} \text{ and } t_r \approx \frac{0.30 \text{ to } 0.45}{\omega} . \quad (6-5)$$

For an overshoot of 10% or greater, 0.45 is the appropriate constant in Equation (6-5). (22). Using this

value, and eliminating  $\omega$  from the two expressions, leads to:

$$\xi \approx \frac{6.67 t_r}{t_s} . \quad (6-6)$$

When  $t_r$  and  $t_s$  are measured for the system under investigation (from Figure 5.19) and used in Equation (6-6), a calculated value of damping factor is found such that:

$$\xi \geq 2.35 . \quad (6-7)$$

This value corresponds to a heavily overdamped, non-oscillating (and no overshoot) response: Yet, the system does overshoot. Clearly then, it will not be possible to express this system response in terms of a second order differential equation.

Several approaches to this problem were explored in the course of this study. Among those worthy of discussion were:

1. Use of the "describing function" technique.
2. Curve fitting procedures involving polynomials.
3. The addition of "poles" to the Laplace transformation as given in Equation (6-1).

Even though all methods were not successful or feasible, the reasoning associated with the success or failure of the divers methods is, it is felt, worthy of discussion.

#### The "Describing Function" Technique

This technique is used in system analysis for systems



containing an element which displays a large departure from linearity. The technique has been used for describing the response of such phenomena as "abrupt saturation," "dead bands," "backlash," etc. The use of this technique presupposes two rather restricting assumptions, i.e.:

- i. The input to the nonlinear device is to be a pure sine wave.
- ii. The higher harmonics in the output of the nonlinear device may be neglected.

The first assumption is so restrictive as to remove any utility for this application that the describing function may usually have. Its greatest usage is in the determination of a stable or unstable situation, not response as a function of time. The input to a shunt motor is usually a step type input. The very fact that the motor exhibits nonlinear relationships prevents the application of the principle of superposition which would permit extrapolation of sinusoidal input results to determine step input response.

#### Curve Fitting Procedures Involving Polynomials

The simplest curve fitting procedures involve fitting the coefficients of the polynomial  $\omega(t)$  to a given set of data points, thus:

$$\omega(t) = a_0 + a_1t + a_2t^2 + a_3t^3 + \dots \text{ etc.} \quad (6-8)$$

Since torque, as a function of time, may be calculated

from Equation (6-8), and this calculation involves derivatives, it is necessary to use a curve fitting procedure which insures as complete correspondence as possible between the describing polynomial and the actual data. A curve passing through the data points, but with no restriction placed on its locus between selected points may lead to false results and conclusions in both speed and torque calculations. A quadratic expression is the highest order polynomial which can be depended upon to pass through the selected points and to insure a "smooth" curve between the selected points. Since a quadratic equation fitting requires only three sets of data points and three sets of data points are insufficient to adequately describe the  $\omega$  versus  $t$  curve, such as in Figure 5.19, some means of using a succession of quadratic equations must be resorted to for a successful application. One method of doing this is to use quadratic equations which are delayed or shifted until specified times. This technique is possible by virtue of the ability to express some function of time as being zero until some specified time has elapsed.

For example, if  $U(t)$  denotes a unit step function,  $U(t - a)$  denotes also a unit step function, except in the latter case, the value of the function is zero until time  $t=a$  has elapsed. Whereas, the Laplace Transform of  $U(t)$  is  $\frac{1}{s}$ , the transform of  $U(t - a)$  is found to be  $\frac{e^{-as}}{s}$ . (21). Indeed, multiplying the Laplace Transform of any function by  $e^{-as}$  has the affect of shifting the time function "a"

units in time to the right on a rectangular coordinate systems. This can be illustrated by considering a polynomial,  $\omega(t)$ , as plotted in Figure 6.2. If it is desired that the value of this polynomial be zero for times less than or equal to  $t_1$ , it is customary to express the function as  $U_{-1}(t - t_1)\omega(t)$ , where  $U_{-1}(t - t_1)$  represents a step function of unit magnitude delayed until time  $t_1$ . If  $\omega(t) = a_0 + a_1t + a_2t^2$ , the Laplace transform,  $F(S)$ , of the delayed function is

$$F(S) = L[U_{-1}(t - t_1)\omega(t)] \quad (6-9)$$

where  $L$  denotes the transformation process. If  $T = t - t_1$ , then  $t = T + t_1$

and

$$L[U_{-1}(t - t_1)\omega(T + t_1)] = e^{-t_1 S} L[\omega(T + t_1)] \quad (6-10)$$

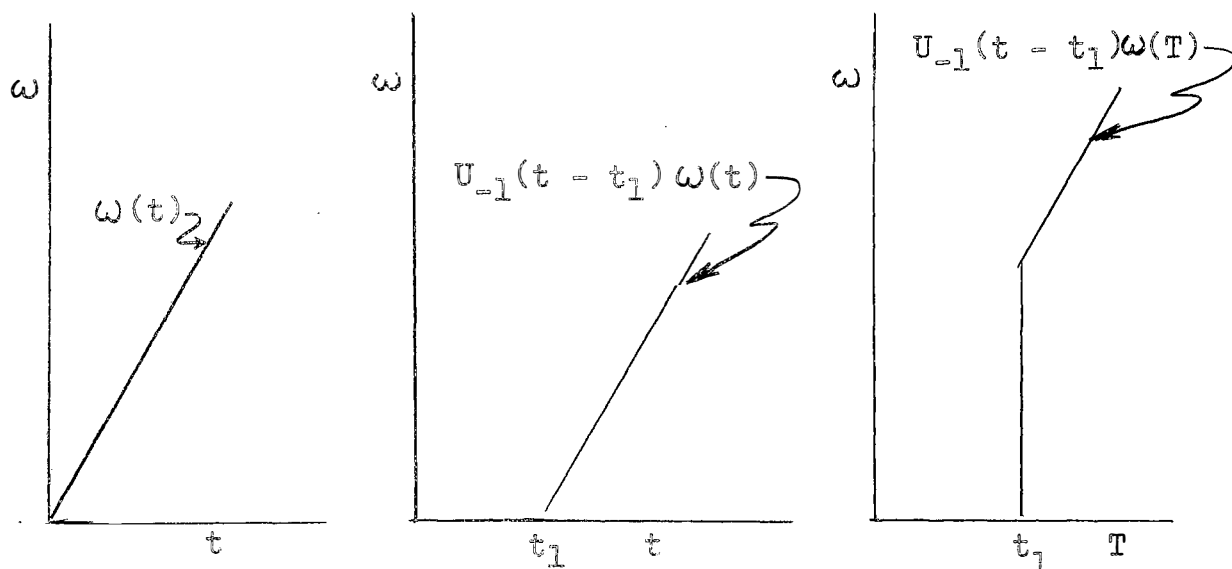


Figure 6.2. Delay and Shift Using Laplace Transforms

Assume a typical  $\omega$  versus  $t$  curve as shown in Figure 6.3. A smooth curve through three points, 2, 3, and 4 can be expressed as

$$\omega(t) = a_0 + a_1 t + a_2 t^2$$

changing this to a function of  $T = t - t_1$ , using it in Equation (6-10), and expanding yields

$$\begin{aligned} L[U_{-1}(t - t_1)\omega(T + t_1)] &= e^{-t_1 s} L[\omega(T + t_1)] \\ &= e^{-t_1 s} L[a_0 + t_1 a_1 + a_2 t_1^2 + T(a_1 + 2t_1 a_2) + \\ &\quad + a_2 T^2]. \end{aligned} \quad (6-11)$$

The delayed polynomial then has the Laplace transform:

$$\begin{aligned} \omega(s) &= e^{-t_1 s} \left[ \frac{(a_0 + a_1 t_1 + a_2 t_1^2)}{s} + \frac{(a_1 + 2t_1 a_2)}{s^2} + \right. \\ &\quad \left. + \frac{2a_2}{s^3} \right]. \end{aligned} \quad (6-12)$$

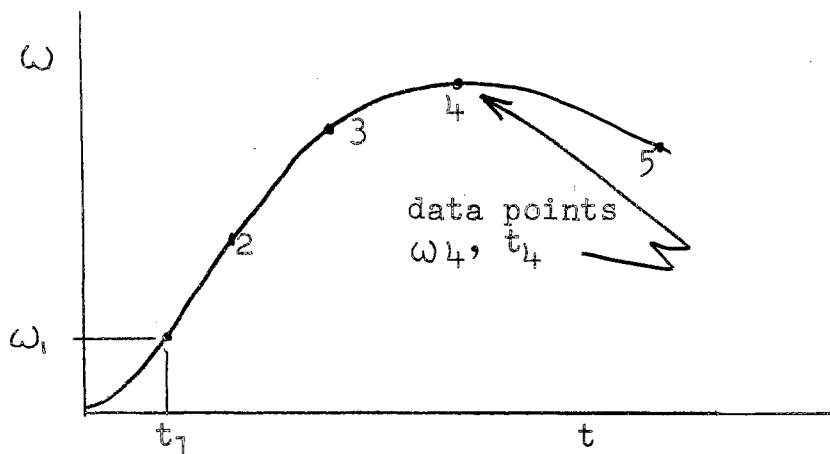


Figure 6.3. Typical  $\omega$  Versus  $t$  Characteristic

If the negative of Equation (6-11) is manipulated in the same fashion except using a unit step delayed until time  $t_3$ , the time function shown in Figure 6.4 can be generated. It's Laplace transform is:

$$\omega(s) = e^{-t_1 s} \left[ \frac{(a_0 + a_1 t_1 + a_2 t_1^2)}{s} + \frac{(a_1 + 2t_1 a_2)}{s^2} \right] +$$

(Continued on next page)

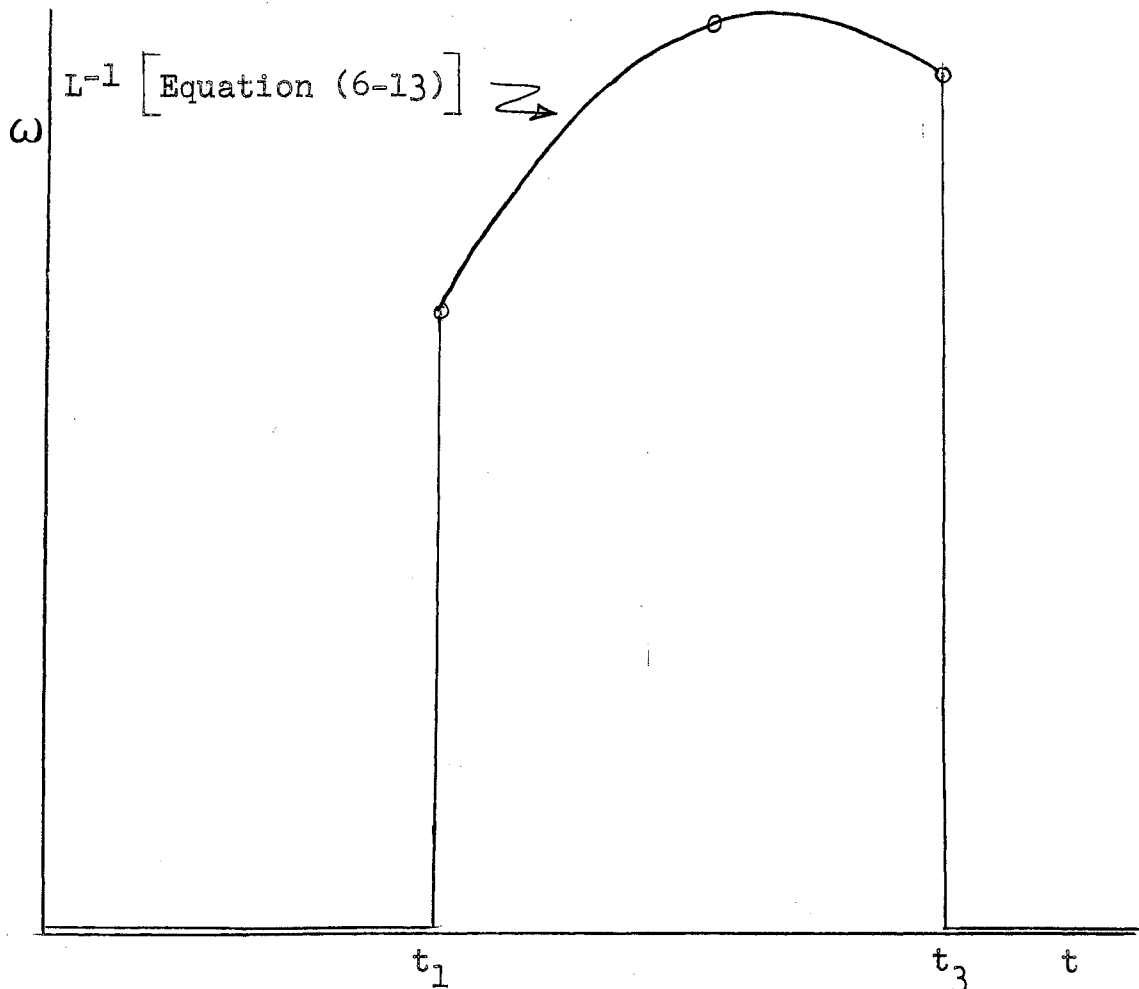


Figure 6.4. Generating Non-Periodic Functions by Delay and Shift

$$\begin{aligned}
& + \frac{2a_2}{s^3} \Big] - e^{-t_3 s} \left[ \frac{a_0 + a_1 t_3 + a_2 t_3^2}{s} + \right. \\
& \left. + \frac{a_1 + 2t_3 a_2}{s^2} + \frac{2a_2}{s^3} \right] \quad (6-13)
\end{aligned}$$

Equation (6-13) transforms back to the time domain as:

$$\omega(T) = (a_0 + a_1 t_1 + a_2 t_1^2) + (a_1 + 2t_1 a_2)T + a_2 T^2$$

or, since  $T = t - t_1$

$$\omega(t) = a_0 + a_1 t + a_2 t^2 \quad (6-14)$$

for  $t_1 < t \leq t_3$ .

By utilizing sequences of combinations of three successive data points, it is thus possible to represent the speed-time characteristic, obtained experimentally, by a Laplace transform. The motor transfer function  $\omega(S)/V(S)$  can then be obtained since  $\omega(S)$  as determined here is for a step voltage input,  $V(S) = \frac{V}{s}$ . Thus:

$$\frac{\omega(S)}{V(S)} = \frac{s\omega(S)}{V} \quad (6-15)$$

This transfer function appears to be a much more reliable representation than the function derived from linear analysis.

The coefficients for use in the several quadratic equations used here can be found either by writing three simultaneous equations involving the three data points or by an application of Lagrange's interpolation method. If

$\omega_i, t_i; \omega_j, t_j; \omega_k, t_k$  are three successive data points, the former method requires simultaneous solution of:

$$\begin{aligned} a_0 + a_1 t_i + a_2 t_i^2 &= \omega_i \\ a_0 + a_1 t_j + a_2 t_j^2 &= \omega_j \\ a_0 + a_1 t_k + a_2 t_k^2 &= \omega_k \end{aligned} \quad (6-16)$$

for the coefficients  $a_0, a_1$ , and  $a_2$ .

Lagrange's Interpolation Method involves evaluation of:

$$\begin{aligned} \omega = & \frac{(t - t_j)(t - t_k)}{(t_i - t_j)(t_i - t_k)} \omega_i + \frac{(t - t_i)(t - t_k)}{(t_j - t_i)(t_j - t_k)} \omega_j \\ & + \frac{(t - t_i)(t - t_j)}{(t_k - t_i)(t_k - t_j)} \omega_k, \end{aligned} \quad (6-17)$$

from which  $a_0, a_1, a_2$  are found as coefficients of  $t^0, t^1, t^2$ .

Calculated results using this method are presented in Section 4 of this chapter.

#### Addition of "Poles" to Modify Equation (6-1)

The form of Equation (6-1) and the actual behavior pattern of the motor suggested the possibility of adding to Equation (6-1) to obtain an expression of the following

type:

$$\omega(s) = \omega_{\infty} \left[ \frac{1}{s(1 + \frac{2\xi}{\omega} s + \frac{s^2}{\omega^2})(s + p_4)(s + p_5) \dots} \right] \quad (6-18)$$

where  $p_4, p_5 \dots$  are additional "poles" in the  $s$ - or complex plane. (22). The addition of poles has two effects, i.e.: (1) additional derivatives of the step function response at  $t = 0$  (resulting in a slower starting response, and (2) a change in amplitude and phase of the damped oscillation term in the time expression.

Unfortunately, no analytical technique for pole location is available, other than the time honored method of 'cut and try'. This investigator simulated a second order system using cascaded passive network of resistance and capacitance elements sized to behave (transfer function-wise) as a linear shunt motor. Additional passive networks with adjustable elements were then placed in series to simulate the addition of poles corresponding to  $p_4$  and  $p_5$ . With a step voltage input, the output was recorded and, by means of adjusting pole location, an attempt was made to reproduce actual motor output behavior. It was found that the addition of each pole has very slight affect on the transient response to a step input. The only possibility would be to use a large number of additional poles and the necessity for executing a unique, composite adjustment of each pole position makes this approach unworkable.



### Calculation of Response Using Curve Segments

The sets of data points shown in Table VI-II were taken from the speed response of the motor used in this investigation (plotted in Figure 5.19) for the condition of no series field and with the shunt field at rated excitation at time  $t = 0$ . The coefficients of the quadratic equations representing the various response curve segments were calculated using the Lagrange Interpolation Formula and are presented in Table VI-II. The curve segments are plotted, using the calculated coefficients, in Figure 6.5. Using the delay and shift techniques associated with Laplace transformation methods, as discussed earlier, the Laplace transformation of speed as a function of time is (using coefficients from Table VI-II):

$$\begin{aligned} \omega(s) = & \frac{224}{s^2} + \frac{14360}{s^3} + e^{-0.1s} \left[ \frac{2}{s} - \frac{470}{s^2} - \frac{22920}{s^3} \right] + \\ & + e^{-0.2s} \left[ -\frac{86}{s} + \frac{2050}{s^2} + \frac{3960}{s^3} \right] + \\ & + e^{-0.3s} \left[ \frac{3}{s} + \frac{60}{s^2} + \frac{200}{s^3} \right] + \\ & + e^{-0.4s} \left[ \frac{153}{s^2} + \frac{3065}{s^3} \right] + \\ & + e^{-0.5s} \left[ -\frac{3.5}{s} + \frac{667}{s^3} \right] + \end{aligned}$$

(Continued on page 232)

TABLE VI-II

DATA POINTS,  $\omega$  VERSUS  $t$  (Figure 5-19)

$\omega$	$t$				
0	0				
34	0.055				
94	0.1				
172	0.2				
204	0.3				
202	0.4				
188	0.5				
186	0.7				
1. $\omega = 0 + 224t + 7180t^2$			$a_0^1 = 0$	$a_1^1 = 224$	$a_2^1 = 7180$
2. $\omega = -66 + 2050t - 4280t^2$			$a_0^2 = -66$	$a_1^2 = 2050$	$a_2^2 = -4280$
3. $\omega = -30 + 1470t - 2300t^2$			$a_0^3 = -30$	$a_1^3 = 1470$	$a_2^3 = -2300$
4. $\omega = 6 + 1170t - 1700t^2$			$a_0^4 = 6$	$a_1^4 = 1170$	$a_2^4 = -1700$
5. $\omega = 190 + 97t - 167t^2$			$a_0^5 = 190$	$a_1^5 = 97$	$a_2^5 = -167$
6. $\omega = 270 - 236t + 166t^2$			$a_0^6 = 270$	$a_1^6 = -236$	$a_2^6 = 166$

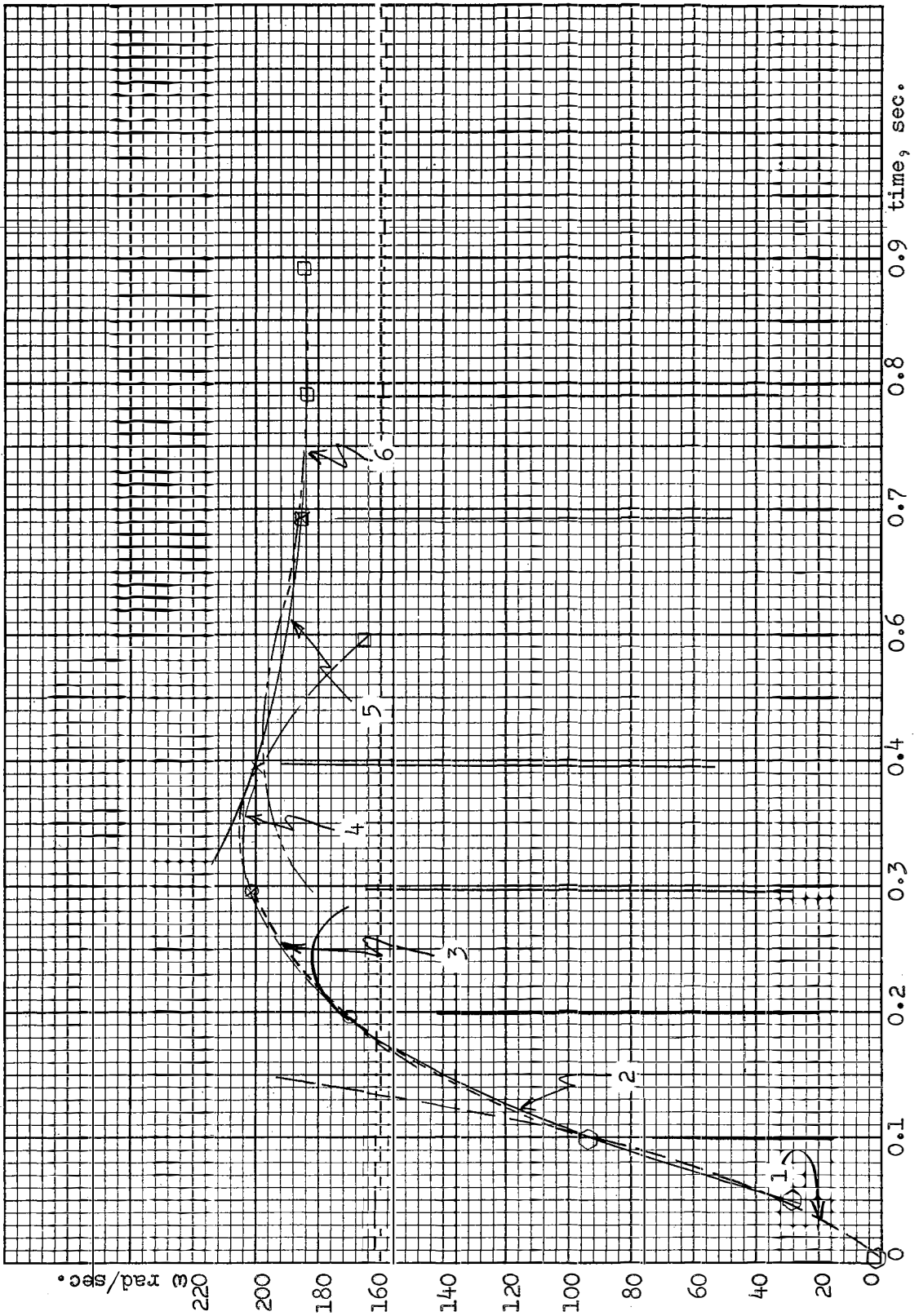


Figure 6.5. Curve Fitted Segments (Speed Versus Time)

$$+ e^{-0.7s} \left[ \frac{4}{s^2} - \frac{333}{s^3} \right]. \quad (6-19)$$

The speed response used in these calculations was for a step input voltage of 115 volts;  $V(S) = 115/s$ . Dividing each side of Equation (6-19) by  $V(S)$  will yield the motor transfer function.

Since the nonlinearity exhibited by the motor is a result of shunt field to armature circuit coupling more than as a result of saturation of the iron core, the transfer function as obtained above should be valid over the rated voltage range of the motor.

Since the general torque expression is:

$$T = J \frac{d\omega}{dt} + C_1 + C_2\omega \quad (6-20)$$

torque, as a function of time can be calculated over the various time intervals. Using the previously established values of:

$$C_1 = 0.1427 \text{ newton-meters}$$

$$C_2 = \frac{6.07}{1000} \text{ newton-meters/radian}$$

$$J = 0.0032 \text{ Kg-meters-sec}^2$$

the calculated values of torque are:

$$0 < t < 0.1$$

$$T = 0.85 + 27.2t + 43.6t^2$$

$$0.1 \leq t < 0.2$$

$$T = 4.5 - 15t - 27t^2$$

$$0.2 \leq t < 0.3$$

$$T = 4.661 - 5.80t - 13.97t^2$$

$$0.3 \leq t < 0.4$$

$$T = 3.924 - 3.78t - 10.32t^2$$

$$0.4 \leq t < 0.6$$

$$T = 1.606 - 0.480t - 1.013t^2$$

$$0.6 \leq t < 0.7$$

$$T = 1.02 - 0.37t + t^2$$

$$t \geq 0.7$$

$$T = 1.28 \text{ newton meters.} \quad (6-21)$$

Values of torque for various times were calculated and are shown in Figure 6.6 along with torque calculated from the linearized equations and the observed torque reproduced from Figure 5.20. The torque, as calculated from Equation (6-21), leaves a lot to be desired from the accuracy standpoint, but it is a considerably better representation in several respects, i.e., the torque calculated by Equation (6-21) shows a maximum of less than twice observed torque, whereas the torque calculated from the linearized analysis

has a peak of approximately six times the observed value and the linearized version reaches steady state in 0.15 seconds, whereas the observed torque and the torque calculated by Equation (6-21) both reach steady state about  $t = 0.70$  seconds. Also, by Equation (6-21), the torque behaves as the observed torque in that there is an undershoot below the ultimate value while the linear version appears to be slightly over-damped.

This method of speed and torque calculation is far superior to procedures based on linearized versions of the shunt motor and gives nearly exact reproductions of speed versus time and a usable transfer function for the motor even though the torque calculations are in error. It is felt by this investigator that the probable source of error lies in a possible oversimplification of the system friction because of the neglect of coulomb friction; that is, "static" friction. A non-zero value of input is necessary to overcome this type of friction and it is a different value than will be obtained by projecting the rolling friction and rotating torques back to zero speed (which is a standard procedure and the one used in this analysis). This "threshold" behavior is a consequence of phenomena that exists on a microscopic scale and can be characterized only in statistical terms. Also, some error will have been introduced in arbitrarily selecting data points from the speed versus time response because the  $t$  location of a specific  $\omega$  data point will have a great deal of influence

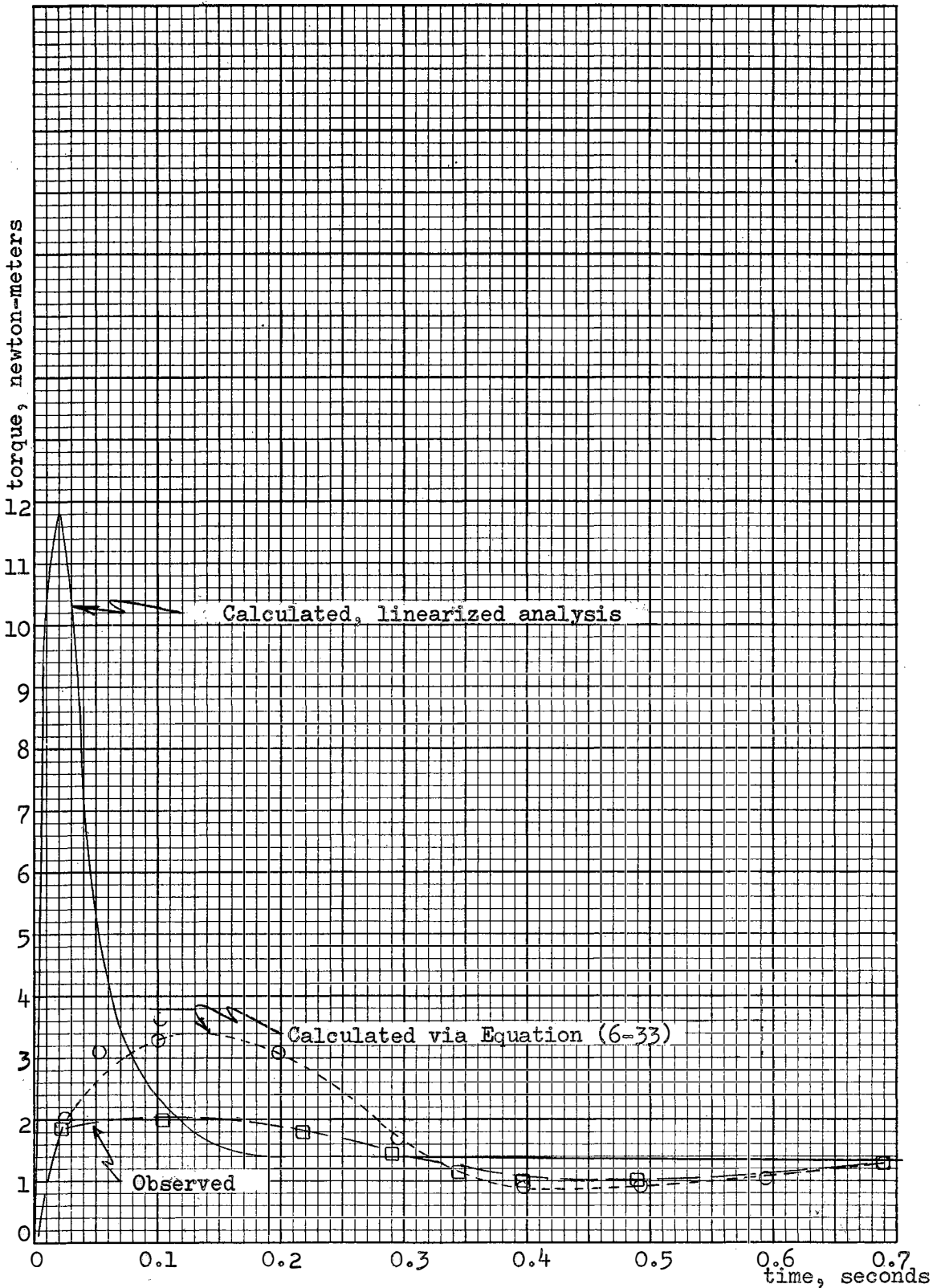


Figure 6.6: Torque Versus Time, Observed and Calculated

on  $\frac{d\omega}{dt}$  in the vicinity of the data point and this results in a large portion ( $J \frac{d\omega}{dt}$ ) of the developed torque in the calculations.



## CHAPTER VII

### SUMMARY AND CONCLUSIONS

#### Summary

It is common practice in system analysis procedures to consider the widely used shunt connected d.c. motor as a linear device. The differential equations written to describe the motor behavior are ordinary linear differential equations.

The set of equations necessary to completely describe performance are presented as Equations (3-3) through (3-7), followed by the necessary assumptions that "linearize" the motor and simplify the analysis procedure sufficiently to enable closed loop analysis techniques to be employed.

Derivations of performance expressions, based on the simplifying assumptions, are presented for various configurations in Chapter III.

The factors neglected by the simplifying assumptions are investigated in Chapter IV. In this chapter, the use of Frohlich's representation of the magnetic structure is utilized to derive quantitative expressions for the evaluations of (i) the current-time response of a nonlinear circuit, (ii) the demagnetizing affect of armature reaction,

and (iii) the affect of brush shift on torque output and induced voltage. Although these effects have been investigated by others, the investigations were of qualitative or graphical nature. The results presented in this thesis allow, for the first time, evaluation of these phenomena in the design stage.

Chapter V is concerned with methods of obtaining experimental transients as well as presenting observed results for a d.c. motor subjected to various initial conditions and load situations. These results are compared with performance as calculated for the motor using the linear type analysis and are found to have wide discrepancies with respect to calculated performance. The discrepancies are so great as to lead one to conclude that the linear type version of response is very nearly worthless from a quantitative standpoint.

Chapter VI concerns itself with a derivation for an experimental procedure from which calculations can be made resulting in performance expressions which agree quite well with reality, and from which a transfer function can be obtained for use in system analysis.

### Conclusions

Two choices are available for obtaining more faithful representation of the transient behavior of direct current shunt connected motors. The form of the motor, as presently designed can be accepted "as is", and recognized as a

device which will not behave as predicted by simplified linearized equations, or steps can be taken in the design of the motor which will minimize the factors contributing to the departure of actual from predicted performance.

If the former option is chosen, resort to the experimentally determined transfer function procedure developed in this thesis will lead to more accurate results. The degree of accuracy is a function of the total number of data points utilized. In the results presented in Chapter VI, a minimum number of points were used; the transfer function relating speed output to voltage input was nearly an exact duplication of the observed performance while the torque-time response calculation displayed only one-sixth the error present when calculated by linearized equations.

Specifications for a new design in which de-emphasis, or elimination if possible, of factors contributing to the performance discrepancies noted in this thesis should be determined after consideration of the following parameters.

#### A. Brushes and Rigging

The quantitative results derived in Chapter IV-D predict the effect of brush shift and indicate that it results in either magnetizing or demagnetizing effect in the magnetic structure (depending upon the direction of shift relative to rotational direction of the armature). In control system work, since the requirement is for rotation in both directions, brushes must be on neutral. This requirement

dictates the use of a commutating field, or interpole, for commutation assistance.

Since the resistance introduced into the armature circuit by the brush system is difficult to predict and is also highly variable (being a function of current density, speed, atmospheric conditions, physical wear of the brushes, etc.), the armature resistance should be made as large as possible in order to minimize exterior manifestations of the variations introduced by the brushes. This will, incidentally, aid commutation.

#### B. Armature Windings

High armature resistance is desirable from the standpoint of the factors mentioned in (A), but more important from a transient standpoint is that it will reduce armature to shunt field coupling by virtue of decreasing the resultant current within the closed circuits formed by armature winding, commutator segments and brushes during switching or transient periods. The coupling arises from other sources also (see below) but it appears to this investigator to be the dominate over-all factor responsible for discrepancies noted above. As pointed out in Chapter IV, the induced voltage, during dynamic conditions, is as much as 37% less than one would predict from the regular open circuit characteristic of the motor.

The demagnetizing effect of the coupling, due to circulating currents in portions of the armature, can also be

lessened by avoiding the use of complex armature winding arrangements, such as duplex, triple reentrant, etc., that consist of multiturn connections to the commutator segments upon which the brush system must be such as to span three or four segments. This results in a larger number of short circuited armature turns than would be present in a simple lap or wave winding.

### C. Use of Additional Windings

In Chapter IV-C, this author developed a quantitative analysis of the demagnetizing effect of armature reaction, utilizing the constants of Frohlich's Equation as they relate to a specific magnetic circuit. Since armature reaction is one of the factors with the most pronounced effect upon net core excitation (and the so called torque constant) the use of compensating windings located in the pole faces appear justified regardless of motor size, if transient response is critical.

A series field for compounding a motor is often considered desirable, especially for high torque (at low speed) type loads. This usage is commonly specified because of the impression, widely held in industry, that the series field ampere turns, per se, are responsible for additional torque. If the magnetic circuit is operated above its knee, the additional ampere turns contributed by the series field will result in a negligible increase in flux. However, the torque is increased by virtue of the decreased

magnetic circuit demagnetization due to armature to shunt field coupling. This coupling is decreased several orders of magnitude when a small series field is present. For this reason, this author prefers to designate the series winding as a stabilizing winding, rather than a compounding winding.

A mathematical derivation of the benefits of a commutating, or interpole winding, is presented for the first time in Chapter IV. The advantage accrues from two standpoints, i.e., because of the polarity of the winding, it tends to neutralize armature circuit inductance which is a motor parameter subject to broad variations in value and because of the fact that "under" commutation results in a direct magnetizing effect. If a winding of a number of turns such that it would be over strength with full armature current is installed, it can be adjusted to provide the proper strength for commutation in the steady state by shunting it with a resistor to divert a portion of the armature current and reduce the net ampere turns to the proper value. During transient periods, because of the self inductance of the winding, a larger percentage of armature current is diverted, resulting in "under" commutation and direct magnetizing effect, thus neutralizing other demagnetizing influence.

#### D. Core Fastening Methods

The method of fastening the core laminations and the

motor frame should be carefully designed to insure no closed conducting paths within which current can circulate during transient periods. These circulating currents are in such a direction as to demagnetize the main field during load increases. If closed paths are unavoidable, care should be taken to select fasteners of as high resistivity as possible in order to restrict the magnitude of the induced currents.

#### E. Core Material, Configuration and Excitation Requirements

A procedure for qualitatively evaluating core materials and configurations with respect to response time was developed during this investigation. The evaluation is with respect to initial permeability and magnetizing requirements and uses Frohlich's Equation as a basis of comparison of the various materials. For minimum response time and minimum eddy current effects, the design should utilize a low resistivity, high permeability core material with the fewest number of turns on the exciting winding consistent with the maximum allowable exciting current. High permeability and low resistivity tend toward relatively large eddy current time constants in the core itself but this results in minimum disturbance in the excitation winding from the eddy currents.

It is felt by this author that positive steps can be taken in both analysis and design to insure more faithful

representation of the transient behavior of d.c. motors, resulting in an increased accuracy of over-all system performance predictions. It is hoped that the derivations and developments originating during this investigation and presented in this thesis will contribute to the over-all problem.



### SELECTED BIBLIOGRAPHY

1. Hansen, K. L. "Analysis of Starting Characteristics of D.C. Motor," Trans. AIEE, Vol. 36 (1917).
2. Koenig, H. E. "Transient Response of D.C. Dynamos," Trans. AIEE, Vol. 69, I (1950).
3. Vowels, R. E. and W. G. Forte. "Electromechanical Analysis of a Separately Excited D.C. Machine," Trans. AIEE, Vol. 71, I (1952).
4. White, David C. and Herbert H. Woodson. Electromechanical Energy Conversion. New York: John Wiley and Sons, (1959).
5. Jones, R. W. Electric Control Systems. New York: John Wiley and Sons, (1950).
6. McClinton, A. T., E. L. Brancato and R. Panoff. "Transient Characteristics of D.C. Motors and Generators," Trans. AIEE, Vol. 68 (1949).
7. Adkins, Bernard. The General Theory of Electrical Machines. New York: John Wiley and Sons, (1957).
8. Rudenberg, Reinhold. Transient Performance of Electric Power Systems. New York: McGraw-Hill, (1950).
9. Fitzgerald, A. E. and C. Kingsley. Electric Machinery. New York: McGraw-Hill, (1952).
10. Ku, Y. H. Electric Energy Conversion. New York: Ronald Press, (1958).
11. Rao, C. V. G. "Solution of Nonlinear Differential Equations for Rotating Oscillator," Journal, Franklin Institute 265 (1958).
12. Linville, T. M. "Current and Torque of D.C. Machines on Short Circuit," Trans. AIEE, Vol. 65 (1946).

13. Linville, T. M. and A. G. Darling. "Rate of Rise of Short Circuit Current of D.C. Motors and Generators," Paper, AIEE 52-71 (December, 1951).
14. Cybulski, John, E. L. Brancato and J. P. O'Connor. "Transient Performance of D.C. Machinery I," Paper, AIEE 53-85 (1952).
15. Ahlquist, R. W. "Equations of Motion of D.C. Machine," Trans. AIEE, Vol. 73, III B (1954).
16. Radiation Lab. Theory of Servomechanisms. New York: McGraw-Hill, (1947).
17. Moore, Robt. C. "How Much Torque From D.C. Dynamic Braking," Control Engineering (Magazine), (April, 1961).
18. Saunders, Robert M. "Measurement of D.C. Machine Parameters," Trans. AIEE, Vol. 70 (1951).
19. STANDARDS - ASA Standards, Rotating Electrical Machinery, C50-1943, American Standards Assn., New York, (1943).  
  
AIEE, No. 501, Test Code for D.C. Machines, New York, (July, 1941).  
  
NEMA, Standards for Motors and Generators MG1, National Electric Manufacturing Assn., New York (1949).
20. LePage, W. R. Analysis of Alternating Current Circuits. New York: McGraw-Hill, (1954).
21. Nixon, Floyd E. Handbook of Laplace Transformation. New Jersey: Prentice-Hall, (1960).
22. Truxal, John G. Control System Synthesis. New York: McGraw-Hill, (1955).

## APPENDIX A

In order to calculate  $i$  versus  $t$  for the sample calculation in Chapter IV, Sub-section A, an IBM 1620 computer was utilized. In the sample calculations, the stipulation was made that 5.0 amperes exciting current and a maximum flux of 0.0125 webers corresponding to 5.0 amps excitation would be used. A range of values of  $D$  and  $N$  were chosen, such that:

$$\begin{aligned} 0.015 < D < 0.03 & \quad \text{in increments of } D = .005 \\ 500 < N < 1500 & \quad \text{in increments of } N = 500. \end{aligned}$$

Defining  $D$ ,  $N$ ,  $N_{\max}$  and  $I_s$  constrained the value  $G$ . The time for current build up to various values of  $i$ , where  $0.5 < i < 4.95$  in increments of  $i = 0.5$  were made using Equation (4-16) which is, with values:

$$\epsilon^t = \epsilon \frac{1.56 Ni}{62.5 \times 10^4 [50 - (5 - i)(0.0125)]} \frac{0.0125N(D - .0125)}{62.5D} \left[ \frac{5D - (5 - i)(0.0125)}{D - 0.0125(5 - i)} \right]$$

This information was used to plot Figures 4.4 through 4.10.

## GOTRAN PROGRAM

310000300002  
360000000300

```
1 PAUSE‡
D=0.015‡
DO 10 I=1,4‡
D5=5.0*D‡
XX=D-0.0125‡
E=500.0‡
DO 11 J=1.3‡
C=2.0E-4*E‡
C=C*XX‡
C=C/D‡
PRINT, D,E‡
F=0.50‡
DO 12 K=1,9‡
X=5.-F‡
Y=X*0.0125‡
Z=D5-Y‡
B=Z/X‡
B=B/XX‡
A=2.5E-6*E‡
A=A*F‡
A=A/Z‡
AA=LOG(B)‡
T=C*AA‡
T=T+A‡
PRINT, F,T‡
12 F=F+0.5‡
PAUSE‡
11 E=E+500.‡
10 D=D+.005‡
GO TO 1‡
END‡
```

## SAMPLE PRINT OUT

3.0000000E- 2	500.00000
.50000000	1.6837276E- 2
1.0000000	3.3306037E- 2
1.5000000	4.9778861E- 2
2.0000000	6.6680390E- 2
2.5000000	8.4563303E- 2
3.0000000	.10425632
3.5000000	.12721721
4.0000000	.15661330
4.5000000	.20240671

3.0000000E- 2	1000.0000
.50000000	3.3674551E- 2
1.0000000	6.6612072E- 2
1.5000000	9.9557719E- 2
2.0000000	.13336077
2.5000000	.16912659
3.0000000	.20851264
3.5000000	.25443440
4.0000000	.31322661
4.5000000	.40481340

3.0000000E- 2	1500.0000
.50000000	5.0511829E- 2
1.0000000	9.9918111E- 2
1.5000000	.14933658
2.0000000	.20004117
2.5000000	.25368990
3.0000000	.31276898
3.5000000	.38165163
4.0000000	.46983993
4.5000000	.60722013

## VITA

Howard Britton Hamilton  
Candidate for the Degree of  
Doctor of Philosophy

**Thesis:** FACTORS AFFECTING THE TRANSIENT RESPONSE OF  
DIRECT CURRENT MOTORS

**Major Field:** Electrical Engineering

**Biographical:**

**Personal Data:** Born in Augusta, Kansas, October 28,  
1923, the son of Silas H. and Ora J. Hamilton.

**Education:** Graduated from Augusta High School in  
1941; received the Bachelor of Science degree in  
Electrical Engineering in June, 1949 from the  
University of Oklahoma, Norman, Oklahoma; re-  
ceived the Master of Science degree in Electrical  
Engineering in June, 1955, from the University  
of Minnesota, Minneapolis, Minnesota; completed  
the requirements for the Doctor of Philosophy  
degree in June, 1962.

**Professional experience:** Electrical Engineer with  
the General Electric Company, Schenectady,  
New York from June, 1949 to September, 1953;  
Instructor in Mechanical Engineering from Sep-  
tember, 1953 to June, 1954; Assistant Professor  
and Head, Electrical Engineering Department from  
September, 1955 to June, 1958 at the University  
of Wichita, Wichita, Kansas; Unit Chief at  
Boeing Airplane Company, Wichita, Kansas from  
September, 1958 to September, 1960; Associate  
Professor of Electrical Engineering from Septem-  
ber, 1960 to the present (currently on leave of  
absence). Participated in Boeing Airplane  
Company Summer Faculty Program during the Summer  
of 1954.

**Membership in Scientific and Professional Societies:**  
Member, Past Section Chairman and Member Rotating  
Machinery Committee of American Institute of  
Electrical Engineers; Registered Professional  
Engineer in Kansas; Member Kansas Engineering  
Society, Tau Beta Pi, Sigma Tau, Eta Kappa Nu, and  
Phi Eta Sigma.